



Rôle de la phosphodiésterase 2A dans la physiopathologie du syndrome de l'X fragile

Sébastien Delhaye

► To cite this version:

Sébastien Delhaye. Rôle de la phosphodiésterase 2A dans la physiopathologie du syndrome de l'X fragile. Biologie cellulaire. Université Côte d'Azur, 2021. Français. NNT: 2021COAZ6014 . tel-04637384

HAL Id: tel-04637384

<https://theses.hal.science/tel-04637384>

Submitted on 6 Jul 2024

HAL is a multi-disciplinary open access archive for the deposit and dissemination of scientific research documents, whether they are published or not. The documents may come from teaching and research institutions in France or abroad, or from public or private research centers.

L'archive ouverte pluridisciplinaire **HAL**, est destinée au dépôt et à la diffusion de documents scientifiques de niveau recherche, publiés ou non, émanant des établissements d'enseignement et de recherche français ou étrangers, des laboratoires publics ou privés.



THÈSE DE DOCTORAT

Rôle de la phosphodiesterase 2A dans
la physiopathologie du syndrome de l'X
Fragile

Sébastien DELHAYE

Institut Pharmacologique Moléculaire et Cellulaire

**Présentée en vue de l'obtention
du grade de docteur en** Sciences de la Vie et de la
Santé
d'Université Côte d'Azur

Mention : Interactions moléculaires et cellulaires

Dirigée par : le Dr Barbara BARDONI

Soutenue le : 1^{er} juillet 2021

Devant le jury, composé de :
Présidente du jury : Michèle STUDER,
Directrice de recherche, *Université Côte D'Azur*

Rapportrice externe : Julie PERROY,
Directrice de recherche, *Université Montpellier*

Rapportrice externe : Susanna PIETROPAOLO,
Chargée de recherche, *Université de Bordeaux*

Examinateuse : Ingrid BETHUS,
Maître de conférences, *Université Côte D'Azur*

Examinateuse : Lucia CIRANNA,
Professeure, *Università di Catania*

Directrice de thèse : Barbara BARDONI,
Directrice de recherche, *Université Côte D'Azur*



Résumé

Le Syndrome de l'X Fragile (SXF) est la forme la plus fréquente de déficience intellectuelle héréditaire. Le phénotype des patients SXF est complexe. En effet, ils présentent aussi des traits autistiques, de l'hyperactivité et un déficit de l'attention. Au niveau du cerveau, le phénotype majeur est la présence d'épines dendritiques plus nombreuses, plus longues et plus fines. Ces anomalies morphologiques sont associées à des formes altérées de plasticité synaptique chez le modèle murin de SXF, la souris *Fmr1-KO*. Le SXF est causé par l'expansion (plus de 200 fois) du triplet nucléotidique CGG dans le 5'UTR du gène Fragile X Mental Retardation 1 (*FMR1*). L'hyperméthylation de cette région du gène *FMR1* et, surtout de son promoteur, induit la suppression de l'expression de *FMR1* et donc l'absence de la protéine FMRP codé par ce dernier. Une expansion entre 50 et 200 fois du triplet est considérée comme une prémutation et est associée à deux autres maladies : le syndrome du tremblement-ataxie lié au X Fragile (FXTAS), une maladie neurodégénérative, et l'insuffisance ovarienne liée à la prémutation de l'X Fragile (FXPOI).

FMRP se lie à l'ARNm et est impliquée dans la régulation de plusieurs étapes du métabolisme de l'ARN, en particulier dans la modulation de la traduction de plusieurs protéines synaptiques. Aucune thérapie n'est aujourd'hui disponible pour traiter les patients atteints de SXF.

J'ai montré que FMRP module l'expression de la Phosphodiesterase 2A (PDE2A) au niveau synaptique. PDE2A est une enzyme impliquée dans la dégradation de l'AMPc et du GMPc, deux seconds messagers qui jouent un rôle critique dans le développement et la différenciation des neurones. Quand FMRP est absente, le niveau et l'activité de PDE2A sont augmentés et, en conséquence, les niveaux d'AMPc et de GMPc sont réduits dans le cortex et l'hippocampe.

J'ai montré que le traitement avec un inhibiteur spécifique de la PDE2A, le BAY

60-7550, rétablit les déficits sociaux chez les souris *Fmr1*-KO jeunes et adolescentes, la morphologie anormale des épines dendritiques et la Long Term Depression mGluR-dépendante exagérée. Afin de valider par une approche génétique que la réduction du niveau (et de l'activité) de la PDE2A pourrait avoir un rôle thérapeutique pour le SXF, j'ai croisé la lignée *Pde2a^{+/−}* avec les souris *Fmr1*-KO et analysé le phénotype comportemental, la morphologie neuronale et les voies de signalisation liées à l'AMPc et au GMPc dans l'hippocampe et le cortex des souris générées par ce croisement. En effet, j'ai pu montrer que les animaux *Fmr1*-KOx*Pde2a^{+/−}* ont un phénotype sociocognitif normal comparé aux les animaux *Fmr1*-KO et *Pde2a^{+/−}*. En effet, les souris *Pde2a^{+/−}* ont un comportement très similaire à celui des animaux *Fmr1*-KO même si les altérations moléculaires dans le cerveau apparaissent inversées comparées à celles des souris *Fmr1*-KO.

Dans leur ensemble, mes résultats montrent l'importance des voies AMPc et GMPc qui dépendent de PDE2A dans la pathophysiologie de FXS et dans le neurodéveloppement. En effet, j'ai identifié un nouveau modèle de maladies du développement du cerveau dû à la réduction du niveau d'activité de *Pde2a^{+/−}*.

Dans la première partie de mon doctorat, j'ai contribué à l'identification de la morphologie des neurones corticaux obtenus à partir d'un modèle murin de FXTAS.

Mots-clés : Syndrome de l'X Fragile, Déficience Intellectuelle, Trouble du spectre de l'autisme, AMPc, GMPc, PDE2A

Abstract

Fragile X Syndrome (FXS) is the most common form of inherited intellectual disability (ID). In addition to ID, patients might exhibit autistic features, hyperactivity and attention-deficit disorder, language dysfunction and seizures. Approved and effective therapies are not yet available for FXS. The main hallmark of FXS in the brain is the presence of immature and denser dendritic spines. This abnormality is associated with altered synaptic plasticity in our animal model of FXS, the *Fmr1*-KO mice. FXS is caused by a CGG repeat expansion with a number of repeats higher than 200 in the 5'UTR of the Fragile X Mental Retardation 1 (*FMR1*) gene. Methylation of this region and of its surrounding sequences, including the promoter of *FMR1*, results into the silencing of the gene and the loss of its encoded protein, FMRP. An expansion with a number of repeats variable between 50 and 200 is considered as a premutation and is associated with two pathological conditions other than FXS: The Fragile X-associated Tremor Ataxia Syndrome (FXTAS), and the Fragile X associated Primary Ovarian Insufficiency (FXPOI).

FMRP is an RNA-binding protein implicated in various steps of RNA metabolism. In particular, it plays a role in the translational regulation of a subset of synaptic proteins.

We showed that FMRP modulates the synaptic expression of Phosphodiesterase 2A (PDE2A), an enzyme implicated in the degradation of cAMP and cGMP. In the absence of FMRP, the levels and the activity of PDE2A are increased, and, consequently, cAMP/cGMP levels are reduced in the cortex and hippocampus of *Fmr1*-KO mice.

The blockade of PDE2A with a specific and powerful inhibitor of PDE2A, Bay 607550, rescues various *in vitro*, *ex vivo* and *in vivo* FXS phenotypes. In particular, I contributed to this study by showing that the treatment with Bay 60-7550 rescues social deficits in young and adolescent *Fmr1*-KO mice and abnormal dendritic spine

morphology in hippocampus. In order to validate this new therapeutic target for FXS, I crossed *Pde2a^{+/}* mice with *Fmr1*-KO mice and analyzed their behavior, neuronal morphology and signaling pathways linked to cAMP/cGMP levels in the hippocampus and cortex. I found that double mutant animals (*Fmr1*-KO x *Pde2a^{+/}*) have a normal social and cognitive behavior compared to both *Fmr1*-KO and *Pde2a^{+/}* mice. Indeed, *Pde2a^{+/}* mice display behavioral deficits similar to those characterizing the *Fmr1*-KO mouse, even if the molecular alterations seem to be opposite.

In conclusion, my results highlight the key role of PDE2A-dependent cAMP and cGMP levels and their correlated pathways in neurodevelopment.

Furthermore, in addition to my main project, in the first part of my doctoral stage, I participated to the characterization of neuronal morphology in the mice model of FXTAS showing that this neurodevelopmental marker is dependent on the level of the *Fmr1* mRNA, which displays elevated levels in these mice in the presence of the *Fmr1* premutation.

Key words: Fragile X Syndrome, Intellectual Disability, Autism Spectrum Disorder, cAMP, cGMP, PDE2A

Remerciements

J'aimerais tout d'abord remercier les membres du jury d'avoir accepté d'évaluer mes travaux de thèse. Je remercie les Dr. Julie Perroy et Dr. Susanna Pietropaolo de m'avoir fait l'honneur, en tant que rapportrices, d'avoir consacré du temps à l'évaluation de ma thèse. Merci aux Dr Lucia Ciranna et Dr Michèle Studer de m'avoir accompagné durant ces plus de trois années de thèse en me conseillant au mieux sur ce projet. Enfin, un grand merci au Dr Ingrid Bethus de participer à ce jury, de toujours avoir pris du temps pour discuter avec moi sur mes expériences, et surtout de m'avoir donné envie de me diriger vers la neurobiologie et la recherche, il y a de cela maintenant quelques années. Si je suis là aujourd'hui c'est grâce à toi, et un peu à cause de toi aussi. La boucle est bouclée.

Barbara, je n'aurais pas pu espérer mieux comme directrice de thèse. Point.

Merci de m'avoir soutenu dans les moments difficiles.

Merci de m'avoir fait confiance au quotidien et de m'avoir laissé une liberté aussi grande sur mon sujet. Sauf quand je commençais à parler d'astrocytes. Mais on y viendra tu verras...

Merci de m'avoir fait rire avec tes expressions italiennes traduites en français, le plus souvent très très imagées, et ton franc parler.

« Je peux te dire une chose », merci !

A la BB Team,

Marielle, je crois qu'il est raisonnable de dire que sans toi, je n'aurais jamais réussi à avancer dans ce projet. Même si tu m'as torturé pendant des heures à Animex avant même que je décide de faire ma thèse dans l'équipe (un pari audacieux mais payant), je ne te remercierai jamais assez de m'avoir épaulé au quotidien. De toute façon tu n'avais plus le choix, on est plus que nous deux au labo (insérer emoji triste).

TomTom, le talent à l'état pur, le toucher magique pour faire marcher des clonages, le Papa de l'équipe qui est parti un matin chercher ses clopes et n'est jamais revenu (insérer plusieurs émojis tristes). Merci de m'avoir soutenu en ces débuts de thèse difficiles et de m'avoir fait un peu plus apprécier la biochimie. En même temps, qui n'aimerait pas mélanger de l'eau avec de l'eau dans des tubes. Franchement.

Sara et Gosini, merci les filles pour ces quelques années incroyables avec vous dans le labo et en dehors. Merci pour ces bons moments de travail et d'entraide, et de m'avoir aussi bien accueilli dès le départ. Pas merci pour la raclette aux courgettes et mes surnoms pourris par contre.

Enfin, merci au reste de l'équipe, présent et passé, Mauro, Méline, Maria pour leur accueil et leur gentillesse au quotidien. Et de m'avoir appris la patience aussi.

Bien sûr, je n'oublie pas tous les étudiants ayant franchi les portes de l'enfer : Asma, Nicolas, Alessandra, Erica, Léa, Noa, Ninon, Manon etc etc ...

Je n'oublierai jamais nos petites phrases sur le frigo, un monument envié par tout l'institut.

Je tiens aussi à remercier l'ensemble de l'institut avec qui j'ai eu avec un bon nombre de personnes des échanges très intéressants, très motivants et toujours bienveillants. En particulier :

L'équipe Lalli, j'espère ne pas avoir été trop envahissant à toujours vous demander de me dépanner trois fois par semaine. Un immense merci à Carmen, Mabrouka, Nelly et Enzo pour leur immense gentillesse. Mais décidément, il y a trop d'italiens à cet étage...

Mille merci à Sophie et Fred qui doivent être bien contents de ne bientôt plus me voir. Plus de macros complètement délirantes et bien chiantes à faire. Plus de formation à gogo pour un appareil que j'utiliserais une fois en 4 ans. Et plus de questions débiles de ma part. Mais au moins je n'ai rien cassé. Enfin je crois ...

Merci à Thomas Lorivel pour avoir toujours trouvé un moment pour m'aider pour le comportement et à Animex. Oui tout était dans le PEA Thomas, aie confiance !

Je n'aurais évidemment pas pu survivre cette aventure qu'est la thèse sans mes amis à l'institut ;

Marie, finalement on l'a fait. Merci d'avoir été à mes côtés depuis le début, surtout dans les moments difficiles et pour me dire quand je fais de la merde ! On s'est pas mal débrouillés en fait quand on y pense. Qui l'eût cru !

Maxime, après t'avoir appris tout ce que tu sais aujourd'hui du monde qui t'entoure et au-delà pendant ton stage de master, tu m'as forcé à devenir ton ami. Depuis je fais Salamèche la nuit tombée. Pas merci. Mais merci un peu quand même de me faire rire quand je vois ton crâne luisant s'illuminer au loin dans les couloirs.

Clara, ma collègue du +1, je ne vais pas te remercier parce que c'est plutôt à toi de le faire. Je sais que sans moi tes journées seraient fades et ennuyeuses. Ne pleure pas mon départ, je reviendrai PARCE QU'ON VA L'AVOIR CE PRIX NOBEL !!!

Aurore, merci d'avoir été ma fournisseuse officielle de repas et de faire le taxi tous les midis. Et merci pour tes conseils pour les western blot même s'ils sont toujours aussi laids. Je parle des tiens évidemment.

Grosses pensées à tous mes autres collègues de l'IPMC : Méliné (désolé pour la cuite de la retraite, belle entrée en matière), Daz, Joris, NFL, et tous les autres.

Merci à toute ma famille d'avoir fait semblant de comprendre mon sujet de thèse pendant toutes ces années.

Valentine, je n'ai pas les mots pour te dire à quel point tu m'as été essentielle ces dernières années passées à tes côtés.

Enfin, merci à toutes ces souris tombées au combat. Je ne t'oublierai jamais Ryan.

« Le premier ennemi de la connaissance n'est pas l'ignorance, c'est l'illusion de la connaissance. » Thomas Durand

« Ne suffit-il pas de croire qu'un jardin est beau, sans qu'il faille aussi croire à la présence de fées au fond de ce jardin ? » Richard Dawkins

« Le monde, c'est la preuve » Barbara Bardoni – Juillet 2018

Table des matières

Abréviations	11
Introduction	13
Chapitre 1. Le Syndrome de l'X Fragile.....	13
I. Les troubles du neurodéveloppement.....	13
II. La déficience intellectuelle.....	15
1. Aperçu historique de la DI.....	15
2. Tableau clinique.....	16
3. Epidémiologie et causes.....	17
III. Les troubles du spectre autistique	18
1. Histoire de l'autisme	18
2. Tableau clinique et classification des TSA.....	19
3. Epidémiologie et causes.....	21
4. Traitements	23
5. TSA vs DI	23
IV. Le Syndrome de l'X Fragile	25
1. Découverte du syndrome.....	25
2. Cause, épidémiologie et hérédité	26
3. Tableau clinique	29
4. Le FXTAS	34
5. Modèles animaux.....	35
6. Traitements	43
V. La protéine FMRP et ses ARNm cibles.....	45
1. Le gène <i>FMR1</i>	45
2. La protéine FMRP	46
3. Identification des ARNm cibles de FMRP	50
Chapitre 2 : AMPc/GMPc et PDE2A.....	52
I. AMPc et GMPc, deux seconds messagers à la croisée des chemins.....	52
1. Création et dégradation	52
2. Implication dans de nombreuses voies de signalisation.....	53
3. Rôle de la balance AMPc/GMPc dans les neurones.....	57
4. Rôle dans la plasticité synaptique	57
II. Les phosphodiestérases	60
1. Une grande famille d'enzymes.....	60

2. Rôle dans les troubles du neurodéveloppement	61
3. Modèles animaux.....	63
III. La PDE2A.....	65
1. Biologie de la PDE2A	65
2. Expression et localisation subcellulaire	65
3. Effets de l'inhibition de la PDE2A.....	66
Objectifs de la thèse.....	69
Matériels et méthodes.....	70
Résultats.....	76
I. Effet d'un traitement aigu et chronique en Bay 60-7550 sur les souris <i>Fmr1</i> KO.....	76
II. Rôle de la PDE2A dans la migration corticale au stade embryonnaire	79
III. Effet de la réduction génétique de PDE2A chez la souris <i>Fmr1</i> KO.....	80
IV. Caractérisation de la lignée <i>Pde2a^{+/−}</i>	83
V. Effet de la réduction du niveau d'ARNm de <i>Fmr1</i> sur la morphologie et la protéomique des neurones corticaux de souris modèle du FXTAS.	94
Discussion Projet 1	96
I. Rôle de la PDE2A dans le comportement social, cognitif et anxieux	96
II. Rôle de la PDE2A dans le phénotype cellulaire et moléculaire.....	98
III. Rôle de la PDE2A dans la LTD	103
IV. La souris <i>Pde2a^{+/−}</i> , nouveau modèle de maladie neurodéveloppementale ?	104
Discussion Projet 2	107
Conclusion & Perspectives	109
Publication 1.....	110
Publication 2.....	111
Publication 3.....	112
Annexe 1.....	113
Annexe 2.....	114
Bibliographie	115

Abréviations

AC : Adenylate Cyclase

ADHD : Attention deficit hyperactivity disorder

AMPA : α -amino-3-hydroxy-5-méthylisoazol-4-propionate

AMPc : Adenosine MonoPhosphate Cyclique

ARNm : Acide RiboNucléique messager

BDNF : brain derived neurotrophic factor

CFC : Contextual Fear Conditioning

CLIP : CrossLinking ImmunoPrecipitation

COX4 : Cytochrome c oxidase subunit 4

CRE : cAMP response element

CREB : cAMP response element binding response

DI : Déficit intellectuel

DIV : Days *In Vitro*

DSM : Diagnostic and Statical Manual

E17.5 : stade embryonnaire -jours après accouplement

ERK : extracellular signal-related kinase

EIU : Electroporation *in utero*

FMR1 : Fragile X Mental Retardation 1

FMRP : Fragile X Mental Retardation Protein

FXPOI : Insuffisance ovarienne liée à la prémutation de l'X Fragile

FXTAS : Syndrome du tremblement-ataxie lié au X-Fragile

GABA : acide γ -aminobutyrique

GAF : cGMP-binding PDE, Anabaena adenylyl cyclases, Escherichia coli FhlAs

GC : Guanylate Cyclase

GMPC : Guanosine MonoPhosphate Cyclique

GSK3 : glycogene synthase kinase 3

GWAS : Genome-wide association

Kb : Kilobase

KD : Knock Down

kDa : KiloDalton

KH : K Homology

KI : Knock In

KO : Knock Out

LTD : Long Term Depression

LTP : Long Term Potentiation

mGluR : récepteur métabotropique du glutamate

MWM : Morris Water Maze

NES : Nuclear export signal

NLS : Nuclear localisation signal

NOR : Novel Object Recognition

P13 : Post natal day – jours après la naissance

PDEs : phosphodiesterases

PKA : Protein Kinase A

PKG : Protein Kinase G

PPI : PrePulse Inhibition

QI : Quotient Intellectuel

SNP : Single Nucleotide Polymorphism

SXF : Syndrome de l'X Fragile

TD AH : Trouble du déficit de l'attention avec hyperactivité

TND : Troubles du neurodéveloppement

TSA : Trouble du spectre autistique

USVs : UltraSonic Vocalisations

UTR : Untranslated Region

WT : Wild Type – Sauvage

Introduction

Chapitre 1. Le Syndrome de l'X Fragile

I. Les troubles du neurodéveloppement

Les troubles du neurodéveloppement (TND) regroupent un nombre important de maladies cliniquement hétérogènes qui se caractérisent par des déficits dans la cognition, la communication, le comportement et le fonctionnement moteur. Ils résultent d'un développement atypique du cerveau à différents stades, notamment au niveau de la neurogénèse, la prolifération et la migration des neurones et de la glie ainsi qu'au niveau de la formation des synapses.

Les TND les plus communs incluent les troubles du spectre de l'autisme (TSA), le déficit intellectuel (DI), le trouble du déficit de l'attention avec hyperactivité (Attention Deficit Hyperactivity Disorder, ADHD) ou encore les troubles moteurs. Par extension, les troubles neuropsychiatriques, tels que la schizophrénie et les troubles bipolaires, peuvent rentrer dans cette catégorie ainsi que l'épilepsie. La co-occurrence de plusieurs de ces troubles chez un seul individu est très fréquente. Par exemple, les troubles neuropsychiatriques sont présents chez 30 à 50% des patients atteints de DI (Einfeld et al., 2011), et chez 50% ayant un TSA (Mazefsky et al., 2012).

Les facteurs de causes de ces troubles sont multiples et variés (Fig.1). Ils peuvent être d'ordre génétique (variation du nombre de copies, mutations) de façon majoritaire, ou dans une moindre mesure, d'ordre environnemental *in utero* ou postnatal (expositions à des médicaments, infections, trauma obstétrique, hypoxie, malnutrition, etc...). De nombreuses études de séquençage d'exome ont permis d'associer des milliers de gènes avec des TND comme la DI et les TSA (Najmabadi et al., 2011; Sanders et al., 2012; Xu et al., 2011).

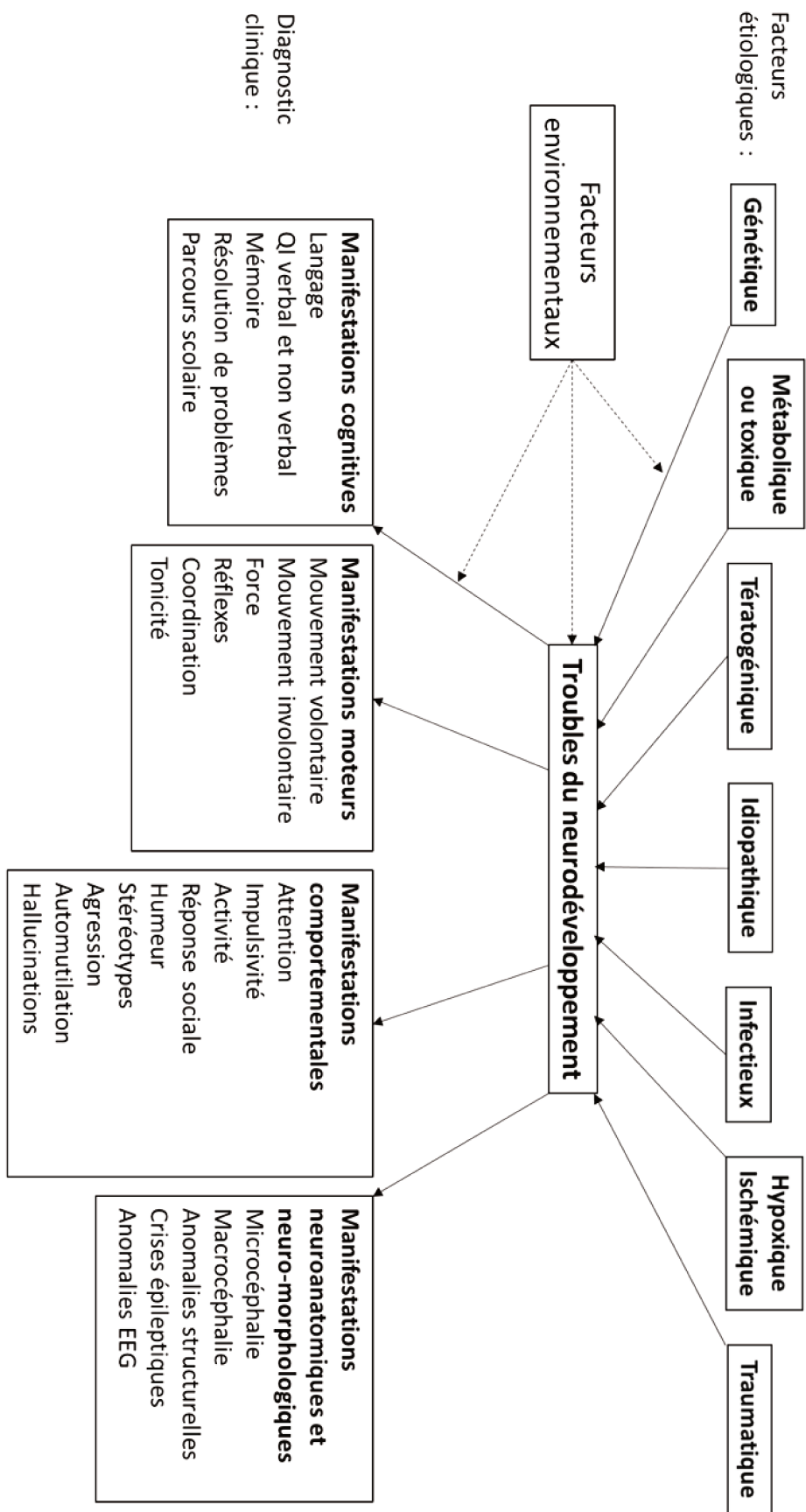


Figure 1. Causes et manifestations des troubles du neurodéveloppement. Adapté de MorenoDe-Luca et al.

II. La déficience intellectuelle

L'Organisation mondiale de la santé (OMS) définit la déficience intellectuelle comme «la capacité sensiblement réduite de comprendre une information nouvelle ou complexe, et d'apprendre et d'appliquer de nouvelles compétences ». Elle est caractérisée par un quotient intellectuel (QI) en dessous de 70 et des limitations du fonctionnement adaptatif.

1. Aperçu historique de la DI

Des traces de l'étude de la déficience intellectuelle sont retrouvées dans les premières civilisations égyptiennes, grecques et romaines anciennes. Dans ces temps-là, la DI n'était pas différenciée des troubles mentaux et faisait déjà l'objet de stéréotypes et de stigmatisation comme jusqu'à très tôt dans notre société récente. Les premières descriptions de DI furent trouvées dans des écrits de l'ancienne Egypte dans lesquels ils s'efforçaient de trouver des traitements à diverses maladies (Scheerenberger, 1983). À l'inverse, dans la Grèce et Rome antique, les populations avaient un regard moins bienveillant envers les personnes ayant des handicaps, allant jusqu'à les tuer par eugénisme, soutenues par certains philosophes de l'époque comme Platon (Richards et al., 2014). C'est au 17ème siècle que la première description de DI comme maladie fut faite par Thomas Willis. Depuis la terminologie décrivant la DI a évolué.

Au début des années 1900, les personnes ayant une DI étaient décrites par les termes « imbécile », « faible d'esprit », « idiot » ou encore « crétin » (Barr, 1904). Par la suite, l'association American Psychiatric Association (APA) publie en 1952 le premier Diagnostic and Statistical manual (DSM-I) qui décrit la condition comme « déficience mentale », puis comme « retard mental » en 1968 dans le DSM-II et enfin le terme « déficience intellectuelle » dans le dernier DSM à date en 2013.

2. Tableau clinique.

La DI est caractérisée par trois aspects précis : des déficits cognitifs, des déficits dans le comportement adaptatif et enfin la survenue de ces déficits pendant la période développementale. Le fonctionnement adaptatif concerne trois domaines principaux : le domaine conceptuel (langage, mémoire), le domaine social et le domaine pratique (autonomie dans la vie quotidienne).

La DI chez un individu est classée en fonction de la gravité des déficits cognitifs et du fonctionnement adaptatif. Cette classification se fait par le test de QI qui permet d'évaluer les performances de l'individu. Le résultat est donné sous la forme d'un score, qui est par définition à 100 dans la population générale. On parle de DI quand le score est inférieur à 70. L'OMS considère comme déficience légère un QI entre 50 et 69, déficience moyenne un QI entre 35 et 49, déficience grave un QI entre 20 et 34 et déficience profonde un QI en dessous de 20.

Bien que des suspicions de DI puissent apparaître dans la petite enfance, une DI peut être diagnostiquée plus formellement à partir de 5 ans. Cependant des enfants ayant une DI plus légère peuvent n'être diagnostiqués que plus tard dans la scolarité, lorsque les tâches cognitives sont plus difficiles (Reschly, 2009).

Les personnes ayant une DI sont particulièrement sujets aux comorbidités. Le plus souvent on retrouve chez ces personnes de l'épilepsie, un retard du langage ou un comportement agressif chez 25% d'entre eux. De plus, la prévalence des troubles psychiatriques est plus élevée chez ces personnes, comme les troubles anxieux, de l'humeur et psychotique (Einfeld et al., 2011).

3. Epidémiologie et causes.

La DI toucherait entre 1 et 3% des personnes dans le monde, avec un ratio de 1,6 homme touché pour 1 femme (Leonard and Wen, 2002).

La première cause connue de DI est d'ordre génétique qui compte pour la moitié des cas, notamment les aberrations chromosomiques (Marrus and Hall, 2017). Le diagnostic génétique de la DI a historiquement commencé par l'identification de la trisomie 21 comme la cause du Syndrome de Down (Lejeune et al., 1959) et du X fragile sur le chromosome X comme la cause du syndrome de l'X Fragile.

L'incidence des DI est aussi liée à des facteurs environnementaux. En effet, la prévalence dans les pays en voie de développement y est deux à trois fois supérieure par rapport aux pays développés, ce qui pourrait s'expliquer par un niveau de vie plus précaire, un risque d'infection et de malnutrition plus important pendant la petite enfance, et un plus haut taux d'accidents périnataux.

D'autres causes externes ont pu être décrites, comme les infections du système nerveux (méningite), traumatismes crâniens, infections pendant la grossesse (rubéole, toxoplasmose) ou encore la prise de drogue ou d'alcool, ce dernier entraînant un syndrome de l'alcoolémie fœtale. Enfin, pour près d'un quart des patients atteints, la cause n'est pas connue à ce jour.

III. Les troubles du spectre autistique

1. Histoire de l'autisme

Le mot « autisme » est dérivé du mot grec « *autós* » qui veut dire « soi-même ». Le psychiatre suisse Eugen Bleuler fut le premier à utiliser ce terme en 1911 dans son ouvrage « *Dementia praecox ou groupe des schizophrénies* » dans lequel il décrit le retrait psychique et délire hallucinatoire de patients schizophrènes.

Cependant, le premier cas documenté d'autisme date de 1747 et fut celui de Hugh Blair de Borgue, un lord écossais. Son plus jeune frère, tuteur légal de Blair, réussit à annuler son mariage, en invoquant son incapacité à s'engager dans un contrat de mariage. En effet, il était décrit comme perdant son « bon sens » et ayant une « folie silencieuse ». Hugh Blair montrait des difficultés à avoir des relations sociales, manque de tact et un regard anormal, ainsi que des difficultés de langage et écholalie, la répétition systématique des phrases. De plus, il avait des comportements stéréotypés et anormaux, comme la collection de plumes d'oiseaux et de brindilles et le fait de s'assoir toujours à la même place à l'Eglise (“Autism in History,” n.d.).

Près de deux cents ans plus tard, durant les années 1940, Leo Kanner, psychiatre américano-autrichien, et Hans Asperger, pédiatre autrichien, redéfinissent les caractéristiques des enfants autistes que l'on connaît aujourd'hui. En 1943, Kanner décrit les symptômes d'isolement sociale, comme des difficultés à interagir avec les autres, et de troubles du langage chez un groupe de 11 enfants non atteints de troubles psychiatriques connus (Kanner, 1968). En 1944, Asperger décrit quant à lui 4 enfants souffrant d'isolement sociale, n'éprouvant que peu de sentiments pour les autres mais n'ayant pas de difficultés de langage. Ces enfants pouvaient avoir des compétences exceptionnelles en mathématique ou en science avec des façons de penser créatives et originales mais avec des intérêts très restreints (Asperger, 1991) (Frith U, 1991). Ces recherches amèneront à un nouveau sous-groupe des troubles du spectre de l'autisme,

le Syndrome d'Asperger, officiellement défini cliniquement par Lorna Wing en 1981 (Wing, 1981).

Depuis les débuts de Kanner et Asperger, l'autisme a été défini comme un trouble rare et restreint jusqu'à être aujourd'hui une condition très étudiée, commune et très vaste/hétérogène, d'où sa nouvelle dénomination « trouble du spectre de l'autisme » adopté en 2013 dans la 5e édition du Manuel diagnostique et statistique de l'Association américaine de psychiatrie (DSM-5).

2. Tableau clinique et classification des TSA

L'autisme est aujourd'hui considéré comme un ensemble de troubles, différents entre chaque individu en fonction de ses capacités sociales et cognitives. Le terme « spectre » permet de rendre compte de cette diversité.

Historiquement, les enfants décrits comme autistes avaient des déficits dans trois domaines principaux, appelé « triade autistique » :

- L'interaction sociale
- La communication verbale et non verbale
- Et des comportements répétitifs et restreints

C'est cette triade que l'on retrouve dans le DSM-4 en 1994 avant de passer dans le DSM-5 à deux domaines principaux (Communication sociale et comportement répétitif). Ce changement de taxonomie entraîne des critères plus stricts pour le diagnostic des TSA, et les individus précédemment diagnostiqués en tant qu'Asperger avec le DSM-4 ne le sont plus avec le DSM-5 et perdent leurs accès aux soins spécifiques aux Etats-Unis (Volkmar et al., 2012; Volkmar and McPartland, 2014).

Table I. Critères diagnostiques du TSA. DSM-V (2013)

A. Déficits persistants de la communication et de l'interaction sociale dans différents contextes :
<ol style="list-style-type: none">1. Déficits dans la réciprocité émotionnelle et sociale : allant d'une approche sociale anormale, échec d'établissement d'une conversation, à un manque total d'intérêt et d'émotions.2. Déficits dans la communication non-verbale : allant du contact visuel et langage corporel anormal, difficultés à comprendre les gestes, à une absence totale d'expressions faciales et de communication non-verbale.3. Déficits du développement, du maintien et de la compréhension des relations : allant d'une difficulté à adapter son comportement en fonction des contextes sociaux différents, difficulté à se faire des amis, à une absence d'intérêt pour ses pairs.
B. Comportement, intérêts et activités restreints et répétitifs :
<ol style="list-style-type: none">1. Caractère stéréotypé ou répétitif de mouvements, d'utilisation d'objet ou du langage (battements de mains, alignement de jouets, écholalie, phrase idiosyncratique)2. Intolérance aux changements, inflexible sur les habitudes et patterns de comportement verbal et non verbal (grande détresse face aux changements, rituels pour saluer, besoin de prendre la même route ou de manger la même chose tous les jours).3. Intérêts très restreints et fixes, anormaux dans leur intensité ou dans leur but (fort attachement avec des objets inhabituels, intérêts extrêmement restreints et répétitifs)4. Hyper ou hyporéactivité aux stimulations sensorielles ou intérêt inhabituel pour les aspects sensoriels de l'environnement (indifférence apparente face à la douleur ou la température, réponse aversive envers sons ou textures spécifiques, sent et touche les objets de façon excessive, fascination visuelle pour les lumières et mouvements)
C. Les symptômes doivent être présents dès la période précoce du développement (mais ne doivent pas être nécessairement totalement manifestes avant que les demandes sociales n'excèdent les capacités limitées de la personne, ou peuvent être masqués par des stratégies apprises plus tard dans la vie).
D. Les symptômes causent un déficit cliniquement significatif dans le fonctionnement social, professionnel ou dans d'autres domaines.

E. Ces troubles ne sont pas mieux expliqués par une déficience intellectuelle (trouble du développement intellectuel) ou un retard global du développement.

La personne doit présenter l'ensemble des symptômes de la catégorie A et au moins deux de la catégorie B pour répondre aux critères du TSA d'après le DSM-5.

Au niveau mondial, la Classification Internationale des Maladies (CIM)-10 publiée par l'OMS considère encore à ce jour la triade autistique, et classe les TSA dans les troubles envahissants du développement.

Les premiers signes et symptômes peuvent apparaître entre 6 et 12 mois, mais dans la plupart des cas un diagnostic fiable peut être établi à partir de 24 mois (Guthrie et al., 2013). Les déficits d'interaction sociale et le retard du langage sont les principaux déficits chez les enfants de moins de 3 ans.

Près des trois quarts des enfants atteints de TSA présentent un autre trouble médical, psychiatrique ou neurologique. Comme le montre une récente méta-analyse, entre 25 et 32% sont atteints de trouble du déficit de l'attention avec ou sans hyperactivité (TDAH) (Lai et al., 2019) ce qui représente 66% des patients atteint de TDAH (Davis and Kollins, 2012; Leitner, 2014). La dépression se retrouve chez 11% des enfants atteints de TSA (Lai et al., 2019) et 80% souffrent d'au moins un trouble d'anxiété (Simonoff et al., 2008). D'autres peuvent être atteints d'hyper ou d'hyposensibilité en réaction à différents stimuli externes (son, lumière, odeur ou douleur).

3. Epidémiologie et causes

La prévalence des TSA a constamment augmenté ces 20 dernières années, notamment aux Etats-Unis d'après le Center for Disease Control (CDC). L'incidence passe de 1 enfant atteint pour 150 en 2000 à 1 pour 54 en 2016 (Maenner et al., 2020). Une récente revue estime la prévalence à 1.5% dans les pays développés, soit une personne sur 66 (Lyall et al., 2017). En France, les TSA concerteraient 700 000

personnes et une naissance sur 150 (Haute Autorité de Santé). Les TSA touchent toutes les populations dans le monde, quelle que soit leur origine ou statut socioéconomique.

Il existe cependant une différence en fonction du sexe de l'individu. Les garçons sont quatre à cinq fois plus atteints que les filles (Christensen et al., 2016) bien que d'autres rapports plus récents relativisent cette différence qui serait de 3 pour 1 (Loomes et al., 2017). Cela pourrait s'expliquer par une validation historique des diagnostics sur les garçons, ce ratio pouvant encore évoluer aux vues des futurs progrès de détection. D'autres théories furent proposées pour expliquer ce ratio, comme l'implication des chromosomes sexuels et du rôle des hormones, sans que celles-ci soient confirmées (Baron-Cohen et al., 2011). De plus, les filles sembleraient avoir des symptômes plus sévères associés à plus de comorbidités psychiatriques et de déficience intellectuelle (Hartley and Sikora, 2009).

L'une des premières idées reçues, et depuis réfutée, sur les causes de l'autisme était d'un mauvais traitement, d'une mauvaise éducation de l'enfant par les parents, telle que les prétendues « mères réfrigérateurs ». Aujourd'hui, le consensus concernant les causes du TSA est qu'il provient de facteurs génétiques et environnementaux, bien que la génétique y joue un rôle majeur. En effet des études étudiant la prévalence du TSA chez des jumeaux homozygotes ont montré que si l'un des jumeaux est atteint de TSA l'autre a entre 36 et 95% de risques d'être atteint aussi (Sandin et al., 2017). Chez des jumeaux hétérozygotes ce risque tombe entre 0 et 30% (Hallmayer et al., 2011; Rosenberg et al., 2009). Les frères et sœurs d'enfant avec un TSA ont 2 à 8% de risques d'être eux aussi diagnostiqués, et ce risque monte à 12-20% si l'enfant concerné a des déficits dans l'un des trois domaines altérés dans l'autisme (Bolton et al., 1994).

Bien que la part de la génétique dans l'apparition du TSA est grande, sa diversité l'est tout autant, avec la participation d'allèles, patterns hérités et variations du nombre de copies (CNV) et polymorphisme à nucléotide simple (SNP).

Des symptômes typiques du TSA se retrouvent chez des personnes souffrant de maladies provoquées par des anomalies génétiques ou chromosomiques comme le syndrome de Down, de Rett et de l'X Fragile. Ce dernier, bien que le plus commun, ne représente cependant que 5% des personnes ayant un TSA.

Il a été mis en évidence ces dernières années le rôle significatif des mutations *de novo*, non héritables, dans le TSA, dont ils en seraient responsables dans 15 à 25% des cas (Ronemus et al., 2014). De façon intéressante, la fréquence des mutations *de novo* dans les lignées germinales d'origine paternelle augmente avec l'âge du père (Kong et al., 2012). Enfin, il est important de noter que la présence d'un historique psychiatrique, en particulier la schizophrénie, chez les parents est associé à une augmentation du risque de TSA chez l'enfant (Jokiranta et al., 2013).

4. Traitements

La prise en charge des patients ayant un TSA se divise en deux catégories de traitement, comportemental et pharmacologique. A ce jour, aucun réel traitement pharmacologique pour les TSA n'est disponible. La prise en charge médicamenteuse peut se faire au niveau des comorbidités dont les patients sont affectés, tels que l'anxiété, le TDAH ou l'épilepsie.

Deux antipsychotiques, aripiprazole et risperidone, sont les deux seuls médicaments approuvés par la FDA américaine (Food and Drug Administration) afin de soigner les problèmes d'irritabilité, d'hyperactivité et d'agressivité chez les enfants diagnostiqués TSA et souffrant de ces symptômes.

5. TSA vs DI

L'une des idées fausses sur l'autisme la plus répandue est qu'il est lié à une déficience intellectuelle. Or cette dernière ne rentre pas dans les critères de diagnostic du TSA et n'en a jamais fait partie. Cependant, la co-occurrence de TSA et de déficience intellectuelle est possible. 70% des patients ayant un TSA présentent aussi différents

niveaux de déficience intellectuelle et 10% des individus présentant une déficience intellectuelle auraient aussi un TSA (Newschaffer et al., 2007).

Le Syndrome de l'X Fragile (SXF) est la première cause génétique de TSA, bien que ne représentant de 5% des cas (Mendelsohn and Schaefer, 2008; Muhle et al., 2004). Dans le cas du SXF, tous les individus atteints ont une déficience intellectuelle, mais entre 15 et 60% auraient un TSA. Cet écart entre les différentes études d'épidémiologie s'explique par différentes méthodologies et diagnostics utilisés (Budimirovic and Kaufmann, 2011).

IV. Le Syndrome de l'X Fragile

1. Découverte du syndrome

La première description d'une déficience intellectuelle liée au chromosome X fut faite en 1943 par James Purdon Martin et Julia Bell en rapportant le cas d'une famille dans laquelle ils ont observé la présence de déficience intellectuelle et de démence chez 11 garçons sur 2 générations. Leurs travaux ont permis de comprendre que cette déficience était liée au sexe et était héritable (Martin and Bell, 1943). Ils nomment la maladie le syndrome de Martin-Bell. Du fait de l'absence de problème moteur et sensoriel mais avec la présence d'un déficit de la parole, ils émettent l'hypothèse que le dysfonctionnement cérébral se situe principalement dans le cortex préfrontal. Cependant, ils ne relèvent pas l'une des caractéristiques physiques la plus récurrente, le macroorchidisme, une taille anormale des testicules.

Lubs fut le premier à montrer une anomalie, un pincement, sur le bras long du chromosome X chez quatre hommes d'une même famille et leur mère (Lubs, 1969), ensuite appelé « site fragile » (Hecht and Kaiser-McCaw, 1979). Ce site fragile se présente comme une zone de fragilité de la chromatine, visible sur le chromosome lors d'un caryotype. Pour reproduire cette observation, Sutherland en 1977 démontre l'importance de la culture des cellules en milieu pauvre en folate (Sutherland, 1977). Peu de temps après, Turner lie une macroorchidie à un retard mental lié à l'X chez certains patients (Turner et al., 1980).

Une description plus complète de la maladie, maintenant appelée syndrome de l'X Fragile, fut faite par F. de la Cruz en 1985, notamment sur les caractéristiques physiques et comportementales (de la Cruz, 1985). La cause génique du SXF fut trouvée et séquencée en 1991 et sera nommée le gène *FMR1*, Fragile X Mental Retardation 1 (Oberlé et al., 1991; Verkerk et al., 1991; Vincent et al., 1991).

Deux autres maladies associées à ce gène furent caractérisées par la suite : le syndrome du tremblement-ataxie lié au X Fragile (FXTAS), une maladie neurodégénérative, et l'insuffisance ovarienne liée à la prémutation de l'X Fragile (FXPOI) (Cronister et al., 1991; Hagerman et al., 2001).

2. Cause, épidémiologie et hérédité

Le syndrome de l'X fragile est la première cause de retard mental héréditaire. Le SXF est causé par l'absence de la protéine Fragile X Mental Retardation Protein (FMRP), une protéine se liant à l'ARN ayant un rôle majeur dans la régulation de l'expression d'un grand nombre d'ARN messagers essentiels pour le bon développement et fonctionnement du cerveau particulièrement. Cette absence est due à l'inactivation du gène *FMR1*. En effet, le SXF est causé par l'expansion d'une répétition du triplet nucléotidique CGG dans le 5'-UTR (untranslated region), le promoteur de *FMR1*, dont la localisation en Xq27.3 fut découverte par Krawczun en 1985 (Krawczun et al., 1985). Cette expansion va amener à une méthylation excessive des cytosines de la région et l'inactivation du gène, et le nombre de répétitions définit différents états cliniques. Les individus manifestant le SXF ont la mutation complète et plus de 200 répétitions du triplets CGG, pouvant aller jusqu'à 1000 triplets ininterrompus (Fig.2).

Ceux ayant un nombre de répétitions compris entre 55 et 200 répétitions portent la prémutation et ont une production excessive de FMRP qui est liée au FXTAS et FXPOI. En effet les niveaux d'ARNm de *FMR1* sont 2 à 8 fois plus élevés chez les personnes portant la prémutation, engendrant une séquestration de protéines importantes pour le fonctionnement neuronal par la structure en tête d'épingle qui se forme dans les répétitions CGG (Hagerman and Hagerman, 2013).

A cela s'ajoute certains individus ayant le SXF avec un mosaïcisme de répétitions de CGG de longueurs différentes, avec des cellules présentant la mutation complète et d'autres la prémutation. Un mosaïcisme de méthylation existe aussi, avec des cellules

ayant l'allèle *FRM1* méthylé et d'autres non méthylé. Ces deux types de mosaïque entraînent la production partielle de FMRP, et les individus touchés peuvent présenter un tableau clinique moins sévère que les individus chez qui FMRP est totalement absente.

Enfin, un nombre croissant de patients ayant une mutation ponctuelle ou par délétion, ou encore un shift du cadre de lecture du gène *FMR1* a été reporté (Myrick et al., 2014; Quartier et al., 2017). Les individus ayant ces mutations pouvant amener à une perte de fonction ou l'absence de FMRP ne représentent cependant qu'une faible portion des personnes touchées par le SXF.

La prévalence de la mutation complète du SXF dans la population mondiale est estimée à 1 pour 4000 chez les hommes et 1 pour 7000 pour les femmes, bien qu'une importante méta-analyse remette en cause ces chiffres. En effet, après application d'un modèle statistique permettant de prendre en compte les caractéristiques des populations sur près de 50 études de prévalence, la méta analyse a déterminé une prévalence de 1 pour 7143 hommes et 1 pour 11,111 femmes (Hunter et al., 2014). De plus la prévalence semble varier dans les différentes régions du monde en raison de différences dans les haplotypes prédisposant de l'expansion des CGG en fonction des différences dans les populations et de l'effet fondateur. Ce dernier correspond à la perte de variation génétique lors de l'établissement d'une nouvelle population formée à partir d'un petit nombre d'individus. Par exemple, une très grande prévalence pour le SXF (1 pour 19 chez l'homme et 1 pour 46 chez la femme) a été rapporté à Ricaurte en Colombie (Saldarriaga et al., 2018).

La prévalence de la prémutation serait de 1 pour 855 chez l'homme et 1 pour 591 chez la femme (Hunter et al., 2014). Le FXTAS touche près de 40% des hommes et 16% des femmes ayant la prémutation après 50 ans, alors que le FXPOI apparaît chez 16 à 20% des femmes portant la prémutation (Hagerman and Hagerman, 2013).

L'hérédité du SXF ne suit pas la transmission classique de Mendel car il dépend du nombre de répétitions du triplets CGG dans le promoteur du gène *FMR1*. Le passage de la forme pré-mutée à la mutation complète se fait par l'expansion des répétitions pendant la transmission de la mère porteuse de la prémutation à son enfant. Le risque du passage de la forme pré-mutée à la mutation complète à la descendance dépend du nombre de répétitions dans l'allèle pré-muté, qui peut grimper à 100% à partir de 99 répétitions. Ce risque est aussi lié à l'âge de la mère et au nombre d'interruptions de triplets CGG.

Mais cette expansion ne se fait pas lors de la transmission du chromosome X du père, portant la prémutation, à ses filles ni à ses fils recevant le chromosomes Y. De plus, seulement 1% des hommes ayant la mutation complète et souffrant du SXF auraient une descendance, la majorité ne se reproduisant pas. Chez ces individus, leurs filles hériteront de la forme pré-mutée et ne présenteront pas de déficience. En effet, il y a une perte de la forme mutée lors de la formation des spermatozoïdes et seulement une forme pré-mutée passe (Hagerman and Hagerman, 2002).

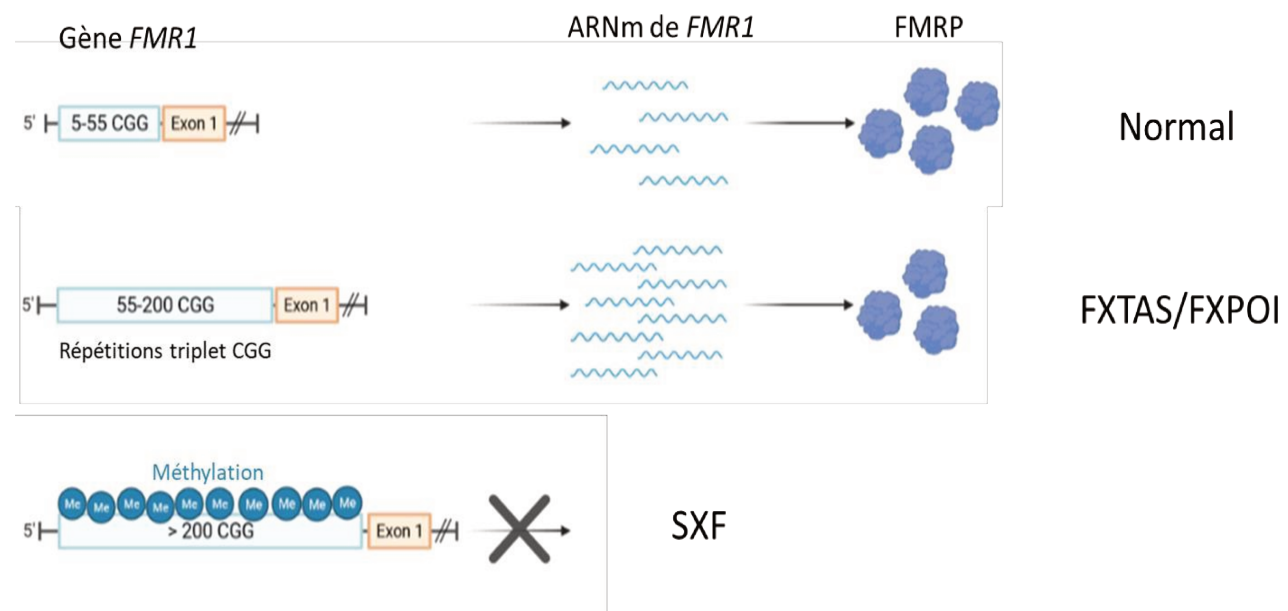


Figure 2. Conséquences de l'expansion de la répétition du triplet CGG. Un individu sain présente un nombre de répétitions de CGG compris entre 5 et 55. On parle de prémutation quand ce nombre varie entre 55 et 200, ce qui engendre l'augmentation de la transcription de l'ARNm de *FMR1* et une légère baisse de FMRP. Lors de la mutation complète, avec plus de 200 répétitions, l'hyperméthylation de la région promotrice provoque l'absence de FMRP et le SXF.

3. Tableau clinique

a. Caractéristiques physiques

Les nouveau-nés, plus tard diagnostiqués comme atteints du SXF, ne montrent pas de caractéristiques ou de symptômes décelables à la naissance. Associé à un historique familiale inexistant, cela rend le diagnostic néonatal impossible. À la naissance, le poids, la taille et la circonférence de la tête des enfants SXF se situent dans des valeurs normales (Lachiewicz et al., 2000). Bien que par la suite les courbes de croissance de taille et de poids semblent suivre une évolution normale, la circonférence du crâne est supérieure à la moyenne à l'âge prépubère et la majorité des enfants SXF développent une macrocéphalie.

Les caractéristiques physiques se précisent et deviennent plus visibles au cours de l'enfance. Plus de 80% des individus ont un ou plusieurs traits physiques qui comprend :

- Une dysmorphie faciale dans plus de 75% des cas, dont un visage allongé, des oreilles proéminentes et/ou une mâchoire prognathe (80% des hommes adultes atteints).
- Une macroorchidie, une taille anormale des testicules qui apparaît à la puberté, chez 95% des hommes adultes. Le volume testiculaire peut atteindre 50 mL, contre 20 à 30 mL chez des jeunes adultes sains. Ce volume s'explique par une augmentation des inclusions lysosomales dans les cellules de Sertoli et des anomalies dans la différenciation des spermatides (Johannisson et al., 1987), qui pourraient engendrer un dérèglement de la spermatogénèse, et donc d'une diminution de la fertilité (Hersh et al., 2011).
- Un tonus musculaire amoindrie, une hypotonie, particulièrement au niveau du visage.

- Une hyperlaxité ligamentaire (67% des patients) qui est une atteinte des tissus conjonctifs se traduisant par une souplesse articulaire particulière. Les mains sont caractérisées par des doigts aplatis et des plis palmaires profonds.
- Un affaissement de la voûte plantaire (« pied plat »).
- Des otites à répétition liées à des infections fréquentes
- Un strabisme dans de plus rares cas (8%)

Ces anomalies physiques peuvent être expliquées en partie par une hypotonie musculaire et dysplasie du tissu conjonctif (Opitz et al., 1984). Une manifestation possible de la dysplasie est un prolapsus de la valve mitrale, retrouvé essentiellement chez les patients adultes (Ramírez-Cheyne et al., 2019). Chez les femmes, le phénotype physique, s'il est présent en premier lieu, y est moins prononcé mais similaire aux hommes.

D'autres problèmes d'ordre médical ont été décrits chez les patients SXF comme des reflux gastro-œsophagiens, constipation, cycle éveil-sommeil ou encore l'épilepsie (Kidd et al., 2014). Bien que généralement bénigne dans le SXF, l'épilepsie touche 20% des patients (Musumeci et al., 1999) et apparaît entre 4 et 10 ans en disparaissant à la puberté le plus souvent (Sabaratnam et al., 2001). Il est intéressant de noter que la présence de l'épilepsie chez les patients SXF est significativement associée à l'autisme (Berry-Kravis et al., 2010).

Enfin, il a été montré assez tôt que les niveaux basals et stimulés d'AMPc dans les plaquettes sont réduits chez les patients atteints de SXF, ce qui constitue un marqueur biochimique important (Berry-Kravis and Huttenlocher, 1992) .

b. Les troubles cognitifs.

Le trouble clinique le plus important associé au SXF est le retard global du développement et la déficience intellectuelle. La sévérité de la déficience intellectuelle varie d'un patient à l'autre et aussi selon le sexe, la gravité de la DI étant moindre chez

les femmes atteintes du SXF (Hessl et al., 2009b; Schneider et al., 2009). Le quotient intellectuel (QI) moyen des individus masculins se situe entre 40 et 51, ce qui est considéré comme un retard mental modéré. Certains patients se retrouvent avec un score encore inférieur et présentent un retard mental profond alors que 18% des individus SXF ont un score supérieur à 70 et ont donc un retard considéré comme léger (Alanay et al., 2007). Le QI des patients est directement corrélé avec le niveau de production de FRMP, et de façon similaire les individus avec un mosaïcisme comme précédemment décrit ont un QI plus élevé (Schneider et al., 2013). Les principales difficultés des patients atteints sont de traiter les informations de façon ordonnée, d'établir des liens de cause à effet ou encore de résoudre des problèmes d'arithmétique (Schneider et al., 2009).

Enfin le retard psychomoteur se retrouve à l'âge moyen des patients SXF lors de la première marche (2.12 ans en moyenne) et des premiers mots (2.43 ans en moyenne) qui sont supérieurs à la moyenne (Alanay et al., 2007).

c. Les troubles comportementaux

Les troubles comportementaux chez les patients SXF sont typiquement plus marqués que les caractères physiques et sont considérés comme un critère important pour poser un diagnostic clinique. Ces principaux troubles sont : l'hyperactivité, qui se retrouve chez 80 à 90% des patients, un déficit de l'attention, l'impulsivité, l'évitement du regard, une altération des interactions et de la communication sociale, écholalie, hypersensibilité à des stimuli (son et/ou lumière), stéréotypies (battements des mains, ...). Ces troubles se retrouvent dans le TSA, dont 67% des garçons SXF et 23% des filles sont diagnostiqués (Bailey et al., 2008; Clifford et al., 2007). Il est décrit que le SXF est la cause monogénique la plus fréquente d'autisme, comptant pour 5% des patients atteints de TSA (Mendelsohn and Schaefer, 2008). La plupart de ces troubles résulte d'un haut niveau d'anxiété et d'une faible capacité d'adaptation à un environnement nouveau.

Certains de ces troubles diminuent au fil du temps après la puberté, comme l'agressivité et les crises de colères. Cependant le comportement peut se détériorer rapidement en étant exposé à l'alcool par exemple (Salcedo-Arellano et al., 2016).

Chez les filles ayant la mutation complète, les troubles comportementaux suivent ceux des garçons en étant moins prononcés (Dahlhaus, 2018).

d. Au niveau du cerveau

Les études structurelles du cerveau par imagerie par résonnance magnétique (IRM) ont montré des altérations volumétriques de certaines régions précises chez les patients atteints du SXF. L'anormalité la plus importante est l'élargissement du noyau caudé, qui est plus prononcé chez les patients que chez les patientes atteintes du SXF (Hallahan et al., 2011; Reiss et al., 1995). Cette anomalie se retrouve tôt dans le développement, dans les trois premières années, et persiste chez l'adulte (Sandoval et al., 2018). Des études d'IRM fonctionnelle montrent une activité réduite (Bruno et al., 2017), et un métabolisme de la choline et du glutamate réduit dans cette région chez des patients SXF par rapport à des sujets sains (Bruno et al., 2013). De façon intéressante, l'élargissement du noyau caudé est négativement corrélé au niveau de FMRP (Gothelf et al., 2008) et positivement corrélé à une aggravation des déficits cognitifs et comportementaux (Sandoval et al., 2018).

Une réduction du vermis du cervelet a aussi été identifiée de façon constante chez les patients (Gothelf et al., 2008; Mostofsky et al., 1998), apparaissant dès un an (Hoeft et al., 2010). De plus, une réduction du volume du cervelet a aussi été observée chez de jeunes patients, corrélée à la présence de TSA (Hoeft et al., 2008), alors que le volume de cette région est positivement corrélé au QI.

De nombreuses altérations modérées du volume sont aussi retrouvées spécifiquement dans certaines régions de la substance grise du lobe cortical, comme une réduction dans les lobes temporal et frontal, ainsi qu'une augmentation du volume dans les lobes pariétal et occipital (Gothelf et al., 2008). Enfin, l'hippocampe serait plus

volumineux chez les patients jeunes (Hoeft et al., 2008), mais cette anomalie ne serait plus retrouvée chez les patients plus âgés.

Des études fonctionnelles ont pu mettre en évidence différents patterns d'activation dans ces régions du cerveau. Par exemple, lors d'une tâche de mémoire de travail, les patients ont une activité neuronale diminuée dans le cortex frontal (Kwon et al., 2001).

Au niveau cellulaire, il a été mis en évidence dans le cerveau de patients atteints du SXF des anomalies morphologiques des contacts synaptiques, les épines dendritiques.

Les premières analyses morphologiques post-mortem du cortex ont montré une augmentation du nombre d'épines dendritiques par rapport à des individus sains (Hinton et al., 1991; Irwin et al., 2001a; Rudelli et al., 1985), une morphologie altérée avec des épines plus longues, fines et immatures (Rudelli et al., 1985), comme les filopodes présents pendant la période post-natale. Ces anomalies signifieraient que les phénomènes de pruning, élimination des épines surnuméraires, et de maturation sont altérés dans le SXF (Fig.3).

Ces anomalies morphologiques et numériques pourraient expliquer et être à l'origine des déficits retrouvés chez les patients, en altérant le fonctionnement de la transmission synaptique. De façon intéressante, des anomalies morphologiques des épines dendritiques ont aussi été observées chez des patients atteints d'autres formes de déficience intellectuelle comme le syndrome de Down (Ferrer and Gullotta, 1990) et de Rett (Armstrong et al., 1995; Kaufmann and Moser, 2000).

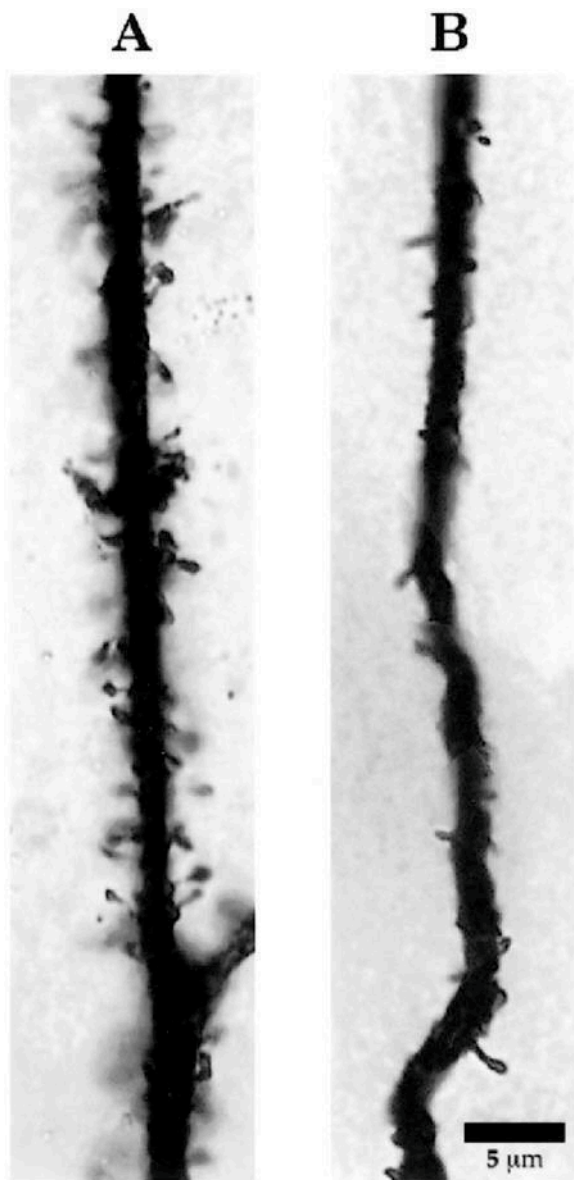


Figure 3. Les épines dendritiques des patients SXF sont plus longues, fines et denses. Golgi staining de neurones montrant la morphologie des épines dendritiques chez une personne atteinte de SXF (A) et chez une personne saine (B). (Irwin et al., 2001b)

4. Le FXTAS

Le FXTAS est une maladie neurodégénérative progressive dépendant de l'âge qui est caractérisée par des tremblements, apparaissant en moyenne deux ans avant une ataxie cérébelleuse, un trouble de la coordination des mouvements (Leehey et al., 2007). D'autres troubles y sont associés comme une déficience cognitive, de l'anxiété ou des troubles parkinsoniens (Hagerman et al., 2001). Ces troubles apparaîtront chez les hommes de plus de 50 ans ayant la prémutation, 17% seront atteint à cet âge et

75% à l'âge de 80 ans (Jacquemont et al., 2004). Une atrophie cérébrale a été décrite dans le cervelet, le thalamus et le striatum (Jacquemont et al., 2003) et le nombre de répétitions du triplet CGG est corrélé à la sévérité de l'atrophie. Le niveau d'ARNm de *FMR1* est augmenté d'un facteur 2 à 8, alors que le niveau de FMRP est normal ou légèrement diminué chez les patients ainsi que chez le modèle murin CCG-KI (Berman et al., 2014; Hagerman, 2013; Schneider et al., 2020; Tassone et al., 2000).

Une autre des caractéristiques neuropathologiques du FXTAS est la présence d'inclusions eosinophiles intranucléaires dans le système nerveux central et périphérique, historiquement identifiées pour la première fois dans des neurones et astrocytes en 2002 (Greco et al., 2002; Jacquemont et al., 2003). Ces inclusions sont particulièrement présentes dans l'hippocampe et le cortex frontal et temporal. Leur constitution est très hétérogène et se compose d'ubiquitine, heat-shock protéines, protéines se liant à l'ARN et réparant l'ADN et plus de 200 autres protéines (Iwahashi et al., 2006; Ma et al., 2019). L'ARNm de *FMR1* fait partie de ces inclusions (Hagerman, 2013). De plus, la traduction de la répétition CGG de la prémutation en protéine riche en polyglycine, FMRpolyG, serait liée aux inclusions nucléaires quand elle est surexprimée (Sellier et al., 2017). Toutefois des études récentes ont émis des doutes sur le réel niveau d'expression du peptide endogène dans les tissus des patients FXTAS (Ma et al., 2019).

5. Modèles animaux

a. Modèle murin *Fmr1* KO

La souris est un modèle animal qui présente de nombreux avantages expliquant sa large utilisation dans le milieu de la recherche. La souris possède près de 99% de ses gènes en commun avec l'Homme (Chinwalla et al., 2002).

Le gène *FMR1* est très conservé parmi les espèces. Chez la souris le gène *Fmr1* est localisé sur le chromosome X comme chez l'humain. Les protéines FMRP de l'humain et de la souris partagent une homologie de séquence de 97% (Claude T.

Ashley et al., 1993), et l'expression et la localisation de FMRP chez la souris dans les différents tissus est similaire à celles chez l'humain (Bakker et al., 2000). Ceci fait du modèle murin un excellent outil dans l'étude du SXF.

Le premier modèle murin du SXF fut produit par le Dutch-Belgian Fragile X Consortium ("Fmr1 knockout mice," 1994). Une copie mutée du gène *Fmr1* contenant la séquence du gène de la néomycine dans l'exon 5 fut insérée par recombinaison homologue dans des cellules souches embryonnaires à la place de la copie d'origine. Ces cellules recombinées furent injectées dans des blastocytes et transférées dans l'utérus de femelles pseudo-gestantes. Des mâles chimères provenant de ces embryons ont été accouplés à des femelles sauvages pour produire des femelles hétérozygotes pour la mutation, et ces dernières, croisées avec des mâles sauvages permettent d'avoir des mâles *Fmr1* KO. On constate une absence totale de la protéine FMRP chez ces animaux, bien qu'une faible quantité d'ARNm de *Fmr1* soit détectable (Yan et al., 2004).

Pour pallier ce problème, un deuxième modèle a été généré en 2006 par l'insertion de sites loxP (locus of crossing over) entre le promoteur et l'exon 1 du gène *Fmr1*. Après croisement avec des souris exprimant la Cre recombinase, la transcription du gène *Fmr1* est totalement supprimée (Mientjes et al., 2006).

Ces deux modèles ne reproduisent pas l'expansion des triplets nucléotidiques CGG que l'on trouve chez l'humain. Cependant lors de l'insertion d'environ 230 répétitions de CGG dans la région 5' UTR du gène *Fmr1* dans un modèle de souris Knock In (KI), la méthylation du promoteur et l'inhibition induite de la transcription n'est pas retrouvées (Brouwer et al., 2007). De plus, FMRP n'est jamais exprimée chez les souris alors que la protéine semble être exprimée jusqu'à la dixième semaine de gestation chez l'embryon humain ayant la mutation complète avant d'être indétectable par la suite (Willemse et al., 2002).

Les souris KO ont un taux de fécondité et une espérance de vie similaires à celles des souris sauvages. Aucune différence au niveau de la morphologie globale et des organes vitaux n'a été décrite. Cependant, on retrouve dans ce modèle un macroorchidisme identique à celui présent chez l'humain.

Aucune anomalie au niveau de l'anatomie du cerveau n'a été observée sur les souris KO de première génération grâce à des études par IRM ("Fmr1 knockout mice," 1994, p. 1; Kooy et al., 1999). Le volume total du cerveau des *Fmr1*-KO est comparable à celui des sauvages. Des différences volumétriques ont été plus récemment observées chez des souris *Fmr1* KO provenant d'une souche différente FVB (Lai et al., 2016).

La morphologie des épines dendritiques chez ce modèle est aussi altérée. En effet, il a été retrouvé des anomalies semblables à celles des patients dans le cortex occipital et somato-sensoriel et l'hippocampe des souris *Fmr1* KO (Comery et al., 1997; Galvez and Greenough, 2005; Grossman et al., 2006; McKinney et al., 2005; Nimchinsky et al., 2001), avec un nombre plus important d'épines dendritiques plus longues et fines, et donc immatures. Des analyses dans la couche V du cortex somato-sensoriel de jeunes souris *Fmr1* KO d'un mois montrent une augmentation de la densité et de la longueur des épines par rapport aux souris sauvages, mais cette différence n'est plus retrouvée à quatre semaines (Galvez and Greenough, 2005; Nimchinsky et al., 2001). Cependant cette normalisation à quatre semaines ne semble pas se maintenir, puisqu'une augmentation de la densité des épines immatures chez la souris adulte *Fmr1* KO est retrouvée dans cette même étude. De façon intéressante, des anomalies sont retrouvées dans d'autres régions du cerveau à des âges plus avancés, comme une plus grande densité d'épines plus longues dans le cortex visuel chez des souris *Fmr1* KO de 16 semaines, plus précisément sur les cellules pyramidales de la couche V marquées par Golgi-Staining (Comery et al., 1997).

La potentialisation et la dépression à long terme, respectivement LTP et LTD, représentent une augmentation et une diminution sur le long terme du signal entre

deux synapses. Ces deux phénomènes sont considérés comme expliquant électrophysiologiquement les processus de mémorisation et de mémoire. Leurs analyses ont montré chez le modèle du SXF :

- Une augmentation de la LTD dépendant du récepteur métabotropique au glutamate (mGluR) dans l'hippocampe (Huber et al., 2002).
- Une réduction de la LTP dans le cortex (Li et al., 2002), associée à une diminution de la sous unité GluR1 du récepteur AMPA.

De nombreuses études ont montré que le comportement social des souris *Fmr1* KO était abnormal. Concernant les interactions sociales, ces souris ne montrent pas de préférence entre un nouveau congénère inconnu et un objet, et engagent moins d'interactions d'affiliation (reniflement, poursuite, grooming) avec une autre souris du même âge et même sexe (Dahlhaus and El-Husseini, 2010; Maurin et al., 2019a; McNaughton et al., 2008) ou du sexe opposé (Pietropaolo et al., 2011). Les souriceaux *Fmr1* KO de 13 jours présentent aussi un déficit de la discrimination sociale dans le test du Homing dans lequel ils sont placés dans une cage contenant 1/3 de litière provenant du nid de la mère, et 2/3 de litière propre et doivent retrouver la litière contenant l'odeur de la mère depuis la partie propre (Maurin et al., 2019a).

Les enfants atteints du SXF ayant un retard du langage, et les vocalisations ultrasoniques (USVs) des rongeurs étant considérées comme relevant dans l'étude des déficits du langage (Fischer and Hammerschmidt, 2011), il est intéressant de s'attarder sur la communication sociale des souris *Fmr1* KO. Ces USVs sont émis lors de l'isolement d'un jeune souriceau de sa mère ou lors de la présentation à un mâle adulte d'une femelle ou de son urine. Les études sur les souris *Fmr1* KO mettent en évidence des anomalies du nombre d'USVs émis, parfois plus de vocalisations (Spencer et al., 2011), parfois moins (Gholizadeh et al., 2014), et certaines études ne montrent aucune différence (Hodges et al., 2017; Pietropaolo et al., 2011). Cette inconsistance dans les résultats pourrait s'expliquer par des différences de protocole et d'âge des souris

étudiées (Reynolds et al., 2016). Une analyse plus profonde au niveau de la fréquence et des types de vocalisations montre une différence marquée entre souris sauvages et *Fmr1* KO, ces dernières faisant des appels à plus haute fréquence et à plus de syllabes par exemple (Belagodu et al., 2016; Hodges et al., 2017).

Un comportement anormal souvent rapporté et constant chez les *Fmr1* KO est une augmentation de leur locomotion dans le test de l'open field (Dahlhaus and ElHusseini, 2010; Pietropaolo et al., 2011; Spencer et al., 2005; Yuskaitis et al., 2010a), cohérente avec l'hyperactivité retrouvé chez les patients atteints du SXF. Le temps passé au centre de l'open field est par ailleurs considéré comme un indicateur d'anxiété et les souris *Fmr1* KO y passent plus de temps que les sauvages (Spencer et al., 2005), montrant une diminution potentielle de l'anxiété environnementale des souris mutantes. D'autres tests d'anxiété vont dans ce sens, comme le zero maze et le elevated plus maze, dans lesquels les souris *Fmr1* KO passent plus de temps dans les quadrants/bras ouverts que les sauvages (Liu and Smith, 2009; Yuskaitis et al., 2010a). Ces résultats nous amènent à penser qu'une anxiété environnementale amoindrie coexiste avec une anxiété sociale augmentée chez le *Fmr1* KO, comme le montrent les anomalies d'interactions sociales précédemment décrites, ainsi que l'augmentation des réponses d'anxiété chez le *Fmr1* KO en face de son reflet dans un miroir (Spencer et al., 2005).

Les souris *Fmr1* KO présentent de plus des comportements stéréotypés similaires à ceux que l'on en retrouve chez les patients. Elles passent plus de temps à se lécher que leurs congénères sauvages ("Evidence for social anxiety and impaired social cognition in a mouse model of fragile X syndrome. - PsycNET," n.d.; Pietropaolo et al., 2011), et enterrent plus de billes lors du test du Marble Burying (Scharkowski et al., 2018; Spencer et al., 2011).

Des anomalies de réponses à des stimulus ont aussi été notées chez les *Fmr1* KO, notamment sur le Prepulse inhibition (PPI) et le sursaut suivant le stimulus. Le PPI

est une mesure de la réponse sensorimotrice qui intervient quand un faible préstimulus diminue la réponse à un stimulus plus fort (pulse) dans les 100 milliseconds. Des déficits de PPI ont été enregistrés chez des patients atteints du SXF (Hessl et al., 2009a). A l'inverse des patients, les souris mutantes ont une augmentation du PPI et un sursaut réduit (Pietropaolo et al., 2011; Spencer et al., 2011).

Concernant les capacités cognitives des souris mutantes, le Dutch-Belgian Fragile X Consortium a historiquement caractérisé la mémoire spatiale du premier modèle *Fmr1* KO grâce au test de la piscine de Morris ou Morris Water Maze (MWM) ("Fmr1 knockout mice," 1994). Le MWM est un test dépendant de l'hippocampe, qui permet d'évaluer la capacité de mémorisation spatiale des souris à localiser une plateforme submergée sous une eau opaque en utilisant des repères visuels (Morris, 1984). Dans l'étude du Consortium, les souris X Fragile mettent significativement plus de temps à apprendre l'emplacement de la plateforme lors du premier jour de l'apprentissage, mais ne présentent pas de différence par rapport aux souris sauvages lors du test final, lorsque la plateforme est retirée et le temps que passe le sujet dans le quadrant contenant auparavant la plateforme est comptabilisé. De façon intéressante, les souris *Fmr1* KO ont un déficit d'apprentissage plus important lors du « reversal », lorsque la plateforme est changée de place après la première série de test. Ceci pourrait indiquer que les souris mutantes ont des difficultés à réagir à un changement d'environnement. Ces résultats sur le « reversal » ont pu être répétés sur des fonds génétiques différents sans pour autant voir une différence lors du test de la première position de la plateforme ("Mildly impaired water maze performance in maleFmr1 knockout mice," 1997; Nolan and Lugo, 2018).

Le test de reconnaissance d'un nouvel objet ou Novel Object Recognition (NOR) est un autre test fréquemment utilisé afin de tester la mémoire des souris mutantes. Il permet de caractériser la mémoire à court et long terme en fonction du temps laissé entre la phase d'apprentissage et la phase de test. Bien que nombreuses variantes existent, le NOR consiste principalement à présenter deux objets identiques lors de la

phase d'apprentissage et de remplacer un des deux objets par un différent lors du test. Les souris ayant tendance à naturellement être attirées par la nouveauté, elles se focaliseront plutôt sur le nouvel objet. Les souris *Fmr1* KO ont des difficultés à différencier les deux objets lors du test : avec 3 minutes (Ventura et al., 2004), 24h d'intervalle chez la souche FVB (Gomis-González et al., 2016; Seese et al., 2020), avec 3 minutes (Felgerolle et al., 2019), 24 h d'intervalle (Costa et al., 2018), chez la souche C57BL/6J.

4.2. Modèle murin du FXTAS.

Un modèle de knock-in (CGG KI) fut développé en remplaçant la répétition triplet nucléotidique endogène CGG8 par la répétition CGG98 humain, reproduisant ainsi la prémutation associée au FXTAS (Bontekoe et al., 1997; Brouwer et al., 2008). De façon similaire aux patients atteints de FXTAS, ces souris présentent des inclusions nucléaires dans le cerveau (Brouwer et al., 2008). De plus, il a été montré que ces souris CGG KI ont des déficits cognitifs lors du test du MWM à 52 semaines et des déficits moteurs au test du rotarod à 70 semaines (Van Dam et al., 2005), et des déficits progressifs de la perception spatiale (Hunsaker et al., 2009). Enfin, les neurones en culture issus d'hippocampes de CGG KI ont des dendrites plus courts et une arborisation dendritique réduite (Chen et al., 2010)

Plus récemment, un modèle murin inductible présentant les inclusions nucléaires spécifiques au FXTAS dès quatre semaines ne montre pas de déficits comportementaux spécifiques (Haify et al., 2020).

4.3. *Rattus norvegicus*.

Plus récemment par rapport à la souris, deux modèles de rats *Fmr1* KO ont été créés par la technique de zinger-finger nucléase (ZNF) en 2009 (Geurts et al., 2009) et de CRISPR-Cas9 en 2017 (Tian et al., 2017). L'avantage de l'utilisation des rats par rapport aux souris est leur cerveau plus gros, la facilité à les entraîner à des tâches plus complexes, et leur distance évolutive avec l'humain plus réduite. On retrouve chez ce

modèle de rat une macroorchidie, une mGluR-LTD exagérée dans l'hippocampe (Tian et al., 2017), une densité d'épines dendritiques élevée (Till et al., 2015) ainsi que des déficits dans des tests du comportement social (Hamilton et al., 2014; Tian et al., 2017). Cependant ce modèle ne présente pas de déficits de vocalisations ou dans l'activité locomotrice, ni dans la mémoire spatiale dans le test du MWM (Hamilton et al., 2014; Till et al., 2015), bien que le modèle de 2017 montre bien des déficits dans le MWM (Tian et al., 2017). Les rats *Fmr1* KO montrent aussi des difficultés dans la reconnaissance d'objet dans une étude plus récente (Asiminas et al., 2019).

4.4. *Drosophila melanogaster*.

Drosophila melanogaster possède un seul gène orthologue FMR1 conservé, nommé *dFMR1*, et la protéine produite dFMRP similaire à 56% à la protéine humaine FMRP, notamment au niveau des domaines fonctionnels (domaines KH et RGG box : voir partie V.2.a) (Wan et al 2000). Le premier mutant *dFMR1* fut produit peu de temps après son clonage (Zhang et al., 2001) et est viable et fertile. Cependant, la viabilité des mutants est étroitement liée et sensible au fond génétique, si bien que certains peuvent être léthaux (Morales et al., 2002). Chez ces mutants, des altérations du comportement reliés au SXF ont été caractérisés, comme des déficits de l'interaction sociale (Bolduc et al., 2010), de la mémoire olfactive (Monyak et al., 2017) mais aussi des altérations de comportement propres à la drosophile comme la parade nuptiale (Gross et al., 2015).

4.5. *Danio rerio*.

Le poisson zèbre est un petit poisson d'Asie du Sud de la famille des Cyprinidés couramment utilisé en laboratoire depuis 1981 pour de nombreuses raisons (Streisinger et al., 1981) : son homologie génomique avec l'humain, sa fertilisation externe, sa transparence embryonnaire et son faible coût logistique. Le premier modèle *Fmr1* KO a été créé en 2009 par la technique de TILLING (Targeting Induced Local Lesions in Genomes) en induisant des lésions à des endroits précis du génome

(den Broeder et al., 2009). Ces animaux présentent une hyperactivité et une augmentation de l'anxiété face à un nouvel environnement (Ng et al., 2013), ainsi qu'une plus grande fréquence de temps passé en banc (*shoaling*) (Wu et al., 2017).

6. Traitements.

A ce jour, aucun traitement spécifique pour le SXF n'est disponible, et la prise en charge clinique se focalise sur le traitement symptomatique des comorbidités et des problèmes psychiatriques. La Sertraline, un inhibiteur spécifique de la recapture de la sérotonine, est par exemple couramment utilisé pour traiter l'anxiété chez les patients SXF.

De nombreux essais cliniques constituant de grands espoirs ont à chaque fois échoués, notamment sur les antagonistes des récepteurs glutamatergiques métabotropiques, mGluR, comme le mavoglurant. En effet, parmi toutes les cibles caractérisées pour traiter le SXF, la voie glutamatergique a été l'une des premières à être testée. La signalisation des mGluR est exagérée en absence de FMRP, ce qui cause une hyperexcitabilité des neurones (Bear et al., 2004). La réduction génétique ou l'inhibition pharmacologique de ces récepteurs a montré un effet positif sur plusieurs phénotypes comportementaux de la souris *Fmr1* KO (Thomas et al., 2012, 2011; Veloz et al., 2012). Les essais cliniques sur les différents antagonistes des mGluR n'ont malheureusement pas conclu à un effet bénéfique chez l'Homme.

Une autre voie de signalisation, la voie inhibitrice GABA, a été également intensément étudiée dans le SXF, dont une altération de l'expression de récepteurs GABA et une diminution de la production de GABA a été observé dans le cadre de la maladie (Adusei et al., 2010). De même que pour la voie mGluR, l'activation de la voie GABAergique a corrigé un certain nombre de phénotypes altérés dans des études précliniques chez la souris et la drosophile, mais leur efficacité chez l'Homme n'a pour l'heure pas été montrée lors des essais cliniques (Braat and Kooy, 2015).

Très récemment, un essai clinique sur l'efficacité d'un inhibiteur de la phosphodiestérase 4D, BPN14770, chez des patients adultes atteints de SXF a montré une amélioration des performances dans l'expression orale, la lecture et dans la vie quotidienne (Berry-Kravis et al., 2021).

Ces essais cliniques ont par ailleurs montré que la réponse au placebo est très importante et que cela démontrait l'absence de mesures quantitatives efficace pour apprécier l'effet réel du traitement sur les différents comportements et capacités des patients. De plus, le début d'essais cliniques sur de jeunes enfants montre l'effort donné à constater l'effet des traitements sur le développement précoce du cerveau qui est altéré.

V. La protéine FMRP et ses ARNm cibles.

1. Le gène *FMR1*.

Le gène *FMR1* fait 38 kilobase (kb) de long et est constitué de 17 exons au niveau de la région Xq27.3 (Eichler et al., 1993). Son transcrit majeur mesure 3.9 kb dont 0.2 correspond au 5'UTR, 1.9 kb à la séquence codante et 1.8 kb au 3'UTR. Les autres transcrits sont produits à partir de différents épissages alternatifs affectant les exons 12, 14, 15 et 17 (Claude T. Ashley et al., 1993; Verkerk et al., 1993). Au niveau du 5'UTR, il a été identifié plusieurs sites de fixations de facteurs transcriptionnels, comme NRF1 et USF1 et 2 (Kumari and Usdin, 2001), qui affecteraient le profil d'expression spatio-temporelle du gène *FMR1* au cours du développement.

Le profil d'expression du gène *FMR1* a été particulièrement étudié au cours du développement embryonnaire par hybridation *in situ* et immunohistochimie sur tissus humains et murins. Chez l'humain et la souris, le gène *FMR1* est exprimé dans l'ensemble des tissus fœtaux et son expression reste élevée dans le cerveau, les ovaires et les testicules à l'âge adulte (Devys et al., 1993; Hinds et al., 1993; Tamanini et al., 1997).

Plus précisément, on a pu observer une forte expression de *FMR1* dans le système nerveux sur des fœtus humain âgés de 8-9 semaines (Abitbol et al., 1993)). A 20 semaines, l'expression est également élevée dans les testicules (Tamanini et al., 1997) et dans le cerveau, particulièrement dans l'hippocampe, à 18-25 semaines (Abitbol et al., 1993).

Bakker et al. ont montré que bien que *FMR1* ne soit pas exprimé durant les deux premiers jours d'embryogenèse, les niveaux d'expression dans tous les tissus augmentent jusqu'au 14eme jour, particulièrement dans ceux d'origine ectodermique qui donneront par exemple le cerveau (Bakker et al., 2000). Par la suite, le pic d'expression de FMRP est atteint treize jours après la naissance, proche du pic de

synaptogénèse (Semple et al., 2013), particulièrement dans le cerveau et les testicules (Bonaccorso et al., 2015).

2. La protéine FMRP

a. Structure de la protéine.

FMRP est une protéine de taille attendue moyenne de 71 kDa d'une séquence de 632 acides aminés (aa). Elle fait partie d'une famille de protéines qui comprend ses deux paralogues FXR1P et FXR2P. Elle est connue pour interagir avec différents partenaires protéiques et des ARNs grâce à plusieurs domaines qui ont été caractérisés dans ses régions N-terminale, C-terminale et centrale (Fig.4).

On retrouve deux domaines d'interaction protéique Tudor (TD) en tandem, appelés Agenet ou Tud1/Tud2 (Ramos et al., 2006)..

Il existe deux domaines KH (K Homology), KH1 et KH2, d'environ 70 aa qui ont pour fonction de reconnaître l'ARN (Valverde et al., 2008, 2007). KH2 semble aussi important pour l'association de FRMP avec les polyribosomes (Darnell et al., 2005). Une RGG box, séquence de 20 à 25 aa riche en glycine et arginine, lie aussi l'ARN (C. T. Ashley et al., 1993). Un troisième domaine d'interaction à l'ARN KH0, a été découvert après les deux précédents, mais qui est aussi un domaine d'interaction protéique (Myrick et al., 2015).

Une séquence d'export nucléaire (NES, nuclear export signal) se trouve dans la région centrale, ainsi qu'une séquence de localisation nucléaire (NLS, nuclear localisation signal) présent dans la région N-terminale du domaine KH0, qui adresse la protéine FMRP au noyau.

FMRP subit des modifications post-traductionnelles par phosphorylation sur différents sites, le plus souvent sur ser499 chez la souris (Ceman et al., 2003). Cette phosphorylation est déclenchée par la voie mGluR qui contrôle la dégradation de FMRP

à la synapse (Nalavadi et al., 2012; Narayanan et al., 2007a). La forme phosphorylée semble être prédominante au niveau des dendrites (Narayanan et al., 2007b).

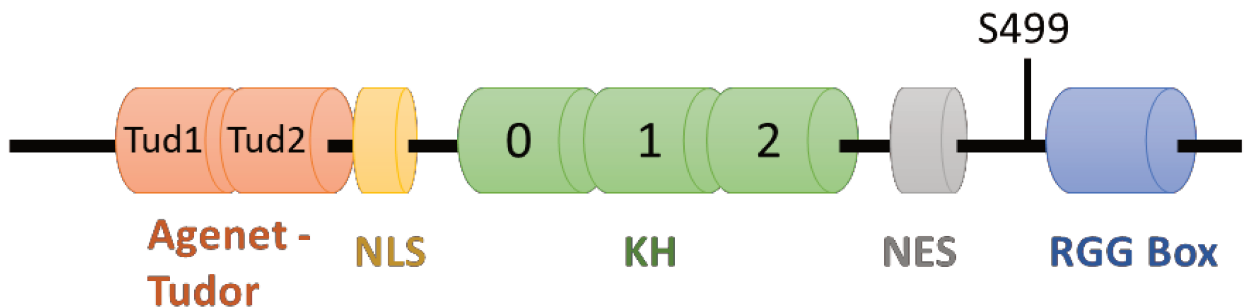


Figure 4. Représentation schématique de la protéine FMRP. NLS : Signal de localisation nucléaire, KH : domaine d'homologie avec hnRNP K, NES : signal d'export nucléaire, RGG : domaine riche en arginine-glycine-glycine, S499, sérine principalement phosphorylée.

b. Une protéine aux fonctions multiples

A) Une navette entre noyau et cytoplasme

Bien que FMRP se retrouve majoritairement dans le cytoplasme, détecté en immunofluorescence (Devys et al., 1993), elle peut être aussi détectée dans le noyau (Feng et al., 1997). FMRP contenant les deux séquences NLS et NES, l'hypothèse est que la protéine ait un rôle de navette entre le noyau et le cytoplasme, recrutant de façon précoce ses ARNs cibles et participant à leur export vers le cytoplasme. De façon intéressante, FMRP a été retrouvé près des pores nucléaires en microscopie électronique (Feng et al., 1997). Dans ce sens, quelques interacteurs nucléaires de FMRP ont été identifiés comme NUFIP1 (NUclear FMRP Interacting Protein) (Bardoni et al., 1999), une protéine liant l'ARN localisée aussi dans les synapses (Bardoni et al., 2003). Chez la Drosophile, Nufip et Tral (Trailer Hitch) ont été identifiées comme composants du complexe protéique contenant aussi Zfrp8. Cette protéine est nécessaire dans le noyau et contrôle la localisation de FMRP dans le cytoplasme. En effet, Zfrp8 et FMRP contrôlent tous deux l'état de condensation de l'hétérochromatine (Tan et al., 2016).

B) Régulation de la traduction

La première observation faite d'une régulation de la traduction par FMRP se retrouve dans la quantité de protéines chez la souris *Fmr1* KO ou chez les patients (Jacquemont et al., 2018). La synthèse protéique basale dans des tranches d'hippocampe de souris *Fmr1* KO est plus élevée par rapport au WT (Osterweil et al., 2010), ce qui suggère que FMRP est tout d'abord un répresseur de la traduction.

La présence de FMRP dans les polyribosomes dans plusieurs lignées cellulaires et dans le cerveau a été observée par sémination après centrifugation sur gradient de sucre et par immunofluorescence montrant une co-localisation (Khandjian et al., 1996).

FMRP semble bloquer les ribosomes lors de la phase d'elongation de la synthèse des protéines. En effet, FMRP co-sédimente dans les gradients de sucre avec les polyribosomes bloqués sur l'ARNm après traitement à la puromycine (Stefani et al., 2004), qui relargue les ribosomes en cours de traduction mais pas ceux bloqués en elongation, ou à l'homoharringtonine (Shah et al., 2020), qui bloque les ribosomes sur le codon start (AUG) mais permet aussi aux autres de continuer l'elongation. Différentes hypothèses expliquent comment FMRP ralentit et/ou bloque la translocation des ribosomes ; en tant que barrage physique (Darnell et al., 2011) ou en bloquant l'association des tRNA avec le ribosome (Chen et al., 2014).

Bien que FMRP soit historiquement reconnue comme un répresseur de la traduction, elle peut aussi moduler positivement la traduction de certains transcrits par la présence de motifs spécifiques sur l'ARN (Bechara et al., 2009; Tabet et al., 2016).

C) Liaison à des motifs spécifiques de l'ARN

G-quadruplex : Le G-quadruplex est une structure particulière de l'ARN riche en guanines. Il est défini par la liaison deux à deux de quatre guanines dans un appariement de type Hoogsteen qui va donner un G-quartet. Le G-quadruplex est un empilement d'au moins deux G-quartets. Le domaine RGG box de FMRP reconnaît et

se lie à cette structure 3D (Maurin et al., 2018; Melko and Bardoni, 2010). De plus, on retrouve le G-quadruplex dans plusieurs ARNs cibles de FMRP, comme *MAP1B* (Microtubule Association Protein 1B), *PP2Ac* (Protein Phosphatase 2A catalytic subunit), *APP* ou *CamKIIa* (Darnell et al., 2001; Melko and Bardoni, 2010; Westmark and Malter, 2007). De façon intéressante, des études avaient montré que FMRP se fixe avec une forte affinité à son ARNm *Fmr1* (Ceman et al., 1999), et le site sur lequel la protéine se fixe est une structure G-quadruplex (Schaeffer et al., 2001).

SosLIP : Il a été montré que FMRP se lie à l'ARNm Sod1 (Superoxyde dismutase 1) et module positivement son expression par une structure secondaire appelé SoSLIP (Sod1 mRNA Stem Loops Interacting with FMRP) (Bechara et al., 2009). Ce motif composé de trois structures stem-loop indépendantes est reconnu par le domaine RGG box de FMRP.

Séquences/motifs spécifiques : Ascano et al. ont identifiés ces deux nouveaux sites de fixation ,ACUK/WGCA , dans des ARNm cibles de FMRP dans des cellules HEK293 surexprimant FMRP. Ces deux motifs sont principalement localisés entre la séquence codante et le 3'UTR des ARNm cibles (Ascano et al., 2012). De façon intéressante, l'ARNm Sod1 contient aussi 29 motifs ACUK/WGCA répétés. Plus récemment, les motifs GWRA, TAY et particulièrement CTGKA ont aussi été montré comme étant des séquences spécifiquement reconnues par FMRP (Maurin et al., 2018).

3. Identification des ARNm cibles de FMRP

L'identification des ARNm ciblés par FMRP est une branche importante de la recherche actuelle et passée sur le SXF. L'utilisation des techniques de CrossLinking ImmunoPrecipitation (CLIP) et de ribosome profiling a permis l'établissement par plusieurs équipes de recherche d'une liste d'ARNm cibles importantes. Concernant le CLIP, en liant de façon covalente FMRP à l'ARN par UV, la précipitation de FMRP par anticorps spécifique permet de récolter les ARNs ciblés par la protéine. L'analyse par séquençage à haut débit permet d'identifier par la suite ces ARNs associés. C'est ce qui a été fait dans mon laboratoire d'accueil, en listant plus de 4000 cibles ARN (Maurin et al., 2018). Maurin et al. ont réalisé un HITS-CLIP (high-throughput sequencing of RNA isolated by CLIP) dans le cortex, l'hippocampe et le cervelet de souris à P13, au pic d'expression de FMRP. Ils ont identifié 1610 nouvelles cibles potentielles dont 57 précédemment liées à l'autisme (SFARI), qui sont impliquées notamment dans les voies de signalisation du calcium et de l'AMPc/GMPc. Parmi ces cibles, l'un des ARN les plus enrichis dans ce CLIP est l'ARNm codant pour la Phosphodiesterase 2A (PDE2A), qui est surexprimée dans les synapses des neurones des souris *Fmr1* KO (Maurin et al., 2018) (Fig.5).

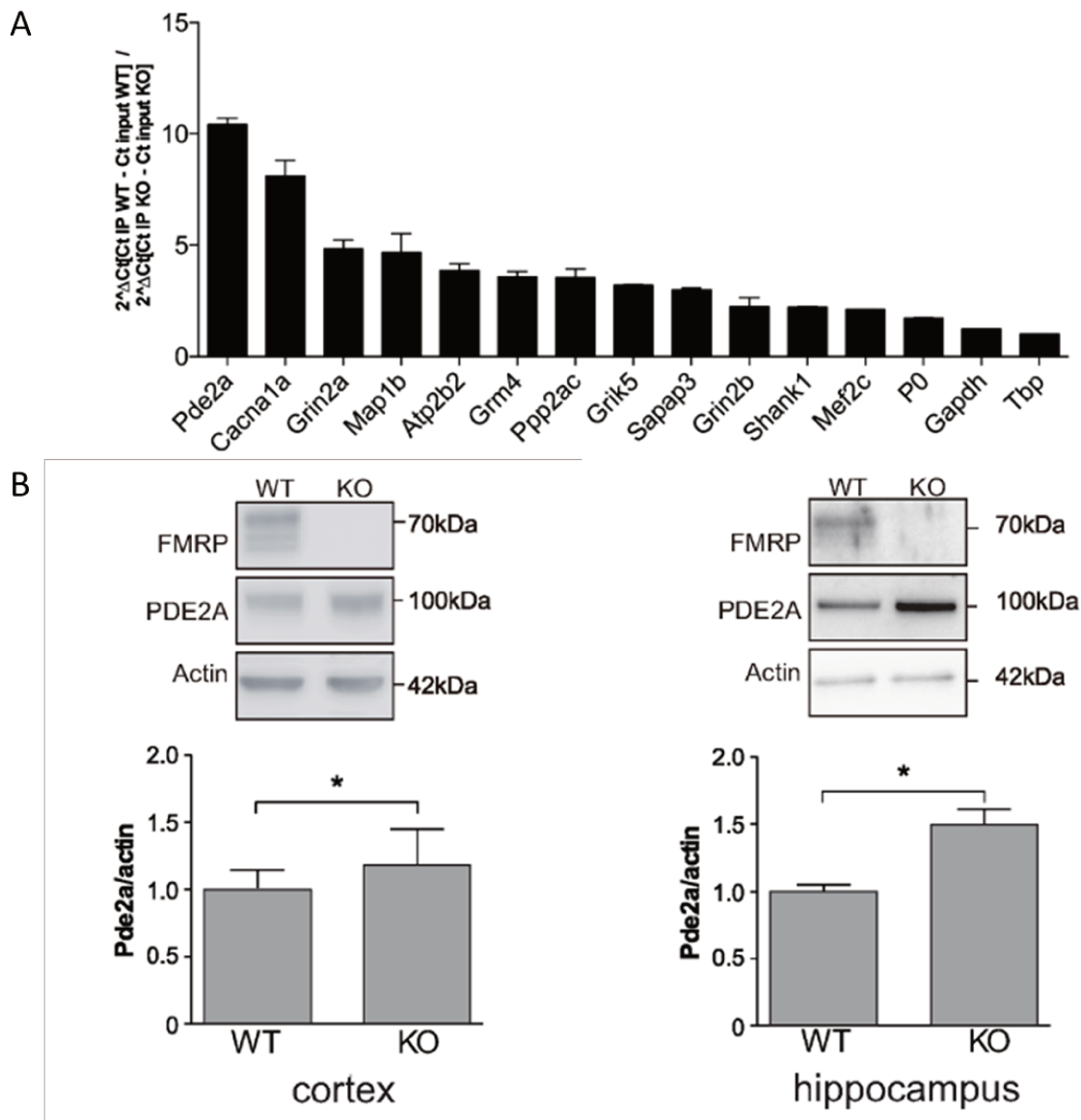


Figure 5. Identification de la dérégulation de PDE2A chez la souris *Fmr1* KO. (A) Validation de l'ARNm *Pde2a* comme cible de FMRP par son enrichissement dans le CLIP de FMRP. (B) Surexpression de PDE2A dans le cortex et l'hippocampe des souris *Fmr1* KO (Maurin et al., 2018).

Chapitre 2 : AMPc/GMPc et PDE2A

I. AMPc et GMPc, deux seconds messagers à la croisée des chemins.

1. Création et dégradation.

L'Adenosine MonoPhosphate cyclique (AMPc) et le Guanosine MonoPhosphate cyclique (GMPc) sont deux seconds messagers régulant un grand ensemble de voies de signalisation (Fig.6).

En 1958, Earl W. Sutherland identifie pour la première fois l'AMPc dans un extrait de foie comme second messager et suggère alors qu'il est un médiateur des effets cellulaires des neurotransmetteurs et des hormones (Butcher and Sutherland, 1962; Rall and Sutherland, 1958), ce qui lui vaudra le Prix Nobel de Physiologie ou médecine. Une trentaine d'années plus tard ce même prix sera décerné à Robert F. Furchtgott, Louis J. Ignarro et Ferid Murad pour leurs travaux sur le rôle du dioxyde d'azote (NO) et du GMPc dans le système cardiovasculaire.

La production d'AMPc est possible grâce aux Adenylyate Cyclases (AC) qui catalysent sa synthèse en partant d'ATP. L'AMPc est principalement synthétisé par des AC transmembranaires, activées par la dissociation de la sous-unité G α du récepteur couplé à la protéine G (GPCR) en réponse à un stimulus extracellulaire, comme une hormone ou un neurotransmetteur. Une seconde source d'AMPc dans la cellule provient des AC solubles régulées par le calcium et le bicarbonate (Kamenetsky et al., 2006). Les différents isoformes d'ACs peuvent être adressés vers des localisations subcellulaires bien distinctes, ce qui permet la génération du signal AMPc de façon ciblée.

De façon analogue, la production de GMPc est due aux Guanylyate Cyclases (GC) en partant de GTP. Ces GC sont divisés en deux catégories : les solubles, activées par le monoxyde d'azote (NO), et les transmembranaires, activées par des peptides

natriurétiques de type C (CNP) (Potter, 2011). Le NO, qui est l'activateur principal de la synthèse de GMPc, est lui-même synthétisé par l'enzyme NOS (Nitric Oxyde Synthase) en réponse à une augmentation des niveaux de Ca^{2+} . Le NO, produit en postsynaptique, agit de façon rétrograde en stimulant les GCs pré-synaptiques.

L'AMPc et le GMPc sont dégradés par une grande famille d'enzyme, les phosphodiesterases (PDEs). La diversité et la localisation des différentes ACs/GCs et PDEs sont déterminantes pour le contrôle spatio-temporel du signal porté par les niveaux d'AMPc et de GMPc. La dégradation des deux seconds messagers par les PDEs vont réduire leur niveau et ramener la Protéine Kinase A (PKA) et la Protéine Kinase G (PKG) à une forme inactive, formant ainsi un rétrocontrôle négatif. De plus, la PKA peut elle-même inhiber l'activité de certaines ACs (Chen et al., 1997; Iwami et al., 1995).

2. Implication dans de nombreuses voies de signalisation.

La cible principale de l'AMPc et du GMPc est la PKA et la PKG, respectivement. Ces deux protéines ont pour fonction de phosphoryler de nombreuses cibles et de moduler le signal des deux seconds messagers, en le multipliant ou en l'éteignant en fonction des protéines ciblées.

La PKA est une holoenzyme formée de deux sous-unités de régulation (R) et deux sous-unités catalytiques (C). La PKA est activée par la liaison de l'AMPc sur les sous-unités R engendrant un changement conformationnel qui libère les sous-unités C (Taylor et al., 1990). Ces sous-unités vont alors pouvoir promouvoir la phosphorylation de certains résidus (sérine et/ou thréonine) des protéines cibles. L'activation de PKA peut se faire de façon indirecte par la CamKII qui active certaines ACs, et donc la production d'AMPc (Mizunami et al., 2014).

La voie principale de la PKA qui est une composante majeure de la plasticité neuronale est la phosphorylation Ser133, et donc l'activation, du facteur de transcription CREB (cAMP response element binding response). CREB phosphorylé (PCREB) interagit directement avec l'ADN sur les régions CRE (cAMP response

element), induisant la transcription de nombreux gènes spécifiques comme les récepteurs AMPA (Borges and Dingledine, 2001), le facteur de croissance BDNF (Brain derived neurotrophic factor) (Esvald et al., 2020) ou d'autres facteurs de transcription comme c-Fos (Sheng et al., 1990).

La voie AMPc/PKA peut aussi aboutir indirectement à la phosphorylation de CREB via la kinase ERK (Extracellular signal-related kinase). CREB est phosphorylée par les protéines kinases Rsk activées par ERK (Impey et al., 1998). PKA semble agir sur l'activation de ERK de deux façons : par la voie de la small G-protein Rap1/kinase B-Raf (Grewal et al., 2000) et par des protéines Epacs qui activent à leur tour Rap1 (de Rooij et al., 1998).

Une autre cible de la PKA est la protéine GSK3 (Glycogene synthase kinase 3). GSK3 est une kinase qui a la particularité d'être constitutivement active, qui est inhibée en réponse à un stimulus par une phosphorylation, et dont les substrats doivent être pré-phosphorylés. GSK3 se réfère en fait à deux paralogues, deux protéines homologues provenant de deux gènes différents, GSK3 α et GSK3 β . Cependant, leurs domaines catalytiques sont pratiquement identiques. Cette enzyme est majoritairement cytosolique, bien que présente aussi dans la mitochondrie et le noyau (Hur and Zhou, 2010).

La phosphorylation en sérine 21 de la GSK3 α et en sérine 9 de la GSK3 β est l'inhibition la plus fréquente de l'activité de GSK3, qui peut être médiée entre autres par la PKA. En effet, la phosphorylation de la sérine provoque le repliement du N-terminal de GSK3 vers le domaine de liaison au substrat, agissant comme un substrat pré-phosphorylé, ce qui va empêcher la phosphorylation des substrats de GSK3 (Frame et al., 2001).

GSK3 phosphoryle particulièrement des substrats déjà phosphorylés, donc issus d'une autre voie de signalisation activée, le plus souvent sur un résidu à 4 résidus en C-terminal de la cible de GSK3. L'action de GSK3 est donc particulièrement limitée dans

le temps et la localisation. GSK3 doit être activé, donc sous forme non-phosphorylée, en même temps que son substrat doit être phosphorylé par une kinase susceptible d'inhiber GSK3. Par exemple, CREB est reconnue par la GSK3 seulement lorsqu'elle est sous forme active, phosphorylée en ser133. GSK3 inactive CREB par la phosphorylation en sérine 129. Or l'inactivation de GSK3 se fait le plus souvent par la phosphorylation de résidu sérine. Un autre signal est donc nécessaire pour lever l'inhibition de la GSK3. Ce paradoxe permettrait de réguler finement les effets de la GSK3 sur CREB (Grimes and Jope, 2001). En plus de CREB, GSK3 régule plusieurs autres facteurs de transcription comme c-Fos/Jun, NF-KappaB ou encore STAT3 (Jope and Johnson, 2004; Sutherland, 2011).

Les protéines Epac lient l'AMPc avec une forte affinité et activent les protéines de la famille des « small GTPases » Ras, Rap1 et Rap2 (de Rooij et al., 1998). L'importance d'Epac a été établie dans l'adhésion cellulaire, les jonctions intercellulaires, l'exocytose ou encore la différentiation cellulaire (Cheng et al., 2008) mais aussi dans la plasticité synaptique.

Enfin, l'AMPc est impliqué au niveau pré-synaptique dans la synthèse et le relargage de neurotransmetteurs comme le glutamate et la dopamine (RodríguezMoreno and Sihra, 2013; Schoffelmeer et al., 1985).

De façon similaire à la PKA, la PKG est un homodimère constitué de deux sous-unités C et R. Chaque sous-unité contient deux sites de liaison au GMPc sur le domaine R. Contrairement à la PKA, la liaison du GMPc n'engendre pas la dissociation de C.

Au niveau post-synaptique, l'activation de la voie GMPc/PKG induit la phosphorylation de CREB, bien que de façon plus minime que AMPc/PKA (Lu and Hawkins, 2002). Cependant, la PKG pourrait indirectement participer à la phosphorylation de CREB en stimulant le relargage de Ca^{2+} depuis les stocks sensibles à la ryanodine. Cela induirait l'activation des protéines Rsk2 activés par ERK, sensible au Ca^{2+} comme décrit précédemment (Impey et al., 1998).

De façon similaire à l'AMPc, au niveau présynaptique, le GMPc est associé au relargage des neurotransmetteurs (Arancio et al., 1996).

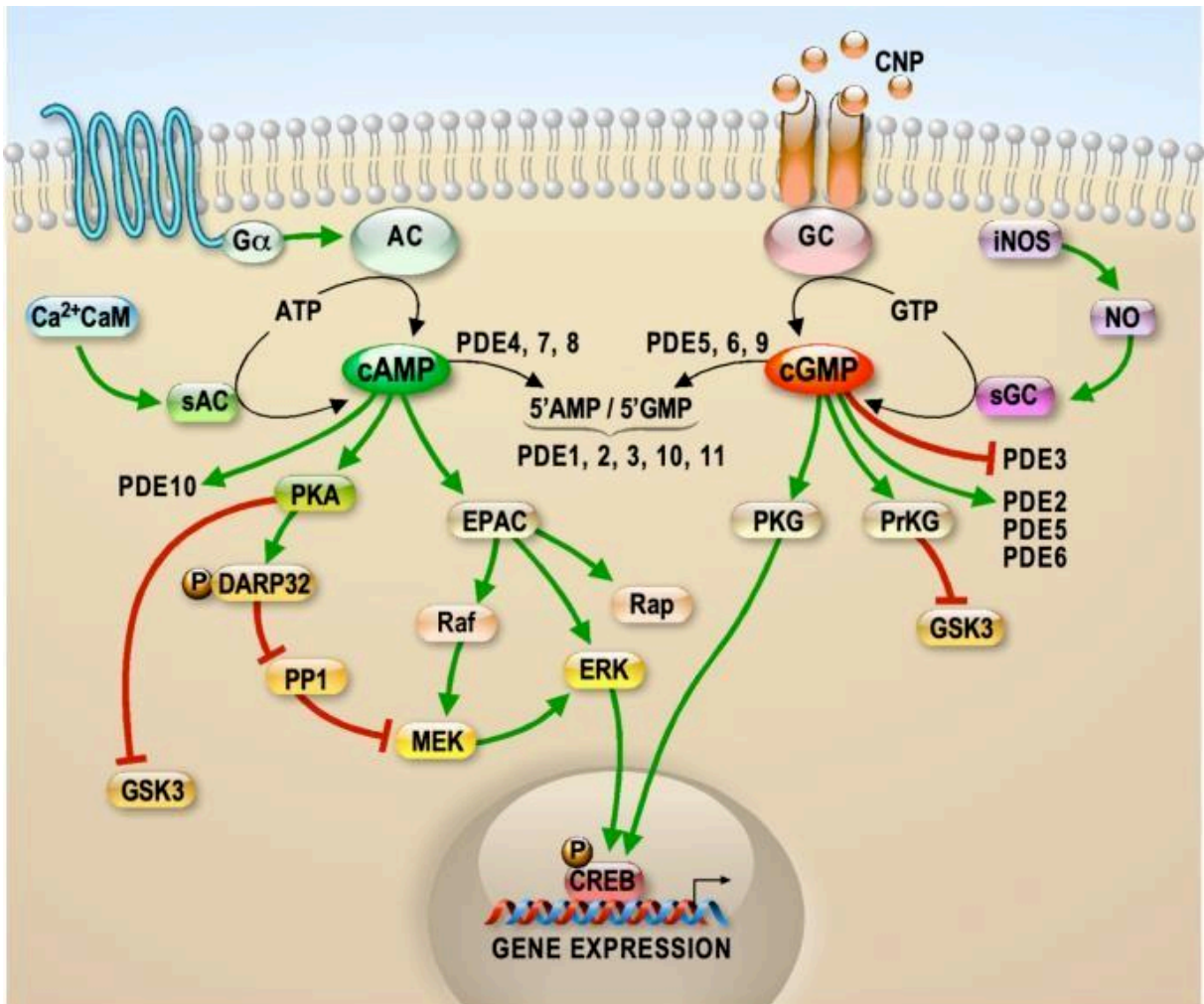


Figure 6. Schéma récapitulant les voies de signalisation impliquant l'AMPc et le GMPc, ainsi que la création et la dégradation spécifique de ces derniers. Les flèches rouges indiquent une inhibition, les flèches vertes une activation. PKA : cAMP-dependent Protein Kinase, Ca²⁺CaM : Ca²⁺/calmodulin-dependent protein kinase II, EPAC : Exchange Protein directly Activated by cAMP, Rap : Ras-related protein, ERK : Extracellular signal-Regulated Kinase, Raf : rapidly accelerated fibrosarcoma, DARP32 : dopamine- and cAMP-regulated neuronal phosphoprotein, PP1 : protein phosphatase-1, MEK : Mitogen-activated protein kinase Kinase, PKG : cGMP-dependent protein kinase, PrKG : protein kinase cGMP-dependent, GSK3 : glycogen synthase kinase 3, iNOS : inducible nitric oxide synthase; NO : nitric oxide, CREB : cAMP response element-binding protein, CNP : C-type natriuretic peptide. (Delhaye and Bardoni, 2021).

3. Rôle de la balance AMPc/GMPc dans les neurones.

La balance entre les niveaux d'AMPc et de GMPc est essentielle pour le modelage des circuits neuronaux et des neurones eux-mêmes. Par exemple, localement pour la polarisation neuronale, la formation de l'axone est favorisée par une concentration élevée d'AMPc mais basse de GMPc (Shelly et al., 2007). A l'inverse, la formation des dendrites est favorisée par une concentration élevée de GMPc et basse d'AMPc (Shelly et al., 2010a).

La différenciation des neurones se fait aussi au niveau des neurotransmetteurs, qui permettent la bonne connectivité du système nerveux avec une balance régulée entre excitation et inhibition. Le choix du neurotransmetteur semble lié aux pics calciques spontanés, et leurs fréquences induisent le devenir en excitateur ou inhibiteur du neurone (Spitzer et al., 2004). Il existe un lien fort entre les pics calciques et l'élévation transitoire d'AMPc qui sont interdépendants (Gorbunova and Spitzer, 2002), ce qui pourrait expliquer le rôle de l'AMPc dans la spécification du neurotransmetteurs.

De plus, la croissance axonale est dépendante de fortes concentrations en AMPc (Cai et al., 2001; Roisen et al., 1972) et est aussi liée aux pics calciques. Une fréquence faible de ces pics de calcium est associée à une croissance axonale forte alors qu'une haute fréquence est visible dans des axones à croissance lente (Gomez and Spitzer, 1999; Tang et al., 2003).

4. Rôle dans la plasticité synaptique

La cascade de signalisation AMPc/PKA est impliquée dans la régulation de la potentialisation à long terme (LTP) au niveau post- et pré-synaptique. Brown et al. ont montré que la LTP induite par Theta Pulse Simulation est dépendante du signal AMPc post-synaptique en inhibant la PP1 (Post-synaptic phosphatase-1), ce qui va augmenter

l'activité de CamKII, une kinase dépendante des niveaux de Ca^{2+} qui peut phosphoryler les récepteurs AMPA (Brown et al., 2000). De même, la PKA phosphoryle la sous-unité GluR1 du récepteur AMPA, ce qui entraîne son insertion dans la zone post-synaptique active (Esteban et al., 2003) et augmente sa probabilité d'ouverture (Banke et al., 2000). La déphosphorylation de ce site Ser845 augmente par ailleurs l'endocytose du récepteur (Lee et al., 2000). De plus, la PKA s'attache à la protéine d'échafaudage AKAP150 pour réguler la phosphorylation de la sous-unité GluR1 et l'incorporation de récepteur AMPA perméable au Ca^{2+} à la synapse lors de la LTD dépendant des récepteurs NMDA (Sanderson et al., 2016). L'étude de l'inhibition et de l'activation pharmacologique ou génétique de la PKA a montré par ailleurs l'importance de l'activité de la PKA dans la LTP dans les tranches hippocampales. L'inhibition de l'activité de la PKA diminue la LTP (Huang and Kandel, 1994; Impey et al., 1996) alors que son activation participe à la génération de la LTP (Frey et al., 1993). Enfin au niveau comportemental, la dérégulation de l'activité de PKA de façon pharmacologique et génétique engendre des déficits de la mémoire spatiale (Abel et al., 1997; Sharifzadeh et al., 2005) et de la mémoire contextuelle (Ahi et al., 2004).

Une autre cible principale de l'AMPc, Epac, semble être impliquée dans la plasticité synaptique. L'activation d'Epac peut induire la LTD dans des tranches d'hippocampe, indépendamment de l'internalisation des AMPAR contenant GluA2/3 et de la voie MAP kinase (Ster et al., 2009). De plus, l'utilisation d'un agoniste d'Epac toujours sur des tranches hippocampales maintient la LTP induite dépendamment de la voie ERK (Gelinas et al., 2008).

En ce qui concerne les cibles de PKA, l'implication de GSK3 dans la plasticité synaptique est décrite depuis quelques années. De façon générale, l'inhibition de GSK3 est nécessaire pour la LTP alors que son activité constitutive est essentielle à la LTD (Hooper et al., 2007). Plus particulièrement, chez la souris sur-exprimant GSK3 β (Hooper et al., 2007) ou exprimant un mutant GSK3 β ne pouvant être inhibé (Dewachter et al., 2009) la LTP est perturbée.

La stimulation de la cascade NMDA/NO/GMPc/PKG joue un rôle important dans la LTP et la LTD, suggérant aussi le rôle du GMPc dans les processus de mémorisation et d'apprentissage. En effet, la LTP produite par stimulation tétanique dans la région CA1 de l'hippocampe est bloquée par des inhibiteurs de GCs et de PKG (Son et al., 1998). De même dans le CA1, la voie NO/GMPc/PKG semble nécessaire à l'induction de la LTD (Reyes-Harde et al., 1999), ainsi que dans le gyrus denté (Wu et al., 1998). De plus, les activateurs de PKG facilitent la LTP en réponse à un faible stimuli tétanique (Arancio et al., 2001; Izquierdo et al., 2000). Le KO de la forme associée à la membrane de la PKG, PKGII, provoque un déficit important de l'apprentissage spatial dans le test du MWM (Wincott et al., 2013). Enfin, l'activateur de la PKG 8-Br-cGMP montre un effet bénéfique dose dépendant sur le test du NOR (Prickaerts et al., 2002).

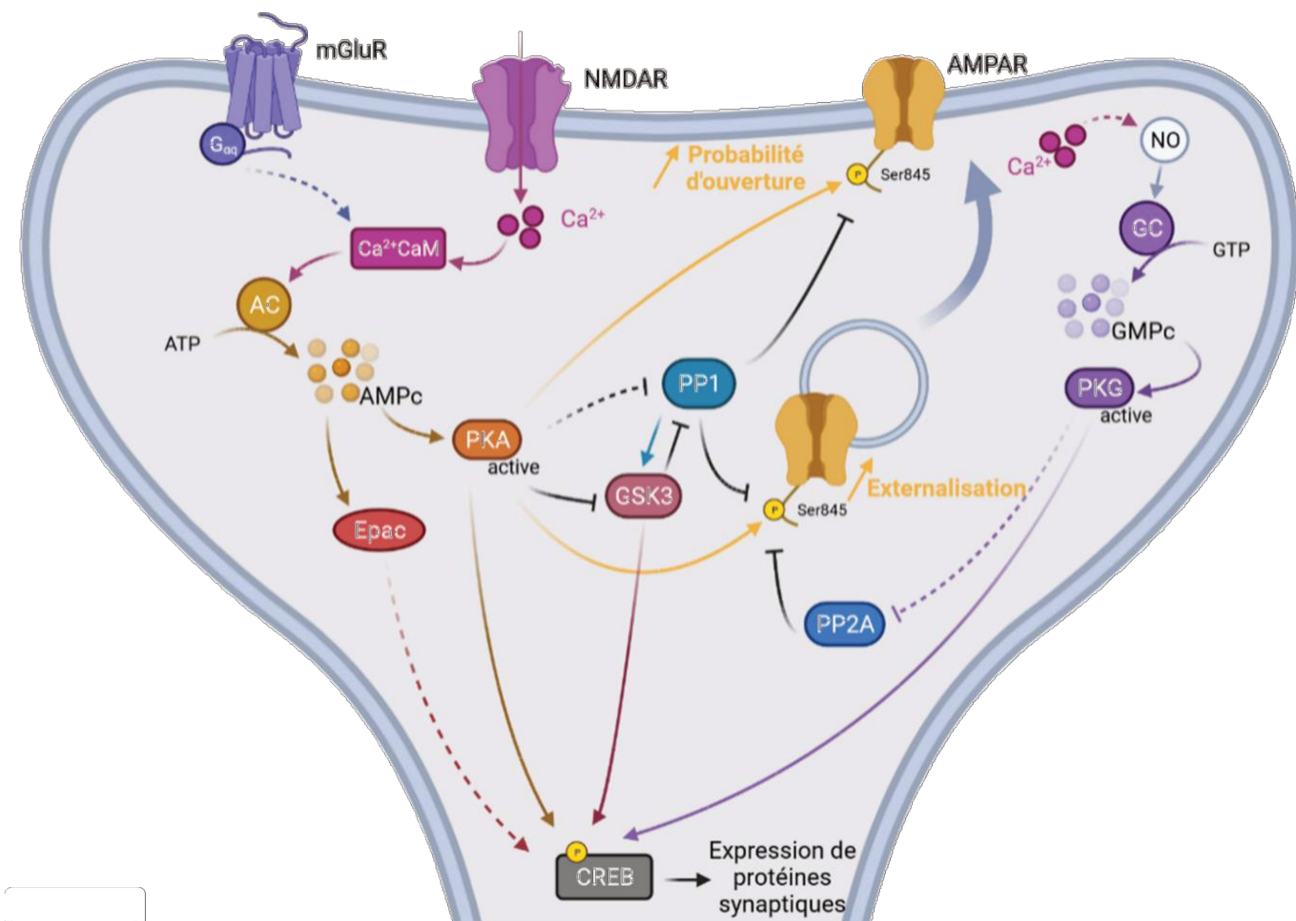


Figure 7. Schéma récapitulant l'implication de l'AMPc et du GMPc dans la plasticité synaptique.
 mGluR : récepteur métabotropique du glutamate, NMDAR : N-methyl-D-aspartate receptor, AMPAR : α -amino-3-hydroxy-5-methyl-4-isoxazolepropionic acid receptor, AC : Adénylate Cyclase, PKA : cAMP-dependent Protein Kinase, Ca²⁺/CaM : Ca²⁺/calmodulin-dependent protein kinase II, EPAC : Exchange Protein directly Activated by cAMP, PP1 : protein phosphatase-1, PP2A : Protein phosphatase 2, GC :

Guanylate Cyclase, PKG : cGMP-dependent protein kinase, GSK3 : glycogen synthase kinase 3, NO : nitric oxide, CREB : cAMP response element-binding protein, (P) Ser845 : phosphorylation en sérine 845.

II. Les phosphodiestérases

1. Une grande famille d'enzymes

L'activité des phosphodiestérases a été décrite pour la première fois en 1886 par le Dr Henry Hyde Salter en observant la capacité bronchodilatatrice de la caféine sur un asthmatique (Boswell-Smith et al., 2006). Le mécanisme n'était pas connu à l'époque mais on sait aujourd'hui que la caféine est un inhibiteur faible non sélectif de PDE. L'activité enzymatique des PDEs est de catalyser l'hydrolyse de la liaison phosphate en 3' de l'AMPc et du GMPc, générant ainsi leur forme inactive 5'AMP et 5'GMP, respectivement. Les phosphodiestérases composent une grande famille, classés en 11 sous-classes de protéines codées par 21 gènes. De nombreux variants d'épissage sont produits depuis ces gènes, résultant en des isoformes à la localisation subcellulaire bien spécifique.

Les PDEs sont réparties en trois groupes en fonction de leur spécificité envers les deux nucléotides : celles spécifiques à l'AMPc (PDE4, PDE7 et PDE8), celles spécifiques au GMPc (PDE5, PDE6 et PDE9), et celles hydrolysant les deux (PDE1, PDE2, PDE3, PDE10 et PDE11). Dans ce dernier groupe, les PDEs ont tout de même une plus grande affinité pour l'un ou l'autre second messager (Azevedo et al., 2014). Cette spécificité est associée à un « switch glutamine », un résidu glutamine très conservé qui permet de réguler la liaison du nucléotide au domaine de liaison (Zhang et al., 2004).

Les différentes structures de ces enzymes, dont la région catalytique et les domaines de régulation, sont partagées entre les isoformes et très conservés entre les espèces. Dans chaque sous-famille de PDEs, les parties N- et C-terminale sont les

régions variables contenant les domaines définissant la localisation subcellulaire de l'isoforme concernée.

2. Rôle dans les troubles du neurodéveloppement

L'implication des PDEs dans les troubles du neurodéveloppement est tout d'abord mise en évidence par les études génétiques qui font le lien entre les deux. Le Science Genetic Association Consortium a conduit une récente étude d'association pangénomique (Genome-wide association ou GWAS) à grande échelle qui a relié certaines variations génétiques dans des gènes codant pour des PDEs avec des capacités cognitives chez l'Homme (Lee et al., 2018). Des SNPs (Single-Nucleotide Polymorphisms) sur *PDE1C*, *PDE2A*, *PDE4B* et *PDE4D* sont significativement associés à la performance cognitive et au niveau de scolarité (Gurney, 2019). La plus grande significativité statistique concerne le SNP rs72962169 dans le gène *PDE2A* associé à un niveau scolaire plus élevé. D'autres études tendent à montrer l'implication des PDEs dans les troubles neurodéveloppementaux.

Un SNP intronique dans le gène *PDE1C* est associé au TSA de façon significative dans une méta-analyse GWAS de près de 16 000 individus (The Autism Spectrum Disorders Working Group of The Psychiatric Genomics Consortium, 2017) et une mutation faux-sens sur le gène *PDE1B* a été identifiée chez des personnes atteintes de TSA (Rubeis et al., 2014) et de schizophrénie (John et al., 2019).

Une mutation homozygote de site d'épissage dans *PDE2A* a été retrouvée chez deux patients atteints d'un syndrome de Rett atypique ayant un retard du développement (Haidar et al., 2020). Une mutation homozygote entraînant la perte de fonction de *PDE2A* a été associée à un trouble du mouvement précoce héréditaire et à un déficit intellectuel (Salpietro et al., 2018). De même, dans une récente publication, une mutation homozygote avec apparition d'un codon stop a été repérée chez deux enfants de la même famille ayant une dyskinésie paroxystique, caractérisée par des mouvements involontaires, et un déficit intellectuel (Douummar et al., 2020). Dans cette

même étude, un troisième patient atteint de ces mêmes troubles présente une double mutation hétérozygote, l'une étant une mutation non-sens donnée par la mère, l'autre une mutation de site d'épissage donnée par le père (Table II).

Table II. Mutations de <i>Pde2a</i> connues chez des patients				
	Mutation	Atteinte sur PDE2A	Phénotype	Référence
1 patient	Mutation homozygote faux-sens(c.1439A>G)(Asp480Gly)	Mutation dans domaine GAF-B	Trouble moteur, déficience intellectuelle	Salpietro et al., 2018
2 patients (famille consanguine)	Mutation homozygote de site d'épissage (c.323+1G>A)	Exon 4 - Protéine tronquée ?	Syndrome de Rett atypique, régression, retard du développement	Haidar et al., 2020
2 patients (frère et sœur)	Mutation homozygote avec apparition de codon stop (c.1180C>T) (Gln384*)	?	Dyskinésie, retard du développement, épilepsie, réseau mitochondrial altéré	Douummar et al., 2020
1 patient	Double mutation hétérozygote : une faux-sens (c.446C>T)(Pro149Leu) et une de site d'épissage (c.1922+5G>A)(Ala618Val)	En amont des domaines GAF-A et B	Dyskinésie, retard du développement, réseau mitochondrial altéré	Douummar et al., 2020

De plus, des patients ayant un trouble bipolaire ont des niveaux réduits d'ARNm de *PDE2A* dans l'hippocampe, le cortex entorhinal et le striatum, tandis que des patients atteints de schizophrénie, trouble bipolaire et de dépression ont des niveaux réduits dans l'amygdale. Enfin des patients atteints de schizophrénie montrent des niveaux réduit d'ARNm de *PDE2A* au niveau du cortex frontal (Farmer et al., 2020).

Des mutations dans les gènes *DISC1* et *PDE4B* réduisant l'interaction entre ces deux protéines, réduisant l'activité de *PDE4B*, est corrélé à la schizophrénie (Millar, 2005). De façon intéressante, un SNP dans le gène *PDE4B* est associé à un effet protecteur envers la schizophrénie chez les femmes (Pickard et al., 2007) et différents polymorphismes sont associés à un effet protecteur contre les troubles paniques chez des sujets russes (Malakhova et al., 2019).

Enfin, une mutation dans le gène *PDE4D* a été montrée comme étant une cause de l'acrodysostosis de type 2 (ACRDYS2), une maladie caractérisée par une DI sévère (Linglart et al., 2012; Michot et al., 2012).

3. Modèles animaux.

Quelques modèles animaux KO pour certaines PDEs commencent ces dernières années à faire leur apparition et à être caractérisés, nous donnant des informations précieuses sur le rôle de ces enzymes sur le comportement, certaines maladies ou encore de l'implication des PDEs dans la plasticité synaptique.

Le knock-down de *Pde1b* dans l'hippocampe améliore la mémoire spatiale et contextuelle dans les tests du labyrinthe de Barnes et du Contextual Fear Conditioning (CFC) (McQuown et al., 2019), tandis que le KO total présente une hyperactivité locomotrice, des déficits dans la mémoire spatiale (Reed et al., 2002), ainsi qu'un phénotype antidépressif (Hufgard et al., 2017).

Le modèle murin KO *Pde2a* a été généré mais est léthal au stade embryonnaire E17 à cause d'une défaillance cardiaque.

Les souris *Pde4b*-KO présentent une diminution du PPI et une réponse locomotrice exagérée aux amphétamines, corrélée à une diminution de l'activité dopaminergique et sérotoninergique dans le striatum (Siuciak et al., 2007). Dans deux autres études, les souris *Pde4b*-KO ont des déficits de mémoire associative dans le test de peur conditionnée (Rutten et al., 2011), passent moins de temps dans le compartiment « light » lors du test du Dark-Light et explorent moins lors du test de l'open field (Zhang et al., 2008). De façon intéressante, on trouve dans ce modèle une LTD plus persistante au niveau de l'hippocampe par rapport aux WT en réponse à une induction (Rutten et al., 2011). Quant au modèle murin *Pde4d*-KO, ces souris présentent une diminution de l'immobilité lors du test de suspension par la queue et de nage forcée (Zhang et al., 2002). Ces résultats suggèrent une implication de PDE4B et PDE4D dans le comportement anxieux et la dépression.

Les souris *Pde10*-KO présentent une diminution de l'activité exploratoire, une réponse locomotrice aux amphétamines augmentée ainsi qu'un retard d'apprentissage lors de test d'évitement conditionné (Siuciak et al., 2008).

Enfin, les souris *Pde11a*-KO présentent des ventricules latérales élargis, une augmentation de l'activité dans le CA1, une hyperactivité dans le test de l'open field et un déficit dans la formation de la mémoire sociale (Kelly, 2017; Kelly et al., 2010).

III. La PDE2A

1. Biologie de la PDE2A

La phosphodiestérase 2A (PDE2A) est doublement spécifique en hydrolysant l'AMPc et le GMPc (Rosman et al., 1997). Elle fut identifiée pour la première fois dans le foie de rat en 1971 par Beavo, Hardman et Sutherland (Beavo et al., 1971), et a été clonée et séquencée pour la première fois en 1986 (Sass et al., 1986). Cette enzyme est un homodimère, dont chaque monomère fait environ 105 kDa. Elle est composée en N-terminal de deux domaines GAF (cGMP-binding PDE, Anabaena adenylyl cyclases, Escherichia coli FhlAs), GAF-A et GAF-B. Cette PDE a la particularité d'être activée par l'un de ses substrats, le GMPc, qui se lie sur le domaine GAF-B. Cette capacité permet à l'enzyme de médier la « communication » entre les deux cascades de signalisation provoquées par l'AMPc et le GMPc.

Le résidu glutamine précédemment mentionné régulant la spécificité des PDEs envers leur substrat est dans la PDE2A le Gln859. Dans cette enzyme, ce résidu est capable d'effectuer une rotation libre, lui permettant de former des liaisons hydrogènes avec les deux seconds messagers (C-R Yang 2012)

La PDE2A hydrolyse l'AMPc et le GMPc avec des valeurs de Km similaires (30 μ M pour l'AMPc et 10 μ M pour le GMPc) et une Vmax de 120 μ mol par minute et par mg (Martins et al. 1982). La liaison du GMPc au domaine GAF-B de l'enzyme augmente l'hydrolyse de l'AMPc d'un facteur 5 à 30 (Gesellchen Zaccolo 2011).

2. Expression et localisation subcellulaire

PDE2A est exprimée dans le système nerveux central et périphérique ainsi que dans le reste du corps, comme dans le cœur, les cellules endothéliales ou encore les glandes surrénales. Mais c'est dans le cerveau que l'expression de la PDE2A est la plus importante.

L'expression de PDE2A dans le système nerveux central est principalement située au niveau antérieur (prosencéphale), et se trouve peu au niveau postérieur (rhombencéphale) et moyen (mésencéphale). L'hybridation *in situ* d'ARNm de *Pde2a* dans le cerveau de rat montre des niveaux importants de PDE2A dans la substance grise de la région antérieure, dans le bulbe olfactif, les cellules pyramidales de l'hippocampe et dans le noyau médian de l'habenula (Stephenson et al., 2012). Des patterns d'expression similaires se retrouvent en immunohistochimie. Au niveau du cortex somato-sensoriel, PDE2A est fortement exprimée dans la couche corticale I, et le neuropile des couches II et III. Un plus faible marquage se trouve aussi dans le neuropile de la couche V et dans la couche IV. Dans l'hippocampe, la PDE2A est exprimée fortement dans le CA1 et la région terminale des mossy fiber du CA3 (Stephenson et al., 2012). Le pattern d'expression dans le cortex de rat est similaire à celui du cortex chez l'humain, le primate, le chien et la souris (Stephenson et al., 2009) De plus, la PDE2A est retrouvée préférentiellement dans les axones et les terminaisons des neurones.

PDE2A est en réalité composée de 3 variants, au rôle et localisation différente, PDE2A1, PDE2A2 et PDE2A3. PDE2A1 est soluble dans la cellule, tandis que PDE2A2/3 sont associés à la membrane (Noyama and Maekawa, 2003). Plus particulièrement, le variant PDE2A2 est associé aux membranes des mitochondries, au niveau de la matrice (Acin-Perez et al., 2011). Cependant, une autre étude a conclu à la localisation de ce variant plutôt au niveau de l'espace intermembranaire et de la membrane externe de la mitochondrie (Monterisi et al., 2020). Enfin, le variant PDE2A3 est associé à la membrane des synapses par myristoylation et palmitoylation (Russwurm et al., 2009).

3. Effets de l'inhibition de la PDE2A

De façon surprenante, malgré la forte présence de la PDE2A au sein du système nerveux et notamment limbique, ses inhibiteurs n'ont pas suscité autant d'attention que ceux des autres PDEs. L'un des inhibiteurs de la PDE2A les plus étudiés et

commercialement disponible est le Bay 60-7550, ayant une sélectivité pour la PDE2A 50 fois supérieure que pour la PDE1C et au minimum 100 fois supérieur que pour les autres PDEs (Boess et al., 2004). L'inhibition de la PDE2A par le Bay 60-7550 a montré des effets bénéfiques sur l'apprentissage, la mémorisation et la plasticité synaptique. En effet, l'administration de Bay 60-7550 permet à des rats d'avoir des performances améliorées dans les tests de reconnaissance d'un nouvel objet à 24h d'intervalle, et de reconnaissance d'un congénère (Boess et al., 2004). Dans cette même étude, l'inhibition de PDE2A augmente la LTP induite dans la région CA1 de l'hippocampe. D'autres études montrent l'effet bénéfique de l'administration de Bay 60-7550 sur les performances de rats lors de test de reconnaissance de nouvel objet (Bollen et al., 2015; Domek-Łopacińska and Strosznajder, 2008).

Dans des modèles de neuro-dégénération, l'injection de Bay 60-7550 a aussi montré des effets bénéfiques lors des tests de MWM dans des modèles de maladie d'Alzheimer (Ruan et al., 2019; L. Wang et al., 2017) et de NOR dans un modèle d'ischémie (Soares et al., 2017).

De plus, l'administration de Bay 60-7550 à des souris soumises à un stress aigüe et prolongé est bénéfique sur le comportement anxieux associé à ce modèle lors des tests d'anxiété, caractérisant l'effet anxiolytique de cet inhibiteur (Chen et al., 2021). Une utilisation du Bay 60-7550 contre l'alcoolisme serait possible étant donné son effet inhibiteur de la consommation et de la préférence à l'alcool chez la souris (Shi et al., 2018).

De façon intéressante, le rôle de la PDE2A dans la douleur est suggéré par l'effet bénéfique du Bay 60-7550 sur l'inflammation radiculaire et l'allodynie mécanique chez un modèle de rat souffrant d'hernie discale lombaire (J.-N. Wang et al., 2017).

D'autres inhibiteurs de la PDE2A, moins utilisés, ont pour autant montré d'autres effets bénéfiques chez différents modèles animaux. Hcyb1 a un effet neuroprotecteur et antidépressif chez la souris (Liu et al., 2018), tandis que TAK-915 améliore les déficits

cognitifs et sociaux dans un modèle de rat schizophrène (Nakashima et al., 2018) et améliore le déclin cognitif lié à l'âge chez la souris (Nakashima et al., 2019).

A ce jour, un seul inhibiteur spécifique de la PDE2A de Pfizer a été testé au cours d'un essai clinique afin de traiter la migraine, mais les résultats n'ont pas été communiqués.

Objectifs de la thèse

La dérégulation de l'expression de l'ARNm et/ou de la protéine pour laquelle FMR1 code est à la base de plusieurs pathologies – notamment le SXF et le FXTAS – qui peuvent avoir un impact dans le développement du cerveau. L'étude des réseaux moléculaires jouant un rôle dans la physiopathologie de ces maladies est donc essentielle à l'identification de nouvelles cibles thérapeutiques. D'autre part, la capacité de corriger les phénotypes au niveau préclinique (*in vitro*, *ex-vivo* ou *in vivo* dans des modèles animaux) représente la première étape pour la mise en place de thérapies innovantes et efficaces chez les patients.

Pour le SXF, je me suis concentré sur l'étude de l'impact que la modulation du niveau d'expression de PDE2A – dont FMRP règle la traduction – a dans le développement du cerveau, par des expériences de comportement et de caractérisations moléculaires et cellulaires. En partant de l'observation que le niveau d'expression de PDE2A dans le cortex et l'hippocampe des souris *Fmr1* KO est augmenté, j'ai utilisé plusieurs approches complémentaires entre elles :

- La réduction pharmacologique de l'activité de PDE2A dans la souris modèle du SXF.
- La réduction génétique du niveau d'expression de PDE2A, par croisement des souris *Fmr1* KO avec la lignée *Pde2a^{+/−}*.
- La sur-expression de PDE2A dans le cortex d'embryons WT.

Pour le FXTAS et les souris CGG-KI, j'ai étudié l'impact de la modulation d'un des éléments physiopathologiques connu de la maladie - le niveau d'ARNm de *Fmr1* - sur des phénotypes neuronaux liés au développement (e.g. morphologie des épines, taille du premier neurite).

Matériels et méthodes

La plupart des matériels et méthodes utilisés sont complètement décrits dans les articles en annexe à la fin de cette thèse. Concernant mes derniers résultats non publiés à ce jour, les matériels et méthodes nouvellement utilisés sont listés ci-dessous.

1. Souris *Pde2a^{+/−}*

Les souris *Pde2a^{+/−}* (B6; 129P2-PDE2A<tm1Dgen>/H; EM:02366) nous ont été données par le Dr Emanuela Pellegrini et le Dr Fabio Naro, Università la Sapienza – Rome (Italy)

Ces souris transgéniques sont génotypées par le set de primers suivant :

Pde2a screen F1: 5'-CTGCCTGATGGTGAAGAAAGGCTA-3',

Pde2a screen F2: 5'-GGGCCAGCTCATTCCCTCCCACCATC-3',

Pde2a screen R: 5'-TGAGCAGACCCCTATGGAAGGTG-3'

2. Novel Object Recognition (NOR)

2.1 Apparatus

Ce test est réalisé dans une arène de 20cm sur 38cm et des parois de 30cm. Les parois sont opaques et blanches. Les souris sont testées par groupe de quatre à l'âge de 2 mois. Les deux sets d'objets différents sont des petites bouteilles de shampoing vertes et des boîtes de lamelles blanches et vides. Les objets et l'arène sont nettoyés à l'éthanol 70% puis à l'eau entre chaque souris.

2.2 Procédure

Les animaux sont tout d'abord habitués à l'arène vide pendant cinq minutes les deux jours précédent le test. Durant la phase d'apprentissage, les animaux sont placés dans l'arène avec deux objets identiques (soit deux bouteilles, soit deux boîtes) pendant dix minutes. Cinq minutes ou une heure après, une seconde phase de test

permet aux animaux d'explorer l'arène avec cette fois un des deux objets remplacé par un de l'autre set. La disposition des objets et le choix des sets utilisés pour chaque souris est aléatoire afin d'éviter tout biais de préférence d'objet et d'emplacement.

Lors de ces deux phases de test, le temps d'exploration est enregistré manuellement à l'aide d'un logiciel de comptage développé à l'institut (BTT, S. Moreno). L'exploration d'un objet est définie quand le nez de l'animal est dirigé vers l'objet à moins de 2 cm. Quand l'animal se trouve sur l'objet ce comportement n'est pas considéré comme exploratoire envers l'objet.

Un index de discrimination est calculé lors de la seconde phase du test, qui est corrigé par le temps total d'exploration, et qui correspond à la formule suivante : $(\text{temps d'exploration du nouvel objet} - \text{temps d'exploration de l'ancien objet}) / (\text{temps d'exploration total})$. Le temps d'exploration total durant les deux phases est calculé afin de vérifier l'effet des génotypes sur l'exploration de façon général. Les animaux présentant des temps d'exploration anormaux, inférieurs à 10s, sont exclus de l'analyse.

3. Piscine de Morris (MWM)

La piscine utilisée est circulaire, de 90cm de diamètre et 100 cm de profondeur, remplie d'une eau opacifiée et maintenue entre 23 et 24 °C. Une plateforme de 8cm de diamètre est utilisée pour la Cue Task et la phase d'apprentissage (Trial), à 1cm sous la surface de l'eau, et est enlevée le jour du Probe Test. La plateforme est repositionnée à l'opposé lors du Reversal. Quatre indicateurs spatiaux sont accrochés aux murs aux quatre points cardinaux et un rideau sépare la piscine du reste de la pièce. Lors de la Cue Task un bouchon flotteur est placé sur la plateforme afin de vérifier les capacités visuelles et locomotrices des animaux. Chaque jour de test, les animaux sont relâchés dans l'eau 4 fois, à chaque point cardinal, sauf le jour du Probe Test où elles sont testées une fois depuis l'Ouest. Les animaux ont 90 secondes pour trouver la plateforme, et

doivent rester 30 secondes sur celle-ci. Si une souris n'atteint pas la plateforme dans le temps imparti, elle est aidée à la rejoindre et doit y rester 30 secondes.

Le test se compose de deux jours de Cue Task, quatre jours d'apprentissage Trial et d'un jour de Probe Test

Le temps de latence avant de trouver et de rester sur la plateforme est mesuré pour chaque souris, ainsi que le temps passé dans chaque quadrant le jour du Probe Test par le logiciel Anymaze.

4. Zero Maze élevé (ZME)

L'appareil du ZME est une plateforme en forme de « O » surélevée qui est divisée en deux sections fermées par des parois et deux sections ouvertes. Chaque animal est placé au départ à l'entrée d'une section fermée et laissé rentrer de lui-même dans cette zone. Le test dure 5 minutes, durant lequel la latence de sortie dans la zone ouverte, le nombre de transitions et le temps passés dans ces zones est comptabilisé. L'animal est considéré dans une section quand ces quatre pattes sont dans ladite section.

5. Western Blot

Les hippocampes congelés sont broyés puis resuspendus et lysés dans un tampon de lyse particulier pour étudier les phosphorylations. Ce tampon contient 1% Triton X100, 20 mM Tris HCl (pH7.6), 150 mM NaCl, 5 mM orthovanadate, 1mM PMSF, 30mM β -Glycérophosphate, 10mM NaF et un cocktail d'inhibiteurs de protéases et phosphatases. Après sonication, centrifugation et récupération du surnageant, du NuPAGE LDS Sample Buffer (4x) et du NuPAGE Sample Reducing Agent (10x) (Invitrogen) sont rajoutés. Les échantillons sont dénaturés à 95°C ou 35°C (pour les mGluR5) pendant 10 minutes. L'électrophorèse des échantillons est réalisée sur gels pré-coulés NuPAGE 4-12% Bis-Tris (Invitrogen) et migrés pendant 1.5h à 150V dans du

tampon NuPAGE MOPS SDS Running Buffer (Invitrogen). Les protéines sont ensuite transférées sur membrane de nitrocellulose pendant 1.5h à 100V constant.

Par la suite, les membranes sont saturées dans 5% de lait TBS-0.1%Tween pendant 1h, puis incubées sur la nuit à 4°C avec les anticorps primaires suivant : anti-GAPDH (Millipore, 1:5000), anti-PDE2A (Abcam, 1 :1000), anti-GSK3β (CellSignaling, 1 :1000), anti-GSK3β(ser9) (CellSignaling, 1 :1000) et anti-COX4 (SantaCruz, 1 :1000)

Les membranes sont lavées trois fois avec du TBS-0.1%Tween et incubées avec l'anticorps secondaire (1 :5000) pendant 1h à température ambiante. Après trois lavages en TBS-0.1%Tween, les membranes sont révélées avec Immobilon Western (Millipore). La quantification de l'intensité des bandes se fait avec ImageJ.

6. Electroporation *in utero* (EIU)

L'électroporation *in utero* a été réalisée sur des cerveaux d'embryons de souris au stade E14.5, en ciblant la région corticale (Fig.7). Les électroporations ont été faites avec les électrodes connectées à l'électroporateur NEPA GENE. Les paramètres suivants ont été utilisés : 4 pulses de 50V, P(on) 50ms, P(off) 1s, et 5% decay rate. Les mères sont anesthésiées par un mélange kétamine (1mg/kg)/xylazine(10mg/kg) par injection intra-péritonéale, avec un anesthésique local Lidocaïne (2mg/kg) au niveau de l'ouverture et un antidouleur Buprénorphine en sous-cutanée.

Le plasmide a été produit par clonage du gène *Pde2a* dans un plasmide contenant le promoteur du gène *Cdk5*, permettant l'expression spécifique dans les neurones, et le gène codant pour la protéine GFP, transfété dans des bactéries Stbl2 (ThermoFischer). La solution finale de plasmide à 1µg/µl contenant du tampon endo-free TE et du colorant fast-green 1X est injectée dans un des deux ventricules de l'embryon par micro-injecteur. Le plasmide *Cdk5-GFP* est électroporé dans les mêmes conditions comme contrôle. La mère est ensuite sacrifiée et les embryons récupérés au stade E17.5, 72h plus tard.

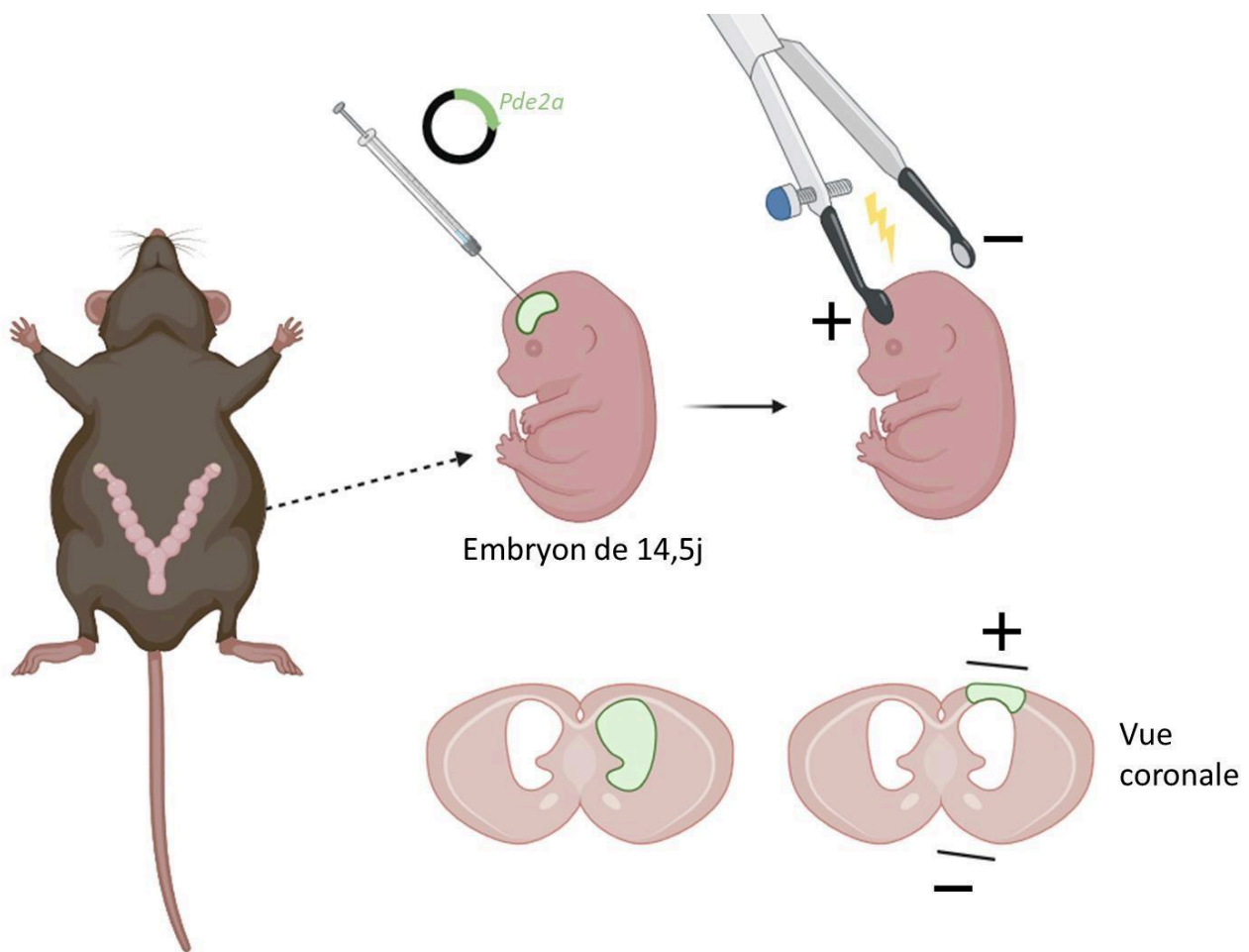


Figure 8. Protocole d'électroporation *in utero*. Après injection de la solution contenant le plasmide et le Fast Green dans un des ventricules, les embryons sont électroporés avec les électrodes d'une façon à cibler les couches corticales, comme présenté ici.

7. Immunohistochimie :

Les cerveaux perfusés en PFA 4% de souris de 13 jours et les cerveaux des embryons issus de l'EIU ayant passés 24h en PAF 4% ont été coupés au vibratome en tranches de 40 μ m.

En fluorescence : Les coupes flottantes sont initialement placées 5 minutes dans du NH₄Cl puis perméabilisées dans du Triton 0.3%/PBS pendant 10 minutes à température ambiante. Elles sont ensuite saturées pendant 2 heures dans 2.5% Goat

Serum/PBS (Blocking) puis incubées sur la nuit à 4°C avec l'anticorps primaire. Du True Black1X en EtOH 70% est mis sur les coupes pendant 10 minutes. Après lavages au PBS, les coupes sont ensuite incubées avec l'anticorps secondaires pendant 2 heures à température ambiante et les noyaux sont marqués au DAPI (1 :1000) pendant 10 minutes. Les anticorps utilisés dans cette étude sont : anti-CUX1 (Millipore, 1 :200), anti-Ctip2 (Abcam, 1 :200) et anticorps secondaires conjugués-Alexa594 (1 :200).

En visible : Après perméabilisation identique, les coupes flottantes sont placées dans du PBS/0.3%H₂O₂ pour bloquer les peroxydases endogènes, puis dans la solution de Blocking et incubées avec l'anticorps primaire anti-GFP (Invitrogen, 1 :1000) sur la nuit à 4°C. Les coupes sont ensuite incubées dans la solution GAR-HRP (DAKO) pendant 30 minutes. Les coupes sont enfin plongées une à une dans la solution de révélation DAKO liquid DAB afin de chronométrier le temps de coloration. Seules les coupes marquées sont ensuite montées sur lames.

Analyse par macro sur Fuji (ImageJ) créée par F. Brau de la plateforme imagerie de l'IPMC. La macro segmente le cortex en dix sections égales et compte le nombre de cellules marquées par section en fluorescence, ou compte l'intensité en enlevant le fond en visible (coupes issues de l'EIU).

8. Statistiques :

Les datas sont analysées par Two-Way Anova avec comme facteurs les différents génotypes et/ou le traitement. Les datas de caractérisation de la lignée *Pde2a^{+/−}* sont analysées par t-test paramétrique quand le nombre de valeurs est suffisant et suivant une loi normale, non-paramétrique sinon. Les datas sont exprimées en moyenne ± SEM. Les tests statistiques appropriés pour chaque expérimentation sont décrits dans les légendes des figures correspondantes. Les analyses statistiques et les figures ont été réalisées sur GraphPad Prism version 6.0.

Résultats

I. Effet d'un traitement aigu et chronique en Bay 60-7550 sur les souris

Fmr1 KO

A mon arrivée dans le laboratoire, l'ARNm de *Pde2a* a été identifié comme cible de FMRP à un moment clé du développement neuronal, tandis que PDE2A est surexprimé dans le cerveau des *Fmr1* KO. Les bénéfices de l'inhibition pharmacologique de PDE2A sur les phénotypes *in vitro* et *ex vivo* du modèle murin du SXF ont pu être montrés par la suite. En effet, le traitement au Bay 60-7550 rétablit la morphologie neuronale, axonale et des épines dendritiques, et la LTD dépendant des mGluR exagérée chez le *Fmr1* KO (voir Publication 1). Pour aller plus loin, nous avons voulu caractériser l'effet du Bay 60-7550 sur les déficits comportementaux des souris *Fmr1* KO, à savoir un déficit de discrimination sociale dans le test du Homing, et une diminution de l'interaction sociale à l'adolescence, d'une façon semblable aux patients SXF. La dose de Bay 60-7550 utilisée a été choisie en amont lors de tests de vocalisations ultrasoniques (USVs) pour avoir une dose sans effet chez les souris WT.

J'ai pu montrer que l'inhibition de PDE2A par une injection intra-péritonéale unique de Bay 60-7550 améliore les performances des souriceaux *Fmr1* KO de 13 jours lors du test du Homing, au niveau de la latence et du temps passé dans la litière d'origine (Fig.9A-B). De façon intéressante, les performances des souriceaux WT ne sont pas altérées par le traitement. A l'inverse, cette injection unique n'a pas permis de rétablir de façon significative les déficits d'interaction sociale des souris *Fmr1* KO d'un mois (Fig.9C).

J'ai traité de façon chronique avec le Bay 60-7550 les souris du 5^{ème} au 21^{ème} jour après la naissance et testé leurs capacités sociales après un intervalle de 9 jour sans traitement. Cette période de traitement choisie se situe autour du pic d'expression de FMRP et de la synaptogénèse, et correspond à une période de développement chez les

enfants SXF quand les premiers symptômes apparaissent. Ce traitement chronique permet de rétablir les déficits d'interaction sociale des souris *Fmr1* KO (Fig.9D), sans avoir d'effet sur les souris WT, montrant que l'inhibition précoce et chronique de PDE2A a des effets sur le long terme spécifiquement sur le phénotype SXF.

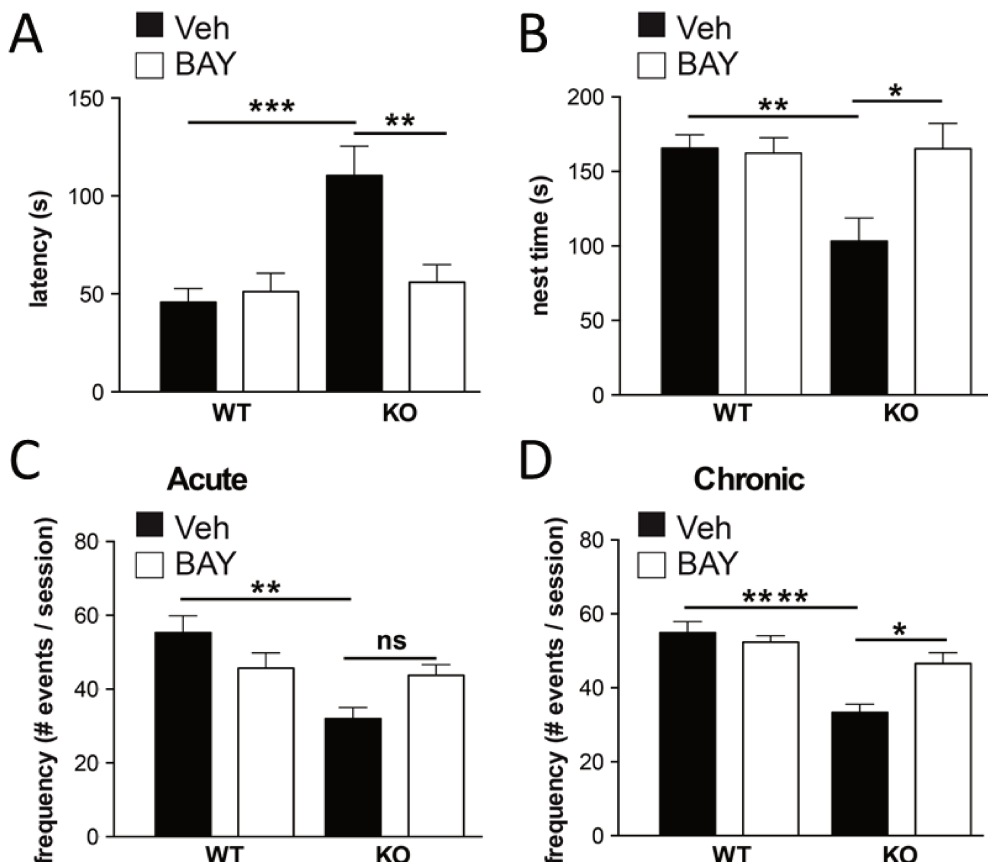


Figure 9. L'inhibition de la PDE2A rétablit les déficits du comportement social des souris *Fmr1* KO. A) Les souris *Fmr1* KO mettent plus de temps à rejoindre la litière de leur cage d'origine ($F_{genotype(1,45)}=11.79$, $P=0.001$; $F_{treatment(1,45)}=5.86$, $P=0.02$; $F_{genotypextreatment(1,45)}=8.81$, $P=0.005$) et B) passent moins de temps dans cette zone ($F_{genotype(1,45)}=5.51$, $P=0.02$; $F_{treatment(1,45)}=5.37$, $P=0.02$; $F_{genotypextreatment(1,45)}=6.63$, $P=0.013$) dans le test du homing à P14 (n : WT-Veh = 14 ; WT-Bay = 16 ; KO-Veh = 9 ; KO-Bay = 10). Ces deux déficits sont normalisés chez les souris *Fmr1* KO traitées au Bay 60-7550. L'interaction sociale a été évaluée à P30 C) avec un traitement unique ($F_{genotype(1,57)}=7.53$, $P=0.008$; $F_{treatment(1,57)}=0.05$, $P=0.82$; $F_{genotypextreatment(1,57)}=5.43$, $P=0.02$) (n : WT-Veh = 18 ; WT-Bay = 22 ; KO-Veh = 12 ; KO-Bay = 9) et D) un traitement chronique ($F_{genotype(1,36)}=28.71$, $P<0.0001$; $F_{treatment(1,36)}=4.358$, $P=0.0440$; $F_{genotypextreatment(1,36)}=9.539$, $P=0.0039$) (n : WT-Veh = 11 ; WT-Bay = 14 ; KO-Veh = 8 ; KO-Bay = 7). Les datas sont représentées en moyenne ± SEM (adjusted P value : *P<0.05, **P<0.01, ***P<0.001). Le Two-way ANOVA puis le test post hoc Tukey de comparaison multiple ont été utilisés.

Enfin, par la technique du Golgi Staining (Du, 2019), j'ai pu analyser l'effet du traitement chronique et précoce du Bay 60-7550 sur la morphologie des épines dendritiques dans la région CA1 de l'hippocampe. Le traitement permet de rétablir la longueur anormale des épines dendritiques chez les souris *Fmr1* KO de 3 mois de sur le long terme (Fig.10).

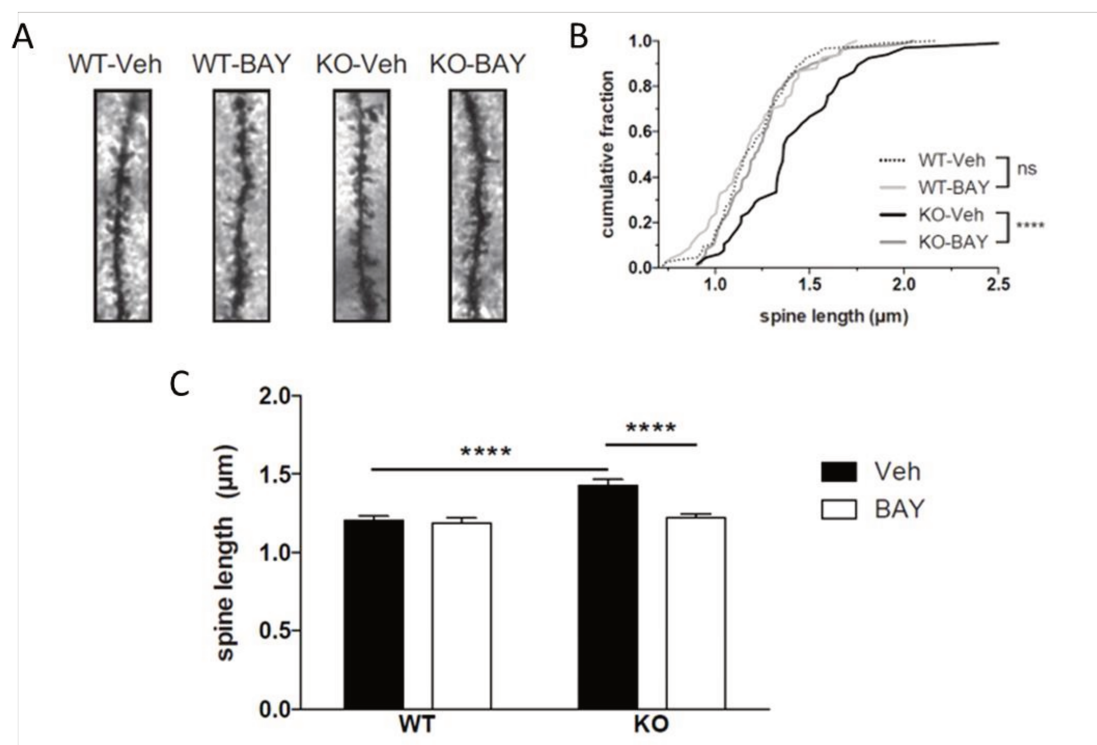


Figure 10. L'inhibition chronique et précoce de PDE2A améliore la maturation des épines dendritiques dans l'hippocampe. A) Photos représentatives de la région CA1 de l'hippocampe de chaque groupe qui ont été marqués au Golgi Staining. Les tranches de cerveau provenant de 3 animaux de chaque condition ont été analysées. La longueur des épines a été analysée sur ImageJ avec une macro maison B) L'effet du traitement sur la distribution cumulative de la longueur des épines a été analysé par le test Kolmogorov-Smirnov (nombre d'épines : WT-Veh $n=118$; WT-Bay $n=67$; KO-Veh $n=64$; KO-Bay $n=142$) ($****: p<0,0001$; n.s.: not significant). C) Moyenne de la longueur des épines dendritiques \pm SEM, analysée par Two-way ANOVA ($F_{genotype(1,313)}=19.86$, $P<0.0001$; $F_{treatment(1,313)}=14.84$, $p=0,0001$; $F_{genotype \times treatment(1,313)}=10.56$; $p=0.0013$) ($****adjusted P < 0.0001$).

II. Rôle de la PDE2A dans la migration corticale au stade embryonnaire

Afin de comprendre l'implication éventuelle de la surexpression PDE2A dans l'altération de la migration corticale chez les souris *Fmr1* KO, j'ai réalisé des électroporations *in utero* sur des embryons de souris de 14.5 jours avec un plasmide cdk5-GFP, permettant une expression neuronale spécifique, dont j'ai intégré l'ADN de PDE2A. Cela me permet donc de mimer la surexpression de PDE2A retrouvée dans notre modèle *Fmr1* KO, tout en s'affranchissant de toutes les autres altérations moléculaires liées à l'absence de FMRP.

Après récupération des cerveaux à E17.5 et marquage de la GFP par immunohistochimie en visible sur les coupes, j'ai quantifié la migration des neurones électroporés au travers du cortex. La surexpression de PDE2A par le plasmide ralentit la migration corticale radiale des neurones par rapport aux neurones électroporés avec le plasmide contrôle, notamment de façon significative sur les couches corticales supérieures (Fig.11).

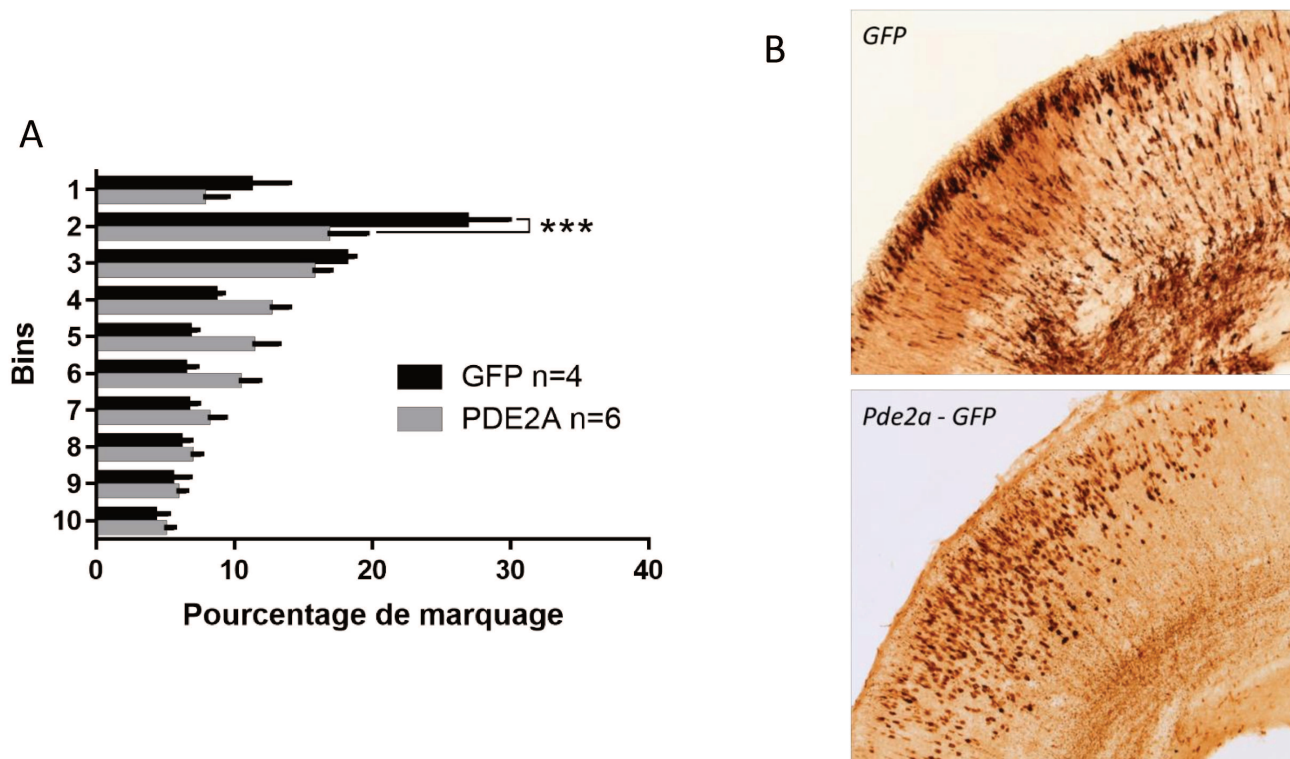


Figure 11. La surexpression de PDE2A ralentit la migration corticale des neurones électroporés. (A) Fréquence de distribution des neurones électroporés par pourcentage de marquage dans le cortex divisé en 10 segments. (B) Images représentatives des coupes de cerveau d'embryons à E17.5. Datas représentés en moyenne \pm SEM, analysés par Two-Way Anova ($F_{plasmide(9,70)} = -1.642e-013$, $P > 0.9999$; $F_{bins(9,70)} = 23$, $P < 0.0001$; $F_{interaction(9,70)} = -3.873$, $P = 0.0005$) (adjusted pvalue : *** $P < 0.0005$)(n : cdk5-GFP = 4, cdk5-Pde2a-GFP = 6).

III. Effet de la réduction génétique de PDE2A chez la souris *Fmr1* KO

1. La réduction génétique de PDE2A rétablit une partie des déficits du comportement social des souris *Fmr1* KO

Afin de montrer l'importance de la PDE2A dans le phénotype de nos souris *Fmr1* KO, j'ai entrepris le croisement entre ces souris et une nouvelle lignée *Pde2a^{+/−}*, afin de réduire génétiquement l'activité de la PDE2A, qui est surexprimé dans le modèle du SXF. Je me suis d'abord intéressé à l'impact de ce croisement sur le comportement social de nos souris.

Lors du test du Homing, la réduction génétique de PDE2A chez les sourceaux double mutants *Fmr1* KO x *Pde2a^{+/−}* ne permet pas de rétablir les déficits de discrimination sociale présents chez les sourceaux *Fmr1* KO, mettant significativement plus de temps à retrouver la litière d'origine que les WT (Fig.12A). De plus, les sourceaux *Pde2a^{+/−}* ne semblent pas avoir de phénotype particulier lors de ce test.

En ce qui concerne les interactions sociales à l'adolescence, lors du test du jeu social, les souris *Fmr1* KO x *Pde2a^{+/−}* vont établir un nombre d'interactions similaires à celui des souris WT (Fig.12B). La réduction génétique de PDE2A chez ces souris permet donc de rétablir les déficits de comportement social des souris *Fmr1* KO. De façon intéressante, dans ce test les souris *Pde2a^{+/−}* présentent un défaut d'interaction, similaire aux souris *Fmr1* KO. Un niveau trop ou peu élevé de PDE2A est donc associé à un déficit de comportement social à l'adolescence.

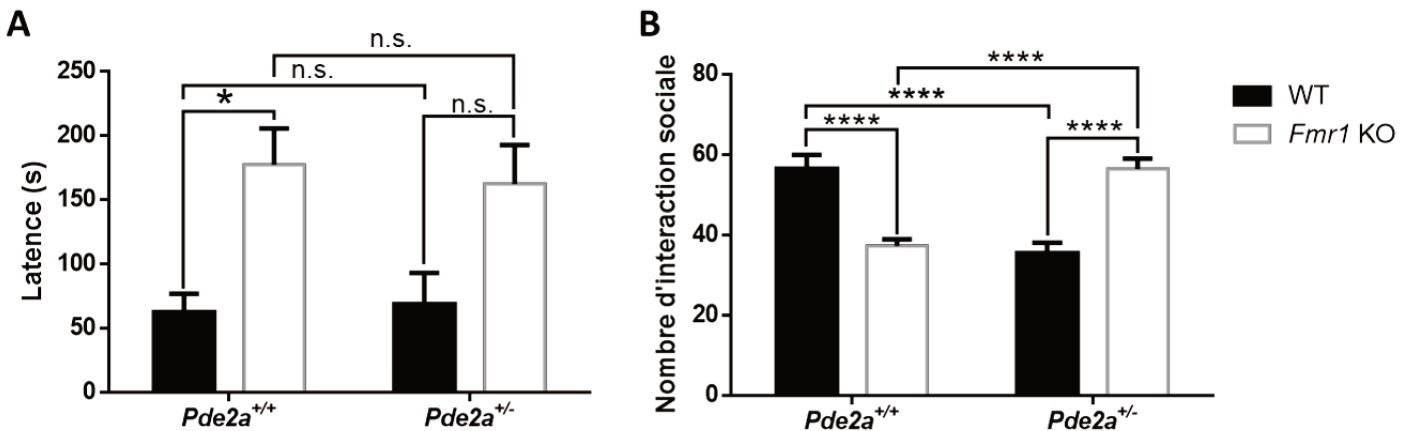


Figure 12. Rôle de la PDE2A dans le comportement social des souris Fmr1 KO et Pde2a+/-.
(A) La réduction génétique de PDE2A chez la souris Fmr1 KO ne rétablit pas les déficits de discrimination sociale dans le test du Homing ($F_{genotypeFmr1(1,50)}=12.42$, $P=0.0009$; $F_{genotypePde2a(1,50)}=0.02316$, $P=0.8797$; $F_{interaction(1,50)}=0.1311$, $P=0.7189$) (n : WT = 10 ; Fmr1 KO = 19 ; Pde2a+/- = 10 ; Fmr1 KO x Pde2a+/- = 15). **(B)** Les souris Fmr1 KO x Pde2a+/- performance de façon similaire au WT lors du test du jeu social, tandis que les souris Pde2a+/- ont des déficits d'interaction sociale similaires aux Fmr1 KO ($F_{genotypeFmr1(1,66)}=0.1327$, $P=0.7169$; $F_{genotypePde2a(1,66)}=0.1081$, $P=0.7433$; $F_{interaction(1,66)}=64.05$, $P<0.0001$) (n : WT = 15 ; Fmr1 KO = 22 ; Pde2a+/- = 15 ; Fmr1 KO x Pde2a+/- = 18). Datas présentés en moyenne ± SEM (adjusted P value : * $P<0.05$, *** $P<0.0001$), analysés par Two-Way Anova et comparaison multiple de Tukey en post hoc.

2. Rétablissement de la reconnaissance du nouvel objet par la réduction de PDE2A dans le double mutant

Par la suite, les performances cognitives de ces souris à l'âge adulte ont été caractérisées par le test de la reconnaissance du nouvel objet, couramment utilisé pour montrer les déficits des souris Fmr1 KO. Après deux jours d'habituation de 10 minutes dans l'arène du test, les souris y sont remises le troisième jour en présence de deux objets identiques à explorer pendant 10 minutes. Après un intervalle de 5 minutes, la souris est replacée dans son arène avec un des deux objets changé par un autre différent, et sa mémoire à court terme est donc testée avec cet intervalle. Le comportement curieux et exploratoire normal des souris va les amener à préférer le nouvel objet lors de la phase de test. Les souris Fmr1 KO ont des déficits de reconnaissance du nouvel objet profond, ne préférant pas un objet à l'autre,

contrairement aux WT (Fig.13). La réduction de PDE2A chez les *Fmr1* KO (*Fmr1* KO x *Pde2a^{+/−}*) permet de rétablir significativement ces déficits. Lors de ce test, de façon concordante avec le comportement social, les souris *Pde2a^{+/−}* présentent elles aussi des déficits lors de ce test, en reconnaissant le nouvel objet aussi mal que les souris *Fmr1* KO. Le niveau d'expression de PDE2A, qu'il soit plus faible ou plus fort par rapport à la normale, engendre donc des déficits lors de cette tâche faisant appel à la mémoire à court terme.

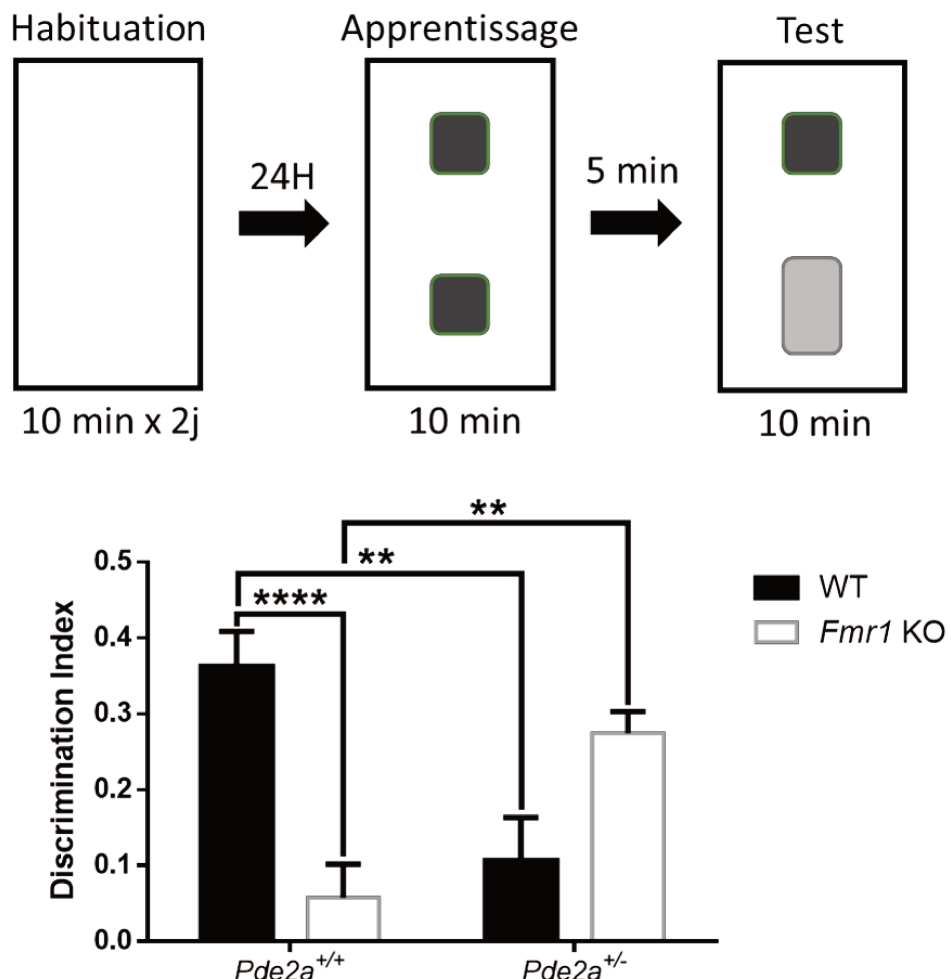


Figure 13. Rôle de la PDE2A lors du test de la reconnaissance d'un nouvel objet. La réduction génétique de PDE2A permet de rétablir la mémoire à court terme des souris *Fmr1* KO x *Pde2a^{+/−}* lors de ce test. Les souris *Pde2a^{+/−}* ont un déficit lors de ce test similaire aux souris *Fmr1* KO ($F_{genotype\ Fmr1(1,37)}=2.434$, $P=0.1272$; $F_{genotype\ Pde2a(1,37)}=0.1969$, $P=0.6598$; $F_{interaction(1,37)}=28.69$, $P<0.0001$) (n : WT = 12 ; *Fmr1* KO = 9 ; *Pde2a^{+/−}* = 8 ; *Fmr1* KO x *Pde2a^{+/−}* = 12). Données présentées en moyenne \pm SEM (adjusted P value : ** $P<0.01$, **** $P<0.0001$), analysées par Two-Way Anova et comparaison multiple de Tukey en post hoc.

IV. Caractérisation de la lignée *Pde2a^{+/}*-

1. Le comportement social, cognitif et anxieux est altéré chez les souris *Pde2a^{+/}*-

Etant donné les précédents résultats obtenus sur les souris *Pde2a^{+/}*-, j'ai voulu caractériser de façon plus précise les déficits comportementaux de ces souris. Les animaux ont donc passé une batterie de test de comportement social, cognitif et d'anxiété en plus de ceux précédemment présentés.

Tout d'abord, il m'a semblé important de caractériser les vocalisations ultrasoniques des sourceaux *Pde2a^{+/}* étant donné les résultats précédents sur les déficits d'interactions sociales de cette lignée. En effet, les déficits de communication sociale font aussi partie des troubles caractéristiques des TSA et sont donc pertinent dans la caractérisation comportementale de cette lignée en tant que possible nouveau modèle de maladie du neurodéveloppement. Lors de la mesure des vocalisations à P10, il apparaît que les sourceaux *Pde2a^{+/}* émettent près de deux fois moins de vocalisations ultra-soniques par rapport aux WT quand ils sont séparés de leur mère (Fig.14A). Ces souris présentent donc une diminution de la communication sociale à un stade du développement précoce, en plus des déficits d'interaction sociale précédemment décrits à l'adolescence.

Le test de la reconnaissance du nouvel objet (NOR) a été reconduit, avec cette fois un intervalle de temps d'une heure, une tâche plus complexe pour les souris faisant appel à la mémoire à long terme. Les souris *Pde2a^{+/}* discriminent encore une fois moins bien le nouvel objet que les souris WT (Fig.14B).

Enfin, je me suis intéressé au comportement d'adaptation à un nouvel environnement anxiogène chez ces souris, étant donné la dominance de ce type de trouble chez les patients atteints de TSA ou d'autres NDD. Lors du test du Zero Maze élevé, les souris *Pde2a^{+/}* mettent plus de temps à sortir du bras fermé pour la première

fois que les souris WT. Cependant, malgré une certaine tendance, elles ne passent pas significativement moins de temps dans les bras ouverts par la suite (Fig.14C).

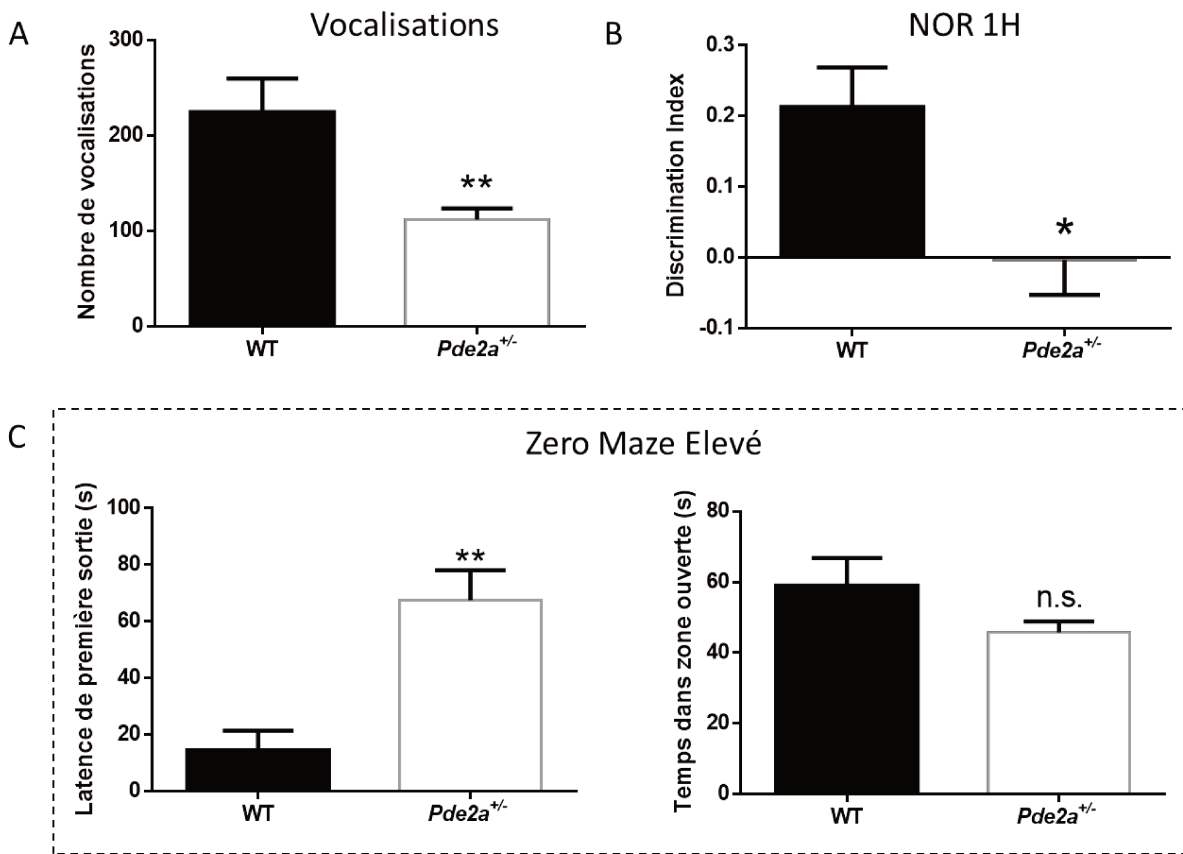


Figure 14. Les souris *Pde2a^{+/-}* présentent un phénotype comportemental altéré. A) Les souris *Pde2a^{+/-}* émettent moins de vocalisation quand ils sont enlevés de leur nid à P10. Datas analysés par t test (** $P=0.007$) (n : WT=14, *Pde2a^{+/-}* = 13). (B) Lors du test de la reconnaissance du nouvel objet avec une heure d'intervalle entre l'apprentissage et le test, les souris *Pde2a^{+/-}* ne discriminent pas le nouvel objet de l'ancien. Datas analysées par test de Mann et Whitney (* $P=0.0140$) (n : WT = 7, *Pde2a^{+/-}* = 6). (C) Les souris *Pde2a^{+/-}* mettent plus de temps à sortir du bras fermé du Zero Maze pour la première fois. Datas analysées par test de Mann et Whitney (** $P=0.0012$; n.s. : non significatif) (n : WT = 7, *Pde2a^{+/-}* = 10). Datas présentées en moyenne \pm SEM.

2. La mémoire spatiale des souris *Pde2a^{+/-}* n'est pas altérée lors du MWM

Etant donné les déficits de mémoire lors du test de la reconnaissance d'un nouvel objet des souris *Pde2a^{+/-}*, j'ai voulu caractériser leur performance lors du test de la piscine de Morris (MWM) impliquant la mémoire spatiale dépendant de

l'hippocampe. Lors du premier jour de la Cue Task, évaluant la latence de retour à la plateforme visible, les souris *Pde2a^{+/−}* mettent significativement plus de temps à atteindre la plateforme (Fig.15A). Cette différence n'est plus visible au deuxième jour. Pendant les quatre jours de la phase d'apprentissage, les deux lignées performent de la même façon, en réduisant leur temps de retour à la plateforme invisible (Fig.15B), en s'aidant des indices visuels (Fig15D). Enfin, lors du Probe Test, durant lequel la plateforme est enlevée, les souris WT et *Pde2a^{+/−}* discriminent de la même façon le quadrant correct des autres (Fig.15C).

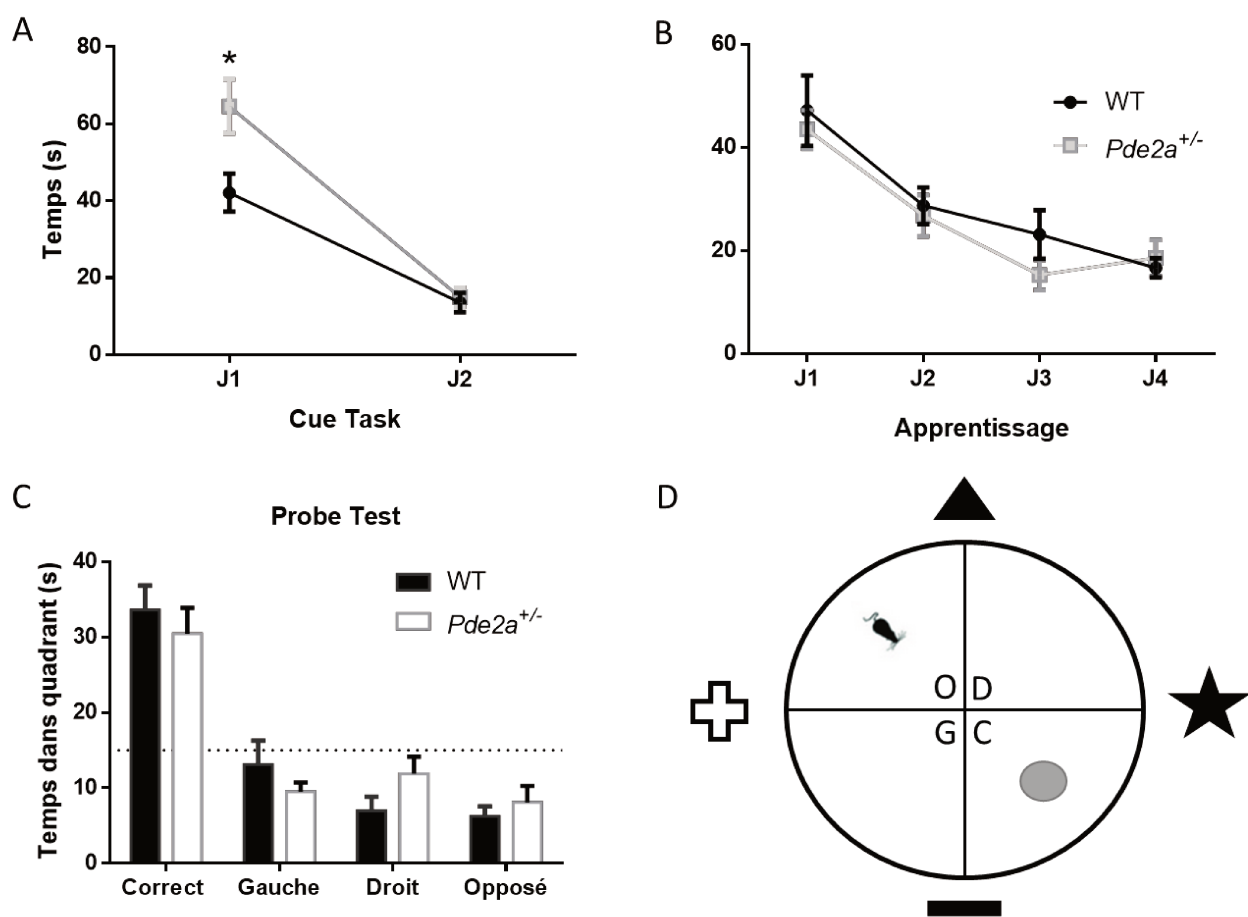


Figure 15. Résultats préliminaires du test du MWM ($n : WT=8, Pde2a^{+/−}=11$) (A-B) Données représentant la moyenne des temps de latence pour retrouver la plateforme des quatre essais par jour lors de la Cue Task et de la phase d'apprentissage. (C) Histogramme représentant le temps moyen passé dans chaque quadrant par chaque lignée en cherchant la plateforme ayant été enlevée pendant 60s. La ligne en pointillée représente le niveau de chance d'être dans le quadrant (60s divisé par 4 quadrants = 15s) (D) Représentation des quadrants de la piscine, l'emplacement de la plateforme immergée lors de la phase d'apprentissage (en gris) et des indices visuels. Données représentées en moyenne \pm SEM, analysées par Two-Way Anova (adjusted p-value : * $p=0.012$)

3. Rôle de la PDE2A dans la croissance du premier neurite des neurones corticaux en culture

Les niveaux d'AMPc et de GMPc sont étroitement liés dans la croissance axonale, le devenir d'un neurite en axone ou dendrite et le devenir du neurone en neurone inhibiteur ou excitateur (Averaimo and Nicol, 2014). Afin de connaître le rôle de PDE2A dans ces phénomènes, j'ai mesuré la taille du premier neurite, prolongement primaire de neurones corticaux en culture pendant 48h, par immunocytochimie (Fig.16A). Une culture par cerveau d'embryon a été faite et génotypée par la suite. Dans les cultures de neurones *Pde2a^{+/-}*, les neurites sont significativement plus longs que ceux des neurones WT (Fig.16B). J'ai pu vérifier la forte diminution d'expression de PDE2A dans les neurones corticaux des embryons *Pde2a^{+/-}* à E14.5 (Fig.16C-D), avant ensemencement en culture. La quantité de PDE2A est donc associée à la croissance des neurites.

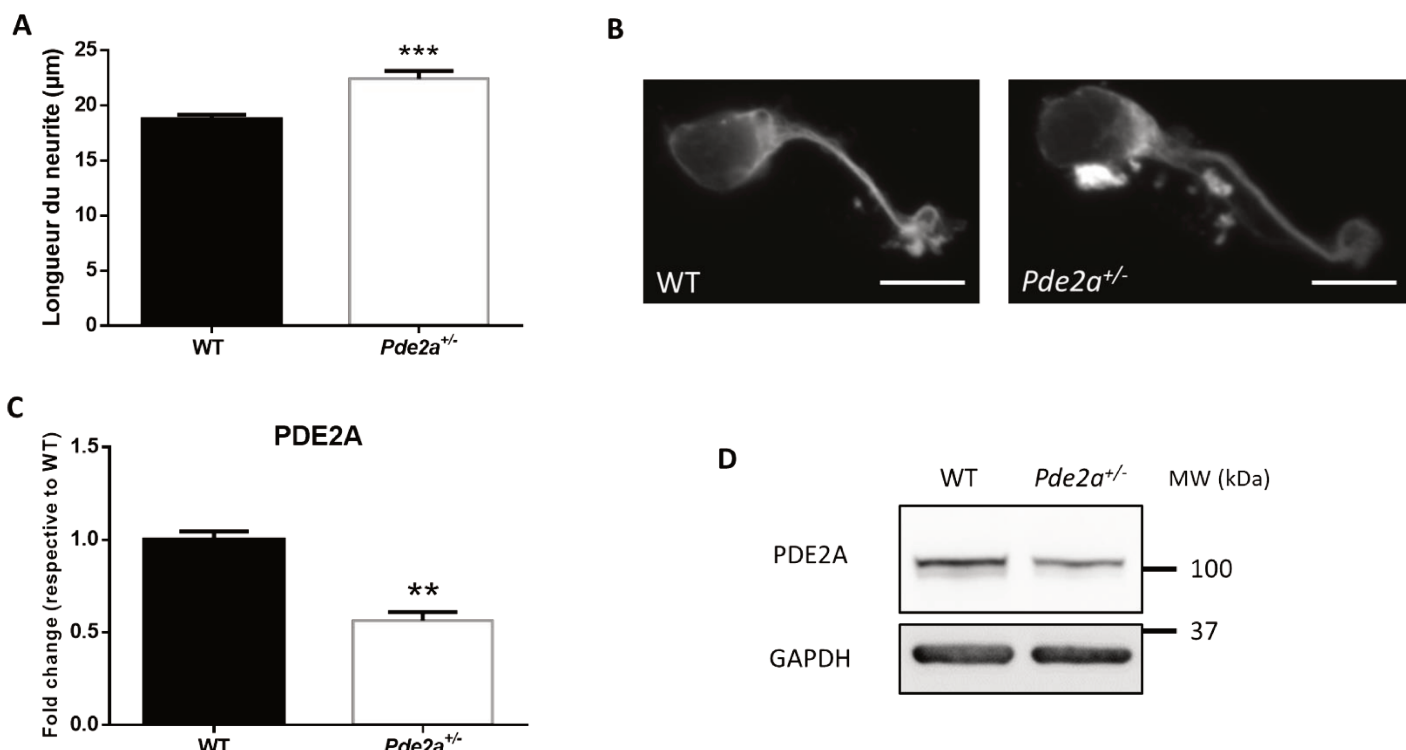


Figure 16. La quantité de PDE2A est corrélée à la croissance des neurites. (A) Histogramme de la longueur du neurite des neurones corticaux WT et *Pde2a^{+/-}* en culture à 2DIV. (Nombre d'embryons : WT=14, *Pde2a^{+/-}*=13 ; une culture par embryon ; entre 116 et 228 neurites mesurés par culture) (B) Images représentatives de neurones corticaux WT et *Pde2a^{+/-}* à 2DIV.

*Barre d'échelle : 10µm (C) Quantification de l'expression de PDE2A par rapport à GAPDH (n : WT=4, *Pde2a^{+/-}*=4) (D) Western Blot montrant la quantité de PDE2A dans un lysat de neurones corticaux au stade embryonnaire E14.5 avant mis en culture. Datas représentées en moyenne ± SEM, analysés par (A) t test et (C) Mann-Whitney test (adjusted p value : **P<0.01, ***P<0.001).*

4. Le positionnement des couches corticales est inchangé chez les souris

Pde2a^{+/-}

En prenant en compte mes résultats obtenus avec la surexpression de PDE2A dans la migration corticale (Fig.11), j'ai voulu quantifier l'impact de la réduction génétique de PDE2A sur l'agencement final des couches corticales. J'ai pour cela marqué sur des tranches de cerveau WT et *Pde2a^{+/-}* par immunohistochimie les couches corticales II et IV par CUX1 et la couche V par Ctip2 (Fig.17B et D). Le cortex est divisé en dix segments identiques et le nombre de cellules marquées est comptabilisé. Aucune différence n'a pu être quantifiée entre les deux génotypes sur le positionnement des différentes couches marquées à ce stade du développement (Fig.17A et C).

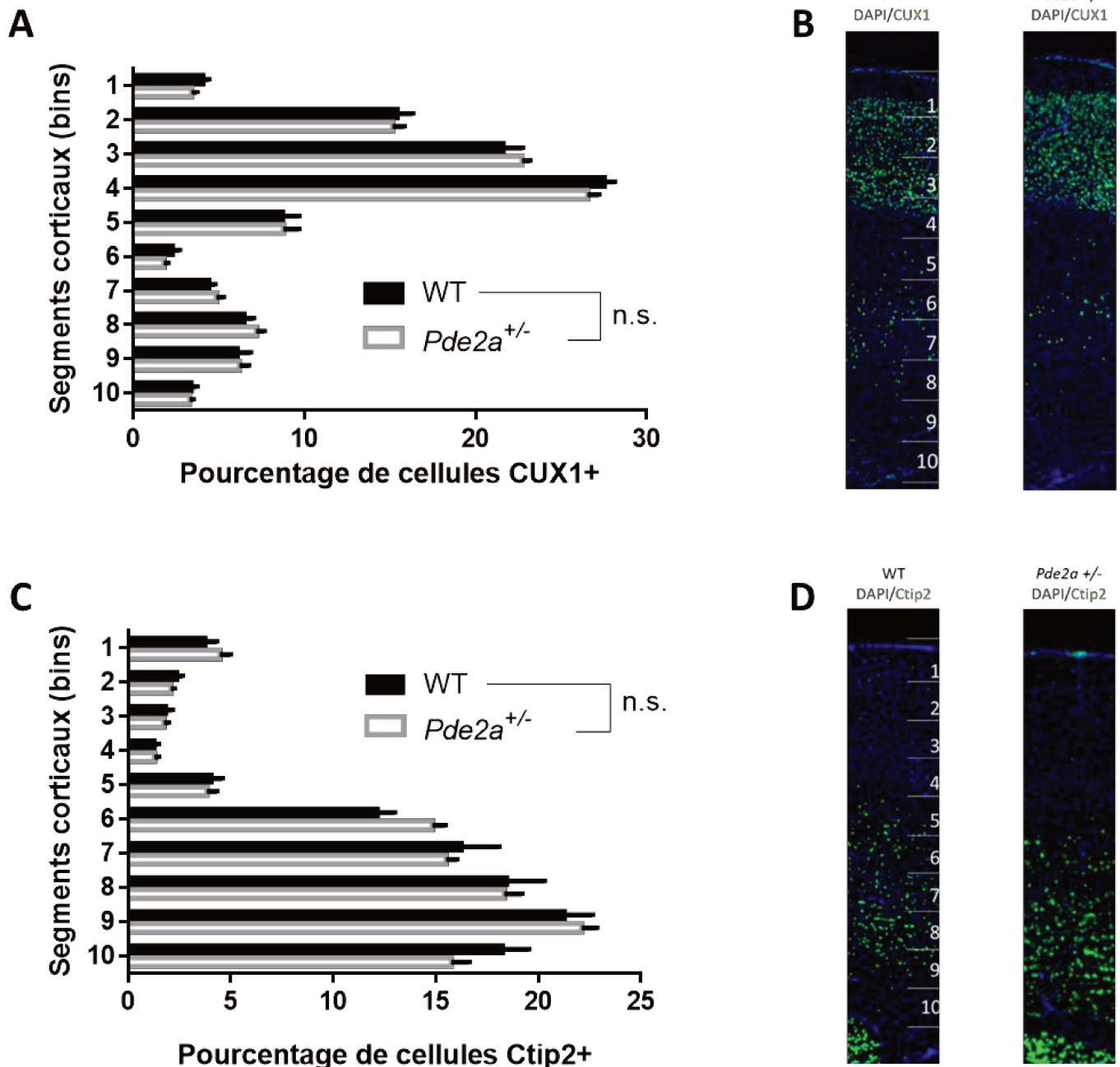


Figure 17. PDE2A n'est pas impliqué dans le positionnement des couches corticales à P13. Fréquence de distribution des cellules CUX1+ (A), marqueur des couches corticales II et IV, et des cellules Ctip2+ (B), marqueur de la couche V, dans le cortex divisé en dix segments égaux de souris WT ($n=7$) et *Pde2a^{+/-}* ($n=9$). Données représentées en moyenne \pm SEM, analysés par TwoWay Anova (A) ($F_{genotype(1,140)}=6.199e-0.13$, $P>0.9999$; $F_{bins(9,140)}=399$, $P<0.0001$; $F_{interaction(9,140)}=0.5512$, $P=0.8347$) (C) ($F_{genotype(1,130)}=4.044e-0.12$, $P>0.9999$; $F_{bins(9,130)}=205.7$, $P<0.0001$; $F_{interaction(9,130)}=1.370$, $P=0.2091$) (B) et (D) Images représentatives montrant la distribution des neurones marqués CUX1 ou Ctip2 dans le cortex.

5. Les souris *Pde2a^{+/−}* ont une LTD mGluR-dépendant fortement altérée

L'inhibition de PDE2A par le Bay 60-7550 rétablit la LTD mGluR-dépendante exagérée dans la région CA1 de l'hippocampe des souris *Fmr1* KO (Maurin et al., 2019b). Ceci indique clairement l'implication de l'AMPc et/ou du GMPc dans cette forme de plasticité synaptique. Nous nous sommes donc intéressés, en collaboration avec la société EphyScience, à l'impact de la réduction génétique sur la réponse électrophysiologique à l'induction de la LTD. Le potentiel post-synaptique d'excitation (field excitatory post-synaptic potential, fEPSP) de neurones pyramidaux de la région CA1 de l'hippocampe a été enregistré après stimulation électrique par électrode. La pente de ce potentiel est mesurée à chaque intensité de simulation afin de caractériser la transmission synaptique basal dans un premier temps. Aucune différence significative de la transmission basale entre les deux génotypes n'a pu être mise en évidence (Fig.18A).

A l'inverse, l'application de DHPG (100µM, 5min), un agoniste des mGluRs de groupe I et V, induit une LTD significativement plus faible dans les tranches d'hippocampes des souris *Pde2a^{+/−}* comparé aux souris WT (Fig.18B-C).

Par western blot et l'utilisation d'anticorps ciblant les récepteurs mGluR5, je me suis intéressé à l'expression de ces récepteurs et leur dimérisation dans ces deux lignées. Mes résultats préliminaires suggèrent que la dimérisation des mGluR5 serait altérée dans l'hippocampe des souris *Pde2a^{+/−}* (Fig.19), pouvant expliquer la résistance à l'induction de LTD par le DHPG.

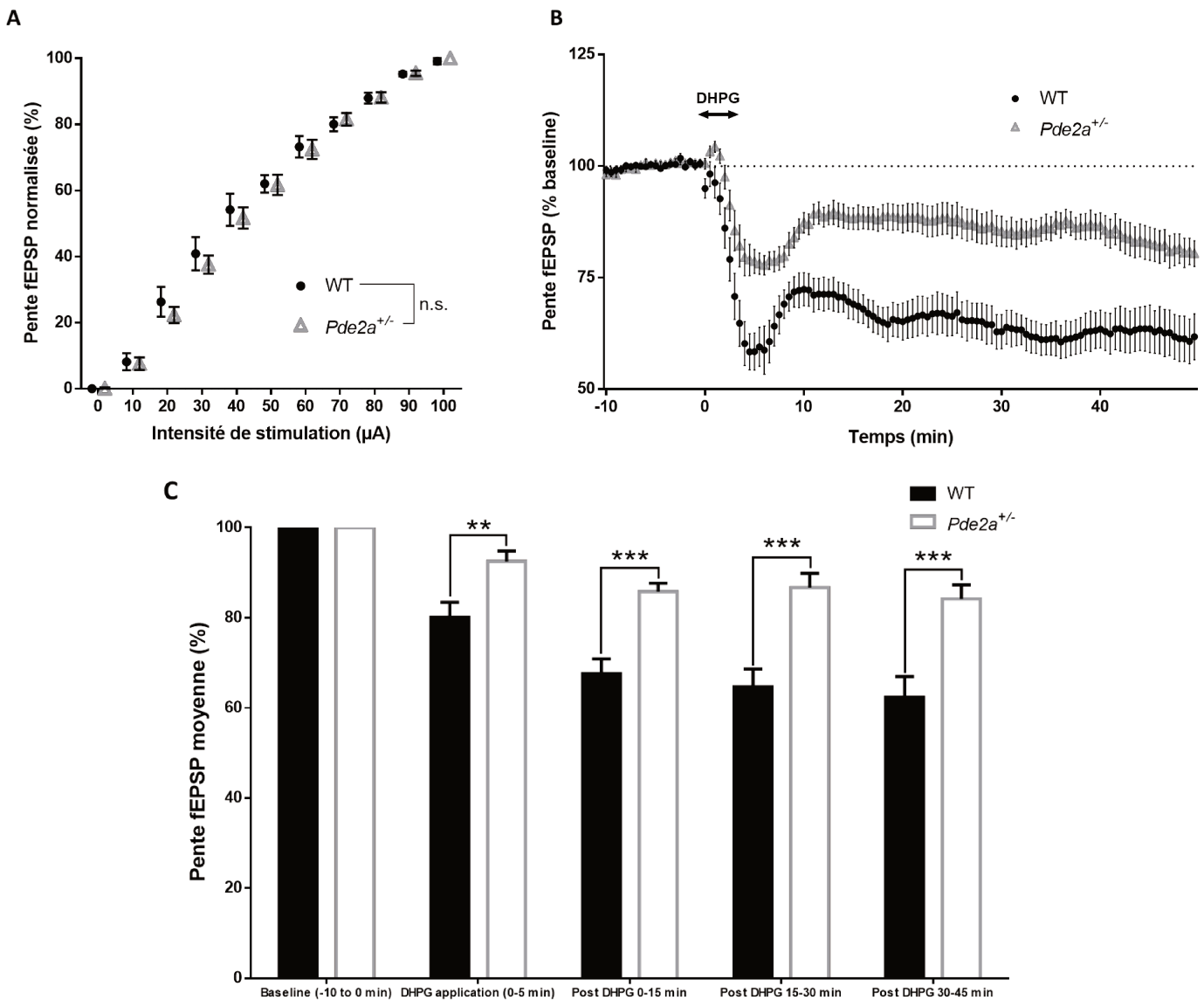


Figure 18. Les souris $Pde2a^{+/-}$ présentent une LTD mGluR-dépendant diminuée dans la région CA1 de l'hippocampe, sans avoir une différence de transmission synaptique basale. (A) Pente fEPSP normalisée en réponse à différentes intensités de stimulation. Données représentées en moyenne \pm SEM, normalisées par rapport à la valeur maximale, analysées par Two-way Anova et comparaison multiple de Sidak (n : WT=10, $Pde2a^{+/-}$ =10) ($F_{genotype}(1,198)=0.4322$, $P=0.5117$; $F_{intensité}(10,198)=347.6$, $P<0.0001$; $F_{interaction}(10,198)=0.2266$, $P=0.9935$) (B) Evolution au cours du temps de la pente fEPSP en réponse à l'induction de la LTP par 100 μ M de DHPG pendant 5 minutes, normalisée par rapport à la valeur basale. (C) Histogramme représentant la moyenne de la pente fEPSP au cours de l'expérience, avant, pendant et après l'application de DHPG. Données représentées en moyenne \pm SEM, analysées par two-tailed unpaired t test (DHPG application : **, $p=0.0066$; Post DHPG 0-15 min : ***, $p=0.0001$; Post DHPG 15-30 min : ***, $p=0.0004$; Post DHPG 30-45 min : ***, $p=0.0009$).

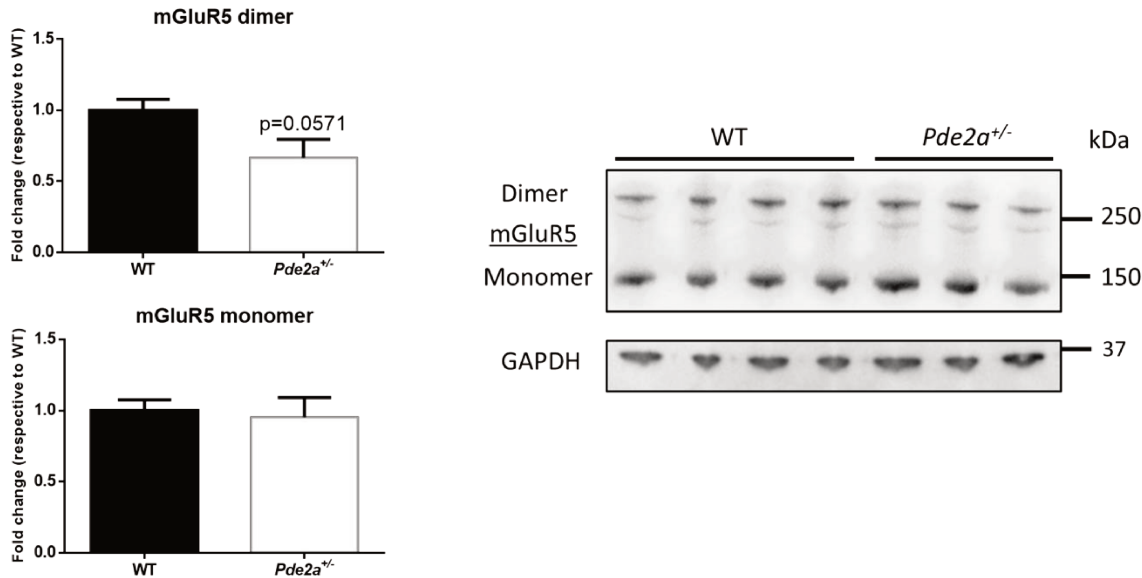


Figure 19. La dimérisation des récepteur mGluR5 semble être altérée chez les *Pde2a^{+/-}*. Quantification des formes monomères et dimères de mGluR5 dans l’hippocampe de souris WT et *Pde2a^{+/-}* d’un mois (n : WT=4, *Pde2a^{+/-}*=3). Datas représentées en moyenne \pm SEM, analysées par test de Mann et Whitney.

6. L’inactivation par phosphorylation de la kinase GSK3 β est altérée dans l’hippocampe des souris *Pde2a^{+/-}*

Afin de caractériser les effets de la réduction génétique de PDE2A sur les voies de signalisations liées à la balance AMPc/GMPc, je me suis intéressé au niveau d’inactivation de la kinases GSK3 β par western blot, par l’utilisation d’anticorps ciblant les formes phosphorylée et non phosphorylée. Cette enzyme a la particularité d’être inhibée par phosphorylation en sérine9 dépendante à la fois des niveaux d’AMPc et de GMPc. GSK3 fait ainsi partie intégrante des voies de signalisations activées par les deux seconds messagers, et peut phosphoryler un grand nombre de substrats dont CREB.

Mes premiers résultats montrent que dans l’hippocampe des souris *Pde2a^{+/-}*, GSK3 β y est moins phosphorylée par rapport aux souris WT, donc plus active (Fig.20), et que le niveau total de GSK3 β est le même entre les deux génotypes.

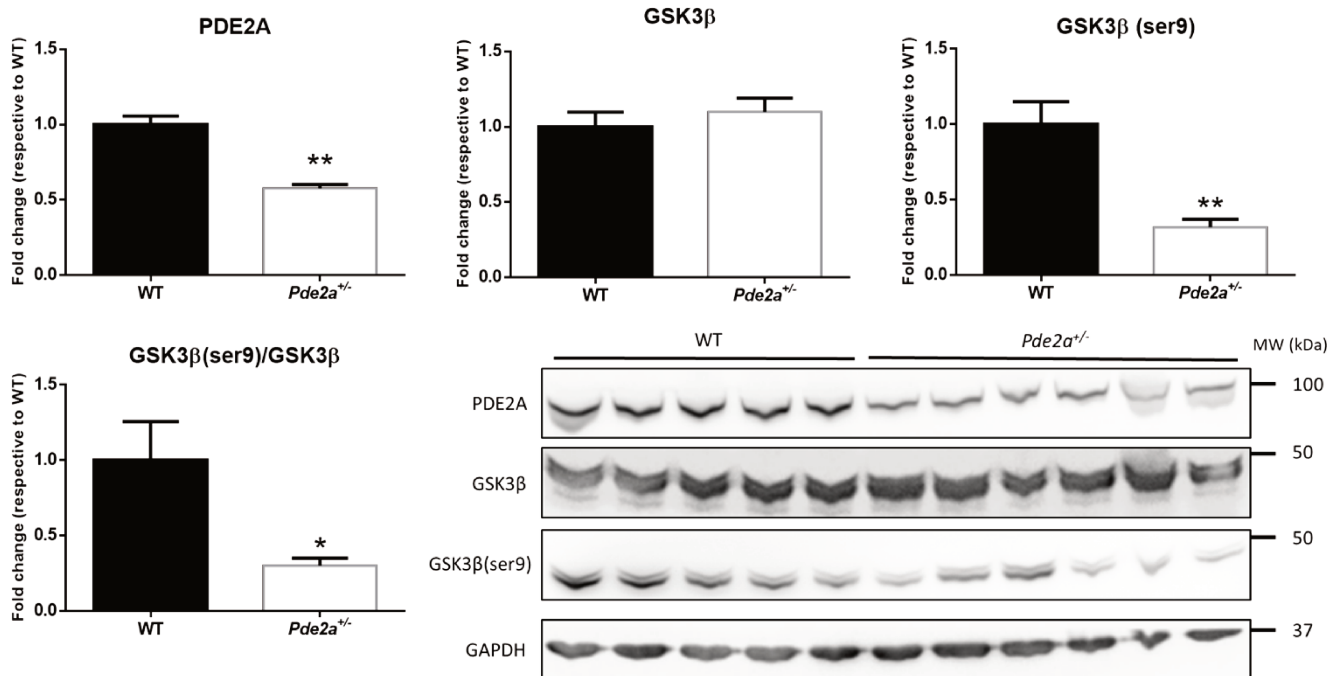


Figure 20. Le niveau de phosphorylation, et donc d'inactivation de GSK3 β est dérégulé chez les souris *Pde2a*^{+/-}. GSK3 β est hyperactive dans l'hippocampe des souris *Pde2a*^{+/-}. Datas représentées en moyenne \pm SEM, analysées par test de Mann et Whitney (*P<0.05, **P<0.01) (n : WT=5, *Pde2a*^{+/-}=6).

7. Les souris *Pde2a*^{+/-} présentent une morphologie mitochondriale altérée.

En prenant en compte la présence d'un isoforme spécifique de PDE2A dans la mitochondrie (Monterisi et al., 2020, p. 2) et la présence de morphologie altérée des mitochondries chez des patients ayant des mutations sur le gène *Pde2a* (Douummar et al., 2020), il paraît important de nous y intéresser dans le cadre de la caractérisation de la lignée *Pde2a*^{+/-}. Pour cela j'ai étudié l'expression d'un marqueur mitochondrial, COX4, et la morphologie des mitochondries par microscopie électronique dans l'hippocampe de souris âgés d'un mois.

Par western blot sur des extraits cellulaires d'hippocampe, j'ai donc pu quantifier une diminution de la présence de COX4 chez les souris *Pde2a*^{+/-} à l'âge d'un mois (Fig.21A). COX4 faisant partie de la chaîne de respiration de la mitochondrie, il en est un marqueur permettant déjà de voir une anomalie chez ces souris, que ce soit au niveau de leur nombre ou de leur forme.

Les images prises par microscopie électronique permettent d'apprécier une altération morphologique des mitochondries dans le CA1 des souris *Pde2a^{+/−}*. On peut remarquer chez les mitochondries *Pde2a^{+/−}* une altération de l'architecture des crêtes mitochondrielles et la présence de vésicules à l'intérieur (Fig.21B).

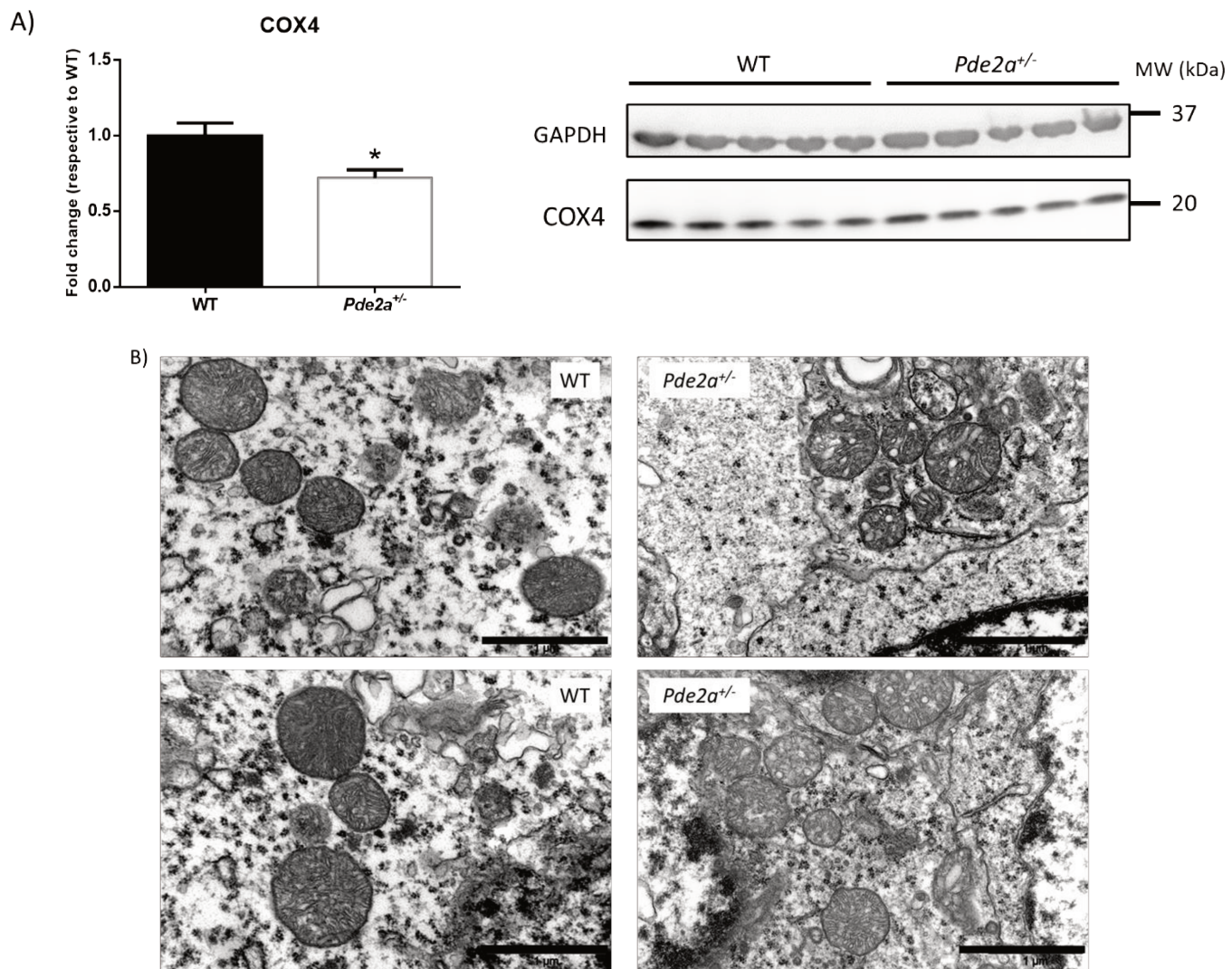


Figure 21. Les souris *Pde2a^{+/−}* ont une altération de la morphologie des mitochondries. (A) Quantification de l'expression de COX4, un marqueur mitochondrial, dans la région CA1 de l'hippocampe des souris WT et *Pde2a^{+/−}* d'un mois. Données représentées en moyenne \pm SEM, analysées par test de Mann et Whitney (*P=0.0381) (n : WT=5, *Pde2a^{+/−}*=5). (B) Images représentatives de mitochondries d'hippocampe de souris d'un mois prises par microscopie électronique. Barre d'échelle = 1 μm.

V. Effet de la réduction du niveau d'ARNm de *Fmr1* sur la morphologie et la protéomique des neurones corticaux de souris modèle du FXTAS.

Le FXTAS est une maladie neuro-dégénérative rare liée à la présence de la prémutation du gène *FMR1*, entre 50 et 200 répétitions du triplet CGG dans le 5'UTR, qui se caractérise par une ataxie et un déclin cognitif. Un des marqueurs moléculaires de cette maladie est une présence élevée d'ARNm de *FMR1* chez les patients FXTAS et dans la souris modèle CGG-KI. Cependant, l'expression de FMRP reste normale, voire légèrement diminuée, malgré la dérégulation du niveau d'ARNm. Dans cette étude, nous avons caractérisé l'impact de la réduction du niveau d'ARNm de *Fmr1* sur la morphologie et la protéomique des neurones corticaux de souris CGG-KI (voir Publication 2).

J'ai pu observer que les neurones CGG-KI avaient une arborisation dendritique réduite et un neurite plus court à 2DIV par rapport au neurones WT. L'utilisation de deux shRNA différents (sh-1a et 1b) réduisant les niveaux d'ARNm de *Fmr1* permet de rétablir ce phénotype morphologique altéré dans les neurones CGG-KI.

Par la suite, je me suis concentré sur la morphologie des épines dendritiques des neurones corticaux en culture à 20DIV. Après transfection permettant l'expression de la GFP, j'ai observé que les neurones CGG-KI transduits ont une densité d'épines plus grande, et qui sont plus longues et larges (Fig.22B-D). Cependant aucune différence de distribution de morphologie spécifique (fine, « stubby », « mushroom ») n'a pu être constatée entre les neurones WT et CGG-KI (Fig.22E-G). Le phénotype morphologique des neurones CGG-KI est rétabli par la transduction des deux shRNA.

Ces résultats montrent l'implication des niveaux élevés d'ARNm de *Fmr1* sur la morphologie altérée des neurones CGG-KI.

Enfin, nous avons montré par analyse protéomique que le rétablissement du phénotype morphologique des neurones CGG-KI par la réduction d'ARNm de *Fmr1* est

aussi associé à un rétablissement du niveau de 29 protéines, dont des protéines liant l'ARN.

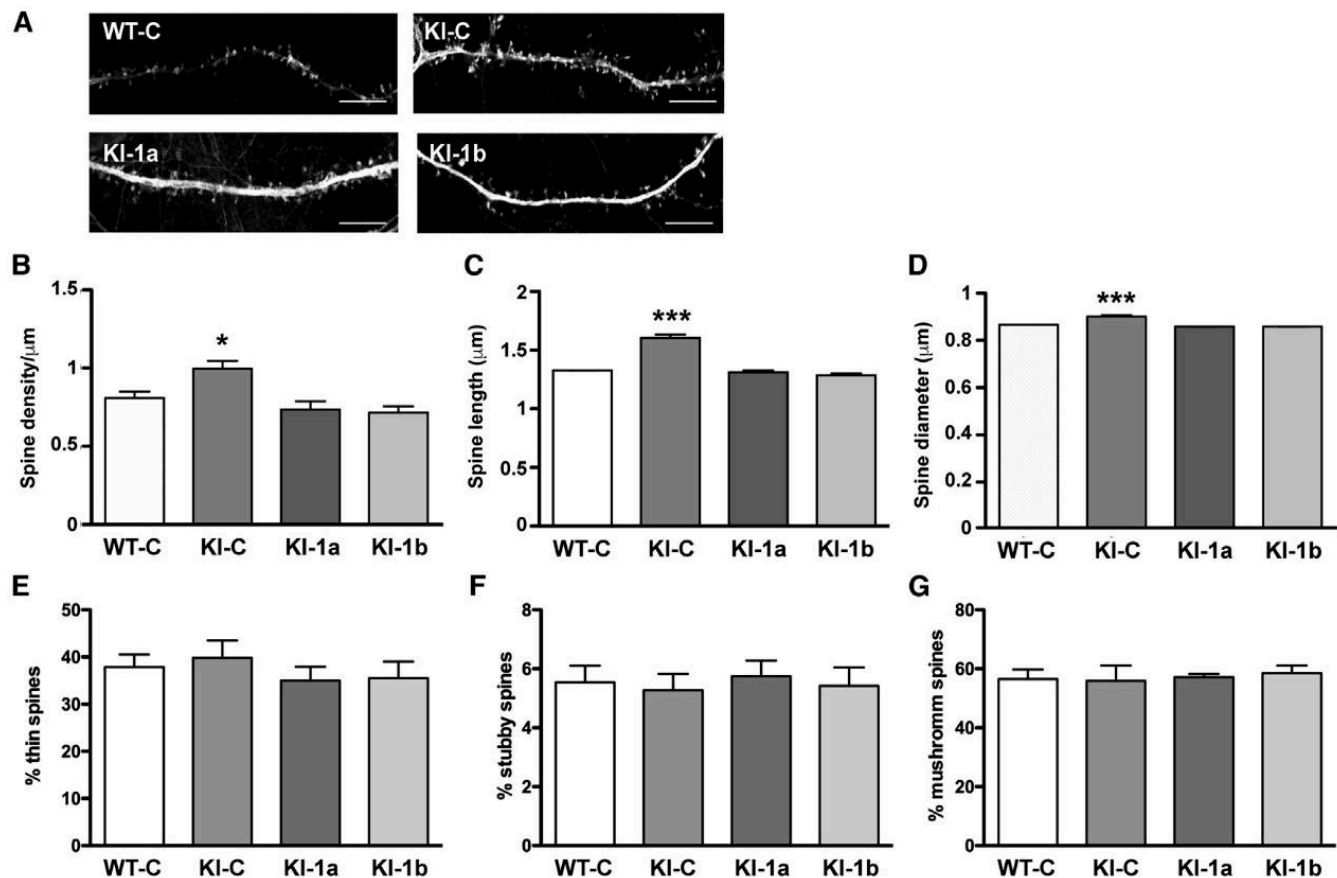


Figure 22. La réduction du niveau d'ARNm *Fmr1* normalise la morphologie des épines dendritiques des neurones corticaux CGG-KI. (A) Images confocales représentatives de la morphologie des épines mesurée par NeuronStudio. Barre d'échelle : 2 μm . (B-G) Histogrammes montrant la moyenne \pm SEM dans chaque culture de la densité(B), la longueur(C) et le diamètre(D) des épines dendritiques, ainsi que le pourcentage d'épines fines (E), sous forme « stubby »(F) et sous forme « mushroom »(G). Datas analysées par one-way Anova avec le test de multiple comparaison de Tukey. (adjusted p value : *P<0.05, ***P<0.001)

Discussion Projet 1

I. Rôle de la PDE2A dans le comportement social, cognitif et anxieux

L'inhibition pharmacologique -de façon chronique ou ponctuelle- de PDE2A par le Bay 60-7550 permet de rétablir les comportements sociaux altérés des souris *Fmr1* KO dont les déficits de communication, de discrimination et d'interaction sociale. De façon similaire, la réduction génétique de PDE2A dans le même modèle murin améliore pour la plupart ces déficits, ainsi que leur capacité cognitive.

La réduction pharmacologique et génétique de l'activité de PDE2A permet de rétablir des déficits comportementaux bien décrits chez les souris *Fmr1* KO, comme les déficits d'interaction sociale et de reconnaissance d'un nouvel objet. De façon surprenante, les souris double mutantes *Fmr1* KO x *Pde2a^{+/−}* ne montrent pas d'amélioration lors du test Homing à P13. Pourtant l'enzyme est exprimée dans un groupe spécifique de neurones dans le bulbe olfactif (Korsak et al., 2017) qui est très impliqué pendant ce test, et le traitement par le Bay 60-7550 permet de rétablir ce déficit. Il pourrait donc y avoir un phénomène de compensation chez les souris doubles mutantes et *Pde2a^{+/−}* avec d'autres phosphodiesterases présentes dans le bulbe olfactif. De la même façon, les souris *Pde2a^{+/−}* performent aussi bien que les souris sauvages, ne montrant pas de signe de déficit de la mémoire spatiale étudiée par MWM. Cependant il me semble essentiel de préciser que je n'ai jamais pu apprécier de déficits lors de ce test chez nos souris *Fmr1* KO non plus.

Il a été montré que l'inhibition de PDE2A permet d'améliorer les capacités cognitives des souris sauvages adultes lors du test du nouvel objet (Boess et al., 2004). A l'inverse, la réduction génétique de PDE2A pendant toute la vie de la souris et de son neurodéveloppement a plutôt tendance à détériorer ses capacités lors de ce test. Les

effets bénéfiques de l'inhibition pharmacologique pourraient s'expliquer par son caractère transitoire et à court terme. Cependant, j'ai pu mettre en évidence un effet bénéfique sur le long terme d'un traitement chronique sur le comportement social et la morphologie des épines dendritiques des souris *Fmr1* KO. Ce traitement n'ayant pas eu d'effet sur les souris sauvages, les faibles doses utilisées lors du traitement chronique peuvent expliquer la différence entre l'impact nul de l'inhibition chronique de la PDE2A chez les souris WT et les déficits présents chez les souris *Pde2a⁺⁻*.

D'une façon intéressante , il est à noter que l'inhibition de la PDE4D par le BNP14770 en traitement chronique permet de rétablir aussi les déficits d'interactions sociales et d'améliorer la morphologie altérée des épines dendritiques des souris *Fmr1* KO (Gurney et al., 2017), d'une façon similaire à mes données. De plus, des résultats positifs d'un essai clinique de Phase II sur des patients adultes atteints du SXF ont été récemment publiés (Berry-Kravis et al., 2021). Pour expliquer ces données, il a été récemment montré que l'inhibition de la PDE2A et de la PDE4D a un effet synergique bénéfique sur le processus de consolidation de la mémoire (Paes et al., 2021). Etant donnée le rôle similaire et en synergie de ces deux phosphodiesterases au niveau synaptique, ces derniers résultats nous confortent dans la validité de la PDE2A comme cible thérapeutique pour le SXF et dont l'inhibition pourrait compléter celle de la PDE4D en thérapie.

De façon générale, ces données sur le rôle de l'AMPc et du GMPc dans la pathophysiologie du SXF montre que leur modulation pourra être une approche thérapeutique. D'autre part l'importance de ces deux seconds messagers a été montré par beaucoup d'autres études. Par exemple, dans le modèle environnemental de TSA par l'injection d'acide valproïque (VPA) chez la souris enceinte, l'inhibition de la PDE2A par le Bay 60-7550 rétablit aussi les défauts de vocalisation et de comportement social (données du laboratoire non publiés). De façon complémentaire, l'inhibition de la PDE5 rétablit l'altération morphologique du tube neural retrouvée chez les embryons en contact de l'acide valproïque (Tiboni and Ponzano, 2015), et l'inhibition de la PDE10A

permet d'améliorer les défauts de comportements sociaux et l'anxiété des rats modèle VPA (Luhach et al., 2021).

Toutefois l'importance d'une précise modulation de PDE2A n'est pas seulement critique dans les comportements socio-cognitifs. En effet, les souris *Pde2a^{+/-}* montrent de façon intéressante un comportement anxieux que l'on ne retrouve pas chez les souris *Fmr1* KO lors du test du Zero Maze élevé. Cependant bien qu'ils mettent plus de temps à sortir du bras fermé, sûr pour eux, ils ne passent pas significativement moins de temps dans les bras ouverts par rapport aux WT. Ceci pourrait être expliqué par une capacité d'adaptation à un nouvel environnement plus lente, suivie d'une phase d'exploration plus intense avec potentiellement une hyperactivité qui reste encore à caractériser. De plus au premier jour de la Cue Task lors du MWM, les souris *Pde2a^{+/-}* sont plus lentes à comprendre le principe de la plateforme submergée pour pouvoir être remises en sécurité. Au deuxième jour de Cue Task, ce comportement n'est plus présent, nous faisant penser à une difficulté d'adaptation liée au stress. PDE2A est fortement exprimée dans le cortex surrénalien et l'hypophyse (Stephenson et al., 2009), où elle pourrait réguler le relargage d'hormones du stress, respectivement l'aldostérone et les glucocorticoïdes, libérées après un stress physique et psychologique. Enfin, il est intéressant de noter que le Bay 60-7550 a été initialement proposé comme anxiolytique et, en effet, son administration a des effets anxiolytiques sur des animaux non stressés (Masood et al., 2009) et des modèles de stress (Soares et al., 2017). Ainsi, ces études semblent donc prouver que différents modes de régulation de l'activité de PDE2A peuvent engendrer des phénotypes comportementaux opposés.

II. Rôle de la PDE2A dans le phénotype cellulaire et moléculaire

Mes résultats ont permis de mettre en évidence le rôle important de la PDE2A dans la physiopathologie du SXF. La présence de déficits du comportement social et des capacités cognitives similaires entre les souris *Fmr1* KO, où la PDE2A est surexprimée, et les souris *Pde2a^{+/-}*, où elle est sous-exprimée, montrent le rôle critique

de la régulation fine des niveaux d'AMPc et de GMPc pour le bon fonctionnement et développement du cerveau. En effet, la dérégulation des niveaux des deux seconds messagers ne se fait pas dans le même sens entre les deux génotypes, mais les déficits y sont similaires.

a) La croissance du neurite

Le rôle critique de la balance AMPc/GMPc dans l'elongation et l'orientation des prolongements neuronaux, axones et dendrites, est bien décrit (Shelly et al., 2010b). Dans ce sens mes résultats montrent que la croissance des neurites de neurones corticaux en culture est corrélée à la quantité de PDE2A présente. De façon intéressante, mon laboratoire a montré que la croissance de ces prolongements dans ces conditions est plus lente chez les neurones *Fmr1* KO par rapport aux WT (voir Publication 1), à l'inverse des neurones *Pde2a^{+/−}* qui présentent une croissance accélérée du neurite à 2DIV. Rappelons que chez la souris *Fmr1* KO, il y a une surexpression de la PDE2A. De plus, l'inhibition spécifique de PDE2A par le traitement en Bay 60-7550 des neurones WT augmente significativement la longueur des neurites, le même phénotype que j'observe dans les cultures de neurones *Pde2a^{+/−}*. A ce stade les réductions pharmacologique et génétique de l'activité de la PDE2A ont le même effet sur ce phénotype, à l'inverse des tests comportementaux. Enfin, dans ce sens, il a été démontré l'effet bénéfique d'inhibiteurs de PDE2A, dont le Bay 60-7550, sur la croissance axonale dans des tranches de cerveau *ex vivo* (Heine et al., 2013, 2011).

En conclusion, ces différents résultats confirment le rôle de PDE2A dans la croissance des neurites. L'étude de la morphologie des épines dendritiques complétera mon étude sur l'impact de l'augmentation de l'AMPc et du GMPc chez les souris *Pde2a^{+/−}*.

b) Le phénotype mitochondrial

La PDE2A2 est une isoforme de PDE2A (Delhaye and Bardoni, 2021) spécifiquement exprimé dans la mitochondrie qui régule la voie de signalisation

AMPc/PKA, dont l'activation est souvent associée à une mitophagie plus faible, une forme spécifique d'autophagie éliminant les mitochondries défectueuses. En effet, PKA phosphoryle DRP1 (dynamin-related protein 1), qui est une protéine essentielle pour la fission mitochondriale (Monterisi et al., 2020), et inhibe sa capacité à induire la fission, ce qui va favoriser au final l'élongation mitochondriale (Cribbs and Strack, 2007). Il n'est donc pas étonnant de constater des défauts de morphologie mitochondriale chez des patients ayant différentes mutations sur *PDE2A* (Douummar et al., 2020). En effet, le marquage par Mitotracker montre dans les fibroblastes de ces patients un réseau de mitochondrie désorganisé. En figure 21, les images en microscopie électronique du CA1 des souris *Pde2a^{-/-}* à un mois suggèrent un déséquilibre dans la balance fusion/fission ou dans la mitophagie des mitochondries.

De l'autre côté, la diminution d'expression de COX4 que j'ai identifiée par WB dans les extraits d'hippocampe obtenus des mêmes souris pourrait être corrélée à ces déficits. En effet, il a été montré qu'en condition d'hypoxie la PKA phosphoryle COX4 et induit sa dégradation et la diminution de son activité (Prabu et al., 2006). La diminution de PDE2A2 dans la mitochondrie, entraînant une élévation d'AMPc et donc de l'activité de PKA, pourrait donc être directement responsable de la diminution de COX4 en agissant sur sa dégradation, sans pour autant être liée à un déficit du nombre de mitochondrie.

c) Le phénotype moléculaire

GSK3 est une des kinases ayant le plus grand nombre de substrats dans la plupart des cellules (Sutherland, 2011). Elle est impliquée dans une large variété de processus du neurodéveloppement comme la neurogénèse, la migration et la morphologie cellulaire et est en aval d'un grand nombre de voies de signalisation dont celles dépendant de l'AMPc et du GMPc (Beurel et al., 2015). En effet, la modulation prédominante de son activité se fait par sa phosphorylation dépendante de la PKA, de la PKG, de la voie PI3K/AKT et d'autres kinases (Beurel et al., 2015; Lin et al., 2007;

Yoshimura et al., 2006). Différentes études ont montré dans l'hippocampe des souris *Fmr1* KO âgées d'un mois un niveau de phosphorylation de GSK3 β comparable aux souris WT (Min et al., 2009)(Guo et al., 2012; Yuskaits et al., 2010b). Cette diminution serait cohérente avec une diminution du niveau d'AMPc nécessaire à la phosphorylation de GSK3 β et donc compatible avec l'augmentation de l'activité de PDE2A dans l'hippocampe des souris *Fmr1* KO, comme nous l'avons montré (Maurin et al., 2019b).

J'ai montré que le niveau de phosphorylation de GSK3 β est réduit dans l'hippocampe des souris *Pde2a^{+/−}*, ce qui signifie que son niveau d'activation est augmenté par rapport aux WT. Il est connu que la PKA peut bloquer directement l'activité de GSK3 β en le phosphorylant. Si c'était le cas pour la PKA dont l'activité dépend de PDE2A, on s'attendrait plutôt à un niveau de phosphorylation plus élevé que chez le WT et donc à l'inactivation de GSK3 β . Donc la phosphorylation de GSK3 β au niveau du neurone totale pourrait être dérégulée de façon indirecte par la diminution de PDE2A, en passant par la dérégulation d'une autre voie régulant cette phosphorylation précédemment mentionnée. Alternativement, la compensation de ce phénotype avec l'augmentation du niveau d'expression d'autres PDEs pourrait expliquer le phénotype des souris *Pde2a^{+/−}*. En effet, par exemple, la surexpression de PDE10A chez la souris *Pde1b* KO a été observée (Hufgard et al., 2017). Il sera quand même important de quantifier le niveau de phosphorylation de GSK3 à la synapse où les compensations pourraient être différentes puisque toutes les PDEs ne sont pas localisées dans ce compartiment neuronal.

Il est intéressant de noter que GSK3 β est retrouvée dans la mitochondrie, contrairement à GSK3 α , et est connue pour réguler leur activité (Yang et al., 2017). L'inhibition par phosphorylation de GSK3 β augmente la biogénèse des mitochondries (Undi et al., 2017), et atténue l'apoptose mitochondriale induite par céramide en inactivant les caspases 2 et 8 (Lin et al., 2007). Il est ainsi possible que la sur-activation chez les souris *Pde2a^{+/−}* de GSK3 β par la diminution de la phosphorylation en Ser9 ait

un effet inverse à cette inhibition et soit aussi impliquée dans les déficits morphologiques relevés.

d) La migration corticale

En se basant sur le rôle de PDE2A dans la croissance axonale, j'ai émis l'hypothèse que cette enzyme pouvait aussi avoir un rôle dans la migration des neurones lors du développement et notamment dans l'architecture corticale, dont les couches supérieures sont les plus immuno-marquées pour PDE2A chez le rat (Stephenson et al., 2012). Il est par ailleurs intéressant de noter que chez la souris *Fmr1* KO il existe une altération de la distribution des couches corticales persistant à l'âge adulte (Lee et al., 2019), de la même façon que chez le *GSK3 :NeuroD6* KO où la migration corticale radiale est compromise(Morgan-Smith et al., 2014). Chez la souris *Pde2a⁺⁻*, l'agencement des couches corticales n'est pas altéré par rapport aux souris WT à 13 jours après la naissance. Il est néanmoins possible qu'à l'inverse de chez le *Fmr1* KO, et de façon similaire à la croissance du neurite, la réduction de PDE2A entraîne une accélération de la migration radiale corticale, invisible à cet âge. Dans ce sens, j'ai entrepris de sur-exprimer PDE2A dans les neurones corticaux par la technique de l'électroporation *in utero*. Chez le *Fmr1* KO, dans lequel PDE2A est surexprimé, la migration corticale entre les âges embryonnaires E14.5 et E17.5 est altérée (La Fata et al., 2014). J'ai donc voulu savoir quelle était la part de PDE2A dans ce déficit. En augmentant l'expression de PDE2A par cette technique j'ai pu constater que les neurones électroporés et surexprimant PDE2A ont un retard dans la migration corticale radiale, qui n'est pas aussi fort que dans le modèle *Fmr1* KO dans la littérature. Ainsi la PDE2A semble avoir un rôle dans la migration corticale des neurones, mais son expression altérée à elle seule ne peut expliquer les déficits retrouvés chez le *Fmr1* KO. Ceci est d'ailleurs cohérent avec le fait qu'en absence de FMRP plusieurs voies impliquées dans la migration neuronale sont altérées, comme celles régulées par les RhoGTPase (Abekhoukh and Bardoni, 2014; Gonzalez-Billault et al., 2012) , dont Rac1 qui est par ailleurs lié au modelage du cytosquelette, essentiel dans le processus de

migration, et altéré dans le SXF (Castets et al., 2005; La Fata et al., 2014; Schenck et al., 2003). De façon intéressante, la PKA régule l'activité de plusieurs membres de la famille des RhoGTPase, comme Rac1 et Cdc42, ainsi qu'un grand nombre d'autres protéines ayant un rôle dans la migration, l'adhésion et les mouvements cellulaires (Howe, 2004). Enfin, la PKA peut phosphoryler l'actine, réduisant sa polymérisation (Ohta et al., 1987), et l'intégrine α 4, réduisant sa liaison à la paxillin essentielle à la migration cellulaire (Han et al., 2001), faisant tout deux parties du cytosquelette. Ces éléments permettent de comprendre l'importance de l'axe AMPc/PKA dans la régulation de la migration cellulaire et donc de l'importance de sa régulation par la PDE2A.

III. Rôle de la PDE2A dans la LTD

La LTD mGluR-dépendante induite est connue pour être exagérée chez les *Fmr1* KO et nous avons montré que l'inhibition de PDE2A par le Bay 60-7550 permettait de rétablir une LTD normal (Voir Publication 1). A l'inverse, ici je montre que les souris *Pde2a^{+/−}* présentent une LTD fortement diminuée. Mes résultats préliminaires sur la dimérisation des récepteurs mGluR5 pourraient expliquer cette altération. En effet, à la membrane, la forme dimérisée représente la forme active des mGluR5. Une diminution de cette conformation expliquerait une plus faible réponse au DHPG, et donc une LTD diminuée.

De plus, il serait aussi important d'étudier l'internalisation des récepteurs AMPA en réponse à la signalisation des récepteurs métabotropiques glutamatergiques, qui est excessive chez le *Fmr1* KO (Nakamoto et al., 2007). En effet, l'état de phosphorylation des sous-unités des AMPAR est associé à leur internalisation et à la LTD. Par exemple, la LTD hippocampale et l'internalisation est diminuée chez des souris ne pouvant avoir la phosphorylation en Ser845 de la sous-unité GluA1, phosphorylée normalement par la PKA (Lee et al., 2010, 2003).

Dans les deux lignées de souris, il semble que la transmission synaptique y soit tout autant altérée, pouvant ainsi expliquer les déficits comportementaux. Il est intéressant de noter que les phénotypes cellulaires et moléculaires peuvent aussi être opposés en aboutissant au même phénotype comportemental comme l'altération de la LTD.

IV. La souris *Pde2a⁺⁻*, nouveau modèle de maladie neurodéveloppementale ?

Des mutations sur le gène *Pde2a* sont présentes chez des patients atteints de déficience intellectuelle et de retard du développement. En considération des différents déficits comportementaux, cellulaires et moléculaires, je peux conclure que la lignée *Pde2a⁺⁻* récapitule une forme de maladie du neurodéveloppement. Cependant il reste de nombreux phénotypes à caractériser afin de pouvoir au mieux catégoriser cette lignée vers une maladie précise du neurodéveloppement, bien que ces troubles partagent très souvent de nombreux déficits. Dans ce sens, l'activité basale des animaux *Pde2a⁺⁻* devrait être étudiée étant donné que différents KO d'autres phosphodiesterases présentent soit de l'hyperactivité pour le *Pde1b* KO, soit de l'hypoactivité pour le *Pde4b* KO et le *Pde10a* KO.

De plus, le test du PPI semble essentiel à réaliser. Ce test est connu pour étudier les modèles animaux de schizophrénie et est surtout utilisé chez les patients atteints de schizophrénie (Swerdlow et al., 2018). Ce test pourrait être utilisé afin de caractériser la lignée *Pde2a⁺⁻* comme modèle de schizophrénie. En effet, ces souris ne présentent pas d'altération de la discrimination-mémoire sociale à 13 jours lors du test du Homing, mais bien une altération des capacités cognitives à l'âge adulte. Ils présentent cependant une altération de la communication sociale à un stade précoce (10 jours). De façon intéressante, il est connu que 30 à 50% des patients développant la schizophrénie pendant l'enfance ont d'abord, plus tôt, des troubles du spectre de

l'autisme (Rapoport et al., 2009). De ce fait, les souris *Pde2a^{+/−}* pourraient représenter un nouveau modèle de schizophrénie apparaissant pendant l'enfance.

Enfin, les patients ayant une mutation sur le gène *PDE2A* présentent notamment des troubles du mouvement. Dans ce sens, il semble intéressant de vérifier les performances motrices des souris *Pde2a^{+/−}* à l'aide du test du Rotarod par exemple. La comparaison entre notre lignée *Pde2a^{+/−}* et les patients ayant ces mutations est cependant difficile. En effet, l'effet des mutations sur la fonction de PDE2A n'a pas été correctement décrite jusqu'à présent dans la plupart des cas. Nous ne savons donc pas si ces mutations entraînent une perte ou un gain de fonction de la protéine, ou affectent différemment l'affinité de PDE2A pour l'AMPc et/ou le GMPc.

De façon étonnante, il est intéressant de noter que l'impact des PDEs dans le neurodéveloppement a donné lieu à peu d'études par l'utilisation de modèles animaux KO. En effet dans de nombreux cas, le phénotype d'animaux KO n'est pas connu, comme c'est le cas pour PDE5 dont l'inhibition pharmacologique a pourtant été intensivement étudiée (Devan et al., 2006; Prickaerts et al., 2002; Zhang et al., 2002). Mais ces inhibiteurs de phosphodiesterase sont le plus souvent administrés en post-natal et ne permettent pas de comprendre le rôle critique des PDEs durant le neurodéveloppement et la synaptogénèse par exemple. Bien qu'étudier une famille de protéines aussi importante dont certains membres n'ont pas des actions spécifiquement centrées au niveau du cerveau, leurs études semblent nécessaires afin de comprendre le rôle de chaque PDE sur le neurodéveloppement normal et pathologique.

La caractérisation de ce nouveau modèle *Pde2a^{+/−}* ouvre donc de nombreuses perspectives de recherche. Par exemple, l'activation des voies de signalisations par l'AMPc est depuis longtemps décrite comme contrôlant la production de cytokine pro-inflammatoire (Teixeira et al., 1997). De faibles concentrations en AMPc favorisent l'inflammation par la production de cytokines comme les interleukines IL-12, IL-17 et

TNF α entre autres (Pieretti et al., 2006), tandis que l'inhibition de GSK3 β permet de réduire la production de ces marqueurs pro-inflammatoire (Ding et al., 2017). De plus, il est connu que la microglie, les macrophages résidant dans le système nerveux central répondant et produisant ces cytokines, est impliquée dans certaines maladies du neurodéveloppement, de par son rôle dans la neurogénèse et la synaptogénèse dont le pruning (Sominsky et al., 2018). De façon intéressante, les souris adultes *Fmr1* KO présentent une microglie moins activée dans le cortex (Lee et al., 2019), allant à l'encontre d'une suractivation retrouvée chez des patients atteints de TSA (Suzuki et al., 2013), mais pouvant expliquer la diminution de l'élimination des synapses médiée par la microglie. L'étude de l'état de la microglie et le statut inflammatoire des souris *Pde2a^{+/−}* serait donc pertinente dans le futur.

Discussion Projet 2

Rôle de l'augmentation des niveaux d'ARNm de *FMR1* sur la morphologie des épines dendritiques dans un modèle murin du FXTAS

Longtemps les porteurs d'une prémutation du triplet de nucléotides CGG dans le gène *FMR1* ont été considérés comme normaux. Cependant, depuis 20 ans des études ont montré qu'ils représentent en fait une population à risque pour les TSA, la dépression et les troubles bipolaires. De plus, les femmes présentent un risque très élevé d'insuffisance ovarienne prématuée (POF = Premature Ovarian Failure) et les hommes peuvent être atteints d'une forme de FXTAS après 50 ans, une maladie neurodégénérative caractérisée par une ataxie et un syndrome parkinsonien. La cause de la neurodégénération a d'abord été expliquée par une mort neuronale associée à la présence d'inclusion nucléaire. Au niveau moléculaire, deux phénotypes particuliers ont été observés : une augmentation des niveaux d'ARNm de *FMR1*, de 2 à 8 fois avec un niveau quasi-normal de FMRP, et la présence d'un peptide riche en polyglycine résultant de la traduction de l'expansion CGG.

Nous nous sommes intéressés au phénotype neurodéveloppemental, caractérisé par une morphologie neuronale anormale a été observée dans les neurones des modèles murins de FXTAS au cours du développement en absence des inclusions nucléaires.

Nous avons utilisé un modèle murin du FXTAS afin de caractériser l'impact de la diminution des niveaux d'ARNm de *Fmr1* au niveau morphologique et moléculaire des neurones en culture. Le rétablissement de la morphologie altérée des neurones FXTAS par la diminution des niveaux d'ARNm de *Fmr1* montre bien que c'est cette présence élevée qui est responsable de la morphologie altérée, et non les inclusions nucléaires qui sont absentes à ce stade du développement. En effet, ces inclusions ne sont

retrouvées que chez des animaux KI-CGG âgés de plus de 12 semaines (Hunsaker et al., 2009). Elles pourraient donc être des mécanismes de défense.

L'analyse protéomique comparative des neurones exprimant le contrôle ou le shRNA spécifique de l'ARNm de *Fmr1* nous a permis de sortir une liste de protéines dérégulées dans les neurones KI-CGG, normalisés après traitement. Plusieurs de ces protéines sont des protéines liant l'ARN, comme Tia1, Hnrnpll et ROAA, laissant penser que les niveaux élevés d'ARNm de *Fmr1* interfèrent avec le métabolisme de l'ARN. De façon intéressante, d'autres protéines dont les niveaux d'expression sont rétablis par la réduction d'ARNm de *Fmr1* sont impliqués dans la régulation du cytosquelette d'actine, qui agit sur la morphologie des neurones et en particulier celle des épines dendritiques. Nous pouvons ici faire le lien direct avec les altérations morphologiques des épines dendritiques que nous avons montrés, dont des épines dendritiques plus longues, avec une tête plus large, et une densité de ces épines augmentée le long des dendrites étudiés. Cependant, la maturation des épines n'est pas altérée, comme le montre nos analyses des différents types d'épines, ce qui suggère que l'élévation du niveau d'ARNm de *Fmr1* n'interfère pas avec la maturation mais a un impact plus subtil sur la morphologie.

Conclusion & Perspectives

Globalement, je suis convaincu d'avoir atteint les objectifs de mon travail en étudiant des cibles thérapeutiques pour le SXF et le FXTAS dont la validation a été faite au niveau préclinique.

Projet 1

Mon travail a permis de mettre en évidence le rôle de PDE2A dans le développement du cerveau en utilisant deux modèles murins du neurodéveloppement, le *Fmr1* KO et le *Pde2a^{+/−}* dont beaucoup de phénotypes peuvent être corrélés à une altération de l'expression de PDE2A et, en conséquence, à une altération du niveau d'AMPc et de GMPc dans le cerveau. Cette conclusion est confortée par la normalisation de plusieurs phénotypes *in vivo* dans le double mutant. Mon travail a d'ailleurs définitivement prouvé l'intérêt de l'inhibition de PDE2A comme thérapie de choix pour le SXF.

La suite de ce projet se fera dans l'analyse plus approfondie des souris doubles mutantes *Fmr1* KO x *Pde2a^{+/−}* afin de comprendre quelles voies de signalisations sont corrigées dans le cerveau de ces souris et de les corrérer à la correction des phénotypes socio-cognitifs, si présents, et des formes de plasticité synaptique altérées chez les souris « parentales », *Fmr1* KO et *Pde2a^{+/−}*.

La caractérisation des souris *Pde2a^{+/−}* devra se poursuivre dans l'étude de plusieurs comportements surtout en corrélation avec ce qui est observé chez les patients ayant des mutations ponctuelles dans le gène PDE2A (précédemment discuté comme la sensibilité avec le PPI et les troubles du mouvement avec le rotarod, ainsi que l'étude de la sensibilité douloureuse). Du point de vue moléculaire, je crois qu'il sera fondamental de comprendre le rôle du niveau d'AMPc et de GMPc dans l'altération de la fonction mitochondriale et dans l'activation de la microglie.

Projet 2

Cette étude a été une preuve de concept sur le rôle de l'ARNm de FMR1 dans la physiopathologie des phénotypes développementaux des neurones FXTAS. L'analyse protéomique comparative a permis d'identifier des protéines différemment exprimées entre les neurones WT et CGG-KI qui ont été corrigées par la réduction de l'expression de FMR1. Ce résultat doit représenter un point de départ pour mettre au point de futures thérapies pour le FXTAS.

Publication 1

ORIGINAL ARTICLE

Involvement of Phosphodiesterase 2A Activity in the Pathophysiology of Fragile X Syndrome

Thomas Maurin  ^{1,2}, Francesca Melancia³, Marielle Jarjat^{1,2}, Liliana Castro  ^{4,5}, Lara Costa⁶, Sébastien Delhaye^{1,2}, Anouar Khayachi¹, Sara Castagnola^{1,2}, Elia Mota^{4,5}, Audrey Di Giorgio⁷, Michela Servadio³, Małgorzata Drozd^{1,2}, Gwénola Poupon¹, Sara Schiavi³, Lara Sardone⁸, Stéphane Azoulay⁷, Lucia Ciranna⁸, Stéphane Martin⁹, Pierre Vincent  ^{4,5}, Viviana Trezza³ and Barbara Bardoni  ^{2,9}

¹Université Côte d'Azur, CNRS, IPMC, F-06560 Valbonne, France, ²CNRS LIA «Neogenex», F-06560 Valbonne, France, ³Department of Sciences, Università RomaTre, I-00145 Roma, Italy, ⁴Sorbonne Université, CNRS, Biological Adaptation and Ageing, F-75005 Paris, France, ⁵Labex BioPsy, F-75005 Paris, France, ⁶Department of Clinical and Experimental Medicine, University of Messina, I-98122 Messina, Italy, ⁷Université Côte d'Azur, CNRS, Institut de Chimie de Nice, F-06108 Nice, France, ⁸Department of Biomedical and Biotechnological Sciences, University of Catania, I-95123 Catania, Italy and ⁹Université Côte d'Azur, INSERM, CNRS, IPMC, F-06560 Valbonne, France

Address correspondence to Barbara Bardoni, Thomas Maurin, CNRS UMR7275, Institute of Molecular and Cellular Pharmacology, 660 Route des Lucioles, Sophia-Antipolis, 06560 Valbonne, France. Email: bardoni@ipmc.cnrs.fr (B.B.); maurin@ipmc.cnrs.fr (T.M.)  orcid.org/0000-0001-6411-1517

Francesca Melancia and Marielle Jarjat equally contributed; Liliana Castro, Lara Costa and Sébastien Delhaye equally contributed to this work; Lucia Ciranna, Stéphan Martin, Pierre Vincent and Viviana Trezza equally contributed to this work

Abstract

The fragile X mental retardation protein (FMRP) is an RNA-binding protein involved in translational regulation of mRNAs that play key roles in synaptic morphology and plasticity. The functional absence of FMRP causes the fragile X syndrome (FXS), the most common form of inherited intellectual disability and the most common monogenic cause of autism. No effective treatment is available for FXS. We recently identified the Phosphodiesterase 2A (*Pde2a*) mRNA as a prominent target of FMRP. PDE2A enzymatic activity is increased in the brain of *Fmr1*-KO mice, a recognized model of FXS, leading to decreased levels of cAMP and cGMP. Here, we pharmacologically inhibited PDE2A in *Fmr1*-KO mice and observed a rescue both of the maturity of dendritic spines and of the exaggerated hippocampal mGluR-dependent long-term depression. Remarkably, PDE2A blockade rescued the social and communicative deficits of both mouse and rat *Fmr1*-KO animals. Importantly, chronic inhibition of PDE2A in newborn *Fmr1*-KO mice followed by a washout interval, resulted in the rescue of the altered social behavior observed in adolescent mice. Altogether, these results reveal the key role of PDE2A in the physiopathology of FXS and suggest that its pharmacological inhibition represents a novel therapeutic approach for FXS.

Key words: autism spectrum disorder, *Fmr1*-KO mice, *Fmr1*-KO rats, fragile X syndrome, phosphodiesterase 2A

Introduction

Fragile X syndrome (FXS) is a rare genetic neurodevelopmental disorder with a prevalence of 1:4000 males and 1:7000 females representing the most common form of inherited intellectual disability (ID) and a leading genetic cause of autism spectrum disorder (ASD). Patients may also exhibit a range of disabling neurological problems including hyperactivity, attention deficit, anxiety and epileptic seizures in addition to facial dysmorphisms and physical abnormalities (Bassell and Warren 2008; Maurin et al. 2014; Castagnola et al. 2017). FXS is caused by the absence of expression of the FMR1 gene, which ultimately leads to the lack of its product, the fragile X mental retardation protein (FMRP), a translational modulator of synaptic proteins and a regulator of mRNA transport at the synapse. Consequently, neurons of both FXS patients and *Fmr1*-KO mice exhibit abnormal dendritic spines associated with altered forms of synaptic plasticity (Bassell and Warren 2008; Maurin et al. 2014; Castagnola et al. 2017). Furthermore, altered volumes of specific brain structures that develop prenatally or early postnatally in young FXS children (Gotheff et al. 2008; Hoeft et al. 2010) and *Fmr1*-KO pups (Lai et al. 2016) have been described. The abundance of many synaptic proteins is altered in the absence of FMRP and, consequently, multiple molecular pathways are dysregulated in *Fmr1*-KO neurons (Maurin et al. 2018). However, despite the research efforts made both at preclinical and clinical levels, approved therapies are not yet available for FXS (Budimirovic et al. 2017; Castagnola et al. 2017; Erickson et al. 2017). Towards this goal, it is essential to have a better understanding of the pathophysiology of FXS and of the role played by FMRP during brain development. Therefore, we used High Throughput Sequencing-Cross Linking Immuno-Precipitation (HITS-CLIP) to identify FMRP RNA targets at postnatal day (PND) 13, an early developmental stage of mouse brain, when FMRP is most highly expressed and synaptogenesis peaks (Maurin et al. 2018). At this age, in hippocampus and in cortex a prominent target of FMRP is the Phosphodiesterase 2A (Pde2a) mRNA (Maurin et al. 2018), which encodes an enzyme involved in cAMP and cGMP degradation (Maurice et al. 2014). PDE2A levels and activity are increased (Maurin et al. 2018 and this study) in *Fmr1*-KO, resulting in reduced levels of cAMP and cGMP, 2 intracellular secondary messengers having key roles in neuronal differentiation, development and function (Shelly et al. 2010; Park et al. 2014). Here, we unravel the pathophysiological relevance of PDE2A activity in FXS by combining *in vitro*, *ex vivo*, and *in vivo* experiments and using 2 rodent models of FXS. We conclude that PDE2A represents a novel therapeutic target to treat children affected by FXS.

Materials and Methods

Neuronal Cultures and Spine Morphology Analysis

Primary cortical neurons were prepared from embryos at E15.5 obtained from pregnant C57Bl/6 *Fmr1*-KO and wild type (WT) mice as previously described (Khayachi et al. 2018). Neurons (17 days *in vitro*) were treated with 0.2 μM BAY607550 or DMSO (control) for 24 h in total. After 5 h of pharmacological treatment, neurons were transduced with attenuated Sindbis viral particles pSinRep5(nsP2726)-expressing GFP at a multiplicity of infection (MOI) of 0.1. Transduced neurons (18 days *in vitro*) were washed twice in PBS at room temperature (RT) after 19 h of transduction, and then fixed (Devader et al. 2015). Sequential confocal images (512 × 220 pixels; Zoom 3.0; Average 4; Speed 7) of GFP-expressing neurons were acquired with a 63X oil-immersion lens (Numerical Aperture NA 1.4) on an inverted Zeiss LSM780

confocal microscope. Z-series of 7–8 images of randomly selected secondary dendrites (3 independent cultures, 24–30 neurons per condition) were analyzed using NeuronStudio software, which allows for the automated detection of immature and mature spines (Rodriguez et al. 2008; Devader et al. 2015).

The dendritic spine morphology analysis was scored and analyzed by trained observers who were unaware of treatment conditions.

cAMP and cGMP Detection

1) ELISA test: Frozen ground hippocampi from PND 13 mice, were resuspended in 10 volumes of 0.1 N HCl and centrifuged to remove debris. Supernatants were used directly for cGMP measurement. ELISA was then carried out according to the manufacturer's instructions (Direct cGMP ELISA kit; Enzo Life Science). 2) cAMP-Glo Max assay: Primary cortical neurons (17–21 days *in vitro*) cultured in 96 wells plates were stimulated in 2 biological replicates with 10 μM Forskolin and 1 μM BAY607550 in dPBS supplemented with CaCl₂ and MgCl₂ for 30 min at 37 °C. cAMP concentration was measured with the cAMP-Glo Max assay (Promega) according to the manufacturer's indications. 3) cAMP Biosensors: Brain slices were prepared from male mice at PND 7–11, transduced with Sindbis viral particles to express the cAMP biosensor Epac-SH^{H150} (Polito et al. 2013). Wide-field images were obtained with an Olympus BX50WI or BX1WI upright microscope with a 40× 0.8 NA water-immersion objective and an ORCA-AG camera (Hamamatsu). Images were acquired with iVision (Biovision, Exton, PA, USA). The excitation and dichroic filters were D436/20 and 455dcx. Signals were acquired by alternating the emission filters with a filter wheel (Sutter Instruments, Novato, CA, USA), HQ480/40 for the donor, and D535/40 for the acceptor. Images were analyzed with custom routines according to the IGOR Pro environment (Wavemetrics, Lake Oswego, OR, USA). The emission ratio was calculated for each pixel as F480/F535. The pseudocolor images display the ratio value coded in hue and the fluorescence of the preparation coded in intensity. The amplitudes of responses were quantified for each neuron as the fractional change in ratio from its own baseline and maximal final ratio response (in the presence of forskolin and IBMX). Responses obtained from CA1 neurons were averaged for each experiment (i.e., brain slice). Data were analyzed with SPSS statistical software version 22.0 (Chicago, IL, USA). Normality in variable distributions and homogeneity of variances across groups were assessed with the Shapiro-Wilk and Levene tests, respectively.

Animals

The experiments were performed following the ARRIVE (Animals in Research: Reporting In Vivo Experiments) guidelines (Kilkenny et al. 2010). *Fmr1*-knockout (KO) and WT mice on a C57BL/6J congenic background were obtained from Prof. R. Willemse (Mientjes et al. 2006), while *Fmr1*-KO and WT rats on a Sprague-Dawley background were purchased from Horizon Discovery (formerly SAGE Labs, USA). All animals were generated and housed in groups of 4 in standard laboratory conditions (22 °C, 55 ± 10% humidity, 12-h light/12-h dark diurnal cycles) with food and water provided ad libitum.

Behavior

Experimental testing was performed between 12:00 and 16:30 each day during the 12-h light period. Only male mice and rats were used. Animal care was conducted in accordance with the

European Community Directive 2010/63/EU. The experiments were approved by the local ethics committee (Comité d'Ethique en Expérimentation Animale CIEPAL-AZUR N. 00788.01; APAFIS#4985-2 016 032 314 169 426 v4APAFIS#8100-2 016 112 217 148 206 v3), by the French Ministry of Research and by the Italian Ministry of Health. The number of animals used in each experiment is indicated in the figure legends.

Electrophysiology

Hippocampal slices were prepared from WT and *Fmr1*-KO mice on a C57BL/6J genetic background at PND 13 as previously described (Costa et al. 2012), following protocols approved by local ethics committee (OPBA, University of Catania) and by the Italian Ministry of Health (N. 35212016-PR). Data were acquired and analyzed with the Signal software (Cambridge Electronic Design, England). Excitatory Post Synaptic Current (EPSC) amplitude was measured as the difference between peak and baseline current. EPSC amplitude values were averaged over 1 min and expressed as % of baseline (mean EPSC amplitude calculated from EPSCs recorded during at least 15 min before [S]-3,5-Dihydroxyphenylglycine [DHPG] application). Different sets of values were compared using the appropriate statistical tests indicated in the corresponding figure legend. The amount of long-term depression (LTD) induced by metabotropic group I glutamate receptor (*mGluR*) was calculated 40 min after LTD induction by DHPG application and is expressed by indicating EPSC amplitude as percentage of baseline (% EPSC).

Drug Treatment

BAY607550 (Cayman) was dissolved in 10% DMSO/8.75% Tween 80/8.75% polyethylene glycol/saline. For the behavioral experiments, BAY607550 or Lu AF64280 (or their vehicles) were administered intraperitoneally (i.p.) 30 min before testing. BAY607550 was administrated at the doses of 0.05 mg/kg at infancy and 0.1 mg/kg at adolescence, while Lu AF64280 was administered at 0.5 mg/kg. Drug doses and pretreatment intervals were based on literature (Boess et al. 2004; Masood et al. 2008, 2009; Ding et al. 2014; Redrobe et al. 2014; Wang et al. 2017) and our pilot data showing that, at the doses used in the present study, drugs did not affect the behavior of WT animals. In one experiment, chronic treatment was carried out by a daily i.p. injection of 0.05 mg/kg BAY607550 to mice from PND 5–21 and mice were tested for social interaction after a washout interval of 9 days. One pup per litter from different litters per treatment group was used in the behavioral experiments, to control for any potential litter effect. Animals were randomly allocated to each treatment group. Coding of the drug solutions ensured that both during experimentation and behavior analysis, the experimenter was unaware of the treatment of the animals. The number of animals per group is indicated in the figure legends.

The Isolation-Induced Ultrasonic Vocalizations Test

The test was performed as previously described (Servadio et al. 2016). Briefly, each pup (at PND 10 for mice and PNDs 5 and 9 for rats) was individually removed from the nest and placed into a black Plexiglas arena, located inside a sound-attenuating and temperature-controlled chamber. Pup ultrasonic vocalizations (USVs) were detected for 3 min by an ultrasound microphone (Avisoft Bioacoustics, Germany) sensitive to frequencies between 10 and 250 kHz and fixed at 10 cm above the arena. Pup axillary temperature was measured before and after the test by a digital thermometer. The emission of USVs was analyzed using Avisoft Recorder software (Version 5.1).

Homing Behavior Test

At PND 14, the litter was separated from the dam and kept for 30 min in a temperature-controlled holding cage. Then, each mouse pup was placed into a Plexiglas box whose floor was covered for 1/3 with bedding from the pup's home cage and for 2/3 with clean bedding. The pup was located at the side of the box covered by clean bedding, and its behavior was video-recorded for 4 min for subsequent analysis. The following parameters were scored using the Observer 3.0 software (Noldus Information Technology): latency (s) to reach the home-cage bedding area; total time (s) spent by the pup in the nest bedding area.

Social Interaction Test

The test was performed as previously described (Terranova and Laviola 2005; Jamain et al. 2008). The 28–30-day-old mice were individually habituated to the experimental apparatus (a Plexiglas cage measuring 30 × 30 × 30 cm³) for 5 min the day before testing. On the test day, the animals were isolated for 2 h before testing, to enhance their social motivation and thus facilitate the expression of social interaction during testing. The test consisted of placing 2 animals (same treatment and weight) into the test cage for 10 min.

The behavior of the animals was recorded using a video camera with zoom lens, DVD recorder and LCD monitor. Behavior was assessed per single animal and analyzed by a trained observer who was unaware of genotype and treatment conditions using the Observer XT software (Noldus, The Netherlands).

The following parameters were scored (Terranova and Laviola 2005; Jamain et al. 2008):

a. Social activities:

1. Social sniffing: sniffing any part of the body of the partner, including the anogenital area.
2. Following: moving in the direction of or pursuing the partner, who moves away.
3. Mutual circle: partners are mutually sniffing each other's anogenital region, while describing tight circles with their reciprocal following movements.
4. Pushing past: the focal animal passes between the wall of the cage and the body of the partner by pushing its own body through the narrow space available.
5. Crawling under/over: the focal animal crawls underneath or over the partner's body, crossing it transversely from one side to the other.
6. Social grooming: chewing and licking the fur of the partner.
7. Social rest: the focal animal is being groomed by the partner.
8. Pushing under: the focal animal pushes its own snout or the whole anterior part of its body under the partner's body, and rests for at least 3 s.
9. Social inactivity: the focal animal is lying flat or standing still (eyes closed or open) while maintaining close physical contact with the partner.

b. Nonsocial activities:

1. Running: the focal animal performs a sudden, rapid, vigorous, and erratic darting, characterized by frequent and sharp changes in direction and without any obvious target.
2. Inactive: Self-explanatory.
3. Exploring: Self-explanatory.

- Digging: the focal animal is digging in the sawdust, pushing and kicking it around, using the snout and/or both the forepaws and hindpaws.

The average frequency of total social activities, quantified as number of events during the 10 min testing session, was graphed.

Statistical Analysis

Results are expressed as mean \pm standard error of the mean (SEM). All statistical analyses were based on biological replicates. Appropriate statistical tests used for each experiment are described in the corresponding figure legends. All statistical analyses were carried out using the GraphPad Prism Version 6.0e.

Results

PDE2A Dysregulation is Involved in the Physiopathology of FXTAS

Pde2a is expressed both in cortex and hippocampus (e.g., supragranular layer of neocortex, CA1 and CA3 regions of hippocampus) (Stephenson et al. 2009, 2012), with a high and homogenous expression in the mouse CA1. To assess whether the increased

abundance of the PDE2A protein in the absence of FMRP that we described (Maurin et al. 2018) is associated with its elevated activity in hippocampus, we measured cAMP levels in single neurons of the CA1 area in *Fmr1*-KO and WT mouse brain slices. For this purpose, we used the Epac-S^{H150} fluorescent biosensor that detects an increase in cAMP levels by a decrease in FRET between the donor and acceptor fluorophores (Polito et al. 2013). These changes were monitored in real-time by ratiometric fluorescence imaging. cAMP synthesis was first stimulated using forskolin, leading to a steady-state biosensor emission ratio. PDE2A was then activated using the NO donor DEANO, which decreased the biosensor ratio. PDE2A activity was then blocked by the addition of the potent and specific PDE2A inhibitor BAY607550 (Boess et al. 2004), which increased the biosensor ratio, revealing the effective contribution of PDE2A in cAMP degradation. A final application of forskolin and the nonselective phosphodiesterase inhibitor IBMX increased the biosensor ratio to its maximum. An example of this analysis in WT neurons is reported in Figure 1A, B. Then we performed these assays in hippocampal slices obtained from PND 7–11 WT and *Fmr1*-KO mice. cAMP levels elicited by forskolin and DEANO stimulation were significantly lower in the absence of *Fmr1* expression, consistent with an elevated PDE2A activity in the *Fmr1*-KO hippocampus (Fig. 1C). We confirmed these findings by a detailed analysis of cAMP

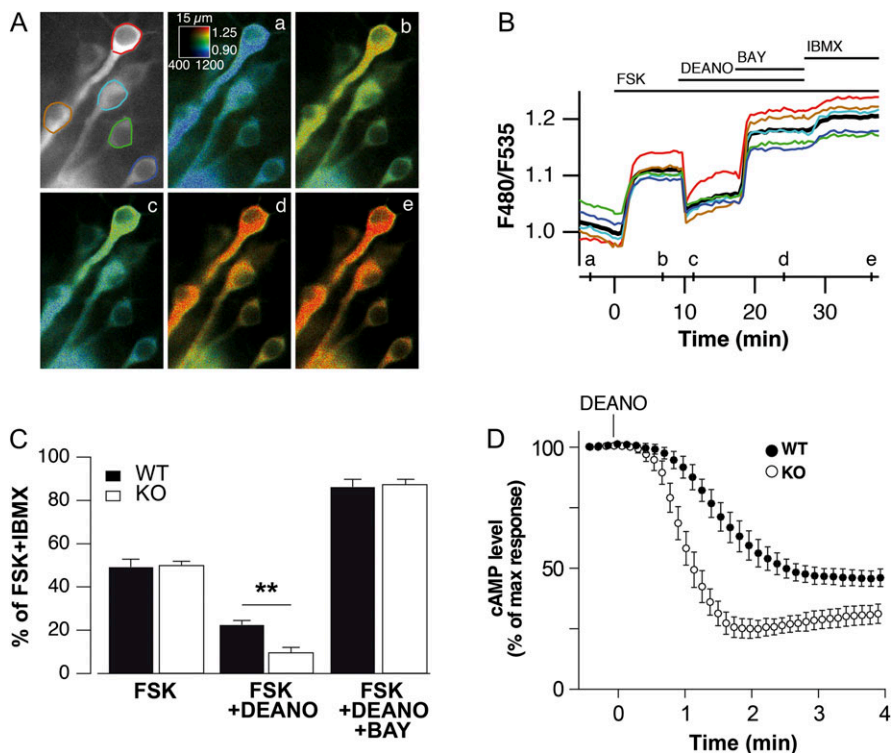


Figure 1. The increased activity of PDE2A results in decreased cAMP levels. (A) Hippocampal brain slices expressing the Epac-S^{H150} biosensor were imaged with wide-field fluorescence microscopy (here exemplified with a measure in a WT brain slice). Images show the raw fluorescence intensity at 535 nm (in gray scale) and the ratio (in pseudocolor), reporting changes in cAMP concentration before stimulation and at different times of the recording during the different treatments (a–e), as indicated by the corresponding lines on the graph in panel “B”. The calibration square on the pseudocolor image indicates from left to right increasing fluorescence intensity levels, and from bottom to top increasing ratio values. The width of the square is used as a scale bar. Its size is indicated above it in micrometers. (B) Each trace on the graph indicates the F480/F535 emission ratio measured on the regions (neuron) delimited by the color contour drawn on the gray scale image (upper left panel). The black trace corresponds to the mean of the 5 colored traces. (C) Quantification of cAMP in WT and *Fmr1*-KO hippocampal slices: the successive responses to forskolin, DEANO and BAY607550 were quantified as a fraction of the maximal response measured in the presence of IBMX. (D) Average ratio response to forskolin (10 μ M), forskolin + DEANO (10 μ M) and forskolin + DEANO + BAY607550 (0.2 μ M) for WT and *Fmr1*-KO. Mean \pm SEM is shown. In each experiment (i.e., brain slices tested, one slice per animal) a variable number of neurons have been considered (between 1 and 6). Results from $n = 12$ WT and $n = 16$ *Fmr1*-KO experiments are shown. Two-way ANOVA followed by Bonferroni multiple comparisons post hoc test revealed a significantly lower level of cAMP in *Fmr1*-KO slices for the FSK + DEANO condition ($F_{\text{genotype}(1,26)} = 640$, $P < 0.001$; $F_{\text{genotype} \times \text{treatment}(1,26)} = 1.25$, $P = 0.278$; $F_{\text{genotype} \times \text{treatment}(1,26)} = 15.76$, $P = 0.001$) followed by Bonferroni multiple comparisons post hoc test (adjusted P value ** $P < 0.01$). (D) Time course measurement of cAMP levels after DEANO application in the presence or in the absence of FMRP.

degradation kinetics in the presence and in the absence of FMRP upon PDE2A activation with DEANO: the decrease in biosensor ratio upon PDE2A stimulation with DEANO was significantly faster in *Fmr1*-KO neurons than in WT (Fig. 1D).

In addition, using an ELISA immuno-assay, we showed that cGMP levels are also significantly decreased in *Fmr1*-KO hippocampi (Supplementary Fig. S1). Collectively, these data indicate that there is an elevated activity of PDE2A in hippocampal *Fmr1*-KO neurons.

Blocking PDE2A Activity Suppresses the Exaggerated LTD in *Fmr1*-KO hippocampus

A hallmark of FXS is the exaggerated LTD induced by mGluR activation in the hippocampal CA3-CA1 synapses (Huber et al. 2002). To assess whether inhibition of PDE2A can prevent the exaggerated synaptic plasticity characterizing FXS hippocampi, we measured LTD expression in the presence and in the absence of BAY607550. AMPA receptor-mediated excitatory postsynaptic currents (EPSCs) were recorded from CA1 pyramidal neurons under whole-cell patch clamp following stimulation of Schaffer collaterals, in the continuous presence of D-AP5 (50 μ M) and bicuculline (5 μ M). Bath application of DHPG (100 μ M, 5 min), an agonist of group I mGluRs, induced a LTD of EPSC amplitude that in WT was not modified in the presence of BAY607550 (50 nM; Fig. 2A,C). The amount of mGluR-LTD is exaggerated in *Fmr1*-KO hippocampi (EPSC amplitude: 40 \pm 9% vs. 78 \pm 9% in *Fmr1* KO vs. WT, $P < 0.05$; Fig. 2B,C), as previously reported (Costa et al. 2012; Castagnola et al. 2017). Intracellular BAY607550 (50 nM) in *Fmr1*-KO mouse hippocampal neurons reverted the exaggerated mGluR-LTD to a level that is not statistically different from WT control recordings (EPSC % amplitude: 78 \pm 9% vs. 86 \pm 7% in WT vs. *Fmr1*-KO treated with BAY607550; Fig. 2B,C). Remarkably, BAY607550 treatment (50 nM) had no effect on mGluR-LTD in WT slices (Fig. 2A–C). These results clearly show the implication of PDE2A-mediated regulation of cAMP and cGMP in the exaggerated mGluR-dependent LTD in *Fmr1*-KO mice.

Inhibiting PDE2A Activity Restores Axonal Length and Spine Maturation in Cultured Cortical *Fmr1*-KO Neurons

The presence of abnormal immature dendritic spines in the brain of FXS patients and in primary neuronal cultures of mouse *Fmr1*-KO models of FXS (Comery et al. 1997; Irwin et al. 2000; Nimchinsky et al. 2001; Antar et al. 2005, 2006) is another hallmark associated with the functional absence of FMRP. Importantly, both cAMP and cGMP have been reported to exert an important role in axonal growth and dendritic spine maturation (Shelly et al. 2010; Shen and Cowan 2010; Averaimo and Nicol 2014; Akiyama et al. 2016). Therefore, to assess the involvement of PDE2A in synaptic morphology, we first analyzed cAMP levels in cultured cortical neurons in the absence or in the presence of PDE2A inhibitors (Supplementary Fig. S2). We then assessed the impact of an inhibition of PDE2A activity on the maturation of dendritic spines (Fig. 3) and on axonal growth (Fig. 4) in *Fmr1*-KO cultured cortical neurons. To quantify the activity of PDE2A in FXS neurons, we measured cAMP levels in cultured *Fmr1*-KO upon forskolin stimulation associated with pan-PDE inhibition with IBMX (Supplementary Fig. S2). This latter treatment led to a significant increase in cAMP levels both in the presence and in the absence of FMRP expression (Supplementary Fig. S2A), while treatment with Rolipram (a specific inhibitor of PDE4) did not (Supplementary

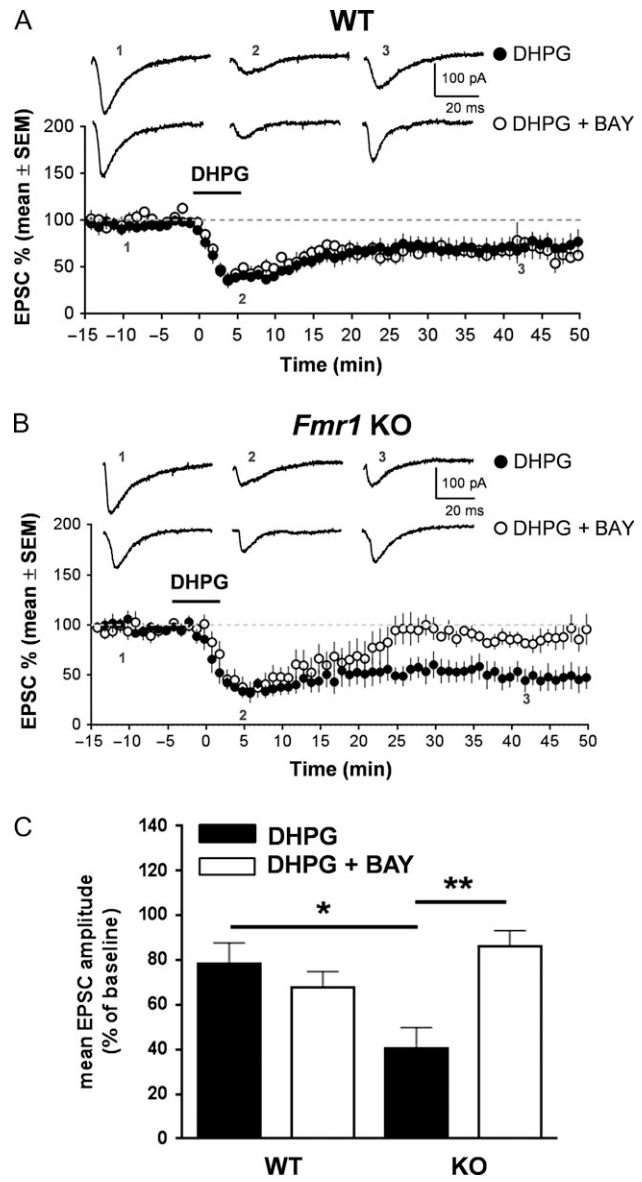


Figure 2. Blockade of PDE2A rescues the exaggerated hippocampal mGluR-dependent LTD in the *Fmr1*-KO brain. (A) DHPG (100 μ M, 5 min) induces a mGluR-LTD of EPSCs recorded from CA1 pyramidal neurons obtained from WT mouse slices ($n = 6$). BAY607550 (50 nM, added intracellularly in the recording pipette) did not modify the amount of mGluR-LTD of EPSCs recorded from CA1 pyramidal neurons in WT slices ($n = 6$). (B) In mouse *Fmr1*-KO slices ($n = 9$), mGluR-LTD was reversed in the presence of intracellular BAY607550 (50 nM). (C) Bar graphs show % EPSC amplitude (mean \pm SEM from groups of neurons) 40 min after application of DHPG in control conditions or in the presence of intracellular BAY607550 (50 nM). Bar graphs show the mean \pm SEM values of EPSC % after the indicated pharmacological treatments. Two-way ANOVA were computed ($F_{\text{genotype}(1,22)} = 1.159$, $P = 0.2933$; $F_{\text{treatment}(1,22)} = 3.919$, $P = 0.2933$; $F_{\text{genotype} \times \text{treatment}(1,22)} = 10.24$, $P = 0.0041$) with Bonferroni's post-tests for multiple comparisons of data sets, using genotype (*Fmr1*-KO or WT) and treatment (BAY607550 or vehicle) as between-subjects factor (adjusted P value: * $P = 0.0276$; ** $P = 0.0037$).

Fig. S2B). Conversely, the specific blockade of PDE2A activity by BAY607550 promoted a significant increase in cAMP levels in *Fmr1*-KO neurons without affecting its abundance in WT neurons (Supplementary Fig. S2C). This finding suggests a PDE2A-dependent regulation of cAMP levels in *Fmr1*-KO neurons.

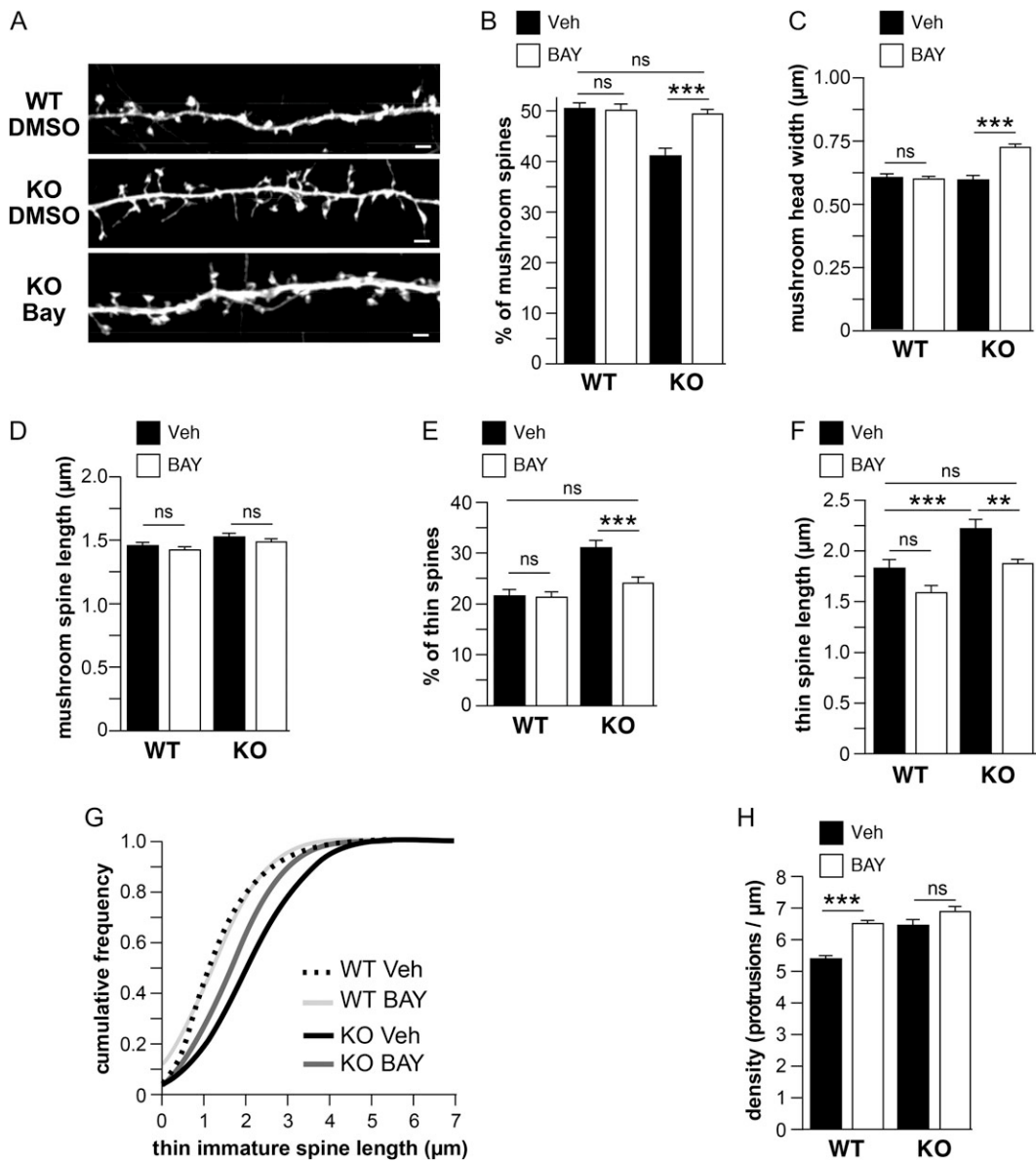


Figure 3. Inhibition of PDE2A activity improves *Fmr1*-KO dendritic spine morphology in cultured cortical neurons. (A) Representative high-resolution confocal images showing GFP-expressing WT and *Fmr1*-KO mouse secondary dendrites treated or not for 24 h with 0.2 μM BAY607550 to block PDE2A activity. Spine morphology was assessed using NeuronStudio software 19 h post-transduction and compared with the measurement obtained from control DMSO-treated neurons. Scale bars: 2 μm. All summary histograms present mean ± SEM values, statistical significance was assessed with 2-way ANOVA. The percentage of mature mushroom spines ($F_{\text{genotype}}(1,110) = 10.98$, $P = 0.0012$; $F_{\text{treatment}}(1,110) = 7.042$, $P = 0.0091$; $F_{\text{genotype} \times \text{treatment}(1,110)} = 8.984$, $P = 0.0034$), (B) mushroom head width ($F_{\text{genotype}}(1,1678) = 18.15$, $P < 0.0001$; $F_{\text{treatment}}(1,1678) = 22.06$, $P < 0.0001$; $F_{\text{genotype} \times \text{treatment}(1,1678)} = 28.41$, $P < 0.0001$), (C) and mushroom spine length ($F_{\text{genotype}}(1,1599) = 7.217$, $P = 0.0073$; $F_{\text{treatment}}(1,1599) = 3.665$, $P = 0.0558$; $F_{\text{genotype} \times \text{treatment}(1,1599)} = 0.002329$, $P = 0.9615$) (D) measured in secondary dendrites of control and BAY607550-treated neurons. The percentage of immature thin spines ($F_{\text{genotype}}(1,111) = 30.25$, $P < 0.0001$; $F_{\text{treatment}}(1,111) = 12.09$, $P = 0.0007$; $F_{\text{genotype} \times \text{treatment}(1,111)} = 8.911$, $P = 0.0035$) (E) and thin spine length ($F_{\text{genotype}}(1,878) = 23.16$, $P < 0.0001$; $F_{\text{treatment}}(1,878) = 17.37$, $P < 0.0001$; $F_{\text{genotype} \times \text{treatment}(1,878)} = 0.6166$, $P = 0.4325$) (F) is presented. The consequence of the BAY607550 treatment on the distribution of the thin spine length is depicted as cumulative frequency curves in (G). (H) Histograms showing the mean ± SEM values of protrusion frequency after the indicated pharmacological treatments. Two-way ANOVA were computed with Bonferroni post hoc test to assess the treatment effect in neurons from each genotype. (Adjusted P value: ** $P < 0.01$; *** $P < 0.001$. $N = \sim 1000$.) Protrusions per condition (3 independent mouse cortical neuron cultures; 24–30 neurons per condition). ns, not significant.

In cultured *Fmr1*-KO neurons (Fig. 3A), the specific inhibition of PDE2A by BAY607550 strongly promoted spine maturation by increasing the number of mushroom spines (Fig. 3B) and reduced the number of immature filopodia (Fig. 3E) to normal WT levels. BAY607550 also had a positive impact on the maturity of *Fmr1*-KO neurons by increasing the head size of mushroom spines (Fig. 3C) and concomitantly reducing the length of thin immature spines to WT levels (Fig. 3F–G). Finally, the

BAY607550 treatment affected neither the length of mature spines (Fig. 3D) nor the density of dendritic protrusions (Fig. 3H) in *Fmr1*-KO neurons.

Abnormal axonal growth has been observed in the fly model of FXS (Morales et al. 2002). Since both cAMP and cGMP fulfill critical roles in axonal growth (Shelly et al. 2010; Shen and Cowan 2010; Averaimo and Nicol 2014; Akiyama et al. 2016), we assessed whether PDE2A activity regulates the length of axons.

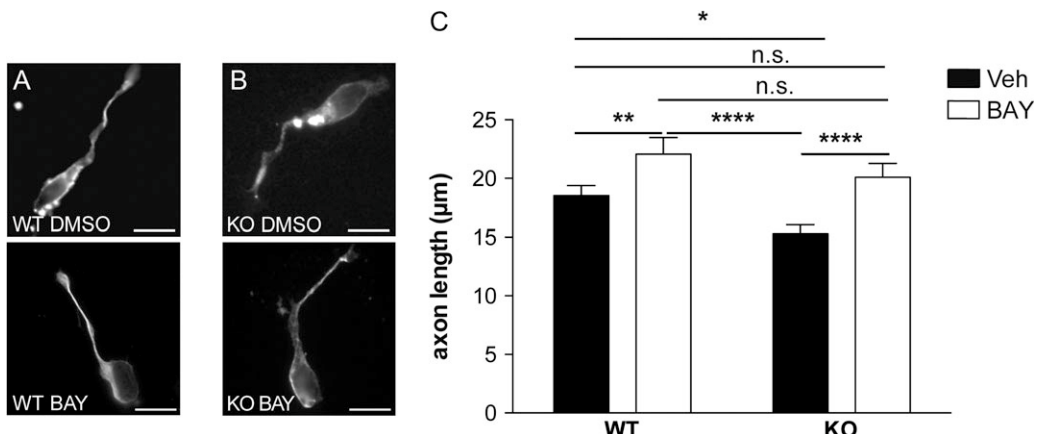


Figure 4. PDE2A activity is associated to axon growth regulation. (A, B) Representative pictures of 2 days in vitro cultured WT (A) and *Fmr1*-KO (B) primary cortical neurons treated with vehicle or 1 μM BAY607550 as indicated (scale bar: 10 μm). (C) Histogram of axon length of WT and *Fmr1*-KO neurons treated with vehicle or with 1 μM BAY607550 for 24 h. Results show the mean axon length ± SEM from 3 independent cultures on 73 randomly selected cells for each condition. Two-way ANOVA with Tukey post hoc test: DMSO:KO versus DMSO:WT. *Adjusted P value = 0.0256; BAY:WT versus DMSO:WT. **Adjusted P value = 0.0081; BAY:KO versus DMSO:WT. ns: Adjusted P value = 0.4114; BAY:WT versus DMSO:KO. ****Adjusted P value < 0.0001; BAY:KO versus DMSO:KO. ***Adjusted P value < 0.0001; BAY:KO versus BAY:WT. ns: Adjusted P value = 0.3547; ns, not significant.

Using an immunocytochemistry-based approach, we measured axon length of 2 days in vitro neurons and showed that *Fmr1*-KO neurons had significantly shorter axons than WT cells (Fig. 4A–C). The blockade of PDE2A for 24 h with BAY607550 was sufficient to fully rescue the axonal growth defect of FXS neurons (Fig. 4).

Critical Role of PDE2A Activity in Defining Social Deficits Displayed by 2 Rodent Models of FXS

The *Fmr1*-KO mouse model of FXS recapitulates the main behavioral traits initially described in FXS patients, such as cognitive deficit and social interaction impairments (Mientjes et al. 2006; Maurin et al. 2014). Since we identified *Pde2a* mRNA as a target of FMRP during the early postnatal life in the mouse brain and since we showed that PDE2A expression was increased in *Fmr1*-KO brains (Maurin et al. 2018), we investigated whether an acute PDE2A blockade in vivo rescued the altered phenotype of *Fmr1*-KO infant (PND 10–14) and adolescent (PND 30) mice in FXS-relevant behaviors (Fig. 5). At infancy, *Fmr1*-KO pups displayed early communicative deficits, since they vocalized significantly less compared with WT pups when separated from the dam and siblings at PND 10 (Fig. 5A,B). Furthermore, *Fmr1*-KO animals showed early deficits in social discrimination, since they were unable to use olfactory cues to discriminate between a neutral odor and their own cage odor in the homing behavior test (Fig. 5C,D). BAY607550 has been shown to efficiently cross the blood-brain barrier when administered i.p., promoting comparable PDE2A inhibition levels as the intracranial injection route (Wang et al. 2017). Our results showed that inhibition of PDE2A activity through i.p. administration of BAY607550 normalized the altered USV profile displayed by PND 10 *Fmr1*-KO mice (Fig. 5B). Remarkably, we validated this result by inhibiting PDE2A with Lu AF64280, another highly specific PDE2A inhibitor (Redrobe et al. 2014). Similar to BAY607550, Lu AF64280 was able to revert the altered USV frequency displayed by *Fmr1*-null pups (Supplementary Fig. S3). This confirms that PDE2A blockade is able to rescue the communicative deficit displayed by *Fmr1*-KO mice in the USV test. Furthermore, we found that treatment with BAY607550 improved the performance of *Fmr1*-KO pups in the homing behavior test (Fig. 5C–E) without

altering the performance of WT pups. Our results pointed out that altered social behavior is a core phenotypic characteristic of the FXS mouse model. Accordingly, compared with WT animals, adolescent *Fmr1*-KO mice showed reduced social interaction, a phenotype that was rescued by PDE2A inhibition (Fig. 5F).

PDE2A is a Therapeutic Target for FXS

The elevated activity of PDE2A may underlie the deficits in communicative and social domains displayed by *Fmr1*-KO mice throughout development. To confirm this possibility, we chronically treated *Fmr1*-KO mice with BAY607550 from PND 5 to PND 21, and tested their social abilities after a washout interval of 9 days. Strikingly, early treatment with BAY607550 reversed the social deficits displayed by *Fmr1*-KO mice at PND 30, showing that the beneficial effects of early PDE2A pharmacological blockade are long-lasting (Fig. 5G). Importantly, the administration of BAY607550 had no effect on the behavior of WT mice (Fig. 5B,D–G), further indicating the specificity of this treatment for the FXS phenotype. Finally, chronically administered BAY607550 rescued the abnormal dendritic spine length in the CA1 region of the hippocampus of *Fmr1*-KO mice (Supplementary Fig. S4). To validate PDE2A as a therapeutic target for FXS, we extended the behavioral analysis to *Fmr1*-KO infant rats. Similar to *Fmr1*-KO mice, *Fmr1*-KO rats vocalized less than WT controls when separated from their mother and siblings at PND 5 and PND 9 (Fig. 6A,B). Remarkably, acute administration of BAY607550 also normalized their altered USV pattern (Fig. 6A,B) and the ability of these infant rats to communicate, without affecting the behavior of WT control animals (Fig. 6A,B).

Discussion

Role of PDE2A in Hippocampus and Cortex Development

We have shown that an elevated amount of the PDE2A protein is present in *Fmr1*-null cortex and hippocampus (Maurin et al. 2018). Due to the heterogeneous pattern of the expression level of PDE2A in these brain regions (Stephenson et al. 2009, 2012), we measured here the PDE2A activity at the single cell level demonstrating that the activity of PDE2A is also significantly increased

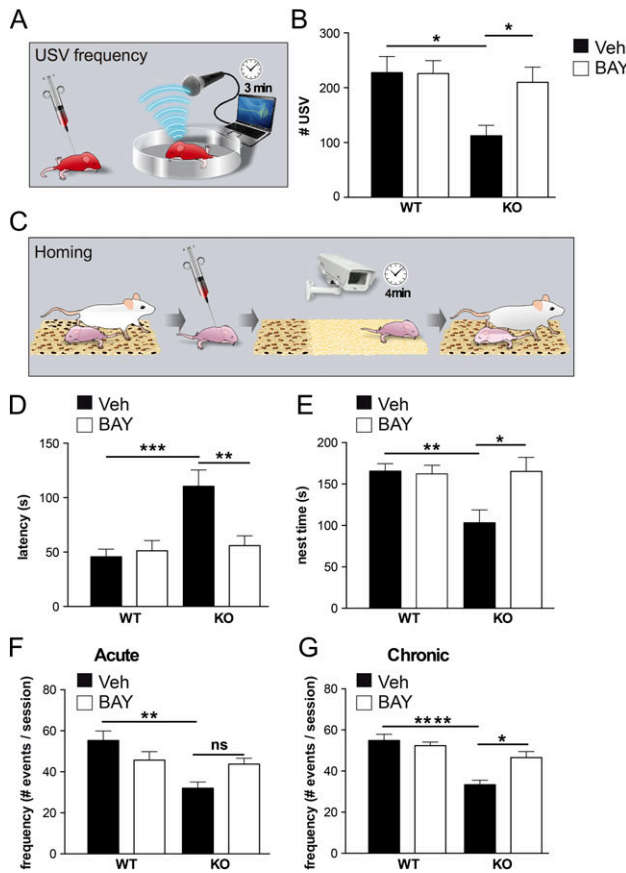


Figure 5. Inhibition of PDE2A activity rescues abnormal behaviors in infant and adolescent *Fmr1*-null mice. (A) Scheme of the USV test performed at PND 10. The 30 min after treatment with BAY607550 or vehicle, pups were separated from the dam and ultrasonic vocalizations (USV) were recorded for 3 min. (B) *Fmr1*-KO mice emit less USVs when removed from the nest at PND 10, and this communicative deficit is reversed upon BAY607550 injection ($F_{genotype(1,63)} = 7.07, P = 0.01; F_{treatment(1,63)} = 3.80, P = 0.05; F_{genotype \times treatment(1,63)} = 4.09; P = 0.04$; n: WT-Veh = 17; WT-Bay = 17; KO-Veh = 16; KO-Bay = 17); (C) presentation of the homing test performed at PND 14; *Fmr1*-KO mice show (D) longer latency to reach the home-cage bedding ($F_{genotype(1,45)} = 11.79, P = 0.001; F_{treatment(1,45)} = 5.86, P = 0.02; F_{genotype \times treatment(1,45)} = 8.81; P = 0.005$) and (E) spend less time in the nest area ($F_{genotype(1,45)} = 5.51, P = 0.02; F_{treatment(1,45)} = 5.37, P = 0.02; F_{genotype \times treatment(1,45)} = 6.63; P = 0.013$) in the homing behavior test at PND 14 (n: WT-Veh = 14; WT-Bay = 16; KO-Veh = 9; KO-Bay = 10); both these parameters are normalized when *Fmr1*-KO mice are treated with BAY 607550. (F, G) Social interaction was evaluated at PND 30, results are reported for acute (F) (n: WT-Veh = 18; WT-Bay = 22; KO-Veh = 12; KO-Bay = 9) ($F_{genotype(1,57)} = 7.53, P = 0.008; F_{treatment(1,57)} = 0.05, P = 0.82; F_{genotype \times treatment(1,57)} = 5.43; P = 0.02$), and chronic treatment (G) (n: WT-Veh = 11; WT-Bay = 14; KO-Veh = 8; KO-Bay = 7) ($F_{genotype(1,36)} = 28.71, P < 0.0001; F_{treatment(1,36)} = 4.358, P = 0.0440; F_{genotype \times treatment(1,36)} = 9.539, P = 0.0039$). Data represent mean \pm SEM (adjusted P value: *P < 0.05, **P < 0.01, ***P < 0.001). Two-way ANOVA was used to assess the effects of BAY607550 in *Fmr1*-KO and WT mice, using genotype (*Fmr1*-KO or WT) and treatment (BAY607550 or vehicle) as between-subjects factor, followed by Tukey multiple comparison post hoc test where appropriate.

in the absence of FMRP. Since an important fraction of PDE2A is localized at the synapse (Russwurm et al. 2009; Maurin et al. 2018), we reasoned that its elevated activity in FXS neurons could impact local cAMP and cGMP homeostasis. It has been reported that the levels of both cAMP and cGMP have critical roles in axon elongation and guidance (Shelly et al. 2010; Akiyama et al. 2016) and in regulating the morphology and growth of dendritic spines

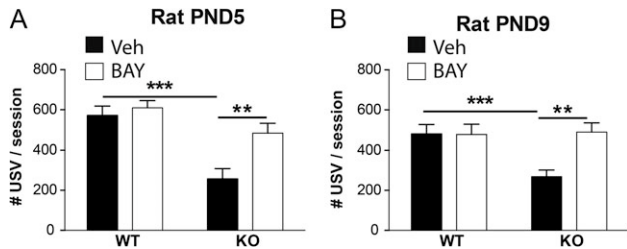


Figure 6. Inhibition of PDE2A activity rescues communication deficit in infant *Fmr1*-KO rats. *Fmr1*-KO rats emit less USVs when removed from the nest at PND 5 and 9, and this communicative deficit is reversed upon BAY607550 injection at (A) PND 5 (n: WT-Veh = 8; WT-Bay = 8; KO-Veh = 9; KO-Bay = 9) ($F_{genotype(1,32)} = 5.67, P = 0.023; F_{treatment(1,32)} = 6.76, P = 0.014; F_{genotype \times treatment(1,32)} = 7.12, P = 0.012$) and (B) at PND 9 (n: WT-Veh = 8; WT-Bay = 10; KO-Veh = 10; KO-Bay = 10) ($F_{genotype(1,30)} = 22.72, P < 0.001; F_{treatment(1,30)} = 8.27, P = 0.007; F_{genotype \times treatment(1,30)} = 4.28; P = 0.047$). Data represent the mean number of emitted USV (\pm SEM) per 3 min-recording session. (Adjusted P value **P < 0.01, ***P < 0.001.) Two-way ANOVA was used to assess the effects of BAY607550 in *Fmr1*-KO and WT rats, using genotype (*Fmr1*-KO or WT) and treatment (BAY607550 or vehicle) as between-subjects factors, followed by Tukey multiple comparison post hoc test where appropriate.

(Dityatev and El-Husseini 2011). Indeed, *Fmr1*-KO neurons show an increased PDE2A activity as well as an increased density of spines compared with WT neurons. Blocking the excess of PDE2A activity in *Fmr1*-KO cells leads to spine maturation without decreasing the protrusion density. In WT cells, there is no effect of the BAY607550 on spine maturation but there is an increase in the density of protrusion suggesting separated roles of PDE2A activity in spine formation and maturation but not in spine elimination. This latter result is consistent with our recent findings showing that the density of spines is restored in *Fmr1*-KO olfactory neurons by depleting CYFIP1, a protein connecting FMRP with actin remodeling via Rac1 (Abekhoukh et al. 2017). Moreover, the reduced length of growing axons that we found in 2 DIV *Fmr1*-KO neurons may result from the elevated levels of PDE2A that lead, in turn, to a reduced concentration of axonal cAMP and cGMP. Indeed, the normal length of growing axons is restored after treatment with the specific PDE2A inhibitor BAY607550. Furthermore, it is known that cGMP stimulates synthesis of glutamate via phosphoglycerate kinase (PGK) (Neitz et al. 2011). Consistent with a reduction of cGMP, glutamate levels are reduced in the *Fmr1*-KO cortex (Davidovic et al. 2011) and hippocampus (Hebert et al. 2014). PDE2A is the only PDE identified so far at the presynaptic active zone, associated with docked vesicles and illustrating the importance of such a compartmentalized action (Maurin et al. 2018). Indeed, cAMP abundance coupled to PKA signaling is critical to modulate assembly/disassembly/priming/recycling of neurotransmitter vesicles and, consequently, for synaptic transmission and plasticity events (Crawford and Mennerick 2012) and basal synaptic transmission (Gomez and Breitenbacher 2013). Here we show that the pharmacological inhibition of PDE2A activity rescues the exaggerated mGluR-dependent LTD in *Fmr1*-KO hippocampal slices, a well-characterized hallmark of *Fmr1*-KO brain (Huber et al. 2002).

As we already explained, cGMP and cAMP are involved in axonal growth, spine maturation and synaptic plasticity. Since PDE2A modulates the level of both cAMP and cGMP, we can suggest that its elevated activity in the absence of FMRP contributes to the definition of a neuronal FXS phenotype characterized by altered dendritic morphology, altered axonal length and exaggerated mGluR-LTD.

PDE2A has a Crucial and Evolutionarily Conserved Role in the Physiopathology of FXS

We show here that *Fmr1*-KO pups have profound deficits in both social communication and social discrimination from the first days of life, as revealed by their altered USV profile and impaired homing behavior, respectively. This, in turn, may alter the proper development of social behavior and social recognition (Terry and Johanson 1996; Melo et al. 2006). In line with this hypothesis, *Fmr1*-KO mice show deficits in social interaction at the adolescent age (Liu and Smith 2009; Dahlhaus and El-Husseini 2010; Kazdoba et al. 2014) that mirror the phenotype observed in FXS patients. Considering the impact of the pharmacological inhibition of PDE2A on the *in vitro* and *ex vivo* FXS phenotypes, we assessed whether the PDE2A inhibitor BAY607550 could revert the altered phenotype displayed by *Fmr1*-KO animals in social communication, social discrimination, and social interaction. Administration of BAY607550 normalizes the USV profile displayed by *Fmr1*-KO mice and rats. In addition, this treatment rescues the altered performance of *Fmr1*-KO pups in the homing behavior test, and increases the frequency of social interactions observed in *Fmr1*-KO mice to similar levels as WT animals. While PDE2A was previously linked to cognitive processes (Gomez and Breitenbucher 2013; Redrobe et al. 2014; Lueptow et al. 2016), here, for the first time, we associate its increased activity with altered social deficits. It is interesting to notice that PDE2A is coexpressed with FMRP in a specific class of neurons in the olfactory bulb (Korsak et al. 2017). These neurons have been shown to play a role in thermosensing and detecting stress in congeners as well as in pheromone sensing behavior (Juifls et al. 1997). This can lead to the speculation that modulating PDE2A activity in these neurons may influence the social behavior. In conclusion, PDE2A may be an attractive target to simultaneously treat the social and communicative dysfunctions characterizing FXS patients. Importantly, mice chronically treated with BAY607550 during the early postnatal development period clearly benefit of the positive effect of this therapy when tested at adolescence. This result strongly suggests that inhibition of PDE2A during infancy has long-term positive effects and provides a strong preclinical rationale for a new therapeutic strategy for FXS patients. Remarkably, we used very low doses of BAY607550 that do not affect the behavior of WT animals. This is important not only because our approach targets a pediatric population but also because low doses should reduce possible toxic side effects of the drug. Interestingly, several trials have been performed in the past with various formulations and dosages of PF-05 180 999 to treat migraine. We note that the trial in which the highest dosage (360 mg) was tested was discontinued for safety issues, nevertheless former trials using lower doses (30 or 120 mg) were completed but results are yet to be published (<https://clinicaltrials.gov>; #NCT01429740 and #NCT01981499). These studies are however encouraging for future therapeutic intervention for central nervous system (CNS) disorders. Indeed, a phase 1 study has been conducted to investigate the pharmacological properties of TAK915 (another PDE2A inhibitor from Takeda pharmaceuticals (Nakashima et al. 2018)) in order to guide dosage in future clinical studies in schizophrenia (<https://clinicaltrials.gov/ct2/show/results/NCT02584569>). We would suggest that TAK915 may also be used to investigate other CNS disorders in the future.

Our data clearly highlight that PDE2A abundance has a pivotal role in the physiopathology of FXS (Maurin et al. 2018). While cGMP metabolism had never been studied in FXS, it has

already been proposed that the convergence of altered pathways in FXS neurons is responsible for an altered abundance of cAMP in this syndrome. All these pathways are mostly postsynaptic signaling cascades and their relevance for FXS up to date was only studied in adult *Fmr1*-KO mice (Choi et al. 2016; Sethna et al. 2017). Inhibition of Pde4D was recently shown to have positive effects on LTD, learning and memory in adult *Fmr1*-KO mice (Gurney et al. 2017). These results provide evidence for the crucial role of cAMP abundance in synaptic plasticity in *Fmr1*-KO mice. However, the PDE4 enzyme family modulates cAMP but not cGMP levels and does not appear to be directly involved in the pathophysiology of FXS since its expression is not deregulated in the synaptosomal preparations obtained from both young and adult *Fmr1*-KO mice (Tang et al. 2015). Furthermore, Pde4D mRNA is not a prominent FMRP target in all the CLIP assays that have been performed so far (Darnell et al. 2011; Ascano et al. 2012; Tabet et al. 2016; Maurin et al. 2018).

Also, up to now, most of the treatments proposed for FXS have been tested in adult mice and, even when successful, their translation to the clinic failed (Budimirovic et al. 2017; Castagnola et al. 2017; Erickson et al. 2017). Considering these unsuccessful results, an increasing amount of data suggests the need to treat patients affected by neurodevelopmental disorders at the earliest possible age (Khalfallah et al. 2017 for review, and this study) and for a long period of time (Erickson et al. 2017). Remarkably, BAY607550 treatment rescues the communication deficits in both *Fmr1*-KO mice and rats. This strongly argues in favor of a conserved contribution of PDE2A activity in the regulation of processes and/or communication circuits underpinning social behaviors. In the same direction, our findings showing the rescue of social interaction after 9 days of washout suggest that the chronic treatment performed in infancy of these mice was sufficient to modify circuits for an extended time-period. Even if these processes should be investigated in depth in the near future, overall these findings further reinforce the translation potential of this targeted therapeutic approach for FXS.

Conclusions

PDE2A is an overlooked phosphodiesterase previously linked to cognitive processes (Boess et al. 2004; Redrobe et al. 2014; Mikami et al. 2017; Nakashima et al. 2018). Here, for the first time, we establish a relationship between its altered expression and defects in axonal growth, maturation of dendritic spines, mGluR-dependent hippocampal LTD and altered social communication, social discrimination and social interaction behaviors at early developmental ages in *Fmr1*-KO animals. FXS is the leading inherited cause of ID and ASD and the *Fmr1*-KO mouse and rat models are not only widely recognized animal models of FXS but also genetic models of ASD. Since we highlight here that PDE2A abundance has a pivotal role in the pathophysiology of FXS, an implication of PDE2A in other forms of autism can be hypothesized and therefore, targeting PDE2A could be considered a generalized pharmacological target to treat social deficits common to both ASD and FXS.

Supplementary Material

Supplementary material is available at *Cerebral Cortex* online.

Funding

Institut National de la Santé et de la Recherche Médicale (INSERM); Centre National de la Recherche Scientifique (CNRS); Université Côte d'Azur (UCA); Agence Nationale de la Recherche: ANR-12-BSV4-0020 to B.B. and ANR-15-CE16-0015 to B.B. and S.M. Fondation Recherche Médicale (FRM) DEQ20140329490 to BB and FRM-ING20140129004 to B.B. and T.M.; Fondation Jérôme Lejeune to B.B. and S.M. FRAXA Foundation to T.M. PV was supported (in part) by the Investissements d'Avenir program managed by the ANR under reference ANR-11-IDEX-0004-02 (LabEx Bio-Psy). VT was in part supported by Grant to Department of Science, Roma Tre University (MIUR-Italy Dipartimenti di eccellenza, ARTICOLO 1, COMMI 314-337 LEGGE 232/2016). S.C. and M.D. are recipient of international PhD fellowships "LabEx Signalife Program" by ANR-11-LABX-0028-01 (to B.B. and SM.).

Author's Contribution

Li.C. and E.M. performed biosensor cAMP experiments under the guidance of P.V. T.M. performed cAMP and cGMP measures in cultured neurons as described in M&M. La.C. and L.S. performed LTD studies under the supervision of Lu.C. S.C. and M.D. performed cortical neuronal cultures under the guidance of T.M. and B.B. S.C. and M.J. performed RT-qPCR studies under the guidance of B.B. A.K. and G.P. performed dendritic spines analysis under the guidance of S.M. M.J. performed axonal studies under the guidance of T.M. and B.B. M.J., S.D., F.M., M.S., and S.S. performed behavioral studies under the supervision of V.T. M.J., S.D., and T.M. performed Golgi staining under the supervision of B.B. A.D.G. synthesized Lu AF64280 under the guidance of S.A. T.M. and B.B. designed the study, T.M., V.T., L.C., P.V., S.M., and B.B. analyzed the data and wrote the article.

Notes

The authors are indebted with E. Lalli and M. Capovilla for critical reading of the article, M. Grossi, M. Beal and C. Gandin for technical help, F. Aguila for graphical artwork and I. Caillé for discussion and gift of some materials. Conflict of interest: The authors declare no competing financial interests.

References

- Abekhoukh S, Sahin HB, Grossi M, Zongaro S, Maurin T, Madrigal I, Kazue-Sugioka D, Raas-Rothschild A, Doulazmi M, Carrera P, et al. 2017. New insights into the regulatory function of CYFIP1 in the context of WAVE- and FMRP-containing complexes. *Dis Model Mech.* 10:463–474.
- Akiyama H, Fukuda T, Tojima T, Nikolaev VO, Kamiguchi H. 2016. Cyclic nucleotide control of microtubule dynamics for axon guidance. *J Neurosci.* 36:5636–5649.
- Antar LN, Dictenberg JB, Plochniak M, Afroz R, Bassell GJ. 2005. Localization of FMRP-associated mRNA granules and requirement of microtubules for activity-dependent trafficking in hippocampal neurons. *Genes Brain Behav.* 4:350–359.
- Antar LN, Li C, Zhang H, Carroll RC, Bassell GJ. 2006. Local functions for FMRP in axon growth cone motility and activity-dependent regulation of filopodia and spine synapses. *Mol Cell Neurosci.* 32:37–48.
- Ascano M Jr., Mukherjee N, Bandaru P, Miller JB, Nusbaum JD, Corcoran DL, Langlois C, Munschauer M, Dewell S, Hafner M, et al. 2012. FMRP targets distinct mRNA sequence elements to regulate protein expression. *Nature.* 492:382–386.
- Averaimo S, Nicol X. 2014. Intermingled cAMP, cGMP and calcium spatiotemporal dynamics in developing neuronal circuits. *Front Cell Neurosci.* 8:376.
- Bassell GJ, Warren ST. 2008. Fragile X syndrome: loss of local mRNA regulation alters synaptic development and function. *Neuron.* 60:201–214.
- Boess FG, Hendrix M, van der Staay FJ, Erb C, Schreiber R, van Staveren W, de Vente J, Prickaerts J, Blokland A, Koenig G. 2004. Inhibition of phosphodiesterase 2 increases neuronal cGMP, synaptic plasticity and memory performance. *Neuropharmacology.* 47:1081–1092.
- Budimirovic DB, Berry-Kravis E, Erickson CA, Hall SS, Hessl D, Reiss AL, King MK, Abbeduto L, Kaufmann WE. 2017. Updated report on tools to measure outcomes of clinical trials in fragile X syndrome. *J Neurodev Dis.* 9:14.
- Castagnola S, Bardoni B, Maurin T. 2017. The search for an effective therapy to treat fragile X syndrome: dream or reality? *Front Syn Neurosci.* 9:15.
- Choi CH, Schoenfeld BP, Bell AJ, Hinchey J, Rosenfelt C, Gertner MJ, Campbell SR, Emerson D, Hinchey P, Kollaros M, et al. 2016. Multiple drug treatments that increase cAMP signaling restore long-term memory and aberrant signaling in fragile X syndrome models. *Front Behav Neurosci.* 10:136.
- Comery TA, Harris JB, Willems PJ, Oostra BA, Irwin SA, Weiler IJ, Greenough WT. 1997. Abnormal dendritic spines in fragile X knockout mice: maturation and pruning deficits. *Proc Natl Acad Sci USA.* 94:5401–5404.
- Costa L, Spatuzza M, D'Antoni S, Bonaccorso CM, Trovato C, Musumeci SA, Leopoldo M, Lacivita E, Catania MV, Ciranna L. 2012. Activation of 5-HT7 serotonin receptors reverses metabotropic glutamate receptor-mediated synaptic plasticity in wild-type and Fmr1 knockout mice, a model of Fragile X syndrome. *Biol Psychiatry.* 72:924–933.
- Crawford DC, Mennerick S. 2012. Presynaptically silent synapses: dormancy and awakening of presynaptic vesicle release. *Neuroscientist.* 18:216–223.
- Dahlhaus R, El-Husseini A. 2010. Altered neuroligin expression is involved in social deficits in a mouse model of the fragile X syndrome. *Behav Brain Res.* 208:96–105.
- Darnell JC, Van Driesche SJ, Zhang C, Hung KY, Mele A, Fraser CE, Stone EF, Chen C, Fak JJ, Chi SW, et al. 2011. FMRP stalls ribosomal translocation on mRNAs linked to synaptic function and autism. *Cell.* 146:247–261.
- Davidovic L, Navratil V, Bonaccorso CM, Catania MV, Bardoni B, Dumas ME. 2011. A metabolomic and systems biology perspective on the brain of the fragile X syndrome mouse model. *Genome Res.* 21:2190–2202.
- Devader C, Khayachi A, Veyssiére J, Moha Ou Maati H, Roulot M, Moreno S, Borsotto M, Martin S, Heurteaux C, Mazella J. 2015. In vitro and in vivo regulation of synaptogenesis by the novel antidepressant spadin. *Br J Pharmacol.* 172:2604–2617.
- Ding L, Zhang C, Masood A, Li J, Sun J, Nadeem A, Zhang HT, O'Donnell JM, Xu Y. 2014. Protective effects of phosphodiesterase 2 inhibitor on depression- and anxiety-like behaviors: involvement of antioxidant and anti-apoptotic mechanisms. *Behav Brain Res.* 268:150–158.
- Dityatev A, El-Husseini A. 2011. Molecular mechanisms of synaptogenesis. New York; London: Springer.
- Erickson CA, Davenport MH, Schaefer TL, Wink LK, Pedapati EV, Sweeney JA, Fitzpatrick SE, Brown WT, Budimirovic D, Hagerman RJ, et al. 2017. Fragile X targeted pharmacotherapy: lessons learned and future directions. *J Neurodev Disord.* 9:7.

- Gomez L, Breitenbucher JG. 2013. PDE2 inhibition: potential for the treatment of cognitive disorders. *Bioorg Med Chem Lett.* 23:6522–6527.
- Gothelf D, Furfaro JA, Hoeft F, Hoeft F, Eckert MA, Hall SS, O'Hara R, Erba HW, Ringel J, Hayashi KM, et al. 2008. Neuroanatomy of Fragile X syndrome is associated with aberrant behavior and the FragileX mental retardation protein (FMRP). *Ann Neurol.* 63:40–51.
- Gurney ME, Cogram P, Deacon RM, Rex C, Tranfaglia M. 2017. Multiple behavior phenotypes of the fragile-X syndrome mouse model respond to chronic inhibition of phosphodiesterase-4D (PDE4D). *Sci Rep.* 7:14653.
- Hebert B, Pietropaolo S, Meme S, Laudier B, Laugerie A, Doisne N, Quartier A, Lefevre S, Got L, Cahard D, et al. 2014. Rescue of fragile X syndrome phenotypes in Fmr1 KO mice by a BKCa channel opener molecule. *Orphanet J Rare Dis.* 9:124.
- Hoeft F, Carter JC, Lightbody AA, Cody Hazlett H, Piven J, Reiss AL. 2010. Region-specific alterations in brain development in one- to three-year-old boys with fragile X syndrome. *Proc Natl Acad Sci USA.* 107:9335–9339.
- Huber KM, Gallagher SM, Warren ST, Bear MF. 2002. Altered synaptic plasticity in a mouse model of fragile X mental retardation. *Proc Natl Acad Sci USA.* 99:7746–7750.
- Irwin SA, Galvez R, Greenough WT. 2000. Dendritic spine structural anomalies in fragile-X mental retardation syndrome. *Cereb Cortex.* 10:1038–1044.
- Jamain S, Radyushkin K, Hammerschmidt K, Granon S, Boretius S, Varoqueaux F, Ramanantsoa N, Gallego J, Ronnenberg A, Winter D, et al. 2008. Reduced social interaction and ultrasonic communication in a mouse model of monogenic heritable autism. *Proc Natl Acad Sci USA.* 105:1710–1715.
- Juifls DM, Fülle HJ, Zhao AZ, Houslay MD, Garbers DL, Beavo JA. 1997. A subset of olfactory neurons that selectively express cGMP-stimulated phosphodiesterase (PDE2) and guanylyl cyclase-D define a unique olfactory signal transduction pathway. *Proc Natl Acad Sci USA.* 94:3388–3395.
- Kazdoba TM, Leach PT, Silverman JL, Crawley JN. 2014. Modeling fragile X syndrome in the Fmr1 knockout mouse. *Intractable Rare Dis Res.* 3:118–133.
- Khalfallah O, Jarjat M, Davidovic L, Nottet N, Cestele S, Mangegazza M, Bardoni B. 2017. Depletion of the fragile X mental retardation protein in embryonic stem cells alters the kinetics of neurogenesis. *Stem Cells.* 35:374–385.
- Khayachi A, Gwizdek C, Poupon G, Alcor D, Chafai M, Cassé F, Maurin T, Prieto M, Folci A, De Graeve F, et al. 2018. Sumoylation regulates FMRP-mediated dendritic spine elimination and maturation. *Nat Commun.* 9:757.
- Kilkenny C, Browne WJ, Cuthill IC, Emerson M, Altman DG. 2010. Improving bioscience research reporting: the ARRIVE guidelines for reporting animal research. *PLoS Biol.* 8:e1000412.
- Korsak LIT, Shepard KA, Akins MR. 2017. Cell type-dependent axonal localization of translational regulators and mRNA in mouse peripheral olfactory neurons. *J Comp Neurol.* 525: 2201–2215.
- Lai JK, Lerch JP, Doering LC, Foster JA, Ellegood J. 2016. Regional brain volumes changes in adult maleFMR1-KO mouse on the FVB strain. *Neurosci.* 318:12–21.
- Liu ZH, Smith CB. 2009. Dissociation of social and nonsocial anxiety in a mouse model of fragile X syndrome. *Neurosci Lett.* 454:62–66.
- Lueptow LM, Zhan CG, O'Donnell JM. 2016. Cyclic GMP-mediated memory enhancement in the object recognition test by inhibitors of phosphodiesterase-2 in mice. *Psychopharmacology (Berl).* 233:447–456.
- Masood A, Huang Y, Hajjhussein H, Xiao L, Li H, Sun J, Nadeem A, Zhang HT, O' Donnell JM, Xu Y. 2009. Anxiolytic effects of phosphodiesterase-2 inhibitors associated with increased cGMP signaling. *J Pharmacol Exp Ther.* 331:690–699.
- Masood A, Nadeem A, Mustafa SJ, O'Donnell JM. 2008. Reversal of oxidative stress-induced anxiety by inhibition of phosphodiesterase-2 in mice. *J Pharmacol Exp Ther.* 326: 369–379.
- Maurice DH, Ke H, Ahmad F, Wang Y, Chung J, Manganiello VC. 2014. Advances in targeting cyclic nucleotide phosphodiesterases. *Nat Rev Drug Discov.* 13:290–314.
- Maurin T, Lebrigand L, Castagnola S, Paquet A, Jarjat M, Grossi M, Popa A, Rage F, Bardoni B. 2018. HITS-CLIP in various brain areas reveals new targets and new modalities of RNA binding by fragile X mental retardation protein. *Nucleic Acids Res.* 46:6344–6355.
- Maurin T, Zongaro S, Bardoni B. 2014. Fragile X syndrome: from molecular pathology to therapy. *Neurosci Biobehav Rev.* 2: 242–255.
- Melo AI, Lovic V, Gonzalez A, Madden M, Sinopoli K, Fleming AS. 2006. Maternal and littermate deprivation disrupts maternal behavior and social-learning of food preference in adulthood: tactile stimulation, nest odor, and social rearing prevent these effects. *Dev Psychobiol.* 48:209–219.
- Mientjes EJ, Nieuwenhuizen I, Kirkpatrick L, Zu T, Hoogeveen-Westerveld M, Severijnen L, Rifé M, Willemse R, Nelson DL, Oostra BA. 2006. The generation of a conditional Fmr1 knockout mouse model to study Fmrp function in vivo. *Neurobiol Dis.* 21:549–555.
- Mikami S, Sasaki S, Asano Y, Ujikawa O, Fukumoto S, Nakashima K, Oki H, Kamiguchi N, Imada H, Iwashita H, et al. 2017. Discovery of an orally bioavailable, brain-penetrating, in vivo active phosphodiesterase 2A inhibitor lead series for the treatment of cognitive disorders. *J Med Chem.* 60:7658–7676.
- Morales J, Hiesinger PR, Schroeder AJ, Kume K, Verstreken P, Jackson FR, Nelson DL, Hassan BA. 2002. Drosophila fragile X protein, DFXR, regulates neuronal morphology and function in the brain. *Neuron.* 34:961–972.
- Nakashima M, Imada H, Shiraishi E, Ito Y, Suzuki N, Miyamoto M, Taniguchi T, Iwashita H. 2018. Phosphodiesterase 2A inhibitor TAK-915 ameliorates cognitive impairments and social withdrawal in N-methyl-d-aspartate receptor antagonist-induced rat models of schizophrenia. *J Pharmacol Exp Ther.* 365:179–188.
- Neitz A, Mergia E, Eysel UT, Koesling D, Mittmann T. 2011. Presynaptic nitric oxide/cGMP facilitates glutamate release via hyperpolarization-activated cyclic nucleotide-gated channels in the hippocampus. *Eur J Neurosci.* 33:1611–1621.
- Nimchinsky EA, Oberlander AM, Svoboda K. 2001. Abnormal development of dendritic spines in FMR1 knock-out mice. *J Neurosci.* 21:5139–5146.
- Park AJ, Havekes R, Choi JH, Luczak V, Nie T, Huang T, Abel T. 2014. A presynaptic role for PKA in synaptic tagging and memory. *Neurobiol Learn Mem.* 114:101–112.
- Polito M, Klarenbeek J, Jalink K, Paupardin-Tritsch D, Vincent P, Castro LR. 2013. The NO/cGMP pathway inhibits transient cAMP signals through the activation of PDE2 in striatal neurons. *Front Cell Neurosci.* 7:211.
- Redrobe JP, Jorgensen M, Christoffersen CT, Montezinho LP, Bastlund JF, Carnerup M, Bundgaard C, Lerdrup L, Plath N. 2014. In vitro and in vivo characterisation of Lu AF64280, a novel, brain penetrant phosphodiesterase (PDE) 2A inhibitor: potential relevance to cognitive deficits in schizophrenia. *Psychopharmacology (Berl).* 231:3151–3167.

- Rodriguez A, Ehlenberger DB, Dickstein DL, Hof PR, Wearne SL. 2008. Automated three-dimensional detection and shape classification of dendritic spines from fluorescence microscopy images. *PLoS One.* 3:e1997.
- Russwurm C, Zoidl G, Koesling D, Russwurm M. 2009. Dual acylation of PDE2A splice variant 3: targeting to synaptic membranes. *J Biol Chem.* 284:25782–25790.
- Servadio M, Melancia F, Manduca A, di Masi A, Schiavi S, Cartocci V, Pallottini V, Campolongo P, Ascenzi P, Trezza V. 2016. Targeting anandamide metabolism rescues core and associated autistic-like symptoms in rats prenatally exposed to valproic acid. *Transl Psychiatry.* 6:e902.
- Sethna F, Feng W, Ding Q, Robison AJ, Feng Y, Wang H. 2017. Enhanced expression of ADCY1 underlies aberrant neuronal signalling and behaviour in a syndromic autism model. *Nat Commun.* 8:14359.
- Shelly M, Lim BK, Cancedda L, Heilshorn SC, Gao H, Poo MM. 2010. Local and long-range reciprocal regulation of cAMP and cGMP in axon/dendrite formation. *Science.* 327:547–552.
- Shen K, Cowan CW. 2010. Guidance molecules in synapse formation and plasticity. *Cold Spring Harb Perspect Biol.* 2:a001842.
- Stephenson DT, Coskran TM, Kelly MP, Kleiman RJ, Morton D, O'Neill SM, Schmidt CJ, Weinberg RJ, Menniti FS. 2012. The distribution of phosphodiesterase 2A in the rat brain. *Neurosci.* 226:145–155.
- Stephenson DT, Coskran TM, Wilhelms MB, Adamowicz WO, O'Donnell MM, Muravnick KB, Menniti FS, Kleiman RJ, Morton D. 2009. Immunohistochemical localization of phosphodiesterase 2A in multiple mammalian species. *J Histochem Cytochem.* 57:933–949.
- Tabet R, Moutin E, Becker JA, Heintz D, Fouillen L, Flatter E, Krézel W, Alunni V, Koebel P, Dembélé D, et al. 2016. Fragile X mental retardation protein (FMRP) controls diacylglycerol kinase activity in neurons. *Proc Natl Acad Sci USA.* 113:E3619–E3628.
- Tang B, Wang T, Wan H, Han L, Qin X, Zhang Y, Wang J, Yu C, Berton F, Francesconi W, et al. 2015. Fmr1 deficiency promotes age-dependent alterations in the cortical synaptic proteome. *Proc Natl Acad Sci USA.* 112:E4697–E4706.
- Terranova ML, Laviola G. 2005. Scoring of social interactions and play in mice during adolescence. *Curr Protoc Toxicol.* Chapter. 13: 13.10.1–13.10.11.
- Terry LM, Johanson IB. 1996. Effects of altered olfactory experiences on the development of infant rats' responses to odors. *Dev Psychobiol.* 29:353–377.
- Wang L, Xiaokaiti Y, Wang G, Xu X, Chen L, Huang X, Liu L, Pan J, Hu S, Chen Z, et al. 2017. Inhibition of PDE2 reverses beta amyloid induced memory impairment through regulation of PKA/PKG-dependent neuro-inflammatory and apoptotic pathways. *Sci Rep.* 7:12044.

Publication 3

Reduction of *Fmr1* mRNA Levels Rescues Pathological Features in Cortical Neurons in a Model of FXTAS

Malgorzata Drozd,^{1,4} Sébastien Delhaye,^{1,4} Thomas Maurin,^{1,4} Sara Castagnola,¹ Mauro Grossi,¹ Frédéric Brau,¹ Marielle Jarjat,¹ Rob Willemse,² Maria Capovilla,¹ Renate K. Hukema,² Enzo Lalli,³ and Barbara Bardoni³

¹Université Côte d'Azur, CNRS, Institute of Molecular and Cellular Pharmacology, 06560 Valbonne Sophia Antipolis, France; ²Department of Clinical Genetics, Erasmus Medical Center, Rotterdam, the Netherlands; ³Université Côte d'Azur, INSERM, CNRS, Institute of Molecular and Cellular Pharmacology, 06560 Valbonne Sophia Antipolis, France

Fragile X-associated tremor ataxia syndrome (FXTAS) is a rare disorder associated to the presence of the fragile X premutation, a 55–200 CGG repeat expansion in the 5' UTR of the *FMR1* gene. Two main neurological phenotypes have been described in carriers of the CGG premutation: (1) neurodevelopmental disorders characterized by anxiety, attention deficit hyperactivity disorder (ADHD), social deficits, or autism spectrum disorder (ASD); and (2) after 50 years old, the FXTAS phenotype. This neurodegenerative disorder is characterized by ataxia and a form of parkinsonism. The molecular pathology of this disorder is characterized by the presence of elevated levels of *Fragile X Mental Retardation 1* (*FMR1*) mRNA, presence of a repeat-associated non-AUG (RAN) translated peptide, and *FMR1* mRNA-containing nuclear inclusions. Whereas in the past FXTAS was mainly considered as a late-onset disorder, some phenotypes of patients and altered learning and memory behavior of a mouse model of FXTAS suggested that this disorder involves neurodevelopment. To better understand the physiopathological role of the increased levels of *Fmr1* mRNA during neuronal differentiation, we used a small interfering RNA (siRNA) approach to reduce the abundance of this mRNA in cultured cortical neurons from the FXTAS mouse model. Morphological alterations of neurons were rescued by this approach. This cellular phenotype is associated to differentially expressed proteins that we identified by mass spectrometry analysis. Interestingly, phenotype rescue is also associated to the rescue of the abundance of 29 proteins that are involved in various pathways, which represent putative targets for early therapeutic approaches.

INTRODUCTION

The *Fragile X Mental Retardation 1* (*FMR1*) gene encodes the fragile X mental retardation protein (FMRP), an RNA binding protein whose functional absence causes fragile X syndrome (FXS), the most common form of intellectual disability (ID) and autism spectrum disorder (ASD). The mutation in the *FMR1* gene causing FXS is the presence of a repeated sequence encompassing >200 CGG repeats in its 5' UTR. Hypermethylation of this sequence determines

gene promoter inactivation, causing the silencing of the *FMR1* gene.¹ Although 6–54 CGG repeats in the 5' UTR of *FMR1* is a polymorphism in normal individuals, a repeat sequence of variable length (55–200 CGG repeats) represents the premutation¹ that can cause fragile X tremor ataxia syndrome (FXTAS) in patients over 50 years of age.^{2,3} This is an adult-onset progressive neurodegenerative disorder leading to a variable combination of ataxia, essential tremor, gait imbalance, parkinsonism, peripheral neuropathy, anxiety, and cognitive decline, occurring predominantly in older men carrying the premutation. It is known that people carrying the premutation have a reduced hippocampal volume that correlates with impaired performance in standardized tests of memory.³ At the cellular level, this disorder is characterized by the presence of eosinophilic, ubiquitin-positive nuclear inclusions, which have been observed throughout the brain, with a high percentage being located in the hippocampus of patients, as well as in the animal model of the disease.^{3,4} Inclusions are negative for tau isoforms, alpha-synuclein, or polyglutamine peptides, reflecting a new class of inclusion disorder.³ At the molecular level, FXTAS is characterized by an elevated (2- to 8-fold) level of *FMR1* mRNA, whereas the level of FMRP is normal or slightly reduced in patients, as well in the CGG-KI mouse model.^{2–4} The *FMR1* mRNA is a component of nuclear inclusions³. The product of repeat-associated non-ATG (RAN) translation of the *FMR1* mRNA was also reported to be involved in the generation of inclusions when overexpressed.^{5,6} Although FXTAS is a late-onset disorder, it is also characterized by a set of developmental hallmarks, such as self-reported memory problems, autism-related traits, attention deficit hyperactivity disorder (ADHD), executive functioning, and psychopathology.⁷ Knockin (KI) mouse models have been generated displaying both neurodegenerative and neurodevelopmental

Received 18 July 2019; accepted 8 September 2019;
<https://doi.org/10.1016/j.omtn.2019.09.018>.

⁴These authors contributed equally to this work.

Correspondence: Barbara Bardoni, Université Côte d'Azur, INSERM, CNRS, Institute of Molecular and Cellular Pharmacology, 06560 Valbonne Sophia Antipolis, France.

E-mail: bardoni@ipmc.cnrs.fr



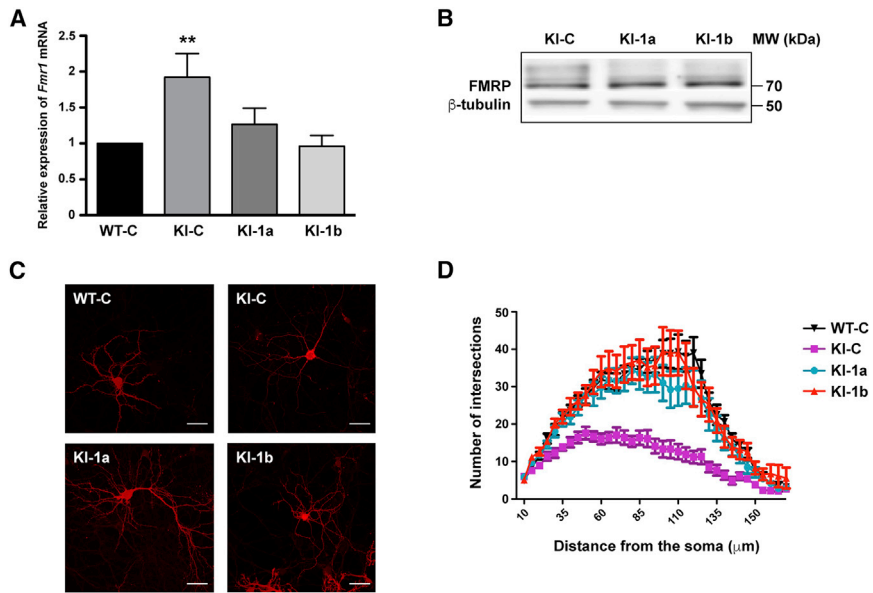


Figure 1. Role of *Fmr1* mRNA Levels in Dendritic Arborization

(A) RNA was prepared from cultured WT and knockin-CGG (KI-CGG) neurons transduced with the control (C) shRNA or two different shRNAs directed against *Fmr1* mRNA (1a and 1b). The level of *Fmr1* mRNA was measured by qRT-PCR using specific primers. Ten different experiments have been carried out for each transduced lentivirus, and a reduction of *Fmr1* levels was observed by using both shRNAs. Results are presented as mean \pm SEM; one-way ANOVA with Tukey's multiple comparisons test, ** $p < 0.01$. (B) Representative western blot analysis of cell cultures of cortical neurons transduced with C, 1a, or 1b shRNAs. FMRP (70 kDa) and β -tubulin (50 kDa) were revealed with specific antibodies. (C) Image of WT and KI-CGG cortical neurons transduced with lentiviruses expressing C, 1a, or 1b shRNAs. Scale bars: 20 μm . (D) Sholl analysis of WT and KI cultured mouse cortical neurons transduced with C or 1a or 1b shRNAs. Reduced arborization of KI-CGG neurons is rescued by *Fmr1* knockdown. Two-way ANOVA was used to compare KI-C and 1a treatments: genotype F(2; 1,527) = 227.9, $p < 0.0001$; treatment (34; 1,527) = 34.12, $p < 0.0001$; interaction F(68; 1,527) = 3.067, $p < 0.0001$; two-way ANOVA was used to compare KI-C and 1b treatments: genotype F(2; 1,318) = 293.6, *** $p < 0.0001$; treatment F(34; 1,318) = 36.21, *** $p < 0.0001$; interaction F(68; 1,318) = 3,803, $p < 0.0001$.

treatment (34; 1,527) = 34.12, $p < 0.0001$; interaction F(68; 1,527) = 3.067, $p < 0.0001$; two-way ANOVA was used to compare KI-C and 1b treatments: genotype F(2; 1,318) = 293.6, *** $p < 0.0001$; treatment F(34; 1,318) = 36.21, *** $p < 0.0001$; interaction F(68; 1,318) = 3,803, $p < 0.0001$.

phenotypes. It was reported that neuronal abnormalities and behavioral alterations in the animal model are present before the appearance of neuronal inclusions. Indeed, cultured hippocampal neurons obtained from a CGG-KI display shorter dendritic length and reduced dendritic complexity.^{4,8–10} In CGG-KI mice, cortical migration is also affected. Indeed, at embryonic day (E) 17, a 2-fold higher percentage of migrating neurons was detected to be oriented toward the ventricle in wild-type (WT) compared with CGG-KI mice.¹¹ All of these abnormalities were observed in inclusion-free cells, because CGG-KI mice display ubiquitin-positive intranuclear inclusions in neurons and astrocytes of the hippocampus and cerebellar internal cell layer starting at 12 weeks of age.^{4,8,9,11} Here we investigated the impact of normalization of *Fmr1* mRNA levels on the morphology and proteomics of cortical cultured neurons obtained from a FXTAS mouse model (CGG-KI)^{8,9} before the generation of nuclear inclusions. By this analysis we have obtained a deeper insight into the physiopathological role of *Fmr1* mRNA levels in FXTAS and identified putative targetable pathways for early treatments.

RESULTS

Hippocampal neurons were isolated from knockin-CGG (KI-CGG) E15.5 mice harboring the CGG premutated allele. It has been shown that these mice display abnormal cortical neuron migration patterns *in utero*.^{10,11} Furthermore, abnormal dendritic architecture and reduced cellular viability have been observed in hippocampal primary neurons of KI-CGG mice, where increased expression of *Fmr1* is already present even if nuclear inclusions are not detected.¹⁰ Indeed, nuclear inclusions appear first in the hippocampus of these mice at the age of 3 months, whereas the same hallmark appears later in the parietal neocortex.^{8,9} We decided to explore whether cultured cortical neurons obtained from these mice have an abnormal

morphology of dendrites and axons during development before the appearance of nuclear inclusions. We studied the dendritic arborization of wild-type (WT) and KI-CGG cortical neurons by Sholl analysis, as previously described,¹² and observed that KI-CGG neurons have a reduced arborization compared with controls (Figures S1A and S1B). To assess whether *Fmr1* mRNA levels impact the morphology of these cultured neurons, we produced lentiviruses expressing two different shRNAs selectively reducing the expression of *Fmr1* mRNA (sh-1a and sh-1b) and one shRNA control (sh-C),¹³ and we used them to transduce cortical cultured neurons obtained from WT and from KI-CGG mice. The infection was performed at 5 DIV (days *in vitro*), and RNA and proteins were prepared from these cultures at 20 DIV. As expected,^{4,13} *Fmr1* mRNA levels were elevated 2-fold in cultured KI cortical neurons compared with WT. sh-1a reduced *Fmr1* transcript levels by 30%, whereas sh-1b reduced them by 50%, (Figure 1A). FMRP levels are not changed in KI cultured neurons compared with WT,^{10,13} and as previously shown in patients.^{2,3} Similarly, the expression level of FMRP was not affected by *Fmr1* knockdown in KI neurons (Figure 1B), as we already observed by transfecting fibroblasts obtained from FXTAS patients with the same shRNAs.¹³ We then analyzed the arborization of WT and KI cortical neurons transduced with *Fmr1* shRNAs. We confirmed that KI neurons transduced with the lentivirus expressing the control shRNA (KI-C) are less arborized than WT neurons transduced with the same lentivirus (Figures 1C and 1D). However, KI neurons transduced with lentivirus expressing either sh-1a or sh-1b displayed a normal dendritic arborization (Figures 1C and 1D).

In 2 DIV neurons we measured the axon length, and we found that they are significantly shorter in *Fmr1*-KI neurons compared with

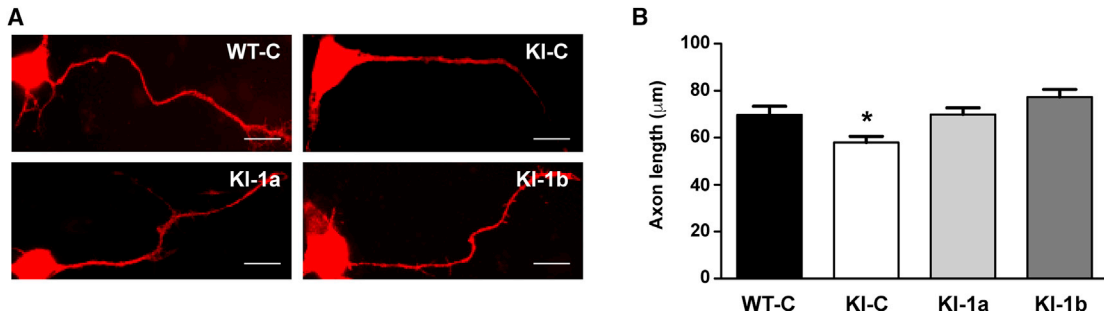


Figure 2. *Fmr1* mRNA Levels Are Associated to Axon Growth

(A) Representative pictures of 2 days *in vitro* cultured WT-C, KI-C, KI-1a, and KI-1b primary cortical neurons. Scale bars: 10 μm. (B) Histogram of axon length of WT and KI cultured neurons transfected with C, 1a, or 1b shRNAs. Results show mean axon length ± SEM of 150 randomly selected cells for each condition from three independent cultures. One-way ANOVA with Tukey's multiple comparisons test, *p < 0.05.

WT (Figure S2). We confirmed that KI-C neurons have shorter axons than WT-C, but the length of these axons was normalized in KI-1a and KI-1b neurons (Figures 2A and 2B).

We then focused on dendritic spine abnormalities. The absence of FMRP causes a peculiar morphology of dendritic spines that has been described in FXS patients and in the mouse model, where it is particularly evident in young animals.^{14,15} Conversely, the study of dendritic spines in the brain of FXTAS patients was never reported, and in *Fmr1* KI mice it was studied only in hippocampi and in the visual cortex from adult animals, displaying an increased length of spines.^{4,16} Here we studied the morphology of dendritic spines of 20 DIV cultured cortical neurons. KI-C spines are longer, denser, and larger than controls. All of these hallmarks are rescued in KI-1a and KI-1b neurons (Figures 3A–3D), indicating that the elevated level of *Fmr1* mRNA causes a set of morphological alterations in KI-CGG neurons. However, the percentage of the different types of spines (thin, stubby, and mushroom) is not significantly different in the two genotypes (Figures 3E–3G).

To get deeper insight into the molecular pathology of FXTAS cultured neurons, we performed a proteomic analysis of neurons that have been transduced with control shRNA or with the shRNAs targeting the *Fmr1* mRNA. Protein extracts of three replicates for each condition were analyzed by nano-liquid chromatography-tandem mass spectrometry (nano-LC-MS/MS) after tryptic digestion.¹⁷ A total of 487 proteins were identified (Table S1), among which 251 have a ratio >2 (upregulation) or <0.5 (downregulation) for at least one of the three comparisons (WT-C versus KI-C, WT-C versus KI-1a, and WT-C versus KI-1b) with a p value <0.10. Interestingly, the abundance of 29 differentially expressed proteins is rescued after reduction of *Fmr1* mRNA by using both specific shRNAs (Table 1). Gene Ontology analysis of these proteins reveals a significant enrichment of proteins involved in different biochemical pathways, among which are GTP binding and RNA binding proteins (Figure 4; Table S2).

DISCUSSION

Two main neurological phenotypes have been described in carriers of the CGG premutation: those exhibiting neurodevelopmental disorders characterized by anxiety, ADHD, social deficits, or ASD, and after 50 years old, FXTAS, a neurodegenerative disorder.³ For some time, nuclear inclusions have been considered as the cause of neurodegeneration, whereas more recent studies suggest that nuclear inclusions may represent a mechanism used by neurons to protect themselves from toxic events.^{4,18–20} So far, two other main physiopathological elements are known to underpin the FXTAS phenotype: the elevated abundance of *FMR1* mRNA² and the presence of a RAN polypeptide.^{5,6} We considered that it is crucial to unravel the role of each element in the molecular pathology of FXTAS to understand the progression of the disorder and its role in pathophysiology. Indeed, it is interesting to remind that neuronal abnormal dendritic morphology (e.g., reduced length and number of dendrites that display longer spines) has been observed in FXTAS neurons at a time of development when nuclear inclusions are not detectable.^{3,4,8–11} These findings suggest that some developmental abnormalities may contribute to the late manifestation of neurodegenerative process and/or that the disease appears, with subtle phenotypes, earlier than predicted up to date. So far, no specific treatment is available for FXTAS patients. A therapy based on allopregnanolone was shown to improve cognitive functioning in patients with FXTAS and to partially alleviate some aspects of neurodegeneration, but no data are known for neurodevelopmental hallmarks,²¹ opening the possibility to search for new targetable pathways in young patients. In this study, we used a murine model of FXTAS to investigate the impact that the reduced level of *Fmr1* mRNA, but not of its encoded protein, has on the morphological and molecular phenotypes of FXTAS cultured neurons. Certainly, by reducing *Fmr1* mRNA levels, we are also supposed to reduce RAN levels, which is possibly involved in the pathophysiology of FXTAS.⁶ However, that peptide was never detected at endogenous levels in neurons so far.^{3,22}

First, we defined phenotypes that were never considered before in cultured cortical neurons obtained from the FXTAS mouse

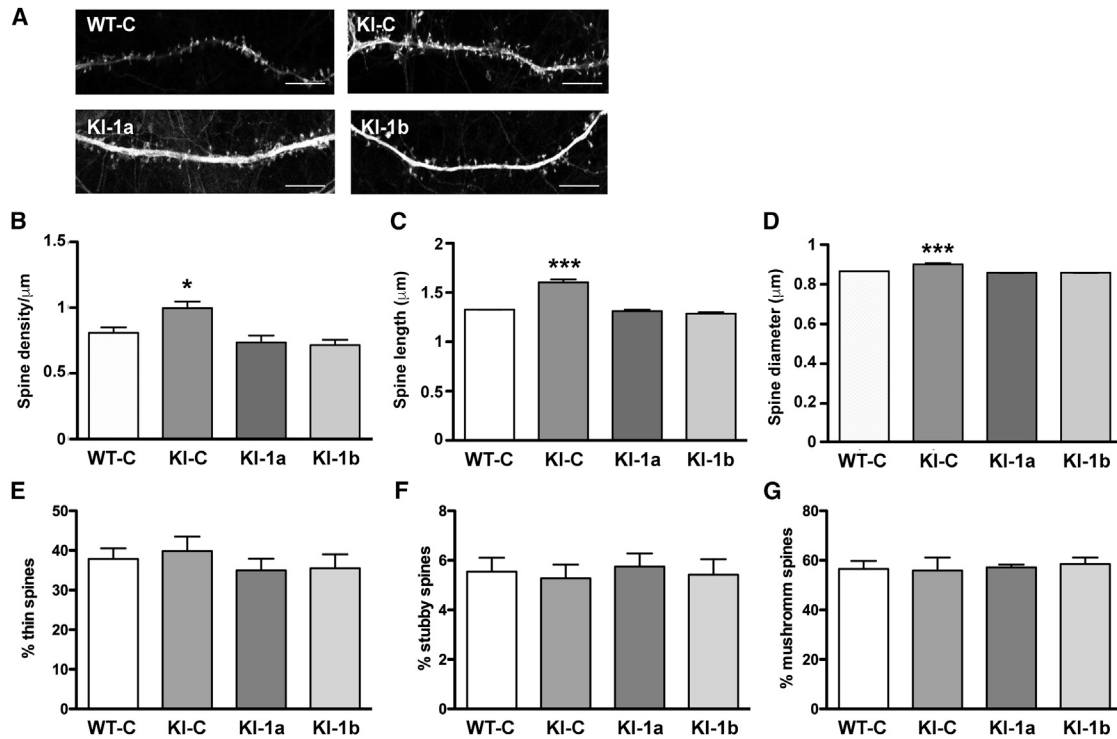


Figure 3. Reduction of *Fmr1* mRNA Levels Normalizes Dendritic Spine Morphology in KI Cortical Neurons

(A) Representative high-resolution confocal images showing dendritic spine morphology were assessed using NeuronStudio software and compared with the measurement obtained from control transduced neurons. Scale bars: 2 μm . All histograms present mean \pm SEM values. Statistical significance was assessed by one-way ANOVA with Tukey's multiple comparisons test. (B–G) Histograms showing the mean \pm SEM values of (B) protrusion frequency in the various cultures, * $p < 0.05$; (C) spine length, *** $p < 0.001$; (D) spine head size, *** $p < 0.001$; (E) percentage of thin spines; (F) percentage of stubby spines; and (G) percentage of mushroom spines.

model: axon length and dendrite morphology. All of these new phenotypes are detected in cells not yet displaying nuclear inclusions, which are known to first appear in hippocampal neurons of 12-week-old KI-CGG mice.⁹ Interestingly, these animals have mild learning and memory deficits,^{4,9} and this behavioral phenotype is consistent with the phenotype that we observed in cultured cortical neurons. Importantly, we confirm that these phenotypes are associated with the levels of *Fmr1* mRNA because they are rescued after the expression of shRNAs specifically targeting this mRNA. We can deduce that an elevated abundance of *Fmr1* mRNA may interfere with normal RNA metabolism. We can predict that the overexpression of *Fmr1* mRNA may also likely interfere with the normal activity of RNA binding proteins or microRNAs (miRNAs) in neuronal soma, and at the synapse by competing for their binding at specific sites or at miRNA response elements (MREs).¹³ All of these considerations suggest that *Fmr1* mRNA metabolism can be regulated by a large number of RNA binding proteins and can be co-regulated with a plethora of other RNAs. For this reason, as the second step of our study, we performed a differential proteomic analysis of neurons expressing control or *Fmr1*-specific shRNAs, and we observed that a set of proteins, whose expression is deregulated in KI-CGG neurons, is normalized after treatment. Consistently, several proteins rescued by *Fmr1*-specific shRNAs are RNA binding proteins (e.g., Tia1,

Hnrnpl, and ROAA). In addition, some proteins whose levels were rescued by the reduction of *Fmr1* mRNA abundance are involved in the regulation of actin cytoskeleton dynamics, which is known to modulate the morphology of neurons and, in particular, of dendritic spines. Defective synaptic actin regulation seems to be involved in different neurodevelopmental and psychiatric disorders.²³ Interestingly, we have shown here that in KI-CGG neurons, dendritic spines are more numerous, and they appear overall longer and with a larger head, but the percentage of the various types of spines is unchanged. These results are consistent with a previous study displaying longer, but not immature, spines in the CGG-KI visual cortex.¹⁶ In addition, our findings suggest that, at least at 20 DIV, the elevated levels of *Fmr1* mRNA do not interfere with the spine maturation process but cause subtle abnormalities of their features, which may have an impact on synaptic transmission. Other rescued proteins belong to the Rab-GTPase family, a sub-class of the RAS superfamily, which spatially and temporally orchestrates specific vesicular trafficking that is critical for synaptic function in neurons in brain developmental disorders,²⁴ as well as in Parkinson's disease.²⁵ Along the same direction, another interesting protein is CLIP2, a cytoplasmic linker factor that is considered as a mediator between organelles and the cytoskeleton.²⁶ Consistent with their role in neurons, mutants of this class of proteins are associated with impaired cognitive

Table 1. Proteins Differentially Expressed in the Different Samples Studied

Name	UniProt Accession Number	WT-C	KI-C	WT-C/ Ki-C	Log (Fold Change)	p Value	KI-1a	WT-C/ Ki-1a	Log (Fold Change)	p Value	KI-1b	WT-C/ KI-1b	Log (Fold Change)	p Value
sp O89023 TPP1_MOUSE	O89023	0.00	0.93	0.00	NA	0.00001	0.00	NA	NA	1.00000	0.00	NA	NA	1.00000
sp P05132 KAPCA_MOUSE	P05132	5.16	10.17	0.51	-0.29	0.00132	5.83	0.89	-0.05	0.81905	4.79	1.08	0.03	0.81905
sp P21126 UBL4A_MOUSE	P21126	0.33	1.53	0.21	-0.67	0.04762	0.66	0.49	-0.31	0.51266	0.38	0.85	-0.07	0.51266
sp P21278 GNA11_MOUSE	P21278	7.43	4.06	1.83	0.26	0.03470	6.49	1.14	0.06	0.69780	7.98	0.93	-0.03	0.69780
sp P24369 PPIB_MOUSE	P24369	8.43	12.31	0.68	-0.16	0.03540	6.73	1.25	0.10	0.68137	9.91	0.85	-0.07	0.68137
sp P30677 GNA14_MOUSE	P30677	2.57	0.93	2.77	0.44	0.04928	2.40	1.07	0.03	0.88974	3.24	0.79	-0.10	0.88974
sp P35283 RAB12_MOUSE	P35283	5.82	3.08	1.89	0.28	0.00979	5.87	0.99	0.00	0.95886	5.51	1.06	0.02	0.95886
sp P52912 TIA1_MOUSE	P52912	0.00	0.93	0.00	NA	0.00001	0.00	NA	NA	1.00000	0.32	0.00	NA	1.00000
sp P56371 RAB4A_MOUSE	P56371	5.81	3.08	1.89	0.28	0.00560	5.87	0.99	0.00	0.94159	5.19	1.12	0.05	0.94159
sp Q80TS3 AGRL3_MOUSE	Q80TS3	0.97	2.16	0.45	-0.35	0.01678	0.37	2.64	0.42	0.17665	0.38	2.53	0.40	0.17665
sp Q8BGH2 SAM50_MOUSE	Q8BGH2	2.28	0.29	7.74	0.89	0.01329	2.07	1.10	0.04	0.79778	2.13	1.07	0.03	0.79778
sp Q8BHC4 DCAKD_MOUSE	Q8BHC4	0.00	0.93	0.00	NA	0.00001	0.31	0.00	NA	0.37390	0.00	NA	NA	0.37390
sp Q8CHT0 AL4A1_MOUSE	Q8CHT0	2.94	0.63	4.64	0.67	0.02926	2.43	1.21	0.08	0.54007	1.95	1.51	0.18	0.54007
sp Q91ZR1 RAB4B_MOUSE	Q91ZR1	5.82	3.68	1.58	0.20	0.02923	5.51	1.05	0.02	0.71442	5.19	1.12	0.05	0.71442
sp Q921F4 HNRLL_MOUSE	Q921F4	0.97	0.00	∞	NA	0.00000	0.98	0.99	0.00	0.98875	0.78	1.24	0.09	0.98875
sp Q922D8 C1TC_MOUSE	Q922D8	1.28	2.78	0.46	-0.34	0.00809	0.92	1.40	0.15	0.72353	1.29	1.00	0.00	0.72353
sp Q99020 ROAA_MOUSE	Q99020	1.63	0.31	5.34	0.73	0.04589	1.69	0.97	-0.02	0.90543	2.19	0.74	-0.13	0.90543
sp Q99PU5 ACBG1_MOUSE	Q99PU5	2.92	1.55	1.88	0.27	0.01399	2.73	1.07	0.03	0.62466	2.61	1.12	0.05	0.62466
sp Q9CPY7 AMPL_MOUSE	Q9CPY7	1.61	3.38	0.48	-0.32	0.00921	2.00	0.81	-0.09	0.53465	1.43	1.13	0.05	0.53465
sp Q9CW03 SMC3_MOUSE	Q9CW03	0.33	1.53	0.21	-0.67	0.04762	0.71	0.46	-0.34	0.64890	0.38	0.85	-0.07	0.64890
sp Q9CYR6 AGM1_MOUSE	Q9CYR6	0.33	1.86	0.18	-0.75	0.01091	0.00	∞	∞	0.37390	0.32	1.04	0.02	0.37390
sp Q9DCN2 NB5R3_MOUSE	Q9DCN2	4.53	6.79	0.67	-0.18	0.00385	4.79	0.95	-0.02	0.62926	4.48	1.01	0.00	0.62926
sp Q9WTX2 PRKRA_MOUSE	Q9WTX2	0.33	1.53	0.21	-0.67	0.04762	0.00	∞	∞	0.37390	0.00	∞	∞	0.37390
sp Q9Z0H8 CLIP2_MOUSE	Q9Z0H8	4.51	8.09	0.56	-0.25	0.04003	4.68	0.96	-0.02	0.88427	5.62	0.80	-0.10	0.88427
tr A0A087WPM2 A0A087WPM2_MOUSE	A0A087WPM2	1.94	2.78	0.70	-0.16	0.00099	1.64	1.18	0.07	0.61624	1.12	1.73	0.24	0.61624
tr A0AUM9 A0AUM9_MOUSE	A0AUM9	0.00	0.93	0.00	NA	0.00001	0.00	NA	NA	1.00000	0.00	NA	NA	1.00000
tr D3YZ68 D3YZ68_MOUSE	D3YZ68	39.80	47.10	0.84	-0.07	0.03447	38.80	1.03	0.01	0.89853	36.50	1.09	0.04	0.89853
tr E9Q7C9 E9Q7C9_MOUSE	E9Q7C9	7.46	9.91	0.75	-0.12	0.03009	5.75	1.30	0.11	0.10120	7.97	0.94	-0.03	0.10120
tr S4R232 S4R232_MOUSE	S4R232	5.50	3.04	1.81	0.26	0.03279	5.50	1.00	0.00	0.99389	5.17	1.06	0.03	0.99389

NA, not applicable.

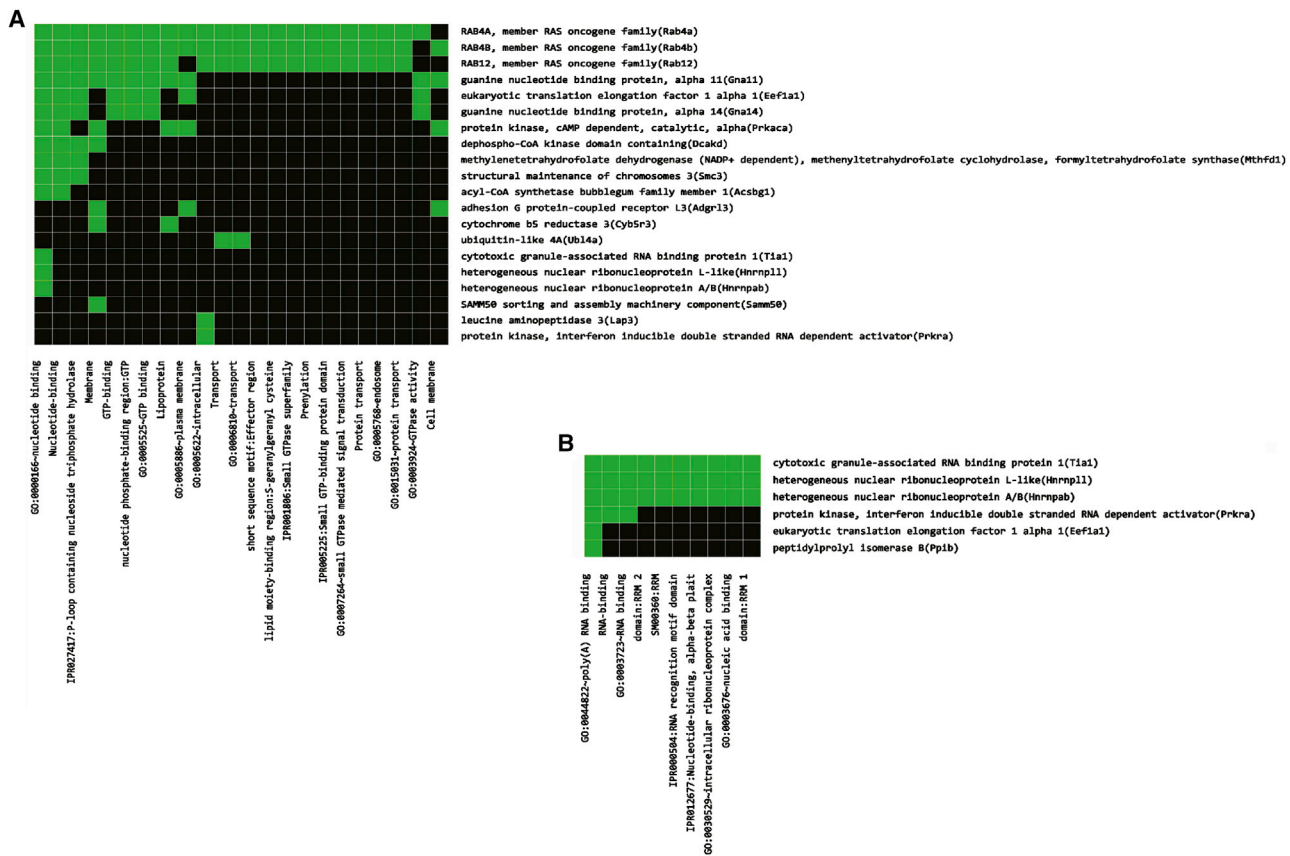


Figure 4. Gene Ontology Classification of Rescued Proteins in KI-CGG Neurons

(A and B) The DAVID Gene Ontology Functional Annotation Clustering tool⁴⁰ was used to show functional classification of rescued proteins in Ki-CGG neurons involved in (A) nucleotide-GTP binding and (B) RNA binding.

functions.^{21,24,27} Importantly, we also found mitochondrial proteins (e.g., pyrroline-5-carboxylate dehydrogenase [Aldh4a1/P5CDH] and Samm50) that are deregulated in CGG-KI neurons, confirming the importance of mitochondria in the pathophysiology of FXTAS, as previously reported by independent studies.^{28,29} This result suggests that an altered mitochondrial function is probably involved in early phenotypes of this disorder. Remarkably, the levels of those proteins were normalized by the reduction of *Fmr1* mRNA abundance. Thus, our data show molecular alterations that may contribute to explain the neurodevelopmental phenotypes of the mouse model and patients carrying the CGG premutation, thus providing an indication for future early therapies to treat CGG-premutation carriers. For instance, Aldh4a1/P5CDH is a mitochondrial matrix NAD(+)-dependent dehydrogenase that catalyzes the second step of the proline degradation pathway, converting pyrroline-5-carboxylate to glutamate. Altered function of this enzyme can result in a deregulation of the glutamate signaling, which is at the basis of various forms of brain disorders, as well as of Parkinson's disease.^{30,31} Thus, Aldh4a1/P5CDH could be a therapeutic target for FXTAS patients during different periods of life and phases of the disorder associated with the CGG premutation. Other targets may be small GTPases by

using, in this case, a strategy based on the modulation of their regulators, as recently proposed.^{32,33} In conclusion, by our approach, we defined altered pathways in FXTAS neurons that are due to the increased levels of *Fmr1* mRNA and impact on neuronal morphology. They represent the molecular pathology underpinning the late FXTAS phenotype. In particular, differentially expressed proteins between WT and CGG-KI neurons are promising pharmacological targetable molecules for early therapeutic intervention for FXTAS. On the other side, future gene therapies could also target the CGG-repeat by excising it, as already shown in an induced pluripotent stem cell (iPSC) line.³⁴

MATERIALS AND METHODS

Animals

The experiments were performed following the Animals in Research: Reporting *In Vivo* Experiments (ARRIVE) guidelines.³⁵ *Fmr1* knockin (KI) and wild-type (WT) mice on a C57BL/6J congenic background were produced as described previously.³⁶ All animals were generated and housed in groups of four in standard laboratory conditions (22°C, 55% ± 10% humidity, and 12-h light/12-h dark diurnal cycles) with food and water provided *ad libitum*. Animal care was

conducted in accordance with the European Community Directive 2010/63/EU. All experiments were approved by the local ethics committee (Comité d’Ethique en Expérimentation Animale CIEPAL-AZUR N. 00788.01).

Lentivirus Generation

Lentivirus particles were produced as previously described.³⁷

Axon Length Measurements

Dissociated neurons were transfected with lentivirus plasmids by using Nucleofector as previously described.¹³ Neurons were cultured for 48 h and then fixed. Axons were labeled with anti-Tuj1 antibody, and the size of individual growing axons (distance from the soma to the tip of the axon) was manually measured using the ImageJ software.¹⁵

Neuronal Culture and Dendritic Spine Morphology Analysis

Primary neurons were prepared from E15.5 pregnant C57BL/6 *Fmr1*^{CGG/Y} and WT mice as previously described.^{12,15} Neurons (5 days *in vitro*) were transduced with lentivirus as previously described.¹² Transduced neurons (20 days *in vitro*) were rinsed twice in PBS at room temperature (RT) after 19 h of transduction and then fixed with 4% paraformaldehyde and Triton-permeabilized. Sequential confocal images (512 × 220 pixels; zoom 3.0; average 4; speed 7) of GFP-expressing neurons were acquired with a 63× oil-immersion lens (NA 1.4) on an inverted Zeiss LSM780 confocal microscope. z series of seven to eight images of randomly selected secondary dendrites were analyzed using the NeuronStudio software, which allows for the automated detection and quantification of dendrite parameters and morphological classification, as previously performed.¹⁵

Protein Extraction and Western Blot Analysis

Immunoblotting was performed as follows: cells or grinded tissues were homogenized in lysis buffer, and debris was removed by centrifugation (20,000 × g, 10 min, 4°C).³⁸ Protein content in the supernatant was measured using the Bradford assay (Bio-Rad), and samples were separated on NuPAGE Bis-Tris 4%–12% gels in MOPS buffer. Separated proteins were transferred to nitrocellulose membranes (Bio-Rad). Membranes were blocked with PBS-Tween (0.05%) and milk (5%), and incubated with primary antibodies overnight.

Antibodies

The monoclonal 1C3 anti-FMRP antibody³⁹ was used at a 1:1,000 dilution, the anti-Tuj1 (BioLegend; TUJ1 1-15-56) antibody was used following the manufacturer’s instructions, and the monoclonal anti-β-tubulin antibody (Sigma) was used at a 1:10,000 dilution.

qRT-PCR

qPCR was performed on a LightCycler 480 (Roche) with MasterMix SYBRGreen (Roche) as previously described.¹³ Primers used to amplify *Fmr1* mRNA were previously reported.³⁷

Protein Identification and Analysis

Proteomic analysis was performed as previously described¹⁷ and resulted in the identification of around 2,000 proteins for each condition. These proteins were then compared to highlight the proteins identified under only one condition or under several conditions (“on/off” effect) and to highlight proteins predominantly identified in one condition relative to another (up if ratio >2, down if ratio <0.5). In order to compile a short list of differentially regulated proteins, a Student’s t test was performed after normalization of the spectral count quantification data. This allowed us to obtain a p value used to make this short list: from the global alignment table of the 2,888 different proteins, we focused on proteins with a p value threshold less than 0.10.

Statistical Analysis

Results are expressed as mean ± SEM. All statistical analyses were based on biological replicates. Appropriate statistical tests used for each experiment are described in the corresponding figure legends. All statistical analyses were carried out using GraphPad Prism version 6.0e.

SUPPLEMENTAL INFORMATION

Supplemental Information can be found online at <https://doi.org/10.1016/j.omtn.2019.09.018>.

AUTHOR CONTRIBUTIONS

M.D., S.D., T.M., S.M., M.G., F.B., M.J., and M.C. performed the experiments; R.W. and R.K.H. provided material; T.M., E.L., and B.B. designed the experiments; M.C., E.L., R.K.H., and B.B. wrote the manuscript.

CONFLICTS OF INTEREST

The authors declare no competing interests.

ACKNOWLEDGMENTS

The authors are grateful to S. Zongaro, P. Hammann, L. Khunn, and S. Abekhoukh for help. This study was supported by CNRS, INSERM, Association Française contre les Myopathies (AFM), Fondation Recherche Médicale (FRM) grant DEQ20140329490, Fondation Recherche sur le Cerveau (FRC), and Agence Nationale de la Recherche grants ANR-15-CE16-0015 and ANR-11-LABX-0028-01. M.D. and S.C. were recipients of a fellowship from the international PhD LabEx “Signalife” Program. S.D. was a recipient of a MRES fellowship.

REFERENCES

- Bardoni, B., Mandel, J.L., and Fisch, G.S. (2000). FMR1 gene and fragile X syndrome. *Am. J. Med. Genet.* **97**, 153–163.
- Tassone, F., Hagerman, R.J., Taylor, A.K., Gane, L.W., Godfrey, T.E., and Hagerman, P.J. (2000). Elevated levels of FMR1 mRNA in carrier males: a new mechanism of involvement in the fragile-X syndrome. *Am. J. Hum. Genet.* **66**, 6–15.
- Hagerman, P. (2013). Fragile X-associated tremor/ataxia syndrome (FXTAS): pathology and mechanisms. *Acta Neuropathol.* **126**, 1–19.
- Berman, R.F., Buijsen, R.A., Usdin, K., Pintado, E., Kooy, F., Pretto, D., Pessah, I.N., Nelson, D.L., Zalewski, Z., Charlet-Bergereaud, N., et al. (2014). Mouse models of the

- fragile X premutation and fragile X-associated tremor/ataxia syndrome. *J. Neurodev. Disord.* 6, 25.
5. Kearse, M.G., Green, K.M., Krans, A., Rodriguez, C.M., Linsalata, A.E., Goldstrohm, A.C., and Todd, P.K. (2016). CGG Repeat-Associated Non-AUG Translation utilizes a cap-dependent scanning mechanism of initiation to produce toxic proteins. *Mol. Cell* 62, 314–322.
 6. Sellier, C., Buijsen, R.A.M., He, F., Natla, S., Jung, L., Tropel, P., Gaucherot, A., Jacobs, H., Meziane, H., Vincent, A., et al. (2017). Translation of Expanded CGG Repeats into FMRpolyG Is Pathogenic and May Contribute to Fragile X Tremor Ataxia Syndrome. *Neuron* 93, 331–347.
 7. Hessl, D., and Grigsby, J. (2016). Fragile X-associated tremor/ataxia syndrome: another phenotype of the fragile X gene. *Clin. Neuropsychol.* 30, 810–814.
 8. Hunsaker, M.R., Arque, G., Berman, R.F., Willemsen, R., and Hukema, R.K. (2012). Mouse models of the fragile X premutation and the fragile X associated tremor/ataxia syndrome. *Results Probl. Cell Differ.* 54, 255–269.
 9. Hunsaker, M.R., Wenzel, H.J., Willemsen, R., and Berman, R.F. (2009). Progressive spatial processing deficits in a mouse model of the fragile X premutation. *Behav. Neurosci.* 123, 1315–1324.
 10. Chen, Y., Tassone, F., Berman, R.F., Hagerman, P.J., Hagerman, R.J., Willemsen, R., and Pessah, I.N. (2010). Murine hippocampal neurons expressing *Fmr1* gene premutations show early developmental deficits and late degeneration. *Hum. Mol. Genet.* 19, 196–208.
 11. Cunningham, C.L., Martínez Cerdeño, V., Navarro Porras, E., Prakash, A.N., Angelastro, J.M., Willemsen, R., Hagerman, P.J., Pessah, I.N., Berman, R.F., and Noctor, S.C. (2011). Premutation CGG-repeat expansion of the *Fmr1* gene impairs mouse neocortical development. *Hum. Mol. Genet.* 20, 64–79.
 12. Abekhoulk, S., Sahin, H.B., Grossi, M., Zongaro, S., Maurin, T., Madrigal, I., Kazue-Sugioka, D., Raas-Rothschild, A., Doulazmi, M., Carrera, P., et al. (2017). New insights into the regulatory function of CYFIP1 in the context of WAVE- and FMRP-containing complexes. *Dis. Model. Mech.* 10, 463–474.
 13. Zongaro, S., Hukema, R., D'Antoni, S., Davidovic, L., Barbry, P., Catania, M.V., Willemsen, R., Mari, B., and Bardoni, B. (2013). The 3' UTR of FMR1 mRNA is a target of miR-101, miR-129-5p and miR-221: implications for the molecular pathology of FXTAS at the synapse. *Hum. Mol. Genet.* 22, 1971–1982.
 14. Nimchinsky, E.A., Oberlander, A.M., and Svoboda, K. (2001). Abnormal development of dendritic spines in FMR1 knock-out mice. *J. Neurosci.* 21, 5139–5146.
 15. Maurin, T., Melancia, F., Jarjat, M., Castro, L., Costa, L., Delhaye, S., Khayachi, A., Castagnola, S., Mota, E., Di Giorgio, A., et al. (2018). Involvement of Phosphodiesterase 2A Activity in the Pathophysiology of Fragile X Syndrome. *Cereb. Cortex* 29, 3241–3252.
 16. Berman, R.F., Murray, K.D., Arque, G., Hunsaker, M.R., and Wenzel, H.J. (2012). Abnormal dendrite and spine morphology in primary visual cortex in the CGG knock-in mouse model of the fragile X premutation. *Epilepsia* 53 (Suppl 1), 150–160.
 17. Rottloff, S., Miguel, S., Bateau, F., Nisse, E., Hammann, P., Kuhn, L., Chicher, J., Bazile, V., Gaume, L., Mignard, B., et al. (2016). Proteome analysis of digestive fluids in Nepenthes pitchers. *Ann. Bot.* 117, 479–495.
 18. Chonchaiya, W., Schneider, A., and Hagerman, R.J. (2009). Fragile X: a family of disorders. *Adv. Pediatr.* 56, 165–186.
 19. Schluter, E.W., Hunsaker, M.R., Greco, C.M., Willemsen, R., and Berman, R.F. (2012). Distribution and frequency of intranuclear inclusions in female CGG KI mice modeling the fragile X premutation. *Brain Res.* 1472, 124–137.
 20. Entezam, A., Bacsic, R., Orrison, B., Saha, T., Hoffman, G.E., Grabczyk, E., Nussbaum, R.L., and Usdin, K. (2007). Regional FMRP deficits and large repeat expansions into the full mutation range in a new Fragile X premutation mouse model. *Gene* 395, 125–134.
 21. Wang, J.Y., Trivedi, A.M., Carrillo, N.R., Yang, J., Schneider, A., Giulivi, C., Adams, P., Tassone, F., Kim, K., Rivera, S.M., et al. (2017). Open-Label Allopregnanolone Treatment of Men with Fragile X-Associated Tremor/Ataxia Syndrome. *Neurotherapeutics* 14, 1073–1083.
 22. Ma, L., Herren, A.W., Espinal, G., Randol, J., McLaughlin, B., Martinez-Cerdeño, V., Pessah, I.N., Hagerman, R.J., and Hagerman, P.J. (2019). Composition of the Intranuclear Inclusions of Fragile X-associated Tremor/Ataxia Syndrome. *Acta Neuropathol Commun* 7, 143.
 23. Yan, Z., Kim, E., Datta, D., Lewis, D.A., and Soderling, S.H. (2016). Synaptic Actin Dysregulation, a Convergent Mechanism of Mental Disorders? *J. Neurosci.* 36, 11411–11417.
 24. Mignogna, M.L., and D'Adamo, P. (2018). Critical importance of RAB proteins for synaptic function. *Small GTPases* 9, 145–157.
 25. Gao, Y., Wilson, G.R., Stephenson, S.E.M., Bozaoglu, K., Farrer, M.J., and Lockhart, P.J. (2018). The emerging role of Rab GTPases in the pathogenesis of Parkinson's disease. *Mov. Disord.* 33, 196–207.
 26. Vandeweyer, G., Van der Aa, N., Reyniers, E., and Kooy, R.F. (2012). The contribution of CLIP2 haploinsufficiency to the clinical manifestations of the Williams-Beuren syndrome. *Am. J. Hum. Genet.* 90, 1071–1078.
 27. Ramakers, G.J. (2002). Rho proteins, mental retardation and the cellular basis of cognition. *Trends Neurosci.* 25, 191–199.
 28. Hukema, R.K., Buijsen, R.A., Raske, C., Severijnen, L.A., Nieuwenhuizen-Bakker, I., Minneboo, M., Maas, A., de Crom, R., Kros, J.M., Hagerman, P.J., et al. (2014). Induced expression of expanded CGG RNA causes mitochondrial dysfunction in vivo. *Cell Cycle* 13, 2600–2608.
 29. Alvarez-Mora, M.I., Rodriguez-Revenga, L., Madrigal, I., Guitart-Mampel, M., Garrabou, G., and Milà, M. (2017). Impaired Mitochondrial Function and Dynamics in the Pathogenesis of FXTAS. *Mol. Neurobiol.* 54, 6896–6902.
 30. Naaijen, J., Lythgoe, D.J., Zwiers, M.P., Hartman, C.A., Hoekstra, P.J., Buitelaar, J.K., and Aarts, E. (2018). Anterior cingulate cortex glutamate and its association with striatal functioning during cognitive control. *Eur. Neuropsychopharmacol.* 28, 381–391.
 31. Carrillo-Mora, P., Sila-Adaya, D., and Villasenor-Aguayo, K. (2013). Glutamate in Parkinson's disease: Role of antiglutamatergic drugs. *Basal Ganglia* 3, 147–157.
 32. O'Gorman Tuura, R.L., Baumann, C.R., and Baumann-Vogel, H. (2018). Beyond Dopamine: GABA, Glutamate, and the Axial Symptoms of Parkinson Disease. *Front. Neurol.* 9, 806.
 33. Gray, J.L., von Delft, F., and Brennan, P. (2019). Targeting the Small GTPase Superfamily through their Regulatory Proteins. *Angew. Chem. Int. Ed. Engl.* Published online March 14, 2019. <https://doi.org/10.1002/anie.201900585>.
 34. Xie, N., Gong, H., Suhl, J.A., Chopra, P., Wang, T., and Warren, S.T. (2016). Reactivation of FMR1 by CRISPR/Cas9-Mediated Deletion of the Expanded CGG-Repeat of the Fragile X Chromosome. *PLoS ONE* 11, e0165499.
 35. Kilkenny, C., Browne, W.J., Cuthill, I.C., Emerson, M., and Altman, D.G. (2010). Improving bioscience research reporting: the ARRIVE guidelines for reporting animal research. *PLoS Biol.* 8, e1000412.
 36. Bontekoe, C.J., Bakker, C.E., Nieuwenhuizen, I.M., van der Linde, H., Lans, H., de Lange, D., Hirst, M.C., and Oostera, B.A. (2001). Instability of a (CGG)98 repeat in the *Fmr1* promoter. *Hum. Mol. Genet.* 10, 1693–1699.
 37. Khalfallah, O., Jarjat, M., Davidovic, L., Nottet, N., Cestèle, S., Mantegazza, M., and Bardoni, B. (2017). Depletion of the Fragile X mental retardation protein in embryonic stem cells alters the kinetics of neurogenesis. *Stem Cells* 35, 374–385.
 38. Maurin, T., Lebrigand, K., Castagnola, S., Paquet, A., Jarjat, M., Popa, A., Grossi, M., Rage, F., and Bardoni, B. (2018). HITS-CLIP in various brain areas reveals new targets and new modalities of RNA binding by fragile X mental retardation protein. *Nucleic Acids Res.* 46, 6344–6355.
 39. Bardoni, B., Castets, M., Huot, M.E., Schenck, A., Adinolfi, S., Corbin, F., Pastore, A., Khandjian, E.W., and Mandel, J.-L. (2003). 82-FIP, a novel FMRP (fragile X mental retardation protein) interacting protein, shows a cell cycle-dependent intracellular localization. *Hum. Mol. Genet.* 12, 1689–1698.
 40. Huang, D.W., Sherman, B.T., Tan, Q., Collins, J.R., Alvord, W.G., Roayaie, J., Stephens, R., Baseler, M.W., Lane, H.C., and Lempicki, R.A. (2007). The DAVID Gene Functional Classification Tool: a novel biological module-centric algorithm to functionally analyze large gene lists. *Genome Biol.* 8, R183.

Publication 2



Role of phosphodiesterases in the pathophysiology of neurodevelopmental disorders

Sébastien Delhayé¹ · Barbara Bardoni²

Received: 4 July 2020 / Revised: 3 December 2020 / Accepted: 9 December 2020

© The Author(s), under exclusive licence to Springer Nature Limited part of Springer Nature 2021. This article is published with open access

Abstract

Phosphodiesterases (PDEs) are enzymes involved in the homeostasis of both cAMP and cGMP. They are members of a family of proteins that includes 11 subfamilies with different substrate specificities. Their main function is to catalyze the hydrolysis of cAMP, cGMP, or both. cAMP and cGMP are two key second messengers that modulate a wide array of intracellular processes and neurobehavioral functions, including memory and cognition. Even if these enzymes are present in all tissues, we focused on those PDEs that are expressed in the brain. We took into consideration genetic variants in patients affected by neurodevelopmental disorders, phenotypes of animal models, and pharmacological effects of PDE inhibitors, a class of drugs in rapid evolution and increasing application to brain disorders. Collectively, these data indicate the potential of PDE modulators to treat neurodevelopmental diseases characterized by learning and memory impairment, alteration of behaviors associated with depression, and deficits in social interaction. Indeed, clinical trials are in progress to treat patients with Alzheimer's disease, schizophrenia, depression, and autism spectrum disorders. Among the most recent results, the application of some PDE inhibitors (PDE2A, PDE3, PDE4/4D, and PDE10A) to treat neurodevelopmental diseases, including autism spectrum disorders and intellectual disability, is a significant advance, since no specific therapies are available for these disorders that have a large prevalence. In addition, to highlight the role of several PDEs in normal and pathological neurodevelopment, we focused here on the deregulation of cAMP and/or cGMP in Down Syndrome, Fragile X Syndrome, Rett Syndrome, and intellectual disability associated with the *CC2D1A* gene.

Introduction

The family of phosphodiesterases

Cyclic adenosine monophosphate (cAMP) and cyclic guanosine monophosphate (cGMP) are second messengers that regulate a variety of signaling pathways via direct interaction with cAMP-dependent protein kinase A (PKA) and cAMP-dependent protein kinase G (PKG), respectively [1].

Adenylate and guanylate cyclases (AC and GC) catalyze the synthesis of cAMP and cGMP starting from ATP and GTP, respectively. In the brain, activation of AC is mediated by heterotrimeric G proteins upon activation of G protein-coupled receptors (GPCRs) by extracellular stimuli (Fig. 1), while soluble AC is directly activated by Ca^{2+} [2] (Fig. 1). In the brain, soluble GC is mainly activated by nitric oxide (NO) and transmembrane GC is activated by C-type natriuretic peptide (CNP) [3] (Fig. 1). cAMP and cGMP are hydrolyzed by phosphodiesterases (PDEs). The enzymatic activity of PDEs was used as one of the initial processes providing evidence for the physiological importance of cAMP. Today, we know that PDEs catalyze the hydrolysis of the 3' phosphate bond of cAMP and cGMP to generate 5' AMP and 5' GMP, respectively [1]. Mammalian PDEs are classified in 11 subfamilies of proteins encoded by 21 different genes, each one displaying multiple splice variants. These spliced variants often have different subcellular localization (Fig. 2) [1, 4]. PDEs are divided into three groups based on their specificity to cyclic nucleotides: specific to cAMP (PDE4, PDE7, and PDE8), specific to

Supplementary information The online version of this article (<https://doi.org/10.1038/s41380-020-00997-9>) contains supplementary material, which is available to authorized users.

✉ Barbara Bardoni
bardoni@ipmc.cnrs.fr

¹ Université Côte d'Azur, CNRS UMR7275, Institute of Molecular and Cellular Pharmacology, 06560 Valbonne, France

² Université Côte d'Azur, Inserm, CNRS UMR7275, Institute of Molecular and Cellular Pharmacology, 06560 Valbonne, France

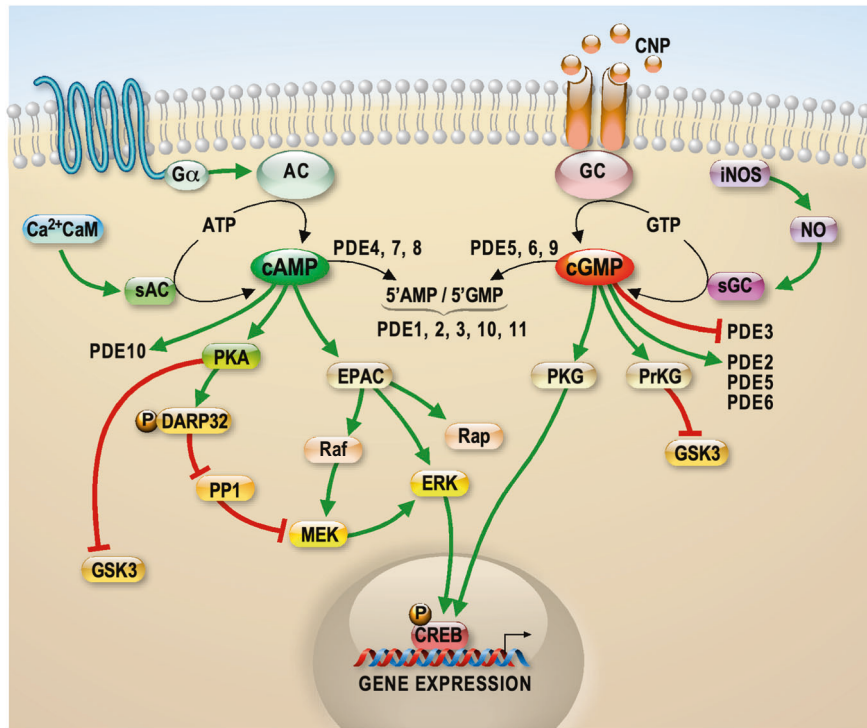


Fig. 1 Neuronal pathways involving PDEs. Schematic of the regulation of cAMP synthesis by Adenylate Cyclases (AC) or s(soluble) AC and of cGMP synthesis by guanylyl cyclases (GC) or s(soluble) GC. Specific degradation of cAMP and cGMP is catalyzed by various PDEs whose specificity is shown. Targets of cAMP and cGMP are shown, as well as well-known neuronal pathways involved in neurodevelopment. Red arrows indicate inhibition while green arrows indicate activation. PKA cAMP-dependent Protein Kinase, Ca²⁺CaM Ca²⁺/calmodulin-dependent protein kinase II, EPAC Exchange Protein

directly Activated by cAMP, Rap Ras-related protein, ERK Extracellular signal-Regulated Kinase, Raf rapidly accelerated fibrosarcoma, DARP32 dopamine- and cAMP-regulated neuronal phosphoprotein, PP1 protein phosphatase-1, MEK Mitogen-activated protein kinase Kinase, PKG cGMP-dependent protein kinase, PrKG protein kinase, cGMP-dependent, GSK3 glycogen synthase kinase 3, iNOS inducible nitric oxide synthase; NO nitric oxide, CREB cAMP response element-binding protein, CNP C-type natriuretic peptide.

cGMP (PDE5, PDE6, and PDE9), and hydrolyzing both cAMP and cGMP (PDE1, PDE2, PDE3, PDE10, and PDE11). The PDEs in the last group have a higher affinity for one of the two cyclic nucleotides [1, 4]. This specificity is associated with a “glutamine switch”, a highly conserved glutamine residue that regulates the binding of the cyclic nucleotide purine ring in the binding domain [5]. The structural features of these enzymes, their regulatory domains, and catalytic regions are common among isoforms and are highly conserved across species. In each subfamily, the main variable regions between each member are the N- and C-terminal domain-containing elements for subcellular localization that is a critical element to define the specific function of each PDE [4, 6]. In Fig. 2, the 11 subfamilies are shown and for each one the functional domains are presented. Moreover, the activity of some PDEs depends on cGMP (PDE2, PDE3, PDE5, and PDE6), while cAMP activates PDE10A [1] (Fig. 1). PDEs are expressed in the cells of all tissues. The precise spatiotemporal expression of PDEs is crucial for the accurate regulation of cAMP and cGMP levels. Indeed, all PDEs appear to be expressed in

the brain according to <http://mousebrain.org/celltypes/> and each PDE displays a specific expression pattern, as illustrated in Supplementary Table I [7]. A study by Lakics et al. compared the expression levels of PDEs in different human brain regions [8]. In Supplementary Table II, we summarize the results of this study indicating the 2–3 most highly expressed PDEs in each of the analyzed brain regions. The expression of PDEs during brain development is poorly studied. In Supplementary Table III, we summarized the studies on this subject reported on Mouse Brain Atlas <https://mouse.brain-map.org/static/atlas>.

Role of PDEs in the brain

In the brain, both cAMP and cGMP are essential during neurodevelopment as well as in maintaining synaptic plasticity, and ultimately in learning and memory [9–11]. Indeed, it has been reported that the levels of both cAMP and cGMP have critical roles in axon elongation and guidance [12, 13] and in regulating the morphology and growth of dendritic spines, where they have opposite

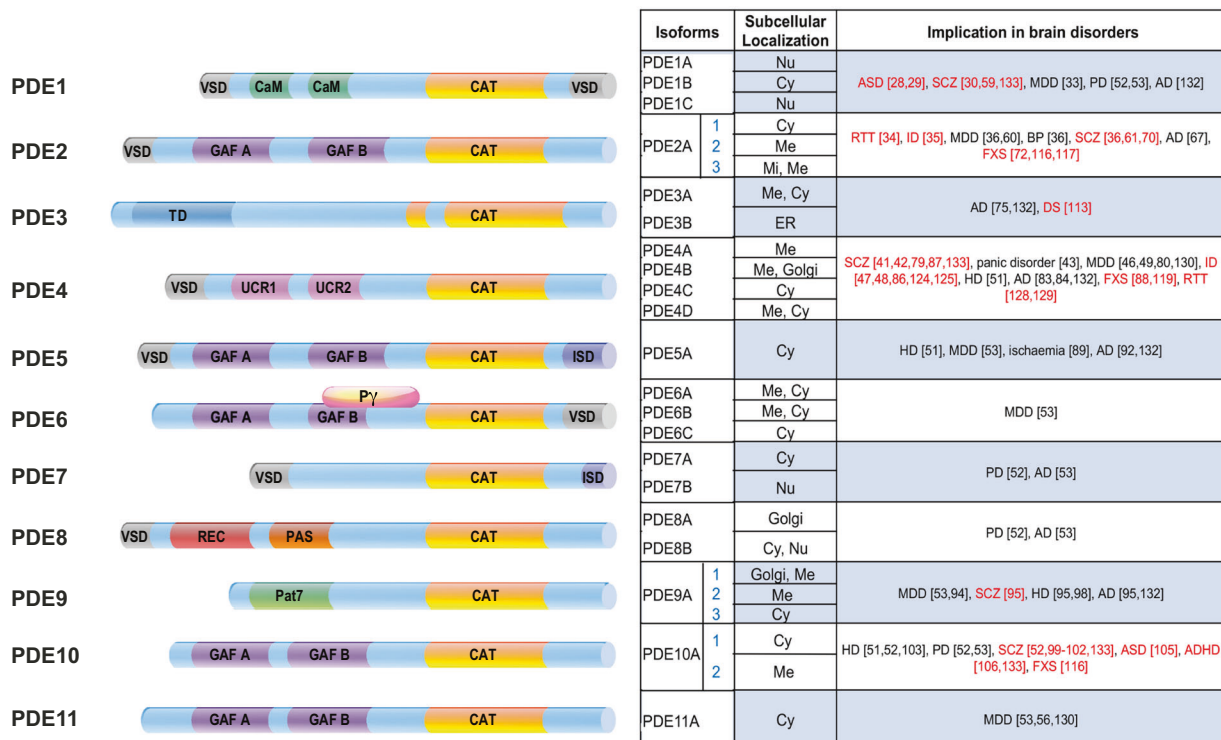


Fig. 2 Structure, localization and implication of PDEs in brain disorders. Left panel. The structure of each PDE subfamily is indicated by representing the various domains. Catalytic domain providing the substrate specificity: CAT. Regulatory domains: GAF: the name is related to the proteins it is found in: cGMP-specific phosphodiesterases, adenylyl cyclases and the bacterial transcription factor FhlA. Ca²⁺/CaM Ca²⁺/calmodulin binding site; PAS Per-ARNT-Sim domain, that is a structural motif. TD transmembrane domain. REC cheY-homologous receiver domain. UCR upstream conserved region. ISD isoform specific domain. Regions that are submitted to alternative splicing have been indicated as VSD variant-specific domain. This domain is called PAT7 in PDE9A variants [148]. Py is part of the PDE6 holoenzyme in rod. Isoforms originated by different genes exist and are indicated for the following subfamily: PDE1 (A, B, and C), PDE3 (A and B), PDE4 (A, B, C and D), PDE6 (A, B and C), PDE7

effect [12]. cAMP abundance coupled to PKA signaling is critical to modulate assembly/disassembly/priming/recycling of neurotransmitter vesicles and, consequently, for synaptic transmission and plasticity events [14]. cGMP signaling can be transmitted through cyclic nucleotide-gated or hyperpolarization-activated cyclic nucleotide-gated ion channels. Furthermore, pharmacological inhibition of soluble GC or PKG slowed down the rate of recycling as well as endocytosis of synaptic vesicles. Indeed, the NO/cGMP/PKG pathway is known to modulate transmitter release and long-term changes of synaptic activity in various brain regions [15]. Overall, the balance between cAMP and cGMP levels is considered to be essential for shaping neuronal circuits [16]. Both cAMP- and cGMP-dependent signaling have been involved in neuronal migration [17]. In particular, a recent study suggested that primary cilium and centrosome

(A and B) and PDE8 (A and B). PDE2, PDE5, PDE9, PDE10 and PDE11 subfamilies are represented by only one member, namely PDE2A, PDE5A, PDE9A, PDE10A and PDE11A. Splicing variants (in blue) of the same protein are indicated when they determine a specific subcellular localization. Middle panel. Localization of each isoform and variant is indicated [4, 6, 148]. Cy Cytosol, Me membrane; Mi mitochondria; Nu Nucleus. Right panel. Brain disorders involving the various PDEs are indicated according to all the genetic and pharmacological information considered in the text. Neurodevelopmental disorders are highlighted in red. AD Alzheimer disease; ASD autism spectrum disorder; BP bipolar disorder; DS down syndrome; HD Huntington disease; ID intellectual disability; FKS fragile X syndrome; MDD major depression disorder, RTT Rett syndrome, SCZ schizophrenia.

integrate the cAMP signaling to favor neuronal migration [18]. Signal transduction starts when cAMP and cGMP induce the activation of PKA and PKG, respectively. Hence, PKA and PKG phosphorylate key proteins of a large array of downstream pathways. As an example, Fig. 1 illustrates the role of PKA and PKG in pathways involved in learning and memory (e.g., cAMP response element-binding protein (CREB) [19]) and in a large number of neurodevelopmental and psychiatric disorders (e.g., GSK3) [20]. Furthermore, cAMP activates the exchange protein directly activated by cAMP (EPAC), which regulates kinases (e.g., ERK and Raf) and Rap GTP-binding protein, a small-GTPase similar to Ras. These factors have key roles in modulation of molecular signaling involved in various aspects of neuronal differentiation, like the establishment of neuronal polarity or axonal growth and cone movement [21–24] (Fig. 1).

Genetic evidence of the implication of PDEs in neurodevelopmental disorders

Recent large-scale genome-wide association studies (GWAS) conducted by the Science Genetic Association Consortium [25] linked genetic variation in some PDE genes with multiple measures of human cognitive function. Single-nucleotide polymorphisms (SNPs) found in *PDE1C*, *PDE2A*, *PDE4B*, and *PDE4D* reached genome-wide significance with educational attainment and cognitive performance [26]. Of note, in this study, the highest statistical significance was reached by SNP rs72962169 in the *PDE2A* gene for GWAS/Educational attainment as measured by the highest level of education achieved (Eduyears), conjoint analysis/Eduyears, and multi-trait analysis/Eduyears [25]. Starting from this information, we considered here the genetic evidence in patients and in transgenic animals (See also Supplementary Table IV) supporting the implication of PDEs in neurodevelopmental brain disorders.

Three *PDE1* genes (*PDE1A*, *PDE1B*, and *PDE1C*) have thus far been identified. Enzyme activity is increased by Ca²⁺/calmodulin binding to the regulatory site located in the N-terminal region of the enzyme [27]. An intronic SNP in the *PDE1C* gene was found to be associated with autism spectrum disorder (ASD; *p* value < 1.0E–04) in a GWAS meta-analysis of 7387 ASD cases and 8567 controls [28]. Inherited missense variants in *PDE1B* gene have also been identified in probands with ASD [29] and with schizophrenia (SCZ) [30]. The knockdown of *Pde1b* in the hippocampus enhances spatial and contextual memory [31]. Conversely, *Pde1b*-knockout (KO) mice display locomotor hyperactivity, spatial learning deficits [32], and antidepressant-like phenotypes [33]. These findings indicate the need to tightly modulate *Pde1b* expression levels by pharmacological approaches to observe an impact on socio-cognitive behavior.

PDE2A is a dual-specific PDE that breaks down both cAMP and cGMP and is activated by cGMP. A homozygous splicing mutation in *PDE2A* was found in two patients with atypical Rett syndrome (RTT), displaying neurodevelopmental delay [34], while a homozygous loss-of-function mutation in *PDE2A* was associated with early-onset hereditary chorea-predominant movement disorder and intellectual disability (ID) [35]. Patients with bipolar disorder showed reduced *PDE2A* mRNA levels in the hippocampus, caudal entorhinal cortex, and striatum, while patients with SCZ, bipolar disorder, and major depressive disorder (MDD) showed reduced *PDE2A* mRNA levels in the amygdala. Furthermore, patients with schizophrenia have reduced *PDE2A* mRNA levels in the frontal cortical region [36]. *Pde2a*-KO mice have been generated but they are lethal during embryogenesis due to cardiac failure [37].

To our knowledge, no studies have been performed on heterozygous animals so far.

The *PDE4* family comprises four genes, *PDE4A–D*, each expressed as multiple variants. The selective modulation of individual *PDE4* subtypes revealed that individual subtypes exert unique and non-redundant functions in the brain [38]. The role of *PDE4* in learning and memory has been studied extensively in the *Drosophila* fruit fly, where only one homolog of the family known as *dunce* (*dnc*) is present, and in mice. Mutational studies in flies have identified *PDE4* as a key modulator of a signaling pathway critical for associative learning, courtship behavior, and neurodevelopment. Deletion of the *dnc* gene in *Drosophila* disrupts learning and memory by preventing the hydrolysis of cAMP, thereby altering the normal spatial and temporal patterning of cAMP signaling [39, 40].

PDE4B interacts directly with *DISC1*, which is a well-known genetic risk factor for mental illness. Mutations in the *DISC1* and *PDE4B* genes reduce the association between both proteins, reducing *PDE4B* activity, which has been shown to be correlated with SCZ [41]. In particular, it was reported that an SNP in *PDE4B* conferred a protective effect against SCZ in women [42]. The implication of the *PDE4B* gene in behavior and mood is also supported by the association of *PDE4B* gene polymorphisms with protection from panic disorder in Russians subjects [43]. *Pde4b*-KO mice show a significant reduction in prepulse inhibition and an exaggerated locomotor response to amphetamine correlated with decreased striatal dopamine and serotonin activity [44]. *Pde4b*-KO mice display enhanced early long-term potentiation following multiple induction protocols, and they exhibit significant behavioral deficits in associative learning using a conditioned fear paradigm [45]. In addition, they display decreased head-dips and time spent in head-dipping in the hole-board test, reduced transitions and time on the light side in the light–dark transition test, and decreased initial exploration and rears in the open-field test were observed [46]. Overall, these studies suggest that *PDE4B* is involved in signaling pathways that contribute to anxiogenic-like effects on behavior [46]. *PDE4D* mutations have been reported as causative for acrodysostosis type 2 with or without hormone resistance (ACRDYS2), a disorder characterized by severe ID [47, 48], leading to the conclusion that altered *PDE4D* levels may affect brain functioning. *Pde4d*-KO mice exhibit decreased immobility in tail suspension and forced swim tests [49], suggesting that *PDE4D* may play a role in the pathophysiology and pharmacotherapy of depression.

PDE10A is a dual-specific PDE that breaks down both cAMP and cGMP. *Pde10*-KO mice display a modest impairment of latent inhibition, a decrease in exploratory locomotor activity, and a delay in the acquisition of conditioned avoidance responses. Furthermore, a decrease in

spontaneous firing in striatal medium spiny neurons and a significant change in striatal dopamine turnover, which is accompanied by an enhanced locomotor response to amphetamines, was observed in these mice [50]. All these data support the strong implication of PDE10A in striatal function, and thus its possible involvement in the pathophysiology of disorders such as Huntington (HD) and Parkinson disease (PD) and SCZ [51–53] (see below).

PDE11A is also a dual-specific PDE that breaks down both cAMP and cGMP. *PDE11A4*, one of the four *PDE11A* splice variants, is involved in the hippocampal formation in humans and rodents, and is highly enriched in the rodent ventral hippocampal formation compared to the dorsal hippocampal formation [54]. *Pde11A*-KO mice show enlarged lateral ventricles and increased activity in CA1, altered formation of social memories and abnormal stabilization of mood [54, 55]. This latter conclusion is also supported by other authors associating *PDE11A* with both MDD and response to antidepressant drugs [56]. Indeed, 16 SNPs in *PDE11A* were studied in patients affected by MDD and sharing 18 common haplotypes. Six haplotypes showed significantly different frequencies between the MDD group and the control group. Furthermore, in patients treated with two different antidepressant drugs—increasing the cGMP/cAMP ratio [57, 58]—the frequency of one haplotype was significantly lower in the remitter group than in the non-remitter group [56].

Pharmacological modulation of PDEs

Similar to the generation of animal models, the identification of specific and powerful inhibitors of PDEs allowed studying the functional role of these enzymes, paving the way for their use in the clinic.

A well-known inhibitor of PDE1B is DSR-141562, which inhibits locomotor hyperactivity and reverses social interaction and novel object recognition in normal mice and rats. This molecule was also shown to improve cognition in the marmoset, a non-human primate [59] by acting through CREB and DARPP32 [32, 59] (Fig. 1). DSR-141562 has been proposed as a therapeutic candidate for positive, negative, and cognitive symptoms in schizophrenia [59].

Many specific PDE2A inhibitors have been generated and characterized. Hcyb1 produces neuroprotective and antidepressant-like effects in mice [60]. TAK-915 shows efficacy in ameliorating cognitive and social impairment in induced rat models of SCZ [61] and it improves cognitive impairment associated with aging in mice [62]. To date, one phase I clinical trial has been reported for this compound (Supplementary Table V). A clinical trial has been carried out using a specific PDE2A inhibitor by Pfizer to treat migraine, but the results have not been communicated to the scientific community (Supplementary Table V). This study

suggests a possible role of PDE2A in pain control. This hypothesis is supported by a study reporting that Bay 60–7550, another well-known inhibitor of PDE2A, alleviates radicular inflammation and mechanical allodynia in a rat model of non-compressive lumbar disc herniation [63]. Bay 60–7550 is likely the most studied PDE2A inhibitor, probably due to its commercial availability. It has been reported to have anxiolytic properties and to ameliorate learning, memory, and synaptic plasticity in normal animals [64–66] and in neurodegeneration models [67, 68]. This drug could also be used for treatment of alcoholism since it was reported to decrease ethanol intake and preference in mice [69]. Despite all these results, no clinical trials testing Bay 60–7550 have been reported, suggesting possible toxicity of this compound. Controversial results concerning the poor ability to cross the blood-brain barrier after oral administration to adult rats [64, 70] and the efficacy of this drug in treating brain disorders when used by intraperitoneal injection in adult and infant mice and rats, might suggest that the bioavailability of Bay 60–7550 in the brain is dependent on the route of administration and/or by the age of the treated subject [65, 71, 72]. PDE2A has been also involved in the pathophysiology of FXS (see below).

Cilostazol is the most studied PDE3-specific inhibitor already used in clinics for the treatment of symptoms of intermittent claudication due to its vasodilator and antiplatelet actions [73]. A clinical trial in patients with mild cognitive impairment is in progress using this compound (Supplementary Table V). This new potential use of cilostazol is based on retrospective study showing that patients using this drug daily as an antiplatelet drug have a decreased risk of developing dementia [74] and reduces the decline in cognitive function in patients with stable AD [75]. In the hippocampus, Cilostazol increases the levels of c-fos and of insulin-like growth factor 1 (IGF-1) [76] and activates CREB in PC12 cells [77].

Several clinical trials have been carried out using roflumilast, a highly specific PDE4 inhibitor. Double-blind studies have shown that acute treatment with roflumilast improves verbal memory performance in elderly and healthy participants [78] and in patients with SCZ [79]. FCPR16 also shows antidepressant-like effects in mice exposed to chronic unpredictable mild stress [80]. Rolipram is another well-known PDE4 inhibitor, whose utilization results into the increased phosphorylation of CREB [81]. Consistently, a single injection of rolipram improves spatial memory deficits in aged mice [82] and memory consolidation of conditioned fear [81]. Furthermore, in the model of Amyloid β -induced memory impairment, mimicking AD, both treatments with rolipram or BPN14770 improve memory performances [83–85]. Rolipram abolishes long-term memory defects in a mouse model of Rubinstein-Taybi syndrome, caused by the presence of a truncated form of

CREB [86] and has antipsychotic properties [87]. This drug was used to improve the phenotype of both fly and mouse models of FXS [88].

PDE5 inhibitors are essential for the vascular effects and treatment of erectile dysfunction. However, PDE5A inhibitors have been implicated in memory function in various studies. In rats, sildenafil, an inhibitor of PDE5, promotes neurogenesis, reduces neurological deficits, and promotes functional recovery after stroke and focal cerebral ischemia [89]. In addition, this drug improves cognition and spatial learning [90, 91]. Sildenafil has been shown to produce long-lasting amelioration of synaptic function, CREB phosphorylation and to increase Brain-Derived Neurotrophic Factor (BDNF) levels [92]. In humans, sildenafil affects selective auditory attention and verbal recognition memory [93]. In particular in AD patients, a single dose of this drug increased cerebral blood flow and the cerebral metabolic rate of oxygen [92].

WYQ-C36D, a high-affinity PDE9A inhibitor, produces antidepressant-like, anxiolytic-like, and memory-enhancing effects in stressed mice [94]. Inhibition of PDE9A in rats with PF-4447943 and PF-4449613 demonstrated the implication of this PDE in tasks depending on hippocampal cholinergic function and sensory gating. These results suggested the utilization of PDE9A inhibitors to treat AD, SCZ, or HD [95]. However, two double-blind randomized controlled phase II studies using two different inhibitors of PDE9A, namely BI 409306 or PF-04447943, failed to prove efficacy in improving cognition in patients with AD [96, 97]. Another clinical trial testing the effect of BI 409306 on SCZ patients is currently ongoing (Supplementary Table V). Recently, the treatment of a HD rat model with PF-4447943 suggested that this drug facilitates striatal cGMP signaling and glutamatergic cortico-striatal transmission. This could help to alleviate motor and cognitive symptoms associated with HD by restoring striatal function [98].

Data obtained by studying a mouse model supported the pivotal role of PDE10A in striatal signaling and striatum-mediated salience attribution, a process that is severely disrupted in patients affected by schizophrenia [99]. Indeed, TAK-063 (Balipodect) and T-251 dose-dependently suppress hyperactivity and improve cognitive deficits, respectively, in MK-801 mice, a model for acute psychosis [99, 100]. A phase II randomized and placebo-controlled clinical trial showed a potential beneficial effect of TAK-063 in subjects with acute exacerbation of SCZ [101]. Two clinical trials are currently testing another PDE10A inhibitor, Lu AF11167, for the treatment of negative symptoms in patients with SCZ (Supplementary Table V). These latter results are consistent with the observation that *Pde10a* mRNA is a target of miR-137, whose absence is associated with SCZ. Partial loss of miR-137 in heterozygous

conditional KO mice results in increased PDE10A levels and in deregulated synaptic plasticity, repetitive behavior, and impaired learning and social behavior. Both treatment with papaverine, a PDE10A inhibitor, and knockdown of *Pde10a* ameliorate the deficits observed in the miR-137 mouse model [102]. PDE10 inhibition increases the expression of BDNF and the phosphorylation of both CREB and the alpha-amino-3-hydroxy-5-methyl-4-isoxazole propionate (AMPA) receptor GLUA1 in a mouse model of HD [103]. Of note, the implication of this receptor in neurodevelopmental disorders is well known [104]. Indeed, recently, papaverin has been reported to attenuate neurobehavioral abnormalities in a rat model of ASD [105] and to ameliorate hyperactivity, inattention and anxiety in a model of attention deficit hyperactivity disorder (ADHD) [106].

Altered activity of PDEs in neurodevelopmental disorders—preclinical conclusion and translational elements

Down syndrome (DS) is the most frequent form of ID (1:600 newborns) and is caused by an extra copy of chromosome 21. A specific region on this chromosome, namely the DS critical region, is necessary and sufficient to produce the main phenotype of DS: cognitive congenital malformations (particularly cardiovascular) and dysmorphic features. Immune disturbances in DS account for autoimmune alopecia, autoimmune thyroiditis and leukemia, respiratory tract infections, and pulmonary hypertension [107]. Several genes in triple dosage have been reported to contribute to ID in patients with DS. The most studied is the *dual-specificity tyrosine phosphorylation-regulated kinase 1A (DYRK1A)* gene encoding a kinase involved in the formation and maturation of dendritic spines from dendrites [108]. Mutations in *DYRK1A* have been found in patients affected by ASD [109]. DYRK1A has CREB among its targets [110], whose activity is regulated by both cAMP and cGMP (Fig. 1), thus suggesting a clear interference of deregulated expression of DYRK1A in cAMP and/or cGMP pathway in DS. Another factor with elevated expression levels in DS is the amyloid precursor protein. This deregulated expression is likely the cause of β -amyloid (A β) plaques that are present in young patients with DS and represent one of the neuropathology hallmarks shared between DS and AD [111]. As reported in Supplementary Table V, several clinical trials to treat AD with PDE inhibitors are currently ongoing. Hence, this information, together with reduced levels of cAMP reported in one of the most-widely used models of DS, the Ts65Dn mouse [112], pushed some authors to study the implication of PDE activity in the pathophysiology of DS. In a recent study, the administration of cilostazol (PDE3 inhibitor) to Ts65Dn mice from fetal to adult age ameliorated cognition and

sensorimotor function in females. The same treatment in males improved their hyperactive locomotion and spatial memory [113]. Overall, these results seem to be consistent with the previous observation that cilostazol promotes the clearance of A β plaques and rescues cognitive deficits in a mouse model [113] of AD and reduces the cognitive decline in patients affected by AD [75].

FXS is caused by the silencing of the *fragile X mental retardation gene (FMR1)*. FXS is the most common form of inherited ID (1:4000 males and 1:7000 females). Patients might also display hyperactivity, attention deficit, ASD, language problems, and seizures [114]. Deregulation of cAMP was one of the first molecular hallmarks defined in FXS patients [115]. *FMR1* encodes the fragile X mental retardation protein (FMRP), an RNA-binding protein that is highly expressed in all brain regions in both neurons and glial cells and mainly involved in translational regulation, being both a repressor and an enhancer of translation [116]. Among the mRNA targets of FMRP, three PDEs, *PDE1A*, *PDE2A*, and *PDE10A*, have been identified [116]. The expression of PDE2A in the cortex and hippocampus is negatively modulated by FMRP both on a translational level and by affecting dendritic transport of encoding mRNAs [116]. Consistently, PDE2A expression levels are elevated in *Fmr1*-KO brains, resulting in reduced levels of both cAMP and cGMP. Treatment of *Fmr1*-KO mice with Bay 60–7550 normalizes the social and cognitive deficits of infant and adolescent *Fmr1*-KO mice, increased the maturity of axons and dendritic spines of *Fmr1*-KO neurons and normalizes the exaggerated hippocampal m-GluR5 long-term depression of *Fmr1*-KO CA1 [72]. Inhibition of PDE2A activity by Bay 60–7550 rescues the release of synaptic vesicles, which is reduced in the absence of FMRP [117]. Consistently, PDE2A is the only PDE associated with docked vesicles [118]. Collectively these findings suggest the implication of PDE2A in the release of neurotransmitters. Another target of FMRP is the mRNA encoding *Pde10a*, whose expression is likely increased in the *Fmr1*-KO mouse brain [116]. Balipodect, an inhibitor of PDE10A, has been accepted by the European Medicine Agency as a potential treatment for FXS (EMADOC-628903358-742). The specific inhibition of PDE4D by BNP14770, a drug developed by Tetra Therapeutics, was shown to be potentially useful for the treatment of FXS. While rolipram—already used to treat FXS animal models [88] inhibits all subtypes of PDE4, BPN14770 is selective for PDE4D. BNP14770 inhibits the enzyme by closing one of the two upstream conserved regions at the regulatory domains across the active site, which limits cAMP access. Daily treatment of *Fmr1*-KO mice for 14 days with BNP14770 improves social interaction and natural behaviors (such as nesting and marble burying), and rescues the altered dendritic spine morphology of *Fmr1*-null neurons

[119]. The details of two clinical trials for this molecule are shown in Supplementary Table V. Positive results obtained in the phase II clinical trial with BNP14770 and enrolling 30 FXS adult male subjects (age 18–41 years) were recently announced: <https://www.fraxa.org/positive-results-reported-in-phase-ii-fragile-x-clinical-trial-of-pde4d-inhibitor-from-tetra-therapeutics/>. It was reported that BPN14770 antagonizes the amnesic effects of scopolamine, increases cAMP signaling in the brain, and increases BDNF and markers of neuronal plasticity associated with memory [85]. This might suggest that this drug will be beneficial to other forms of ID and ASD.

ID associated with the *coiled-coil and C2 domain-containing 1A (CC2D1A)* gene. Functional loss of *CC2D1A* causes a rare form of autosomal recessive ID, sometimes associated with ASD and seizures [120]. While in *Drosophila*, the loss of the ortholog of *CC2D1A*, *lgd*, is embryonically lethal [121], *Cc2d1a* conditional KO mice display deficits in neuronal plasticity and in spatial learning and memory, which are accompanied by reduced sociability, hyperactivity, anxiety, and excessive grooming [122]. The *CC2D1A* gene encodes a transcriptional repressor with essential functions in controlling synapse maturation. This protein regulates the expression of the 5-hydroxytryptamine (serotonin) receptor 1A gene in neuronal cells (HTR1A), likely playing a role in the altered regulation of HTR1A, that is known to be associated with SCZ, anxiety, and MDD [123]. CC2D1A is also localized in cytoplasm where it acts as a scaffold protein in the PI3K/PDK1/AKT pathway [124]. CC2D1A is an interactor of PDE4D regulating its activity and thereby fine-tuning cAMP-dependent downstream signaling [125]. Indeed, it regulates CREB activation in hippocampal neurons by increasing PDE4D activity only in male *Cc2d1a*-deficient mice. Consistently, the male mouse model for CC2D1A-associated disorder shows a deficit in spatial memory that can be restored by inhibiting PDE4D activity. *Cc2d1a*-deficient female mice do not display this phenotype and pharmacological treatment has no effect on their behavior [125].

RTT is a neurodevelopmental disorder that mostly affects girls (1:10000 newborns). In classical RTT, girls display an apparently normal development for 6–18 months before developing severe phenotypes characterized by language problems, deficits in learning and coordination, stereotypies, sleep disturbances, seizures, and breathing deficiencies. Overall, RTT is considered to have a characteristic clinical course of four stages: (I) early-onset stagnation, (II) developmental regression, (III) pseudostationary period, and (IV) late motor deterioration. RTT is caused by mutations in *Methyl CpG binding Protein 2 (MECP2)*, an X-linked gene encoding a transcription factor that binds methylated DNA and acts both as a repressor and enhancer of transcription [126]. The protein modulates a network of

pathways, including the BDNF, PI3K, and ERK pathways [127]. Dysfunction of MECP2 affects morphology and density of dendritic spines, synaptic plasticity, and neuronal migration [126]. Furthermore, reduced cAMP levels were found in neurons of organotypic slices obtained from the brain of a mouse model of RTT due to increased activity of PDE4. Indeed, treatment with rolipram allowed normalization of the growth of neuronal processes and the cAMP transients evoked by electrical stimulation in preBötC neurons [128]. Consistently, reduced levels of CREB and phospho-CREB have been reported in neurons differentiated from human embryonic stem cells and from induced pluripotent stem cells lacking functional MECP2 and displaying an altered arborization. Rolipram rescued these cellular phenotypes as well as several behavioral phenotypes in female RTT mice [129].

Discussion

The results obtained thus far indicate that modulation of PDE activity can be effective for disorders characterized by depressive behavior or memory deficits (Fig. 2) [130, 131]. Clinical trials have mostly addressed the treatment of AD [132] and schizophrenia [133], while two trials are in progress for a form of ASD and only one for depression (Supplementary Table V). We believe that understanding the role of PDE treatment in neurodevelopmental disorders, such as ID, ASD, or both is a very important result obtained from recent studies. Indeed, the pharmacological inhibition of two PDEs (PDE2A and PDE4D) has been associated with multiple autism-like behaviors and cognitive deficit at different ages in mouse models [116, 119, 125]. The inhibition of PDE10A has been proposed for FXS (even if no data have been published yet), ASD [105], and ADHD [106]. The inhibition of PDE3 has been used in DS and is potentially useful for ASD [113]. Indeed, this drug protects against cognitive impairment and white matter disintegration in a mouse model of chronic cerebral hypoperfusion [73], a phenotype characterizing some ASD patients [134]. It is also interesting to consider that low cAMP concentrations favor inflammation due to the increase in IL-8, IL-12, IL-17, IL-22, IL-23, tumor necrosis factor- α , γ -interferon, chemokine C-X-C motif ligand 9 (CXCL9), and CXCL10 levels [135]. This suggests that PDE inhibitors are thought to have anti-inflammatory and neuroprotective effects. Increasing experimental evidence supports the presence of neuroinflammation as a relevant element of neurodevelopmental disorders [136, 137]. This indicates the importance of carrying out specific screenings of the expression levels of PDEs in cohorts of patients affected by idiopathic neurodevelopmental diseases such as ASD and/or ID. To achieve this, it could be useful to measure the

levels of cAMP and/or cGMP in neurons derived from induced pluripotent stem cells or in extracellular vesicles from the central nervous system obtained from fibroblasts and blood, respectively, of these patients. The most accurate method to measure the dynamic levels of these second messengers in real-time is represented by the use of specific FRET-based cAMP (or cGMP) biosensors [18, 138]. This could help to establish therapeutic approaches with molecules modulating the activity of specific PDEs.

PDEs involved in various brain disorders so far (Fig. 2) are cAMP-specific, cGMP-specific or have a double target. This can raise the issue whether an altered cAMP/cGMP ratio could represent a pathophysiological element for these diseases. In this context, a good example is provided by the studies on depression showing that phenotypic improvement can be reached by changing the cGMP/cAMP ratio and then, paradoxically, both by increasing cGMP levels or by reducing cAMP levels [56–58, 130]. Moreover, also PDEs involved in FXS target both cAMP and cGMP [72, 116, 119] (Fig. 1). Indeed, PDE4 is a cAMP-specific isoform, while both cAMP and cGMP are targets of PDE10A and PDE2A, this latter enzyme being stimulated by cGMP (Fig. 1) [1]. PDE1A is activated by Ca^{2+} [1] and is involved in FXS [116], a disorder displaying a deregulated Ca^{2+} homeostasis in brain [139, 140]. We can speculate that an altered cAMP/cGMP ratio is a pathophysiological element in FXS and the modulation of one of those PDEs is sufficient to restore it. This could explain the results in preclinical tests [72, 119] and clinical assays (Supplementary Table V). Thus, it would be difficult to dissect the impact of each PDE in the neurological-psychiatric phenotypes present in FXS. This led to the conclusion that PDE transgenic animals are a main need in the field. Indeed, it is surprising that only a few PDEs have been extensively studied for their impact on brain function by using classical KO animal models. Here, we have reported those models displaying clear psychiatric or neurodevelopmental disorders. In the case of *Pde2a*, the KO phenotype has never been studied since homozygous mutant mice are not viable [37]. In other cases, a phenotype was not known or was never reported (e.g., PDE5). This latter example is very interesting because pharmacological inhibition of PDE5 resulted in potentiating neurogenesis and memory enhancement [89–92]. The use of pharmacological preclinical studies is critical to reach the clinical setting but is not enough to understand the role of PDEs during brain development. Indeed, these drugs are administered only during the post-natal life and often after the weaning, thus missing the possibility to evaluate their impact in early steps of brain development and/or synaptogenesis. Furthermore, genetic silencing of specific PDEs' variants could allow to study the modulation of cAMP and cGMP abundance in subcellular compartments (Fig. 2).

Studying such a large family of proteins is challenging due to their overlapping functions and because of their actions that are not brain specific. However, tools exist today (e.g., conditional KO and optogenetics) to conduct studies focused on the spatio-temporal role of each PDE in normal and pathological brain development and to elucidate their effects on socio-cognitive behaviors at different ages. These studies should also allow the identification of compensation activities by the various members of the PDE family, as suggested, for instance, by the observation that the expression levels of *Pde10a* mRNA are elevated in the striatum of *Pde1b-KO* mice [33].

It is critical that the effects of genes and pathways impacted by the various brain-expressed PDEs be studied in detail in various brain regions and at the synaptic level during brain development. These studies will result in the precise identification of the molecular pathways modulated by each PDE. For instance, an link between PDE3-dependent cAMP signaling with the IGF-1 pathway was established using the specific PDE3 inhibitor cilostazol [76]. Recombinant IGF-1 and some related compounds have emerged as potential therapeutics for the treatment of neurodevelopmental disorders [141]. Trofinetide is a neurotrophic peptide derived from IGF-1 that has a long half-life and is well tolerated. Chronic treatment of *Fmr1*-KO mice with trofinetide corrects learning and memory deficits, hyperactivity, and social interaction deficits displayed by these animals [142]. Thus, a phase II clinical trial for trofinetide was performed. After only 28 days of treatment, improvements in higher sensory tolerance, reduced anxiety, better self-regulation, and more social engagement were observed (NCT01894958). Interestingly, upon the sponsoring of ACADIA Pharmaceuticals Inc., a phase III clinical trial with trofinetide is in progress in 5–15 years old girls affected by RTT (NCT04181723). On the same way and consistent with previous results linking cAMP with BDNF transcription [143], inhibition of PDEs has been reported to increase BDNF levels [52, 53, 85, 92, 103], whose deregulation is involved in the pathophysiology of depression [144], SCZ [133, 145], RTT [126, 146], and FXS [147]. Therefore, we conclude that these findings support the idea of future therapies for psychiatric disorders at the crossroads of pathways involving cAMP and/or cGMP and neurotrophic factors.

Finally, the surprising results from Zamarbide et al. (CC2D1A) and Tsuji et al. (DS) suggest the possibility that a sex-specific regulation (or deregulation) of cAMP or cGMP levels exists [113, 125]. These findings are particularly important for the treatment of ASD and ID, since the ratio of incidence of this disorder is 3:2 in males vs. females, and this could result in a sex-specific treatment. This possibility should be considered for future studies on

PDEs, reinforcing the need to study their relevance for PDE action on brain development and functioning at various ages when sex hormones are present (or not) and they can affect PDE-related pathways differently.

Acknowledgements This study was supported by Inserm, CNRS, Université Côte d'Azur, Fédération Recherche sur le Cerveau, Fondation Jérôme Lejeune, and Agence Nationale de la Recherche: ANR-20-CE16-0016 and ANR-15-IDEX-0001. The authors are grateful to M. Capovilla, E. Lalli, T. Maurin, and D. Tropea for critical reading of the manuscript and discussion and they are indebted to F. Aguila for graphical artwork.

Compliance with ethical standards

Conflict of interest The authors declare that they have no conflict of interest.

Publisher's note Springer Nature remains neutral with regard to jurisdictional claims in published maps and institutional affiliations.

Open Access This article is licensed under a Creative Commons Attribution 4.0 International License, which permits use, sharing, adaptation, distribution and reproduction in any medium or format, as long as you give appropriate credit to the original author(s) and the source, provide a link to the Creative Commons license, and indicate if changes were made. The images or other third party material in this article are included in the article's Creative Commons license, unless indicated otherwise in a credit line to the material. If material is not included in the article's Creative Commons license and your intended use is not permitted by statutory regulation or exceeds the permitted use, you will need to obtain permission directly from the copyright holder. To view a copy of this license, visit <http://creativecommons.org/licenses/by/4.0/>.

References

1. Azevedo MF, Faucz FR, Bimpaki E, Horvath A, Levy I, de Alexandre RB, et al. Clinical and molecular genetics of the phosphodiesterases (PDEs). *Endocr Rev*. 2014;35:195–233.
2. Steegborn C. Structure, mechanism, and regulation of soluble adenylyl cyclases - similarities and differences to transmembrane adenylyl cyclases. *Biochim Biophys Acta*. 2014;1842:2535–47.
3. Potter LR. Guanylyl cyclase structure, function and regulation. *Cell Signal*. 2011;23:1921–6.
4. Bender AT, Beavo JA. Cyclic nucleotide phosphodiesterases: molecular regulation to clinical use. *Pharmacol Rev* 2006;58:488–520.
5. Zhang KYJ, Card GL, Suzuki Y, Artis DR, Fong D, Gillette S, et al. A glutamine switch mechanism for nucleotide selectivity by phosphodiesterases. *Mol Cell*. 2004;15:279–86.
6. Thul PJ, Åkesson L, Wiking M, Mahdessian D, Geladaki A, Ait Blal H, et al. A subcellular map of the human proteome. *Science*. 2017;356:eal3321.
7. Zeisel A, Hochgerner H, Lönnberg P, Johnsson A, Memic F, van der Zwan J, et al. Molecular architecture of the mouse nervous system. *Cell*. 2018;174:999–1014.e22.
8. Lakics V, Karran EH, Boess FG. Quantitative comparison of phosphodiesterase mRNA distribution in human brain and peripheral tissues. *Neuropharmacology*. 2010;59:367–74.
9. Esteban JA, Shi S-H, Wilson C, Nuriya M, Huganir RL, Malinow R. PKA phosphorylation of AMPA receptor subunits

- controls synaptic trafficking underlying plasticity. *Nat Neurosci.* 2003;6:136–43.
10. Son H, Lu YF, Zhuo M, Arancio O, Kandel ER, Hawkins RD. The specific role of cGMP in hippocampal LTP. *Learn Mem.* 1998;5:231–45.
 11. Banke TG, Bowie D, Lee H, Huganir RL, Schousboe A, Traynelis SF. Control of GluR1 AMPA receptor function by cAMP-dependent protein kinase. *J Neurosci.* 2000;20:89–102.
 12. Shelly M, Lim BK, Cancedda L, Heilshorn SC, Gao H, Poo M. Local and long-range reciprocal regulation of cAMP and cGMP in axon/dendrite formation. *Science.* 2010;327:547–52.
 13. Akiyama H, Fukuda T, Tojima T, Nikolaev VO, Kamiguchi H. Cyclic nucleotide control of microtubule dynamics for axon guidance. *J Neurosci.* 2016;36:5636–49.
 14. Crawford DC, Mennerick S. Presynaptically silent synapses: dormancy and awakening of presynaptic vesicle release. *Neuroscientist.* 2012;18:216–23.
 15. Kleppisch T, Feil R. cGMP signalling in the mammalian brain: role in synaptic plasticity and behaviour. *Handb Exp Pharmacol.* 2009;191:549–79.
 16. Averaimo S, Nicol X. Intermingled cAMP, cGMP and calcium spatiotemporal dynamics in developing neuronal circuits. *Front Cell Neurosci.* 2014;8:376.
 17. Kumada T, Lakshmana MK, Komuro H. Reversal of neuronal migration in a mouse model of fetal alcohol syndrome by controlling second-messenger signalings. *J Neurosci.* 2006;26:742–56.
 18. Stoufflet J, Chaulet M, Doulazmi M, Fouquet C, Dubacq C, Métin C, et al. Primary cilium-dependent cAMP/PKA signaling at the centrosome regulates neuronal migration. *Sci Adv.* 2020;6:eaba3992.
 19. Carlezon WA, Duman RS, Nestler EJ. The many faces of CREB. *Trends Neurosci.* 2005;28:436–45.
 20. Portis S, Giunta B, Obregon D, Tan J. The role of glycogen synthase kinase-3 signaling in neurodevelopment and fragile X syndrome. *Int J Physiol Pathophysiol Pharmacol.* 2012;4:140–8.
 21. Li Z, Theus MH, Wei L. Role of ERK 1/2 signaling in neuronal differentiation of cultured embryonic stem cells. *Dev Growth Differ.* 2006;48:513–23.
 22. Albert-Gascó H, Ros-Bernal F, Castillo-Gómez E, Olucha-Bordonau FE. MAP/ERK signaling in developing cognitive and emotional function and its effect on pathological and neurodegenerative processes. *Int J Mol Sci.* 2020;21:4471.
 23. Spilker C, Kreutz MR. RapGAPs in brain: multipurpose players in neuronal Rap signalling. *Eur J Neurosci.* 2010;32:1–9.
 24. Zhong J. RAS and downstream RAF-MEK and PI3K-AKT signaling in neuronal development, function and dysfunction. *Biol Chem.* 2016;397:215–22.
 25. Lee JJ, Wedow R, Okbay A, Kong E, Maghzian O, Zacher M, et al. Gene discovery and polygenic prediction from a genome-wide association study of educational attainment in 1.1 million individuals. *Nat Genet.* 2018;50:1112–21.
 26. Gurney ME. Genetic association of phosphodiesterases with human cognitive performance. *Front Mol Neurosci.* 2019;12:22.
 27. Sharma RK, Wang JH. Purification and characterization of bovine lung calmodulin-dependent cyclic nucleotide phosphodiesterase. An enzyme containing calmodulin as a subunit. *J Biol Chem.* 1986;261:14160–6.
 28. Autism Spectrum Disorders Working Group of The Psychiatric Genomics Consortium. Meta-analysis of GWAS of over 16,000 individuals with autism spectrum disorder highlights a novel locus at 10q24.32 and a significant overlap with schizophrenia. *Mol Autism.* 2017;8:21.
 29. De Rubeis S, He X, Goldberg AP, Paultney CS, Samocha K, Cicek AE, et al. Synaptic, transcriptional and chromatin genes disrupted in autism. *Nature.* 2014;515:209–15.
 30. John J, Bhattacharyya U, Yadav N, Kukshal P, Bhatia T, Nimagaonkar VL, et al. Multiple rare inherited variants in a four generation schizophrenia family offer leads for complex mode of disease inheritance. *Schizophrenia Res.* 2020;216:S288–294.
 31. McQuown S, Xia S, Baumgärtel K, Barido R, Anderson G, Dyck B, et al. Phosphodiesterase 1b (PDE1B) regulates spatial and contextual memory in hippocampus. *Front Mol Neurosci.* 2019;12:21.
 32. Reed TM, Repasky DR, Snyder GL, Greengard P, Vorhees CV. Phosphodiesterase 1B knock-out mice exhibit exaggerated locomotor hyperactivity and DARPP-32 phosphorylation in response to dopamine agonists and display impaired spatial learning. *J Neurosci.* 2002;22:5188–97.
 33. Hufgard JR, Williams MT, Skelton MR, Grubisha O, Ferreira FM, Sanger H, et al. Phosphodiesterase-1b (Pde1b) knockout mice are resistant to forced swim and tail suspension induced immobility and show upregulation of Pde10a. *Psychopharmacology.* 2017;234:1803–13.
 34. Haidar Z, Jalkh N, Corbani S, Abou-Ghoch J, Fawaz A, Mehawej C, et al. A homozygous splicing mutation in PDE2A in a family with atypical Rett syndrome. *Mov Disord.* 2020;35:896–9.
 35. Salpietro V, Perez-Dueñas B, Nakashima K, San Antonio-Arce V, Manole A, Efthymiou S, et al. A homozygous loss-of-function mutation in PDE2A associated to early-onset hereditary chorea. *Mov Disord.* 2018;33:482–8.
 36. Farmer R, Burbano SD, Patel NS, Sarmiento A, Smith AJ, Kelly MP. Phosphodiesterases PDE2A and PDE10A both change mRNA expression in the human brain with age, but only PDE2A changes in a region-specific manner with psychiatric disease. *Cell Signal.* 2020;70:109592.
 37. Assenza MR, Barbagallo F, Barrios F, Cornacchione M, Campano F, Vivarelli E, et al. Critical role of phosphodiesterase 2A in mouse congenital heart defects. *Cardiovasc Res.* 2018;114:830–45.
 38. Richter W, Menniti FS, Zhang H-T, Conti M. PDE4 as a target for cognition enhancement. *Expert Opin Ther Targets.* 2013;17:1011–27.
 39. Byers D, Davis RL, Kiger JA. Defect in cyclic AMP phosphodiesterase due to the dunce mutation of learning in *Drosophila melanogaster*. *Nature.* 1981;289:79–81.
 40. Gervasi N, Tchénio P, Prete T. PKA dynamics in a *Drosophila* learning center: coincidence detection by rutabaga adenyl cyclase and spatial regulation by dunce phosphodiesterase. *Neuron.* 2010;65:516–29.
 41. Millar JK, Pickard BS, Mackie S, James R, Christie S, Buchanan SR, et al. DISC1 and PDE4B are interacting genetic factors in schizophrenia that regulate cAMP signaling. *Science.* 2005;310:1187–91.
 42. Pickard BS, Thomson PA, Christoforou A, Evans KL, Morris SW, Porteous DJ, et al. The PDE4B gene confers sex-specific protection against schizophrenia. *Psychiatr Genet.* 2007;17:129–33.
 43. Malakhova AV, Rudko OI, Sobolev VV, Tretiakov AV, Naumova EA, Kokueva ZG, et al. PDE4B gene polymorphism in Russian patients with panic disorder. *AIMS Genet.* 2019;6:55–63.
 44. Siuciak JA, Chapin DS, McCarthy SA, Martin AN. Antipsychotic profile of rolipram: efficacy in rats and reduced sensitivity in mice deficient in the phosphodiesterase-4B (PDE4B) enzyme. *Psychopharmacology.* 2007;192:415–24.
 45. Rutten K, Wallace TL, Works M, Prickaerts J, Blokland A, Novak TJ, et al. Enhanced long-term depression and impaired reversal learning in phosphodiesterase 4B-knockout (PDE4B^{-/-}) mice. *Neuropharmacology.* 2011;61:138–47.
 46. Zhang H-T, Huang Y, Masood A, Stolinski LR, Li Y, Zhang L, et al. Anxiogenic-like behavioral phenotype of mice deficient in

- phosphodiesterase 4B (PDE4B). *Neuropsychopharmacology*. 2008;33:1611–23.
47. Linglart A, Fryssira H, Hiort O, Holterus P-M, Perez de Nanclares G, Argente J, et al. PRKAR1A and PDE4D mutations cause acrodyssostosis but two distinct syndromes with or without GPCR-signaling hormone resistance. *J Clin Endocrinol Metab*. 2012;97:2328–38.
 48. Michot C, Le Goff C, Blair E, Blanchet P, Capri Y, Gilbert-Dussardier B, et al. Expanding the phenotypic spectrum of variants in PDE4D/PRKAR1A: from acrodyssostosis to acrosyphodysplasia. *Eur J Hum Genet*. 2018;26:1611–22.
 49. Zhang H-T, Huang Y, Jin S-L, Frith SA, Suvarna N, Conti M, et al. Antidepressant-like profile and reduced sensitivity to roflupram in mice deficient in the PDE4D phosphodiesterase enzyme. *Neuropsychopharmacology*. 2002;27:587–95.
 50. Siuciak JA, McCarthy SA, Chapin DS, Martin AN, Harms JF, Schmidt CJ. Behavioral characterization of mice deficient in the phosphodiesterase-10A (PDE10A) enzyme on a C57Bl/6N congenic background. *Neuropsychopharmacology*. 2008;54:417–27.
 51. Cardinale A, Fusco FR. Inhibition of phosphodiesterases as a strategy to achieve neuroprotection in Huntington's disease. *CNS Neurosci Ther*. 2018;24:319–28.
 52. Nthenge-Ngumbau DN, Mohanakumar KP. Can cyclic nucleotide phosphodiesterase inhibitors be drugs for Parkinson's disease? *Mol Neurobiol*. 2018;55:822–34.
 53. Bollen E, Prickaerts J. Phosphodiesterases in neurodegenerative disorders. *IUBMB Life*. 2012;64:965–70.
 54. Kelly MP, Logue SF, Brennan J, Day JP, Lakkaraju S, Jiang L, et al. Phosphodiesterase 11A in brain is enriched in ventral hippocampus and deletion causes psychiatric disease-related phenotypes. *Proc Natl Acad Sci USA*. 2010;107:8457–62.
 55. Kelly MP. A role for phosphodiesterase 11A (PDE11A) in the formation of social memories and the stabilization of mood. *Adv Neurobiol*. 2017;17:201–30.
 56. Luo H-R, Wu G-S, Dong C, Arcos-Burgos M, Ribeiro L, Licinio J, et al. Association of PDE11A global haplotype with major depression and antidepressant drug response. *Neuropsychiatr Dis Treat*. 2009;5:163–70.
 57. Reirerson GW, Mastronardi CA, Licinio J, Wong M-L. Chronic imipramine downregulates cyclic AMP signaling in rat hippocampus. *Neuroreport*. 2009;20:307–11.
 58. Reirerson GW, Mastronardi CA, Licinio J, Wong M-L. Repeated antidepressant therapy increases cyclic GMP signaling in rat hippocampus. *Neurosci Lett*. 2009;466:149–53.
 59. Enomoto T, Tatara A, Goda M, Nishizato Y, Nishigori K, Kitamura A, et al. A novel phosphodiesterase 1 inhibitor DSR-141562 exhibits efficacies in animal models for positive, negative, and cognitive symptoms associated with schizophrenia. *J Pharmacol Exp Ther*. 2019;371:692–702.
 60. Liu L, Zheng J, Huang X-F, Zhu X, Ding S-M, Ke H-M, et al. The neuroprotective and antidepressant-like effects of Hcyb1, a novel selective PDE2 inhibitor. *CNS Neurosci Ther*. 2018;24:652–60.
 61. Nakashima M, Imada H, Shiraishi E, Ito Y, Suzuki N, Miyamoto M, et al. Phosphodiesterase 2A inhibitor TAK-915 ameliorates cognitive impairments and social withdrawal in N-methyl-d-aspartate receptor antagonist-induced rat models of schizophrenia. *J Pharmacol Exp Ther*. 2018;365:179–88.
 62. Nakashima M, Suzuki N, Shiraishi E, Iwashita H. TAK-915, a phosphodiesterase 2A inhibitor, ameliorates the cognitive impairment associated with aging in rodent models. *Behav Brain Res*. 2019;376:112192.
 63. Wang J-N, Zhao X-J, Liu Z-H, Zhao X-L, Sun T, Fu Z-J. Selective phosphodiesterase-2A inhibitor alleviates radicular inflammation and mechanical allodynia in non-compressive lumbar disc herniation rats. *Eur Spine J*. 2017;26:1961–8.
 64. Boess FG, Hendrix M, van der Staay F-J, Erb C, Schreiber R, van Staveren W, et al. Inhibition of phosphodiesterase 2 increases neuronal cGMP, synaptic plasticity and memory performance. *Neuropsychopharmacology*. 2004;47:1081–92.
 65. Domek-Lopacińska K, Strojsnajder JB. The effect of selective inhibition of cyclic GMP hydrolyzing phosphodiesterases 2 and 5 on learning and memory processes and nitric oxide synthase activity in brain during aging. *Brain Res*. 2008;1216:68–77.
 66. Bollen E, Akkerman S, Puzzo D, Gulisano W, Palmeri A, D'Hooge R, et al. Object memory enhancement by combining sub-efficacious doses of specific phosphodiesterase inhibitors. *Neuropsychopharmacology*. 2015;95:361–6.
 67. Ruan L, Du K, Tao M, Shan C, Ye R, Tang Y, et al. Phosphodiesterase-2 Inhibitor Bay 60-7550 ameliorates Aβ-induced cognitive and memory impairment via regulation of the HPA axis. *Front Cell Neurosci*. 2019;13:432.
 68. Soares LM, Meyer E, Milani H, Steinbusch HWM, Prickaerts J, de Oliveira RMW. The phosphodiesterase type 2 inhibitor BAY 60-7550 reverses functional impairments induced by brain ischemia by decreasing hippocampal neurodegeneration and enhancing hippocampal neuronal plasticity. *Eur J Neurosci*. 2017;45:510–20.
 69. Shi J, Liu H, Pan J, Chen J, Zhang N, Liu K, et al. Inhibition of phosphodiesterase 2 by Bay 60-7550 decreases ethanol intake and preference in mice. *Psychopharmacology*. 2018;235:2377–85.
 70. Reneerkens OAH, Rutten K, Bollen E, Hage T, Blokland A, Steinbusch HWM, et al. Inhibition of phosphodiesterase type 2 or type 10 reverses object memory deficits induced by scopolamine or MK-801. *Behav Brain Res*. 2013;236:16–22.
 71. Wang L, Xiaokaiti Y, Wang G, Xu X, Chen L, Huang X, et al. Inhibition of PDE2 reverses beta amyloid induced memory impairment through regulation of PKA/PKG-dependent neuroinflammatory and apoptotic pathways. *Sci Rep*. 2017;7:12044.
 72. Maurin T, Melancia F, Jarjat M, Castro L, Costa L, Delhaye S, et al. Involvement of phosphodiesterase 2A activity in the pathophysiology of fragile X syndrome. *Cereb Cortex*. 2019;29:3241–52.
 73. Kitamura A, Manso Y, Duncombe J, Searcy J, Koudelka J, Binnie M, et al. Long-term cilostazol treatment reduces gliovascular damage and memory impairment in a mouse model of chronic cerebral hypoperfusion. *Sci Rep*. 2017;7:4299.
 74. Tai S-Y, Chien C-Y, Chang Y-H, Yang Y-H. Cilostazol use is associated with reduced risk of dementia: a nationwide cohort study. *Neurotherapeutics*. 2017;14:784–91.
 75. Tai S-Y, Chen C-H, Chien C-Y, Yang Y-H. Cilostazol as an add-on therapy for patients with Alzheimer's disease in Taiwan: a case control study. *BMC Neurol*. 2017;17:40.
 76. Zhao J, Harada N, Kurihara H, Nakagata N, Okajima K. Cilostazol improves cognitive function in mice by increasing the production of insulin-like growth factor-I in the hippocampus. *Neuropsychopharmacology*. 2010;58:774–83.
 77. Zheng W-H, Quirion R. Insulin-like growth factor-1 (IGF-1) induces the activation/phosphorylation of Akt kinase and cAMP response element-binding protein (CREB) by activating different signaling pathways in PC12 cells. *BMC Neurosci*. 2006;7:51.
 78. Blokland A, Van Duinen MA, Sambeth A, Heckman PRA, Tsai M, Lahu G, et al. Acute treatment with the PDE4 inhibitor roflumilast improves verbal word memory in healthy old individuals: a double-blind placebo-controlled study. *Neurobiol Aging*. 2019;77:37–43.
 79. Gilleen J, Farah Y, Davison C, Kerins S, Valdearenas L, Uz T, et al. An experimental medicine study of the phosphodiesterase-4 inhibitor, roflumilast, on working memory-related brain activity and episodic memory in schizophrenia patients. *Psychopharmacology*. 2018. <https://doi.org/10.1007/s00213-018-5134-y>.

80. Zhong Q, Yu H, Huang C, Zhong J, Wang H, Xu J, et al. FCP16, a novel phosphodiesterase 4 inhibitor, produces an antidepressant-like effect in mice exposed to chronic unpredictable mild stress. *Prog Neuropsychopharmacol Biol Psychiatry*. 2019;90:62–75.
81. Monti B, Bertotti C, Contestabile A. Subchronic Rolipram delivery activates hippocampal CREB and Arc, enhances retention and slows down extinction of conditioned fear. *Neuropsychopharmacology* 2006;31:278–86.
82. Wimmer ME, Blackwell JM, Abel T. Rolipram treatment during consolidation ameliorates long-term object location memory in aged male mice. *Neurobiol Learn Mem*. 2020;169:107168.
83. Xu Y, Zhu N, Xu W, Ye H, Liu K, Wu F, et al. Inhibition of phosphodiesterase-4 reverses $\text{A}\beta$ -induced memory impairment by regulation of HPA axis related cAMP signaling. *Front Aging Neurosci*. 2018;10:204.
84. Cui S-Y, Yang M-X, Zhang Y-H, Zheng V, Zhang H-T, Gurney ME, et al. Protection from amyloid β peptide-induced memory, biochemical, and morphological deficits by a phosphodiesterase-4D allosteric inhibitor. *J Pharmacol Exp Ther*. 2019;371:250–9.
85. Zhang C, Xu Y, Chowdhary A, Fox D, Gurney ME, Zhang H-T, et al. Memory enhancing effects of BPN14770, an allosteric inhibitor of phosphodiesterase-4D, in wild-type and humanized mice. *Neuropsychopharmacology*. 2018;43:2299–309.
86. Bourchouladze R, Lidge R, Catapano R, Stanley J, Gossweiler S, Romashko D, et al. A mouse model of Rubinstein-Taybi syndrome: defective long-term memory is ameliorated by inhibitors of phosphodiesterase 4. *Proc Natl Acad Sci USA*. 2003;100:10518–22.
87. Wieschollek V, Manahan-Vaughan D. PDE4 inhibition enhances hippocampal synaptic plasticity in vivo and rescues MK801-induced impairment of long-term potentiation and object recognition memory in an animal model of psychosis. *Transl Psychiatry*. 2012;2:e89.
88. Choi CH, Schoenfeld BP, Weisz ED, Bell AJ, Chambers DB, Hinckley J, et al. PDE-4 inhibition rescues aberrant synaptic plasticity in *Drosophila* and mouse models of fragile X syndrome. *J Neurosci*. 2015;35:396–408.
89. Zhang R, Wang Y, Zhang L, Zhang Z, Tsang W, Lu M, et al. Sildenafil (Viagra) induces neurogenesis and promotes functional recovery after stroke in rats. *Stroke*. 2002;33:2675–80.
90. Prickaerts J, van Staveren WCG, Sik A, Markerink-van Ittersum M, Niewöhner U, van der Staay FJ, et al. Effects of two selective phosphodiesterase type 5 inhibitors, sildenafil and vardenafil, on object recognition memory and hippocampal cyclic GMP levels in the rat. *Neuroscience*. 2002;113:351–61.
91. Devan BD, Bowker JL, Duffy KB, Bharati IS, Jimenez M, Sierra-Mercado D, et al. Phosphodiesterase inhibition by sildenafil citrate attenuates a maze learning impairment in rats induced by nitric oxide synthase inhibition. *Psychopharmacology*. 2006;183:439–45.
92. Sanders O. Sildenafil for the treatment of Alzheimer's disease: a systematic review. *J Alzheimers Dis Rep*. 2020;4:91–106.
93. Schultheiss D, Müller SV, Nager W, Stief CG, Schlotte N, Jonas U, et al. Central effects of sildenafil (Viagra) on auditory selective attention and verbal recognition memory in humans: a study with event-related brain potentials. *World J Urol*. 2001;19:46–50.
94. Huang X-F, Jiang W-T, Liu L, Song F-C, Zhu X, Shi G-L, et al. A novel PDE9 inhibitor WYQ-C36D ameliorates corticosterone-induced neurotoxicity and depression-like behaviors by cGMP-CREB-related signaling. *CNS Neurosci Ther*. 2018;24:889–96.
95. Kleiman RJ, Chapin DS, Christoffersen C, Freeman J, Fonseca KR, Geoghegan KF, et al. Phosphodiesterase 9A regulates central cGMP and modulates responses to cholinergic and monoaminergic perturbation in vivo. *J Pharmacol Exp Ther*. 2012;341:396–409.
96. Frölich L, Wunderlich G, Thamer C, Roehrle M, Garcia M, Dubois B. Evaluation of the efficacy, safety and tolerability of orally administered BI 409306, a novel phosphodiesterase type 9 inhibitor, in two randomised controlled phase II studies in patients with prodromal and mild Alzheimer's disease. *Alzheimer's Res Ther*. 2019;11:18.
97. Schwam EM, Nicholas T, Chew R, Billing CB, Davidson W, Ambrose D, et al. A multicenter, double-blind, placebo-controlled trial of the PDE9A inhibitor, PF-04447943, in Alzheimer's disease. *Curr Alzheimer Res*. 2014;11:413–21.
98. Chakraborty S, Manfredsson FP, Dec AM, Campbell PW, Stutzmann GE, Beaumont V, et al. Phosphodiesterase 9A inhibition facilitates corticostriatal transmission in wild-type and transgenic rats that model Huntington's disease. *Front Neurosci*. 2020;14:466.
99. Suzuki K, Harada A, Shiraishi E, Kimura H. In vivo pharmacological characterization of TAK-063, a potent and selective phosphodiesterase 10A inhibitor with antipsychotic-like activity in rodents. *J Pharmacol Exp Ther*. 2015;352:471–9.
100. Takakuwa M, Watanabe Y, Tanaka K, Ishii T, Kagaya K, Taniguchi H, et al. Antipsychotic-like effects of a novel phosphodiesterase 10A inhibitor T-251 in rodents. *Pharmacol Biochem Behav*. 2019;185:172757.
101. Macek TA, McCue M, Dong X, Hanson E, Goldsmith P, Affinito J, et al. A phase 2, randomized, placebo-controlled study of the efficacy and safety of TAK-063 in subjects with an acute exacerbation of schizophrenia. *Schizophrenia Res*. 2019;204:289–94.
102. Cheng Y, Wang Z-M, Tan W, Wang X, Li Y, Bai B, et al. Partial loss of psychiatric risk gene miR-137 in mice causes repetitive behavior and impairs sociability and learning via increased Pde10a. *Nat Neurosci*. 2018;21:1689–703.
103. Giralt A, Saavedra A, Carreton O, Arumí H, Tyebji S, Alberch J, et al. PDE10 inhibition increases GluA1 and CREB phosphorylation and improves spatial and recognition memories in a Huntington's disease mouse model. *Hippocampus*. 2013;23:684–95.
104. Guang S, Pang N, Deng X, Yang L, He F, Wu L, et al. Synaptopathology involved in autism spectrum disorder. *Front Cell Neurosci*. 2018;12:470.
105. Luhach K, Kulkarni GT, Singh VP, Sharma B. Attenuation of neurobehavioural abnormalities by papaverine in prenatal valproic acid rat model of ASD. *Eur J Pharmacol*. 2020;173663. <https://doi.org/10.1016/j.ejphar.2020.173663>
106. Sharma N, Dhiman N, Golani LK, Sharma B. Papaverine ameliorates prenatal alcohol-induced experimental attention deficit hyperactivity disorder by regulating neuronal function, inflammation, and oxidative stress. *Int J Dev Neurosci*. 2020; <https://doi.org/10.1002/jdn.10076>.
107. Antonarakis SE, Skotko BG, Rafii MS, Strydom A, Pape SE, Bianchi DW, et al. Down syndrome. *Nat Rev Dis Prim*. 2020;6:9.
108. De Toma I, Ortega M, Aloy P, Sabidó E, Dierssen M. DYRK1A overexpression alters cognition and neural-related proteomic pathways in the hippocampus that are rescued by green tea extract and/or environmental enrichment. *Front Mol Neurosci*. 2019;12:272.
109. van Bon BWM, Coe BP, Bernier R, Green C, Gerdts J, Witherspoon K, et al. Disruptive de novo mutations of DYRK1A lead to a syndromic form of autism and ID. *Mol Psychiatry*. 2016;21:126–32.
110. Yang EJ, Ahn YS, Chung KC. Protein kinase Dyk1 activates cAMP response element-binding protein during neuronal differentiation in hippocampal progenitor cells. *J Biol Chem*. 2001;276:39819–24.

111. Lott IT, Head E. Dementia in Down syndrome: unique insights for Alzheimer disease research. *Nat Rev Neurol.* 2019;15:135–47.
112. Dierssen M, Vallina IF, Baamonde C, García-Calatayud S, Lumbierres MA, Flórez J. Alterations of central noradrenergic transmission in Ts65Dn mouse, a model for Down syndrome. *Brain Res.* 1997;749:238–44.
113. Tsuji M, Ohshima M, Yamamoto Y, Saito S, Hattori Y, Tanaka E, et al. Cilostazol, a phosphodiesterase 3 inhibitor, moderately attenuates behaviors depending on sex in the Ts65Dn mouse model of down syndrome. *Front Aging Neurosci.* 2020;12:106.
114. Dahlhaus R. Of men and mice: modeling the fragile X syndrome. *Front Mol Neurosci* 2018;11:41.
115. Berry-Kravis E, Huttenlocher PR. Cyclic AMP metabolism in fragile X syndrome. *Ann Neurol.* 1992;31:22–26.
116. Maurin T, Lebrigand K, Castagnola S, Paquet A, Jarjat M, Popa A, et al. HITS-CLIP in various brain areas reveals new targets and new modalities of RNA binding by fragile X mental retardation protein. *Nucleic Acids Res.* 2018;46:6344–55.
117. García-Font N, Martín R, Torres M, Oset-Gasque MJ, Sánchez-Prieto J. The loss of β adrenergic receptor mediated release potentiation in a mouse model of fragile X syndrome. *Neurobiol Dis.* 2019;130:104482.
118. Boyken J, Grønborg M, Riedel D, Urlaub H, Jahn R, Chua JJE. Molecular profiling of synaptic vesicle docking sites reveals novel proteins but few differences between glutamatergic and GABAergic synapses. *Neuron.* 2013;78:285–97.
119. Gurney ME, Cogram P, Deacon RM, Rex C, Tranfaglia M. Multiple behavior phenotypes of the fragile-X syndrome mouse model respond to chronic inhibition of phosphodiesterase-4D (PDE4D). *Sci Rep.* 2017;7:14653.
120. Manzini MC, Xiong L, Shaheen R, Tambunan DE, Di Costanzo S, Mitialis V, et al. CC2D1A regulates human intellectual and social function as well as NF- κ B signaling homeostasis. *Cell Rep.* 2014;8:647–55.
121. Gallagher CM, Knoblich JA. The conserved c2 domain protein lethal (2) giant discs regulates protein trafficking in *Drosophila*. *Dev Cell.* 2006;11:641–53.
122. Oaks AW, Zamarbide M, Tambunan DE, Santini E, Di Costanzo S, Pond HL, et al. Cc2d1a Loss of function disrupts functional and morphological development in forebrain neurons leading to cognitive and social deficits. *Cereb Cortex.* 2017;27:1670–85.
123. Guan F, Lin H, Chen G, Li L, Chen T, Liu X, et al. Evaluation of association of common variants in HTR1A and HTR5A with schizophrenia and executive function. *Sci Rep.* 2016;6:38048.
124. Al-Tawashi A, Gehring C. Phosphodiesterase activity is regulated by CC2D1A that is implicated in non-syndromic intellectual disability. *Cell Commun Signal.* 2013;11:47.
125. Zamarbide M, Mossa A, Muñoz-Llanca P, Wilkinson MK, Pond HL, Oaks AW, et al. Male-specific cAMP signaling in the hippocampus controls spatial memory deficits in a mouse model of autism and intellectual disability. *Biol Psychiatry.* 2019;85:760–8.
126. Lombardi LM, Baker SA, Zoghbi HY. MECP2 disorders: from the clinic to mice and back. *J Clin Investig.* 2015;125:2914–23.
127. Sanfelix A, Kaufmann WE, Gill M, Guasoni P, Tropea D. Transcriptomic studies in mouse models of Rett syndrome: a review. *Neuroscience.* 2019;413:183–205.
128. Mironov SL, Skorova EY, Kübler S. Epac-mediated cAMP-signalling in the mouse model of Rett Syndrome. *Neuropharmacology.* 2011;60:869–77.
129. Bu Q, Wang A, Hamzah H, Waldman A, Jiang K, Dong Q, et al. CREB Signaling Is Involved in Rett Syndrome Pathogenesis. *J Neurosci.* 2017;37:3671–85.
130. Esposito K, Reierson GW, Luo HR, Wu GS, Licinio J, Wong M-L. Phosphodiesterase genes and antidepressant treatment response: a review. *Ann Med.* 2009;41:177–85.
131. Blokland A, Schreiber R, Prickaerts J. Improving memory: a role for phosphodiesterases. *Curr Pharm Des.* 2006;12:2511–23.
132. Prickaerts J, Heckman PRA, Blokland A. Investigational phosphodiesterase inhibitors in phase I and phase II clinical trials for Alzheimer's disease. *Expert Opin Investig Drugs.* 2017;26:1033–48.
133. Heckman PRA, Blokland A, Ramaekers J, Prickaerts J. PDE and cognitive processing: beyond the memory domain. *Neurobiol Learn Mem.* 2015;119:108–22.
134. Björklund G, Kern JK, Urbina MA, Saad K, El-Houfey AA, Geier DA, et al. Cerebral hypoperfusion in autism spectrum disorder. *Acta Neurobiol Exp.* 2018;78:21–29.
135. Pieretti S, Dominici L, Di Giannuario A, Cesari N, Dal Piaz V. Local anti-inflammatory effect and behavioral studies on new PDE4 inhibitors. *Life Sci.* 2006;79:791–800.
136. Matta SM, Hill-Yardin EL, Crack PJ. The influence of neuroinflammation in Autism Spectrum Disorder. *Brain Behav Immun.* 2019;79:75–90.
137. Hagberg H, Mallard C, Ferriero DM, Vannucci SJ, Levison SW, Vexler ZS, et al. The role of inflammation in perinatal brain injury. *Nat Rev Neurol.* 2015;11:192–208.
138. Zaccolo M, Cesetti T, Di Benedetto G, Mongillo M, Lissandron V, Terrin A, et al. Imaging the cAMP-dependent signal transduction pathway. *Biochem Soc Trans.* 2005;33:1323–6.
139. Ferron L. Fragile X mental retardation protein controls ion channel expression and activity. *J Physiol.* 2016;594:5861–7.
140. Castagnola S, Cazareth J, Lebrigand K, Jarjat M, Magnone V, Delhayé S, et al. Agonist-induced functional analysis and cell sorting associated with single-cell transcriptomics characterizes cell subtypes in normal and pathological brain. *Genome Res.* 2020;30:1633–42.
141. Wrigley S, Arafa D, Tropea D. Insulin-like growth factor 1: at the crossroads of brain development and aging. *Front Cell Neurosci.* 2017;11:14.
142. Deacon RMJ, Glass L, Snape M, Hurley MJ, Altimiras FJ, Biekofsky RR, et al. NNZ-2566, a novel analog of (1-3) IGF-1, as a potential therapeutic agent for fragile X syndrome. *Neuro-molecular Med.* 2015;17:71–82.
143. Esveld E-E, Tuukkine J, Sirp A, Patil S, Bramham CR, Timmusk T. CREB family transcription factors are major mediators of BDNF transcriptional autoregulation in cortical neurons. *J Neurosci.* 2020;40:1405–26.
144. Björkholm C, Monteggia LM. BDNF—a key transducer of antidepressant effects. *Neuropharmacology.* 2016;102:72–79.
145. Libman-Sokołowska M, Drozdowicz E, Nasierowski T. BDNF as a biomarker in the course and treatment of schizophrenia. *Psychiatr Pol.* 2015;49:1149–58.
146. Downs J, Rodger J, Li C, Tan X, Hu N, Wong K, et al. Environmental enrichment intervention for Rett syndrome: an individually randomised stepped wedge trial. *Orphanet J Rare Dis.* 2018;13:3.
147. Nomura T, Musial TF, Marshall JJ, Zhu Y, Remmers CL, Xu J, et al. Delayed maturation of fast-spiking interneurons is rectified by activation of the TrkB receptor in the mouse model of fragile X syndrome. *J Neurosci.* 2017;37:11298–310.
148. Wang P, Wu P, Egan RW, Billah MM. Identification and characterization of a new human type 9 cGMP-specific phosphodiesterase splice variant (PDE9A5): differential tissue distribution and subcellular localization of PDE9A variants. *Gene.* 2003;314:15–27.

Annexe 1

Le laboratoire s'est aussi intéressé à une autre cible de FMRP trouvé par le HITSCLIP, *Cacna1a*, codant pour la sous-unité $\alpha 1$ formant le pore du canal calcique voltagedépendant de type P/Q Cav2.1.

Nous avons montré des déficits d'homéostasie calcique basale dans les neurones de souris *Fmr1* KO par imagerie calcique ratiométrique. Les neurones *Fmr1* KO ont aussi une entrée de calcium altérée en réponse à un stimulus dépolarisant, et ont une expression altérée de Cav2.1 à la surface. Cette étude identifie donc le défaut d'homéostasie calcique comme nouveau biomarqueur cellulaire, nouveau phénotype des neurones *Fmr1* KO.

J'ai pour ma part réalisé pour cette étude la colocalisation de FMRP et Cav2.1 par immunocytochimie et l'immunoprécipitation de Cav2.1 par FMRP dans un extrait de cervelet de souris WT. Ces résultats montrent que FMRP module la localisation subcellulaire et interagit directement avec Cav2.1, pouvant expliquer les défauts retrouvés dans les neurones *Fmr1* KO.



New Insights Into the Role of $\text{Ca}_{\text{v}}2$ Protein Family in Calcium Flux Deregulation in *Fmr1*-KO Neurons

Sara Castagnola^{1,2}, Sébastien Delhaye^{1,2}, Alessandra Folci¹, Agnès Paquet¹, Frédéric Brau¹, Fabrice Duprat³, Marielle Jarjat^{1,2}, Mauro Grossi^{1,2}, Méline Béal^{1,2}, Stéphane Martin³, Massimo Mantegazza³, Barbara Bardoni^{2,3} and Thomas Maurin^{1,2*}

¹Université Côte d'Azur, CNRS UMR7275, IPMC, Valbonne, France, ²CNRS LIA "Neogenex", Valbonne, France, ³Université Côte d'Azur, INSERM, CNRS UMR7275, IPMC, Valbonne, France

Fragile X syndrome (FXS), the most common form of inherited intellectual disability (ID) and a leading cause of autism, results from the loss of expression of the *Fmr1* gene which encodes the RNA-binding protein Fragile X Mental Retardation Protein (FMRP). Among the thousands mRNA targets of FMRP, numerous encode regulators of ion homeostasis. It has also been described that FMRP directly interacts with Ca^{2+} channels modulating their activity. Collectively these findings suggest that FMRP plays critical roles in Ca^{2+} homeostasis during nervous system development. We carried out a functional analysis of Ca^{2+} regulation using a calcium imaging approach in *Fmr1*-KO cultured neurons and we show that these cells display impaired steady state Ca^{2+} concentration and an altered entry of Ca^{2+} after KCl-triggered depolarization. Consistent with these data, we show that the protein product of the *Cacna1a* gene, the pore-forming subunit of the $\text{Ca}_{\text{v}}2.1$ channel, is less expressed at the plasma membrane of *Fmr1*-KO neurons compared to wild-type (WT). Thus, our findings point out the critical role that $\text{Ca}_{\text{v}}2.1$ plays in the altered Ca^{2+} flux in *Fmr1*-KO neurons, impacting Ca^{2+} homeostasis of these cells. Remarkably, we highlight a new phenotype of cultured *Fmr1*-KO neurons that can be considered a novel cellular biomarker and is amenable to small molecule screening and identification of new drugs to treat FXS.

OPEN ACCESS

Edited by:

Regina Dahlhaus,
Friedrich-Alexander-Universität
Erlangen-Nürnberg, Germany

Reviewed by:

Maija Liisa Castrén,
University of Helsinki, Finland
Christina Gross,
Cincinnati Children's Hospital Medical
Center, United States

*Correspondence:

Thomas Maurin
maurin@ipmc.cnrs.fr

Received: 16 April 2018

Accepted: 30 August 2018

Published: 27 September 2018

Citation:

Castagnola S, Delhaye S, Folci A, Paquet A, Brau F, Duprat F, Jarjat M, Grossi M, Béal M, Martin S, Mantegazza M, Bardoni B and Maurin T (2018) New Insights Into the Role of $\text{Ca}_{\text{v}}2$ Protein Family in Calcium Flux Deregulation in *Fmr1*-KO Neurons. *Front. Mol. Neurosci.* 11:342. doi: 10.3389/fnmol.2018.00342

Keywords: Fragile X syndrome, $\text{Ca}_{\text{v}}2.1$, calcium homeostasis, ratiometric calcium imaging, *Cacna1a*

INTRODUCTION

Fragile X syndrome (FXS) is the most common form of inherited intellectual disability (ID) and the leading identified monogenic cause of autism (Maurin et al., 2014; Castagnola et al., 2017). FXS is caused by the silencing of the *Fmr1* gene encoding the Fragile X Mental Retardation Protein (FMRP), an RNA-binding protein modulating the expression of thousands of mRNAs primarily at the translational level in particular, it has been shown to regulate translation at the synaptic level. Furthermore, FMRP has been reported to be involved in different steps of RNA metabolism, indeed it is a component of various ribonucleoproteic complexes (mRNPs), including the RNA granules, the mRNP involved in transport along neurites (Maurin et al., 2014, 2018a).

Several reports have shown that FMRP binds multiple RNAs encoding regulators of ion homeostasis and more particularly involved in the calcium ion pathway (Brown et al., 2001; Miyashiro et al., 2003; Darnell et al., 2011; Ascano et al., 2012; Maurin et al., 2018a).

Furthermore, the search for FMRP-interacting proteins has resulted into the identification of dozens of partners, including ion channels (Bardoni et al., 2006; Ferron, 2016; and this study). Consistently with these findings, ion homeostasis defects in FXS neurons have been described (Chen et al., 2003; Meredith et al., 2007; Brown et al., 2010; Deng et al., 2013; Ferron et al., 2014; Hebert et al., 2014; Zhang et al., 2014; Contractor et al., 2015; Myrick et al., 2015; Wahlstrom-Helgren and Klyachko, 2015; Achuta et al., 2018). In particular, FMRP has been reported to directly interact with two members of the Voltage Gated Calcium Channels (VGCC) family, namely $\text{Ca}_{\text{v}}2.1$ and $\text{Ca}_{\text{v}}2.2$ (Ferron et al., 2014).

Cytosolic calcium concentration is set by the balance between calcium influx and efflux as well as by the exchange of calcium ion with internal stores. Calcium homeostasis is tightly controlled and involves multiple protein complexes such as ATPase pumps, transporters and ion channels in various cellular compartments (Clapham, 2007).

VGCCs respond to plasma membrane depolarization by allowing extracellular calcium ions to flow into cells according to their concentration gradient. Calcium can then act as a second messenger of cell depolarization activating various key intracellular signaling pathways, inducing contraction in muscle cells, protein phosphorylation, secretion and synaptic transmission. VGCCs are heteromers composed by the assembly of a pore-forming subunit (encoded by the corresponding $\alpha 1$ gene) and auxiliary β and $\alpha 2\delta$ proteins (Dolphin, 2016). VGCCs can be distinguished as L-, N-, R- and P/Q-type channels depending on the identity of the pore-forming subunit. L- and T-type VGCCs are found in a great variety of cells, while N-, P/Q- and R-type are mostly expressed in neurons (Catterall, 2011).

The *Cacna1a* gene encodes the P/Q-type VGCC $\text{Ca}_{\text{v}}2.1$, which is critical for the depolarization-evoked release of neurotransmitters at the presynaptic terminals (Simms and Zamponi, 2014). $\text{Ca}_{\text{v}}2.1$ is mostly expressed in the cerebellum, consequently mutations in the *Cacna1a* gene are associated with several neurological disorders such as episodic ataxia and spino-cerebellar ataxia (Zhuchenko et al., 1997). More recently, new mutations in this gene have been identified in four unrelated families with ID, attention deficit, hyperactivity and autism spectrum disorder (Damaj et al., 2015). This suggests that $\text{Ca}_{\text{v}}2.1$ may play a previously under-appreciated role in brain regions other than the cerebellum and could have implicated roles in cognition, memory and social interaction regulation. Indeed, regulation of $\text{Ca}_{\text{v}}2.1$ channels by calcium sensor proteins is required for normal short-term synaptic plasticity, LTP, and spatial learning and memory in mice (Nanou et al., 2016).

We thus investigated calcium homeostasis using ratiometric calcium imaging in *Fmr1*-KO neurons. Our results show that neurons lacking FMRP are not only more sensitive to $\text{Ca}_{\text{v}}2.2$ inhibition but also less sensitive to $\text{Ca}_{\text{v}}2.1$ inhibition compared to wild-type (WT) neurons and this is a consequence of an impaired membrane expression of this channel in the absence of FMRP. We propose here a model in which FMRP is involved in the regulation of the relative membrane expression of P/Q- and N-type VGCCs.

MATERIALS AND METHODS

Primary Neuronal Cultures

Cultures were prepared from the cortex of embryonic stage E14.5 WT and *Fmr1*-KO embryos as previously described (Abekhoush et al., 2017; Maurin et al., 2018a). Neurons (250,000 cells) were plated on ornithine-coated glass coverslips (35 mm diameter) and cultivated in complete medium: Neurobasal (Invitrogen) supplemented with B-27 (Invitrogen) and glutamax (Invitrogen). Neurons were fed weekly by removing 10% of the culture medium and replacing it with fresh complete medium.

Ratiometric Calcium Imaging

Primary cortical neurons Day-In-Vitro 19–23 (DIV 19–23; 13 independent cultures) grown on coverslips were incubated in neurobasal containing 20 μM Fura2-AM (Invitrogen) for 30 min at 37°C. After two washes with HEPES-buffered Tyrode's calcium solution (in mM: 139 NaCl, 15 glucose, 1.25 Na_2HPO_4 dibasic heptahydrate, 1.8 MgSO_4 heptahydrate, 1.6 CaCl_2 dihydrate, 3 KCl, 10 HEPES), coverslips were placed in a metal chamber on an inverted microscope (AxioObserver, Carl Zeiss) equipped with a 300W Xenon lamp (Sutter Instruments) and a Fluor 40 \times NA 1.4 oil immersion objective. Cells were perfused at 22°C throughout the recording with Tyrode's calcium solution. The pharmacological stimulations were performed by supplementing the calcium recording solution with either DiHydroxyPhenylGlycine (DHPG, 100 μM) or KCl (50 mM) or VGCC antagonist (ω -agatoxin-Iva (100 nM); ω -conotoxin GVIA (1 μM); Nitrendipine (1 μM)) or VGCC antagonist (same concentrations) + KCl. A calibration step was performed at the end of every recording by applying successively 0 Ca^{2+} (in mM: 129 NaCl, 15 glucose, 1.25 Na_2HPO_4 dibasic heptahydrate, 1.8 MgSO_4 heptahydrate, 0.5 EGTA, 3 KCl, 10 HEPES), then 0 Ca^{2+} + ionomycin (5 μM) and finally 10 Ca^{2+} + ionomycin (5 μM ; in mM: 129 NaCl, 15 glucose, 1.25 Na_2HPO_4 dibasic heptahydrate, 1.8 MgSO_4 heptahydrate, 10 CaCl_2 dihydrate, 3 KCl, 10 HEPES) solutions. This calibration step allows to quantify the lowest and the highest probe fluorescence $F_{340/380}$ ratio for every Region of Interest (ROI); the maximal value was used subsequently to normalize the fluorescence $F_{340/380}$ measurements. Every recording experiment followed the same protocol:

Tyrode's—40 s; Tyrode's + DHPG—40 s; Tyrode's—60 s; Tyrode's + KCl—20 s; Tyrode's—60 s; Tyrode's + KCl—20 s; Tyrode's—60 s; Tyrode's + VGCC antagonist—60 s; Tyrode's + KCl + VGCC antagonist—20 s; Tyrode's + VGCC antagonist—60 s; Tyrode's + KCl + VGCC antagonist—20 s; Tyrode's + VGCC antagonist—60 s; Tyrode's + KCl + VGCC antagonist—20 s; Tyrode's + VGCC antagonist—60 s; Tyrode's (0 Calcium)—80 s; calibration (see above).

Fura2 was sequentially excited at 340 nm and 380 nm, and the emission monitored at 510 nm. Images were acquired with a cascade 512 EMCCD camera every 2 s using the Metafluor software (Roper Scientific). For each recorded cell, the intracellular calcium concentration $[\text{Ca}^{2+}]_i$ was estimated by measuring the $F_{340/380}$ nm ratio of fluorescence normalized to the

maximal probe fluorescence measured when cells were perfused with the 10 Calcium + ionomycin solution. ω -agatoxin-IVa and ω -conotoxin GVIA were purchased from Smartox, Nitrendipine from Sigma-Aldrich. Resting calcium levels (“baseline”) were measured as the average fluorescence from the first 40 s of each recording. For KCl stimulation, for each cell analyzed we report the results of the mean of two maximal F_{340/380} in two consecutive stimulations. The Drug Response (DR) represents the mean of the two max F_{340/380} in two consecutive stimulations over the mean of the three max F_{340/380} in three consecutive stimulations in the presence of antagonist. The results of the pharmacological stimulations (DHPG, KCl) are reported as fold change over baseline levels. Only cells for which the DHPG stimulation elicited a fold change greater than 1.1 times the baseline levels in F_{340/380} ratio were considered responsive cells.

Immunoprecipitation

Cerebella from WT and *Fmr1*-KO mice were grinded in liquid nitrogen into fine powder and resuspended in 5 v/w with PBS containing 1% Igepal. Samples were cleared with 15 μ l of naked Dynabeads A (Thermofisher) for 30 min at 4°C on a rotating wheel. During this time, 30 μ l of Dynabeads A were incubated with anti-FMRP primary antibody for 1 h at room temperature on a rotating wheel, with 100 μ g of tRNA, ssDNA and BSA. The “pre-clear” beads were then removed and samples were centrifuged for 10 min at 14,000 rpm at 4°C. Supernatants were incubated with antibody-coated beads overnight at 4°C on a rotating wheel. Beads were washed three times with PBS containing 0.1% Igepal and incubated for 15 min at 55°C with 100 mM dithiothreitol and 2× Laemmli sample buffer. Eluted proteins were then resolved on 4%–12% gradient SDS-PAGE using MOPS buffer (Invitrogen).

Biotinylation

Primary neurons plated at the density of 200,000 cells per well were used for biotinylation experiments at DIV 15. Neurons were washed twice with PBS and incubated with EZLink Sulfo-NHS-LC-Biotine (0.3 mg/ml in PBS, Thermo Scientific) for 10 min at 4°C. After a quick wash with PBS, unbound biotin molecules were quenched with 50 mM NH₄Cl for 5 min. After two washes with ice-cold PBS, proteins were extracted using lysis buffer containing 10 mM Tris-HCl pH 7.5, 10 mM EDTA, 150 mM NaCl, 1% Triton X-100, 0.1% SDS and 1% mammalian protease inhibitor cocktail (Sigma-Aldrich). Two-hundred microgram of proteins from each condition were incubated overnight at 4°C with streptavidin-conjugated beads (Sigma-Aldrich). Beads were then washed three times with lysis buffer and resuspended in Laemmli buffer. Proteins were separated in 7% acrylamide-bis-acrylamide gel. Primary antibodies anti β -Actin (Sigma, #A5441; 1/1,000), anti-Ca_v2.1 (Alomone Labs, #ACC-001; 1/1,000) and anti β 3-tubulin (Synaptic Systems, #302302; 1/1,000) were used.

RNA extraction and RT-qPCR were performed as previously described (Maurin et al., 2018a). The sequences of the primers used in this study are provided in Table 1.

TABLE 1 | Sequences of the primers used in this study.

	Forward	Reverse
Cacna1a	GAGTATGACCCCTGCTGCCGT	TGCAAGCAACCCCTATGAGGA
Cacna1b	TGCCTTCTCGAGCTTCATGG	CGCTTGATGGCTTGAGGGGG
Cacna1c	GAACCATATCCTAGGCAATGCAG	AAGAGCCCTTGTCAGGAAA
Cacna1e	TGAGTTGTCGTGCTGGG	GAGGGACATCTTGCAGGAG
c-Kit	GGAGTGTAAAGGCCCTCAACG	TGGGCCTCGATTGCTCTT
Klf4	CAGGATTCATCCCCATCCG	TGGCATGAGCTCTTGATAATGGA
Gfap	CAGATCCGAGGGGGCAA	TGAGCCTGTATTGGGACAAC
Dlg4	GGCGGAGAGGAATTGTCC	AGAATTGGCCTTGAGGGAGGA
Tbp	AGGCCAGACCCCACAAC	GGGTGGTGCTGGCAA

Sequences are presented from 5' to 3' end.

Polyribosome Fractionation

Samples from polyribosome fractionation were described previously (Maurin et al., 2018a). Polyribosome fractionation was performed as described previously (Bechara et al., 2009) on 20%–50% (w/w) continuous sucrose gradients. Fractions were separated on a BR-188 Density Gradient Fractionation System (Brandel). Fold changes in *Cacna1a* mRNA levels between WT and *Fmr1*-KO were assessed by RT-qPCR and were calculated for individual fractions 6–14 according to the formula 2^{-ddC_p} where ddC_p is (C_p *Pde2a* KO fraction_x – C_p *Gapdh* KO fraction_x) – (C_p *Pde2a* WT fraction_x – C_p *Gapdh* WT fraction_x). Results from fractions 6 to 8 (light), 9 to 11 (medium) and 12 to 14 (heavy) were pooled and analyzed together.

Protein Extraction and Western Blot Analysis

Cells and tissues extracts were processed as described previously (Maurin et al., 2018a). Primary antibodies anti β -Actin (Sigma, clone AC-74; 1/1,000) and anti-Ca_v2.1 (Alomone Labs, #ACC-001; 1/1,000) were incubated overnight at 4°C in PBS 0.05%.

Immunocytochemistry on Primary Neurons

Primary neurons grown on glass coverslips were washed three times with PBS at room-temperature and then fixed using 4% Paraformaldehyde (PFA) in PBS for 10 min at room temperature. After rinsing briefly with PBS, free aldehydes were blocked with 50 mM NH₄Cl in PBS for 5 min. Then, a saturation step was performed with PBS containing 10% Fetal Bovine Serum and 0.1% Triton X-100 for at least 20 min. Neurons were incubated with antibodies diluted in PBS containing 10% Fetal Bovine Serum and 0.1% Triton X-100 in a humidified chamber overnight at 4°C. After three PBS washes, neurons were incubated with secondary antibodies for 1 h at RT. After three PBS washes cells were incubated for 3 min in a PBS solution containing DAPI (10 μ g/ml). The glass coverslips were finally washed once with ddH₂O and mounted (Dako Fluorescent Mounting Medium) on glass slides and stored in the dark at 4°C. The polyclonal anti-Ca_v2.1 (Alomone Labs, #ACC-001) antibody was used at a dilution of 1/50. The 1C3 antibody against FMRP was used at a dilution of 1/200 (Castets et al., 2005). Colocalization quantifications of FMRP and Ca_v2.1 in one confocal plan (average of three scans) were carried out using the JACoP plugin for ImageJ (Bolte and Cordelier, 2006). Cells were examined on a TCS SP5 confocal microscope (Leica).

Cell Shape Analysis

We designed an ImageJ (Schneider et al., 2012) dedicated macro to analyze simultaneously the cell shape and the Fura2 fluorescence ratio variations (in time) obtained by sequential excitation at 340 and 380 nm. First, kinetics images of 340 and 380 nm excitation were stacked together and any lateral drift was corrected using the StackReg plugin (Thévenaz et al., 1998). A mask and a list of ROIs for each cell was obtained on the last 340 nm image after a filtering (recursive TopHat followed by an unsharp mask) and a Huang intensity thresholding. Then the 340 and 380 nm images were separated in two stacks and their $F_{340/380}$ ratio calculated after a background measurement and subtraction in each image of the stack. The ROIs were then used on the 340/380 stack to get individual cell measurements of shape parameters (Aspect Ratio, Roundness, Area, Solidity) and $F_{340/380}$ fluorescence ratios during time.

Multivariate Analysis of the Cell Morphology Parameters

Baseline and KCl data were extracted and normalized to the maximal calcium value obtained for each cell with the 10 mM Calcium + ionomycin solution and combined to cell morphology parameters extracted from the images. Both cell morphology, normalized baseline and KCl data were then used for unsupervised analysis. Data were first log10 transformed, then mean-centered and scaled. Then, dimension reduction was performed using Barnes-Hut implementation of t-Distributed Stochastic Neighbor Embedding (tSNE), with perplexity parameter set to 40. K-means clustering was performed on the two-dimension tSNE projection and the optimal number of clusters was determined using the Gap statistic. Significance of the differences between continuous variable distributions was assessed using either Mann-Whitney or Kruskal-Wallis rank sum tests as appropriate. All analyses and graphical representations were performed using the R statistical package or Prism Software 6-2 version (GraphPad Software, Inc., San Diego, CA, USA).

Statistics

The Kolmogorov-Smirnov test was used to assess the normality of the distribution of the datasets. To compare non-normally distributed data, two non-parametric tests were used: the Mann-Whitney test was applied to data of two unpaired samples, while the Kruskal-Wallis test was used to examine the significance of four unpaired groups. Data are expressed as mean \pm SEM, and the *P* values (or adjusted *P* values) < 0.05 were considered statistically significant. RT-qPCR analysis of mRNA expression were analyzed using ANOVA TWO WAY with Sidak's multiple comparisons *post hoc* test. The statistical analysis was performed using Prism Software 6-2 version (GraphPad Software, Inc.).

Animal Experiments

The experiments were performed following the ARRIVE (Animals in Research: reporting *in vivo* Experiments) guidelines (Kilkenny et al., 2010). Animal care was conducted in accordance with the European Community Directive

2010/63/EU. The experiments were approved by the local ethics committee (Comité d'Ethique en Expérimentation Animale CIEPAL-AZUR N. 00788.01; APAFIS#4985-2016032314169426 v4APAFIS#8100-2016112217148206 v3).

RESULTS

Calcium Homeostasis Is Impaired in *Fmr1*-KO Cells

We investigated calcium homeostasis using Fura2 ratiometric imaging in primary neuron cultures derived from the cortex of E14.5 WT and *Fmr1*-KO embryos. According to our immunocytochemistry results, these cultures are enriched in neurons and have limited mature astrocyte content (less than 10% of cells) that are mostly present in cell aggregates (**Supplementary Figures S1A,B**). Therefore, these regions were avoided in subsequent calcium recordings. RT-qPCR analysis of the expression of GFAP and PSD95 markers showed that the absence of FMRP does not affect the relative amounts of astrocytes and neurons in *Fmr1*-KO cultures compared to WT (**Supplementary Figure S1C**). We systematically applied a series of consecutive drug treatments followed by a calibration step that allowed us to quantify the minimum and maximum fluorescence of Fura2 in each analyzed cell. We used the normalized fluorescence ratio ($[F_{340/380}]/\max[F_{340/380}]$) as an indirect quantification of the actual intracellular calcium concentration. By this imaging approach we investigated the functionality of several key parameters of calcium homeostasis in neurons in the presence or in the absence of FMRP.

Cellular Analysis

Our imaging data clearly show the heterogeneity of the neuronal types present in primary neuron cultures (**Figures 1A–C**). Cells differ in size, shape, resting intracellular calcium levels and maximum calcium entry upon KCl stimulation. We wondered whether the absence of FMRP could have different impacts on calcium homeostasis in different cell types. The Fura2 fluorescence ratio and the shape analysis of the ROIs were simultaneously quantified by an ImageJ lab-made macro giving the shape descriptors for each ROI (area, roundness, solidity, circularity). Roundness reflects how circular a ROI is, while solidity and circularity indicate how soft (high scores) or rough (low scores) are the contours of the region. We then performed an unsupervised multivariate analysis (**Supplementary Figures S2A,B**) to group cells according to their size, shape and calcium homeostasis parameters (baseline levels, maximum calcium levels upon KCl stimulation) identifying four distinct and homogeneous groups of cells (**Supplementary Figures S2C–H**). Representative images of ROIs detected in each cluster are shown in **Supplementary Figure S3**. Cells in group 1 and 3 differ in size and in the complexity of their contour, have a higher resting calcium concentration and high calcium entry upon KCl stimulation. Group 2 cells are small with rough contours and display a limited calcium entry following KCl stimulation, characteristics that suggest an astrocytic lineage. Group 4 ROI are small elongated objects that mostly correspond

to neurites (**Supplementary Figure S3**). We considered the repartition of WT and *Fmr1*-KO cells in these clusters and our results indicate a homogeneous distribution of cells from the two genotypes in all clusters (**Supplementary Figures S2I-L**). The number of DHPG-responding cells was also similar in both genotypes (**Supplementary Figure S4**). We focused our analysis on cells belonging to group 1 and 3 which according to this analysis, have neuron characteristics. These cells were subsequently analyzed together. The steady state intracellular Ca²⁺ concentration, measured prior to any pharmacological treatment during the first 40 s of the recording, is elevated in the absence of FMRP (Mann-Whitney test, $P < 0.0001$; **Figure 1D**).

The metabotropic Glutamate receptor pathway has been described to be deregulated in FXS (Huber et al., 2002; Bear et al., 2004). The activation of this pathway with pharmacological agonists like DHPG triggers calcium release from internal stores through IP3 receptors as a consequence of the activation of the Phospholipase C and IP3 second messenger pathway. The calcium ion release from intracellular stores in response to DHPG is variable and not significantly different in the absence of FMRP compared to WT cells at the population level (Mann-Whitney test, $P = 0.9963$, not significant; **Figure 1E**).

We next induced cell depolarization by applying a 50 mM KCl solution onto the cultures, as in these conditions VGCCs are the main determinants of calcium entry in neurons (Mao et al., 2001). VGCCs respond to cell depolarization, upon which they open and allow calcium ion entry through their pore-forming subunit. We thus analyzed for each cell the fold change in $F_{340/380}$ induced by KCl over baseline levels. Our results show that calcium entry through voltage-dependent plasma membrane channels upon KCl-induced neuron depolarization is slightly decreased in *Fmr1*-KO neurons (Mann-Whitney test, $P < 0.0001$; **Figure 1F**). Last, we observed that after the KCl stimulations *Fmr1*-KO neurons had significantly higher mean $F_{340/380}$ ratio over the 40 s that followed the KCl stimulation compared to WT, suggesting a deregulated return to baseline levels in the absence of FMRP (Mann-Whitney test, $P < 0.005$; **Figure 1G**).

Highly specific pharmacological blockers have been identified for all these VGCC subfamilies (Zamponi et al., 2015). For instance, we used specific pharmacological blockers of VGCCs: dihydropyridines, such as nitrendipine, block L-type VGCCs (Peterson et al., 1996) by binding to transmembrane domains of the $\alpha 1$ subunit hence affecting the gating mechanism of the L-type VGCCs. ω -Conotoxin-GVIA (Conotoxin) blocks N-type VGCCs (Ichida et al., 2005) by interacting with the channel pore. ω -Agatoxin IVa (Agatoxin) inhibits P/Q-type VGCCs (Adams et al., 1993) by binding to two extracellular loops of the $\alpha 1$ subunit that are close to the sensor domain of the P/Q-channel. Thus, we used some of these blockers in order to further investigate the molecular determinants of such calcium homeostasis deregulations. Within each neuron expressing or not FMRP, we measured the DR as the ratio of the mean of the maximal depolarization-induced Ca²⁺ entry in the presence of a VGCC-specific antagonist on the mean calcium entry in the absence of a

VGCC-specific antagonist. All the antagonists tested significantly reduced calcium ion entry upon KCl stimulation. Indeed, each antagonist treatment produced a DR that was statistically different from 1, the DR value expected for a drug having no effect (one sample *t*-test, $P < 0.0001$; **Figures 2A–C**). Nevertheless, Nitrendipine (1 μ M) reduced KCl-triggered calcium ion entry similarly in WT and *Fmr1*-KO cells (Mann Whitney test, n.s.: $P = 0.2968$; **Figure 2A**). The ω -Conotoxin-GVIA (Conotoxin; 1 μ M) was more efficient in *Fmr1*-KO cells (Mann Whitney test, $P < 0.0001$; **Figure 2B**). On the contrary, the ω -Agatoxin IVa (Agatoxin; 100 nM) had a fainter effect in *Fmr1*-KO than in WT cells (Mann Whitney test, $P < 0.0001$; **Figure 2C**). These findings strongly suggest that N- and P/Q-type channels are deregulated in *Fmr1*-KO neurons. These results are recapitulated in **Table 2**.

Cacna1a Expression Is Altered in *Fmr1*-KO Primary Neurons

The pore forming unit of P/Q-type VGCC is encoded by the *Cacna1a* gene, whose mRNA is a target of FMRP (Darnell et al., 2011), in particular also during early brain development (at Post-Natal Day 13, PND 13; Maurin et al., 2018a). We therefore investigated how FMRP regulates *Cacna1a* expression in *Fmr1*-KO primary cultured neurons and in cortical extracts of *Fmr1*-KO mouse. We precisely characterized the time course of various $\alpha 1$ gene expression in WT and *Fmr1*-KO primary neurons by RT-qPCR. *Cacna1a* is the most upregulated $\alpha 1$ gene of the Ca_v2 family between DIV 14 and 21, and its expression is reduced in *Fmr1*-KO neurons (**Figures 3A–D**) at DIV 21 compared to WT cells. We therefore investigated whether FMRP modulates *Cacna1a* mRNA half-life by measuring *Cacna1a* stability together with control RNAs in primary neurons treated with the polymerase II inhibitor Actinomycin D. We observed that, consistent with a previous report (Sharova et al., 2009), Actinomycin D treatment triggers a strong decrease in *Klf4* transcript expression (**Figure 3E**) which is not due to cell toxicity, as we could show that in the same conditions *c-Kit* expression is stable over time (**Figure 3F**). In these conditions, *Cacna1a* expression is affected to a similar extent in WT and *Fmr1*-KO neurons (**Figure 3G**), excluding a role of FMRP in regulating *Cacna1a* mRNA stability. We concluded that the decreased expression levels of *Cacna1a* mRNA in *Fmr1*-KO cells do not depend on the half-life of this mRNA in the absence of FMRP but it is likely due to a decreased transcription level. Thus, we analyzed *Cacna1a* translation in the cortex of WT and *Fmr1*-KO mice by quantifying *Cacna1a* mRNA levels in different fractions of polyribosome preparations obtained from WT and *Fmr1*-KO PND 13 mouse cortex. Our results show that *Cacna1a* mRNA polyribosome association is increased in the light and medium polyribosome fractions, which argues in favor of an increased translation of this mRNA in the absence of FMRP (**Figure 3H**).

Western blot analysis of total Ca_v2.1 protein levels in DIV 17–21 primary neurons showed no statistically significant difference between WT and *Fmr1*-KO cells (Mann-Whitney test, $P = 0.7$, not significant; **Figures 4A,B**). We also analyzed Ca_v2.1 expression at the plasma membrane of *Fmr1*-KO and

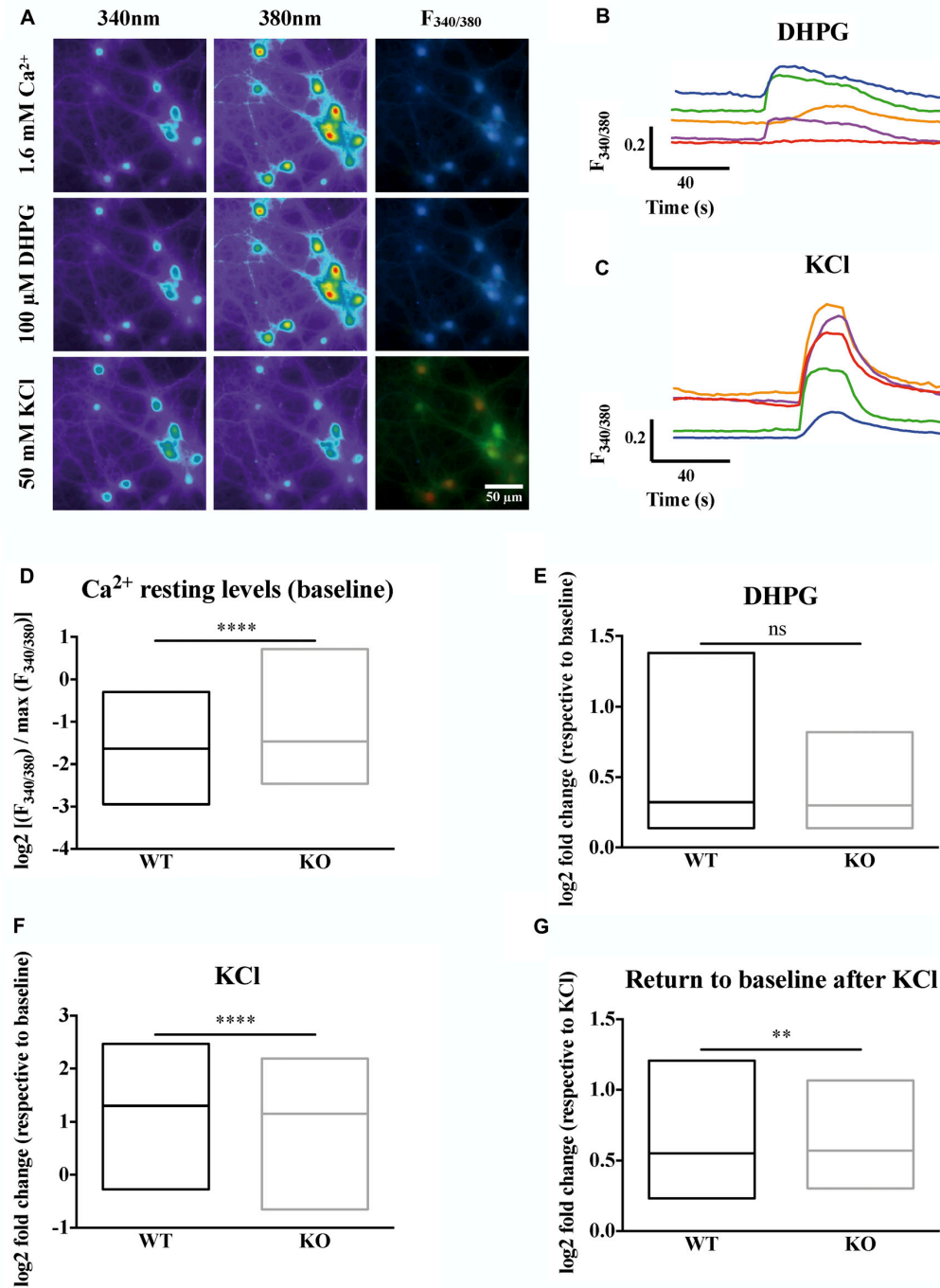


FIGURE 1 | Calcium homeostasis is deregulated in Fragile X mental retardation 1-knockout (*Fmr1*-KO) neurons. **(A)** Profiles of the ratiometric calcium imaging response. Left panels show the emission of Fura2 at 340 nm. Middle panels show the emission of Fura2 at 380 nm. Right panels show the 340 nm/380 nm ratio of fluorescence ($F_{340/380}$). Upper panels show the emission of Fura2 upon 1.6 mM Ca^{2+} perfusion. Middle panels show the emission of Fura2 upon 100 μM DiHydroxyPhenylGlycine (DHPG) perfusion. Lower panels show the emission of Fura2 upon 50 mM KCl perfusion. The scale bar of each panel is 50 μm . **(B)** Sample traces of Fura2 recording upon metabotropic glutamate receptor stimulation with DHPG (100 μM) or **(C)** depolarization with KCl (50 mM) in wild-type (WT) cells. For each cell recorded, the Fura2 fluorescence at each time was normalized to the maximum Fura2 fluorescence ratio observed in the presence of a solution containing 10 mM CaCl_2 and ionomycin (5 μM). The mean stabilized $F_{340/380}$ ratio of Fura2 fluorescence during the first 40 s of recording in the absence of any stimulation is represented in **(D)**. The \log_2 fold change in normalized $F_{340/380}$ after 100 μM DHPG stimulation over baseline normalized ratio is presented in **(E)**. The \log_2 fold change in normalized $F_{340/380}$ after 50 mM KCl stimulation over baseline normalized ratio is presented in **(F)**. The return to baseline following a KCl stimulation is shown for WT and *Fmr1*-KO neurons **(G)**. Mann-Whitney test: **** $P < 0.0001$; ** $P < 0.005$; ns: $P = 0.9963$, not significant. WTn = 697; KOn = 744. These results are summarized in **Table 2**.

TABLE 2 | Results summary.

	Mean \pm SEM WT (<i>n</i>)	Mean \pm SEM KO (<i>n</i>)	P value	P value significance
Figure 1D resting	-1.636 ± 0.016 (697)	-1.459 ± 0.0141 (744)	<0.0001	****
Figure 1E DHPG	0.3221 ± 0.0150 (222)	0.2989 ± 0.0105 (211)	0.9963	ns
Figure 1F KCl	1.297 ± 0.0142 (697)	1.154 ± 0.0147 (744)	<0.0001	****
Figure 1G After KCl	0.5509 ± 0.0054 (697)	0.5709 ± 0.0051 (744)	0.0038	**
Figure 2A Nitrendipine response	0.3497 ± 0.0215 (121)	0.3273 ± 0.0196 (138)	0.2968	ns
Figure 2B Conotoxin response	0.1088 ± 0.0087 (222)	0.1681 ± 0.0090 (219)	<0.0001	****
Figure 2C Agatoxin response	0.1478 ± 0.0085 (213)	0.0961 ± 0.0087 (249)	<0.0001	****

Mann-Whitney test was used to assess statistical significance.

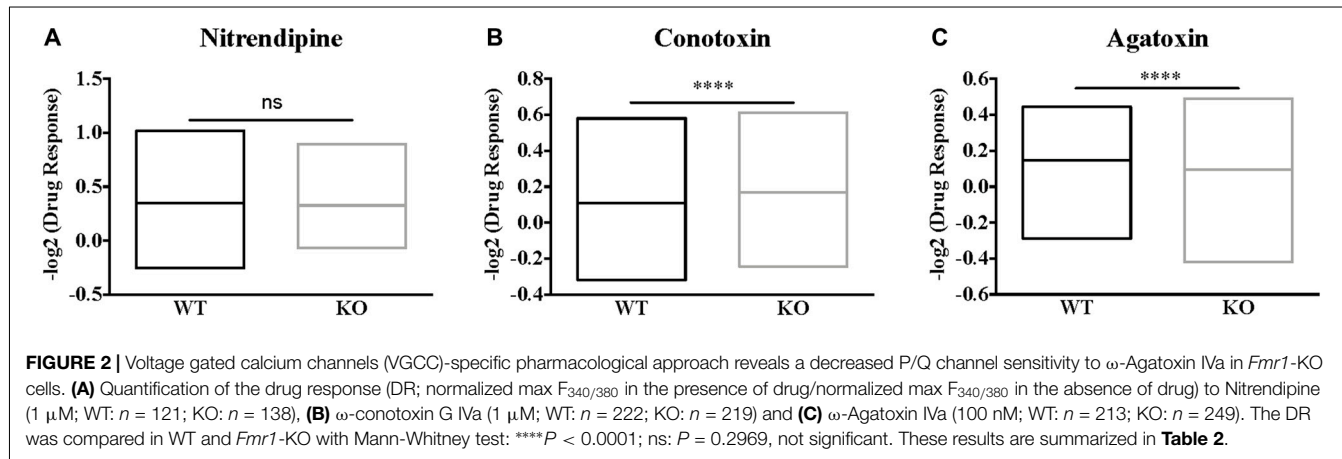


FIGURE 2 | Voltage gated calcium channels (VGCC)-specific pharmacological approach reveals a decreased P/Q channel sensitivity to ω -Agatoxin IVa in *Fmr1*-KO cells. **(A)** Quantification of the drug response (DR; normalized max $F_{340/380}$ in the presence of drug/normalized max $F_{340/380}$ in the absence of drug) to Nitrendipine (1 μM ; WT: *n* = 121; KO: *n* = 138), **(B)** ω -conotoxin G IVa (1 μM ; WT: *n* = 222; KO: *n* = 219) and **(C)** ω -Agatoxin IVa (100 nM; WT: *n* = 213; KO: *n* = 249). The DR was compared in WT and *Fmr1*-KO with Mann-Whitney test: **** P < 0.0001; ns: P = 0.2969, not significant. These results are summarized in **Table 2**.

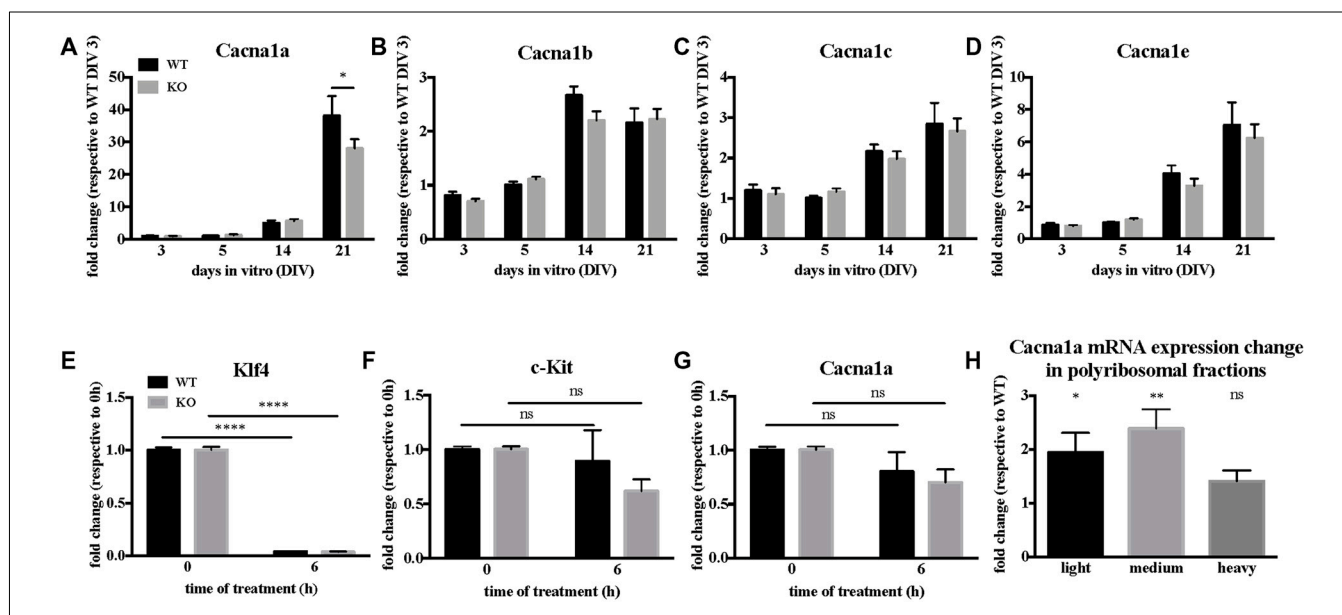


FIGURE 3 | *Cacna1a* expression is deregulated in the absence of Fragile X Mental Retardation Protein (FMRP). **(A)** In vitro time-course of *Cacna1a*, **(B)** *Cacna1b*, **(C)** *Cacna1c* and **(D)** *Cacna1e* mRNA expression. Results are presented as the mean \pm SEM, ANOVA two way Sidak's multiple comparisons post hoc test: * P < 0.05. Quantification of *Klf4* **(E)**, *c-Kit* **(F)** and *Cacna1a* **(G)** mRNA levels upon actinomycin D treatment in Day-In-Vitro (DIV) 19–20 neuronal cultures. The mRNA levels of *c-Kit* as well as those of *Klf4* are used for comparison according to stability data from Sharova et al. (2009). Results are presented as the mean \pm SEM, ANOVA two way with Sidak's multiple comparisons test: **** P < 0.0001; ns, not significant (*c-Kit*: $P_{\text{WT}} = 0.8386$; $P_{\text{KO}} = 0.0694$. *Cacna1a*: $P_{\text{WT}} = 0.4902$; $P_{\text{KO}} = 0.1071$). **(H)** Quantification of *Cacna1a* mRNA relative expression levels (*Fmr1*-KO/WT) in light, medium and heavy polyribosomal fractions, respectively. Results are presented as the mean \pm SEM, One-sample t-test: * P < 0.05; ** P < 0.001; ns: P = 0.0717, not significant.

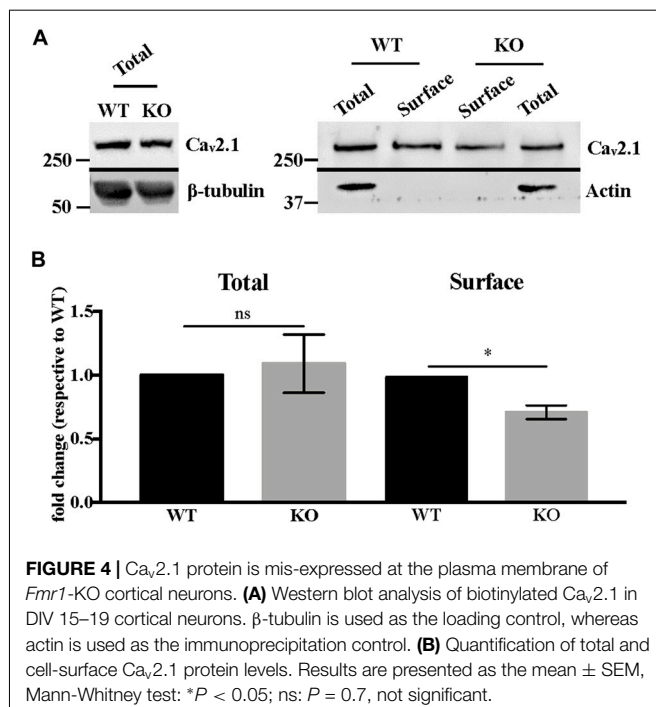


FIGURE 4 | $\text{Ca}_v2.1$ protein is mis-expressed at the plasma membrane of *Fmr1*-KO cortical neurons. **(A)** Western blot analysis of biotinylation assay of $\text{Ca}_v2.1$ in DIV 15–19 cortical neurons. β -tubulin is used as the loading control, whereas actin is used as the immunoprecipitation control. **(B)** Quantification of total and cell-surface $\text{Ca}_v2.1$ protein levels. Results are presented as the mean \pm SEM, Mann-Whitney test: *P < 0.05; ns: P = 0.7, not significant.

WT primary neurons by performing biotinylation assay. Our results show that $\text{Ca}_v2.1$ protein is less expressed at the cell surface of *Fmr1*-KO neurons (Mann-Whitney test, P < 0.05; **Figures 4A,B**).

Since it was reported that, when overexpressed, FMRP directly interacts with both $\text{Ca}_v2.1$ and $\text{Ca}_v2.2$ (Ferron et al., 2014), we assessed whether $\text{Ca}_v2.1$ and FMRP are colocalized in cortical neurons. Using double immunofluorescent staining and confocal microscopy, we observed and quantified their colocalization using Mander's coefficients both in soma and in neurites (**Figures 5A–C**). These findings were also confirmed by biochemistry experiments performed on cerebellar extracts from PND 13 mice in which we showed that endogenous $\text{Ca}_v2.1$ co-immunoprecipitates with FMRP (**Figure 5D**).

DISCUSSION

We and others have shown that among the FMRP mRNA targets many encode ion channels, sensors of intracellular ion concentration and other regulators of ion homeostasis (Brown et al., 2001; Darnell et al., 2011; Maurin et al., 2018a). Nonetheless, the direct interaction of FMRP with ion channels has been reported previously (Brown et al., 2010; Ferron et al., 2014; Myrick et al., 2015; Ferron, 2016). Also, it is not surprising that deregulations of expression levels as well as activities of ion channels have been shown in *Fmr1*-KO neurons (Chen et al., 2003; Meredith et al., 2007; Brown et al., 2010; Deng et al., 2013; Ferron et al., 2014; Zhang et al., 2014; Deng and Klyachko, 2016), some directly implicating VGCC deregulation in FXS (Chen et al., 2003; Meredith et al., 2007; Deng et al., 2013; Ferron et al., 2014; Zhang et al., 2014). Even if some of the conclusions of various studies were not completely convergent (Meredith et al.,

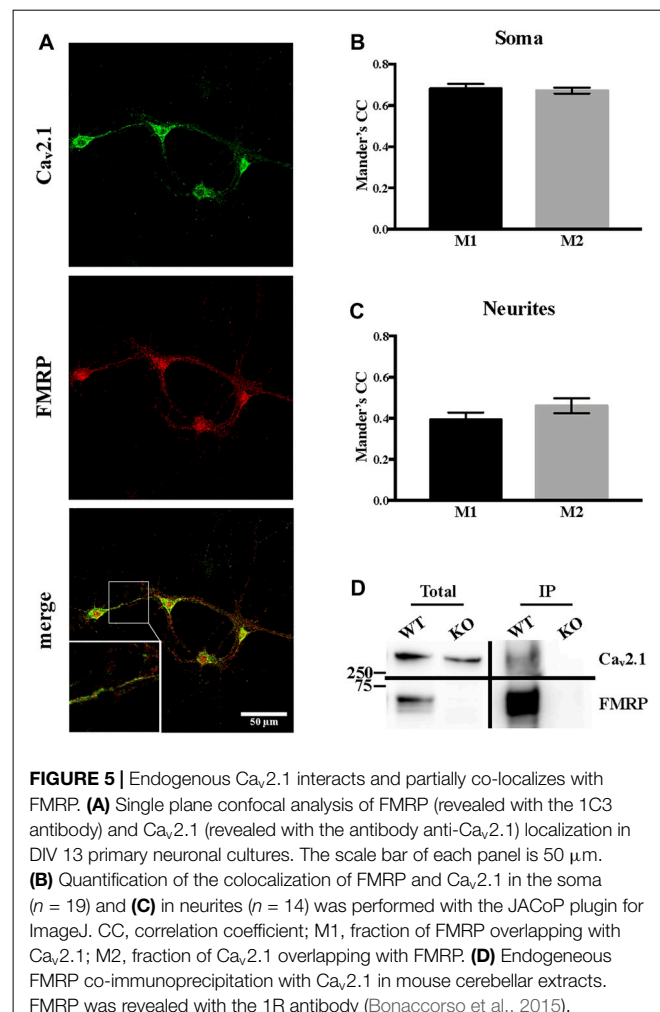


FIGURE 5 | Endogenous $\text{Ca}_v2.1$ interacts and partially co-localizes with FMRP. **(A)** Single plane confocal analysis of FMRP (revealed with the 1C3 antibody) and $\text{Ca}_v2.1$ (revealed with the antibody anti- $\text{Ca}_v2.1$) localization in DIV 13 primary neuronal cultures. The scale bar of each panel is 50 μm . **(B)** Quantification of the colocalization of FMRP and $\text{Ca}_v2.1$ in the soma (n = 19) and **(C)** in neurites (n = 14) was performed with the JACoP plugin for ImageJ. CC, correlation coefficient; M1, fraction of FMRP overlapping with $\text{Ca}_v2.1$; M2, fraction of $\text{Ca}_v2.1$ overlapping with FMRP. **(D)** Endogenous FMRP co-immunoprecipitation with $\text{Ca}_v2.1$ in mouse cerebellar extracts. FMRP was revealed with the 1R antibody (Bonaccorso et al., 2015).

2007; Ferron et al., 2014; Zhang et al., 2014), collectively these works suggest that the Ca^{2+} signaling-associated pathways may be involved in the physiopathology of FXS. For this reason, we decided to study calcium homeostasis in live, cultured neurons in the presence and in the absence of FMRP, using calcium imaging.

FMRP Regulates VGCC Expression and Function

VGCCs play key roles in neurons, notably by regulating membrane excitability, neurotransmitter release and gene expression modulation (Simms and Zamponi, 2014). Alterations in the plasma membrane expression of these channels lead to pathological phenotypes, ranging from ataxia, ID, ASD and epilepsy (Yue et al., 1997; Damaj et al., 2015). Thus, to gain further insight in the Ca^{2+} pathway-associated molecular pathology in FXS, we carried out a pharmacological approach using VGCC-specific antagonists in our cellular model. We showed that both N- and P/Q-type VGCC inhibition differently affected KCl-mediated entry in WT and *Fmr1*-KO neurons. Indeed, blocking N-type VGCCs was more efficient in *Fmr1*-KO than in WT neurons and conversely, P/Q-type inhibition had less effect in *Fmr1*-KO neurons, suggesting that both $\text{Ca}_v2.2$

and $\text{Ca}_v2.1$ activities are deregulated in the absence of FMRP. Interestingly, *Cacna1a* mRNA is a target of FMRP in various brain regions (Maurin et al., 2018a) and here we show that:

1. The membrane levels of $\text{Ca}_v2.1$ channels are reduced in *Fmr1*-KO neurons, consistent with the reduced sensitivity to P/Q-type VGCC inhibition with Agatoxin. Since the intracellular levels of $\text{Ca}_v2.1$ do not appear to be altered (**Figure 4**), we conclude that $\text{Ca}_v2.1$ direct interaction with FMRP could play a role in its function/localization in the absence of the partner. Also, the altered actin cytoskeleton organization described in different FXS cell lines (Castets et al., 2005; Nolze et al., 2013; Abekhoush and Bardoni, 2014; Abekhoush et al., 2017) may explain the reduced membrane expression of $\text{Ca}_v2.1$, since cytoskeleton is the route for the correct subcellular localization of mRNAs (Bramham and Wells, 2007). It is worth reminding that altered sublocalization of membrane proteins (encoded by mRNA targets of FMRP) have been already described, such as diacylglycerol lipase- α (DGL- α ; Jung et al., 2012), Homer 1 (Giuffrida et al., 2005; Aloisi et al., 2017) and Kv4.2, (Gross et al., 2011). Similarly, $\text{Ca}_v2.1$ could be one of the deregulated elements. Interestingly, FMRP binds the mRNAs of other of its interacting proteins such as FMRP, CYFIP2, FXR1, $\text{Ca}_v2.2$ (Darnell et al., 2011; Maurin et al., 2018a), suggesting a tight regulation of a FMRP-containing complex in a FMRP-dependent manner. Furthermore, the multiple mRNA targets of FMRP likely generate a network of interactions among FMRP-dependent pathways whose functional consequences are not easily predictable only considering the main role of FMRP as a translational repressor.
2. Even if the level of the mRNA encoding *Cacna1a* is slightly decreased in *Fmr1*-KO neurons at DIV21 (**Figure 3A**), the translational upregulation of this mRNA (as predicted by the increased polyribosome association of $\text{Ca}_v2.1$ mRNA in *Fmr1*-KO brain compared with WT; **Figure 3H**) counterbalances the reduced mRNA level of *Cacna1a* in mature neurons. As in a yin-yang effect, this leads to unaltered total $\text{Ca}_v2.1$ levels. We did not find any FMRP-dependent effect on RNA stability of *Cacna1a*, leading to the conclusion that the reduced level of *Cacna1a* mRNA in *Fmr1*-KO neurons is rather due to an indirect transcriptional deregulation.

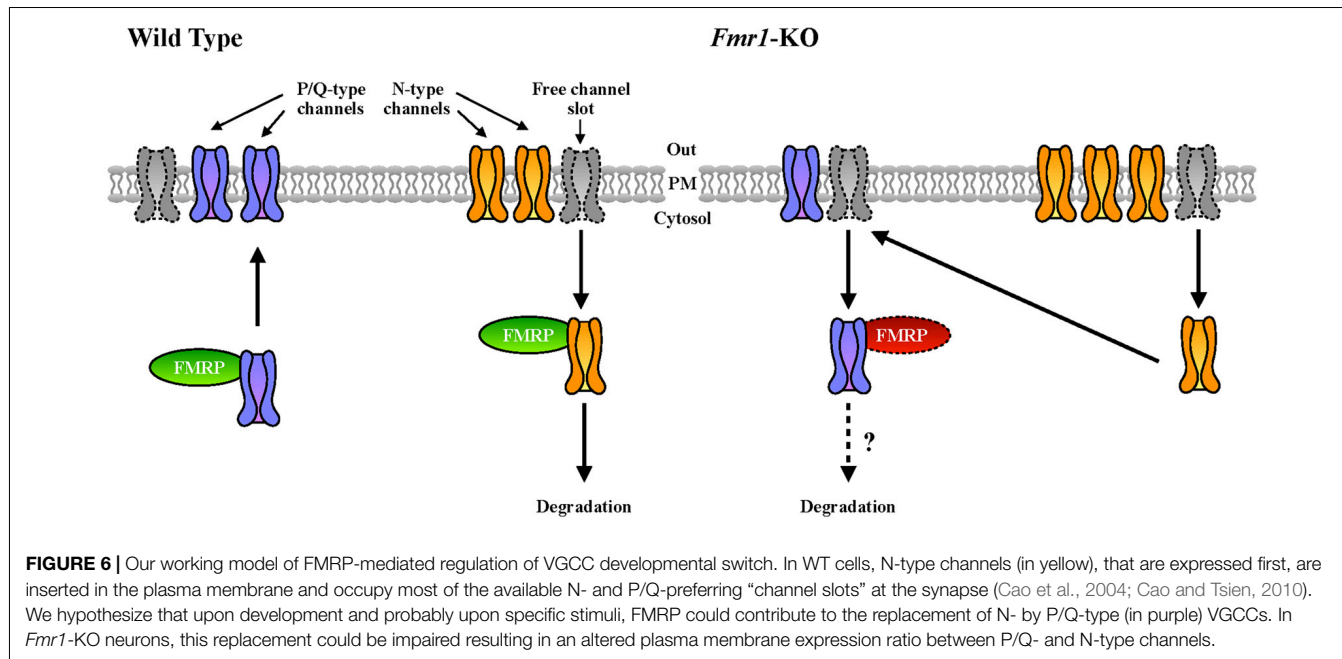
Pre-synaptic Calcium Channels in FXS and ASD

$\text{Ca}_v2.2$ was previously described to be more expressed and present at the plasma membrane of cells in the absence of FMRP (Ferron et al., 2014). This is consistent with the increased sensitivity to conotoxin that we observed in *Fmr1*-KO neurons compared to WT. At the molecular level, this abnormality was explained on the basis of the interaction (by overexpression) between FMRP and both $\text{Ca}_v2.2$ and $\text{Ca}_v2.1$ channels (Ferron et al., 2014). Interestingly, we confirmed here this latter finding by showing that the interaction between the endogenous proteins also occurs in brain (**Figure 5D**). Remarkably, we showed here that in *Fmr1*-KO cells $\text{Ca}_v2.1$

expression deregulation is opposite to the one of $\text{Ca}_v2.2$ (Ferron et al., 2014). As we already stated, FMRP also binds $\text{Ca}_v2.1$ mRNA transcripts, indeed strongly suggesting a central role of FMRP in the regulation of P/Q- and N-type channels relative expression. Interestingly, it was shown that in cultured hippocampal synapses, P/Q- and N-type channels have preferred plasma membrane slots (Cao et al., 2004; Cao and Tsien, 2010) and according to this model, there are exclusive N-type channel slots and P/Q- preferring slots that can be used by N-type channels. For instance, in neurons expressing mutated P/Q-channels that lead to familial hemiplegic migraine type disease, N-type channel currents are increased, either by an increased release probability or rather by an increased N-type expression at the plasma membrane (Cao and Tsien, 2010). Collectively, these findings suggest that some P/Q-type channel slots can actually be occupied by N-type channels upon P/Q-type deficiency. Since FMRP has been shown previously to regulate N-type expression by targeting this channel to the proteasome (Ferron et al., 2014), it is tempting to speculate that FMRP is a molecular adaptor regulating the relative plasma membrane expression of N- and P/Q-type channels. In addition, by regulating the subcellular mRNA localization and/or translation of these channel types, it may also directly modulate their presence at the plasma membrane (**Figure 6**). Future studies will clarify the precise molecular mechanisms underpinning this deregulation in FXS, but it is interesting to underline here that an imbalance between the levels and the activities of N- and P/Q-type channels, could have some impacts on the physiopathology of FXS. Indeed, the differences in N- and P/Q-type inactivation kinetics, their various effects on short term plasticity (Inchauspe et al., 2004) and their different sensitivity to G-protein-coupled receptor-mediated inhibition of neurotransmitter release may have strong impacts on the functioning of synapses (Bourin et al., 1996). Noteworthy, P/Q-type channel activity, but not N-type, mediates GABA release in fast spiking interneurons in rat pre-frontal cortex (Zaitsev et al., 2007). This suggests that abnormal GABA secretion at the temporoammonic branch of the perforant path in the *Fmr1*-KO mouse model (Wahlstrom-Helgren and Klyachko, 2015) could be related to $\text{Ca}_v2.1$ expression defects. Furthermore, it was reported that the maximal inhibition by the GABAB receptor agonist baclofen was greater for EPSCs mediated by N-type channels than for those mediated by P/Q-type channels (Ishikawa et al., 2005). Consequently, in *Fmr1*-KO mice it is likely that the compensation of P/Q- by N-type channels have strong consequences on GABAB inhibition by weakening its effect on presynaptic release, likely leading to network hyper-excitability.

Impairment of Calcium Homeostasis as a New Phenotype of *Fmr1*-KO Neurons. Is It a Novel Biomarker?

Implications of our findings are twofold, biological and clinical. Indeed, the FXS research field actively seeks new treatments and biomarkers to evaluate their efficiency (Castagnola et al., 2017; Maurin et al., 2018b) and, to date, the main cellular



biomarker of cultured *Fmr1*-KO neurons is represented by their abnormal dendritic spine morphology, whose analysis requires exquisite expertise (Khayachi et al., 2018). Conversely, using spectroscopy, calcium concentration measurements can be routinely performed in most laboratory settings, making it an easy and robust marker to monitor drug efficacy. Here, we applied this technique to primary cultured neurons but it will also be possible to perform it in iPS-derived neurons thus obtaining, for the first time, a molecular marker that can be functionally quantified. This can be useful for diagnostic purposes and particularly as a follow-up for specific therapies. Indeed, the search for specific and easily measurable biomarkers for FXS as well as for ASD is urgent. For instance, since 2009 one of the conclusions of the Outcome Measures Working Groups for Fragile X was “...research on biomarkers for detecting treatment response in FXS was in its infancy, but this was an area of utmost importance” (Berry-Kravis et al., 2013). More recently, the accurate analysis of 22 double-blind controlled clinical trials in FXS finalized between 2008 and 2015 led to the conclusion that the readouts employed to evaluate the outcome of treatments were in general of moderate/poor quality (Budimirovic et al., 2017). Last but not least, this cellular biomarker could be used as the readout for screenings of small-molecule (singular) libraries (Bardoni et al., 2017) to define new treatments opportunities for FXS.

Study Limitations

There are several limitations of this study that one may consider:

1. Our ImageJ macro analysis resulted in the identification of four types of cells, which is clearly underestimating the complexity of the cell population. We nevertheless trust that this approach will be useful to identify a cell type of

interest in the future, associating morphological parameters with molecular/physiological determinants; interestingly, Ota et al. (2018) very recently published a study highlighting the benefits of identifying cells according to their shape;

2. In agreement with the expression levels of $\text{Ca}_{v}2.1$, we focused our study on mature neuron cultures. This VGCC deregulation may not be observed in different culture settings;
3. The polyribosome fractionation experiments were performed on cortex extracts from PND 13 mice, preventing the identification of actively translating ribosomes through pharmacological inhibition. Therefore, we can only speculate that the increased presence of *Cacna1a* mRNA in light and medium fractions reflects an increased translation of this mRNA in *Fmr1*-KO mice;
4. The working model describing the putative role of FMRP in the regulation of N- and P/Q-type VGCCs at the plasma membrane (**Figure 6**) awaits a molecular mechanism and therefore is speculative. It nevertheless may be considered as a starting point for future analyses.

AUTHOR CONTRIBUTIONS

TM, FD and AF designed the experiments. SC, SD, AF, MB, MJ, MG and TM performed the experiments. FB designed and wrote the macro in ImageJ. AP performed the unsupervised multivariate analysis. TM, SC, AF, AP, MM, SM and BB analyzed the data. TM, SC and BB wrote the manuscript.

FUNDING

This study was supported by Université Côte d’Azur (UCA); Institut National de la Santé et de la Recherche Médicale

(INSERM); Centre National de la Recherche Scientifique (CNRS); Agence Nationale de la Recherche: ANR-12-BSV4-0020, ANR-12-SVSE8-0022 and Fondation pour la Recherche Médicale (FRM) DEQ20140329490 to BB; Investments for the Future, through the LABEX SIGNALIFE program: #ANR-11-LABX-0028-013, Fondation Jérôme Lejeune and ANR-15-CE16-0015 to BB and SM; FRM-ING20140129004 to BB and TM; FRAXA Foundation to TM. Bioinformatics analysis were performed at the UCAGenomiX platform of the IPMC, a member of the national infrastructure “France Génomique” (ANR-10-Infra-01). SC is recipient of an international Ph.D. fellowship from the “LABEX SIGNALIFE program.”

ACKNOWLEDGMENTS

The authors are grateful to Prof. M. Lazdunski, M. Doghman and M. Drozd for discussion.

SUPPLEMENTARY MATERIAL

The Supplementary Material for this article can be found online at: <https://www.frontiersin.org/articles/10.3389/fnmol.2018.00342/full#supplementary-material>

FIGURE S1 | Cortical primary neuronal cultures show a negligible level of astrocytic growth. **(A)** Fluorescent analysis showing the level of GFAP (in green) in Day-In-Vitro (DIV) 12 WT primary neuronal cultures compared to the total number of cells (DAPI staining in blue for nuclei). **(B)** Percentage of GFAP-positive cells (20 imaged regions; $n = 261$ DAPI-positive cells; $n = 23$ GFAP-positive cells).

REFERENCES

- Abekhoush, S., and Bardoni, B. (2014). CYFIP family proteins between autism and intellectual disability: links with Fragile X syndrome. *Front. Cell. Neurosci.* 8:81. doi: 10.3389/fncel.2014.00081
- Abekhoush, S., Sahin, H. B., Grossi, M., Zongaro, S., Maurin, T., Madrigal, I., et al. (2017). New insights into the regulatory function of CYFIP1 in the context of WAVE- and FMRP-containing complexes. *Dis. Model. Mech.* 10, 463–474. doi: 10.1242/dmm.025809
- Achuta, V. S., Moykkynen, T., Peteri, U. K., Turconi, G., Rivera, C., Keinanen, K., et al. (2018). Functional changes of AMPA responses in human induced pluripotent stem cell-derived neural progenitors in Fragile X syndrome. *Sci. Signal.* 11:eaan8784. doi: 10.1126/scisignal.aan8784
- Adams, M. E., Myers, R. A., Imperial, J. S., and Olivera, B. M. (1993). Toxicity of rat brain calcium channels with omega-toxins from spider and cone snail venoms. *Biochemistry* 32, 12566–12570. doi: 10.1021/bi00210a003
- Aloisi, E., Le Corf, K., Dupuis, J., Zhang, P., Ginger, M., Labrousse, V., et al. (2017). Altered surface mGluR5 dynamics provoke synaptic NMDAR dysfunction and cognitive defects in Fmr1 knockout mice. *Nat. Commun.* 8:1103. doi: 10.1038/s41467-017-0119-2
- Ascano, M. Jr., Mukherjee, N., Bandaru, P., Miller, J. B., Nusbaum, J. D., Corcoran, D. L., et al. (2012). FMRP targets distinct mRNA sequence elements to regulate protein expression. *Nature* 492, 382–386. doi: 10.1038/nature11737
- Bardoni, B., Capovilla, M., and Lalli, E. (2017). Modeling Fragile X syndrome in neurogenesis: an unexpected phenotype and a novel tool for future therapies. *Neurogenesis* 4:e1270384. doi: 10.1080/23262133.2016.1270384
- Bardoni, B., Davidovic, L., Bensaïd, M., and Khandjian, E. W. (2006). The Fragile X syndrome: exploring its molecular basis and seeking a treatment. *Expert Rev. Mol. Med.* 8, 1–16. doi: 10.1017/s1462399406010751
- (C) Quantification of *Gfap* and *Psd95* (*Dlg4* transcript) mRNA levels in DIV 20 cortical neurons ($n = 3$ independent cultures). Results are presented as the mean \pm SEM, Mann-Whitney test: ns, not significant (*Gfap*: $P = 0.3701$; *Psd95*: $P = 0.6200$).
- FIGURE S2** | Unsupervised analysis of the shape and calcium homeostasis parameters of primary neuron cultures leads to the identification of four different groups of Regions-of-Interest (ROIs). Shape and calcium homeostasis parameters were first visualized in 2-dimension space using t-Distributed Stochastic Neighbor Embedding (t-SNE), then K-means clustering was performed on the 2-dimension t-SNE projection, and the optimal number of clusters, was determined using the Gap statistic. **(A)** t-SNE representation of the data, with cells colored by genotype. The distribution of WT (black dots) and *Fmr1*-KO (red dots) is homogeneous and vastly overlapping in all clusters. **(B)** t-SNE representation of the data, with cells colored by cluster. The distribution of the parameters of interest by clusters are presented using boxplots. The boxplots are defined as 25th percentile–75th percentile, the horizontal line corresponds to the median value, and whiskers extend to the min-max values. **(C)** Area covered by the cells, **(D)** cell circularity, **(E)** cell solidity, **(F)** cell roundness, **(G)** cell resting intracellular calcium concentration and **(H)** maximal KCl-triggered intracellular calcium concentration. **(I–L)** Number of cells from each genotype in the various experiments: ω -agatoxin-I Va (Aga), ω -conotoxin GV Ia (Cono), Nitrendipine (Nitren) or in the absence of VGCC antagonist (NoDrug) show the homogeneous WT and *Fmr1*-KO cell distribution in all identified clusters.
- FIGURE S3** | Representative images of ROIs identified using the ImageJ macro. Left panels are pseudo-colored images of stabilized unstimulated cells **(a, d, g, j)**. Middle panels represent the same cells during KCl stimulation **(b, e, h, k)**. Right panels show the macro output result **(c, f, i, l)**. The ROIs are encircled by a yellow line and the numbers indicate to which cluster ROI were attributed.
- FIGURE S4** | The percentage of DHPG-responsive cells is similar in WT and *Fmr1*-KO neurons. Cells in which the pharmacological stimulation elicited at least a 1.1 fold change in the $F_{340/380}$ ratio compared to baseline $F_{340/380}$ were considered DHPG-responsive and were counted in each cell cluster.
- Bear, M. F., Huber, K. M., and Warren, S. T. (2004). The mGluR theory of Fragile X mental retardation. *Trends Neurosci.* 27, 370–377. doi: 10.1016/j.tins.2004.04.009
- Bechara, E. G., Didiot, M. C., Melko, M., Davidovic, L., Bensaïd, M., Martin, P., et al. (2009). A novel function for Fragile X mental retardation protein in translational activation. *PLoS Biol.* 7:e16. doi: 10.1371/journal.pbio.1000016
- Berry-Kravis, E., Hessel, D., Abbeduto, L., Reiss, A. L., Beckel-Mitchener, A., Urv, T. K., et al. (2013). Outcome measures for clinical trials in Fragile X syndrome. *J. Dev. Behav. Pediatr.* 34, 508–522. doi: 10.1097/DBP.0b013e31829d1f20
- Bolte, S., and Cordelieres, F. P. (2006). A guided tour into subcellular colocalization analysis in light microscopy. *J. Microsc.* 224, 213–232. doi: 10.1111/j.1365-2818.2006.01706.x
- Bonacorso, C. M., Spatuzza, M., Di Marco, B., Gloria, A., Barrancotto, G., Cupo, A., et al. (2015). Fragile X mental retardation protein (FMRP) interacting proteins exhibit different expression patterns during development. *Int. J. Dev. Neurosci.* 42, 15–23. doi: 10.1016/j.ijdevneu.2015.02.004
- Bourinet, E., Soong, T. W., Stea, A., and Snutch, T. P. (1996). Determinants of the G protein-dependent opioid modulation of neuronal calcium channels. *Proc. Natl. Acad. Sci. U.S.A.* 93, 1486–1491. doi: 10.1073/pnas.93.4.1486
- Bramham, C. R., and Wells, D. G. (2007). Dendritic mRNA: transport, translation and function. *Nat. Rev. Neurosci.* 8, 776–789. doi: 10.1038/nrn2150
- Brown, V., Jin, P., Ceman, S., Darnell, J. C., O’Donnell, W. T., Tenenbaum, S. A., et al. (2001). Microarray identification of FMRP-associated brain mRNAs and altered mRNA translational profiles in fragile X syndrome. *Cell* 107, 477–487. doi: 10.1016/s0092-8674(01)00568-2
- Brown, M. R., Kronengold, J., Gazula, V. R., Chen, Y., Strumbos, J. G., Sigworth, F. J., et al. (2010). Fragile X mental retardation protein controls gating of the sodium-activated potassium channel Slack. *Nat. Neurosci.* 13, 819–821. doi: 10.1038/nn.2563

- Budimirovic, D. B., Berry-Kravis, E., Erickson, C. A., Hall, S. S., Hessl, D., Reiss, A. L., et al. (2017). Updated report on tools to measure outcomes of clinical trials in fragile X syndrome. *J. Neurodev. Disord.* 9:14. doi: 10.1186/s11689-017-9193-x
- Cao, Y. Q., Piedras-Renteria, E. S., Smith, G. B., Chen, G., Harata, N. C., and Tsien, R. W. (2004). Presynaptic Ca²⁺ channels compete for channel type-prefering slots in altered neurotransmission arising from Ca²⁺ channelopathy. *Neuron* 43, 387–400. doi: 10.1016/j.neuron.2004.07.014
- Cao, Y. Q., and Tsien, R. W. (2010). Different relationship of N- and P/Q-type Ca²⁺ channels to channel-interacting slots in controlling neurotransmission at cultured hippocampal synapses. *J. Neurosci.* 30, 4536–4546. doi: 10.1523/JNEUROSCI.5161-09.2010
- Castagnola, S., Bardoni, B., and Maurin, T. (2017). The search for an effective therapy to treat fragile X syndrome: dream or reality? *Front. Synaptic Neurosci.* 9:15. doi: 10.3389/fnsyn.2017.00015
- Castets, M., Schaeffer, C., Bechara, E., Schenck, A., Khandjian, E. W., Luche, S., et al. (2005). FMRP interferes with the Rac1 pathway and controls actin cytoskeleton dynamics in murine fibroblasts. *Hum. Mol. Genet.* 14, 835–844. doi: 10.1093/hmg/ddi077
- Catterall, W. A. (2011). Voltage-gated calcium channels. *Cold Spring Harb. Perspect. Biol.* 3:a003947. doi: 10.1101/cshperspect.a003947
- Chen, L., Yun, S. W., Seto, J., Liu, W., and Toth, M. (2003). The fragile X mental retardation protein binds and regulates a novel class of mRNAs containing U rich target sequences. *Neuroscience* 120, 1005–1017. doi: 10.1016/s0306-4522(03)00406-8
- Clapham, D. E. (2007). Calcium signaling. *Cell* 131, 1047–1058. doi: 10.1016/j.cell.2007.11.028
- Contractor, A., Klyachko, V. A., and Portera-Cailliau, C. (2015). Altered neuronal and circuit excitability in fragile X syndrome. *Neuron* 87, 699–715. doi: 10.1016/j.neuron.2015.06.017
- Damaj, L., Lupien-Meilleur, A., Lortie, A., Riou, E., Ospina, L. H., Gagnon, L., et al. (2015). CACNA1A haploinsufficiency causes cognitive impairment, autism and epileptic encephalopathy with mild cerebellar symptoms. *Eur. J. Hum. Genet.* 23, 1505–1512. doi: 10.1038/ejhg.2015.21
- Darnell, J. C., Van Driesche, S. J., Zhang, C., Hung, K. Y., Mele, A., Fraser, C. E., et al. (2011). FMRP stalls ribosomal translocation on mRNAs linked to synaptic function and autism. *Cell* 146, 247–261. doi: 10.1016/j.cell.2011.06.013
- Deng, P. Y., and Klyachko, V. A. (2016). Increased persistent sodium current causes neuronal hyperexcitability in the entorhinal cortex of Fmr1 knockout mice. *Cell Rep.* 16, 3157–3166. doi: 10.1016/j.celrep.2016.08.046
- Deng, P. Y., Rotman, Z., Blundon, J. A., Cho, Y., Cui, J., Cavalli, V., et al. (2013). FMRP regulates neurotransmitter release and synaptic information transmission by modulating action potential duration via BK channels. *Neuron* 77, 696–711. doi: 10.1016/j.neuron.2012.12.018
- Dolphin, A. C. (2016). Voltage-gated calcium channels and their auxiliary subunits: physiology and pathophysiology and pharmacology. *J. Physiol.* 594, 5369–5390. doi: 10.1113/jphysiol.2016.202722
- Ferron, L. (2016). Fragile X mental retardation protein controls ion channel expression and activity. *J. Physiol.* 594, 5861–5867. doi: 10.1113/jphysiol.2016.202705
- Ferron, L., Nieto-Rostro, M., Cassidy, J. S., and Dolphin, A. C. (2014). Fragile X mental retardation protein controls synaptic vesicle exocytosis by modulating N-type calcium channel density. *Nat. Commun.* 5:3628. doi: 10.1038/ncomms4628
- Giuffrida, R., Musumeci, S., D'Antoni, S., Bonaccorso, C. M., Giuffrida-Stella, A. M., Oostra, B. A., et al. (2005). A reduced number of metabotropic glutamate subtype 5 receptors are associated with constitutive homer proteins in a mouse model of fragile X syndrome. *J. Neurosci.* 25, 8908–8916. doi: 10.1523/JNEUROSCI.0932-05.2005
- Gross, C., Yao, X., Pong, D. L., Jeromin, A., and Bassell, G. J. (2011). Fragile X mental retardation protein regulates protein expression and mRNA translation of the potassium channel Kv4.2. *J. Neurosci.* 31, 5693–5698. doi: 10.1523/JNEUROSCI.6661-10.2011
- Hebert, B., Pietropaolo, S., Meme, S., Laudier, B., Laugéray, A., Doisne, N., et al. (2014). Rescue of fragile X syndrome phenotypes in Fmr1 KO mice by a BKCa channel opener molecule. *Orphanet J. Rare Dis.* 9:124. doi: 10.1186/s13023-014-0124-6
- Huber, K. M., Gallagher, S. M., Warren, S. T., and Bear, M. F. (2002). Altered synaptic plasticity in a mouse model of Fragile X mental retardation. *Proc. Natl. Acad. Sci. U.S.A.* 99, 7746–7750. doi: 10.1073/pnas.122205699
- Ichida, S., Abe, J., Komoike, K., Imanishi, T., Wada, T., Masuko, T., et al. (2005). Characteristics of omega-conotoxin GVIA and MVIIIC binding to Cav 2.1 and Cav 2.2 channels captured by anti-Ca²⁺ channel peptide antibodies. *Neurochem. Res.* 30, 457–466. doi: 10.1007/s11064-005-2681-5
- Inchauspe, C. G., Martini, F. J., Forsythe, I. D., and Uchitel, O. D. (2004). Functional compensation of P/Q by N-type channels blocks short-term plasticity at the calyx of Held presynaptic terminal. *J. Neurosci.* 24, 10379–10383. doi: 10.1523/JNEUROSCI.2104-04.2004
- Ishikawa, T., Kaneko, M., Shin, H. S., and Takahashi, T. (2005). Presynaptic N-type and P/Q-type Ca²⁺ channels mediating synaptic transmission at the calyx of Held of mice. *J. Physiol.* 568, 199–209. doi: 10.1113/jphysiol.2005.089912
- Jung, K. M., Sepers, M., Henstridge, C. M., Lassalle, O., Neuhofer, D., Martin, H., et al. (2012). Uncoupling of the endocannabinoid signalling complex in a mouse model of fragile X syndrome. *Nat. Commun.* 3:1080. doi: 10.1038/ncomms2045
- Khayachi, A., Gwizdek, C., Poupon, G., Alcor, D., Chafai, M., Casse, F., et al. (2018). Sumoylation regulates FMRP-mediated dendritic spine elimination and maturation. *Nat. Commun.* 9:757. doi: 10.1038/s41467-018-03222-y
- Kilkenny, C., Browne, W. J., Cuthill, I. C., Emerson, M., and Altman, D. G. (2010). Improving bioscience research reporting: the ARRIVE guidelines for reporting animal research. *PLoS Biol.* 8:e1000412. doi: 10.1371/journal.pbio.1000412
- Mao, B. Q., Hamzei-Sichani, F., Aronov, D., Froemke, R. C., and Yuste, R. (2001). Dynamics of spontaneous activity in neocortical slices. *Neuron* 32, 883–898. doi: 10.1016/s0896-6273(01)00518-9
- Maurin, T., Lebrigand, K., Castagnola, S., Paquet, A., Jarjet, M., Popa, A., et al. (2018a). HITS-CLIP in various brain areas reveals new targets and new modalities of RNA binding by Fragile X mental retardation protein. *Nucleic Acids Res.* 46, 6344–6355. doi: 10.1093/nar/gky267
- Maurin, T., Melancia, F., Jarjet, M., Castro, L., Costa, L., Delhayé, S., et al. (2018b). Involvement of phosphodiesterase 2A activity in the pathophysiology of fragile X syndrome. *Cereb. Cortex* doi: 10.1093/cercor/bhy192 [Epub ahead of print].
- Maurin, T., Zongaro, S., and Bardoni, B. (2014). Fragile X syndrome: from molecular pathology to therapy. *Neurosci. Biobehav. Rev.* 46, 242–255. doi: 10.1016/j.neubiorev.2014.01.006
- Meredith, R. M., Holmgren, C. D., Weidum, M., Burnashev, N., and Mansvelder, H. D. (2007). Increased threshold for spike-timing-dependent plasticity is caused by unreliable calcium signaling in mice lacking Fragile X gene FMR1. *Neuron* 54, 627–638. doi: 10.1016/j.neuron.2007.04.028
- Miyashiro, K. Y., Beckel-Mitchener, A., Purk, T. P., Becker, K. G., Barret, T., Liu, L., et al. (2003). RNA cargoes associating with FMRP reveal deficits in cellular functioning in Fmr1 null mice. *Neuron* 37, 417–431. doi: 10.1016/s0896-6273(03)00034-5
- Myrick, L. K., Deng, P. Y., Hashimoto, H., Oh, Y. M., Cho, Y., Poidevin, M. J., et al. (2015). Independent role for presynaptic FMRP revealed by an FMR1 missense mutation associated with intellectual disability and seizures. *Proc. Natl. Acad. Sci. U.S.A.* 112, 949–956. doi: 10.1073/pnas.1423094112
- Nanou, E., Scheuer, T., and Catterall, W. A. (2016). Calcium sensor regulation of the CaV2.1 Ca²⁺ channel contributes to long-term potentiation and spatial learning. *Proc. Natl. Acad. Sci. U.S.A.* 113, 13209–13214. doi: 10.1073/pnas.1616206113
- Nolze, A., Schneider, J., Keil, R., Lederer, M., Hüttelmaier, S., Kessels, M. M., et al. (2013). FMRP regulates actin filament organization via the armadillo protein p0071. *RNA* 19, 1483–1496. doi: 10.1261/rna.037945.112
- Ota, S., Horisaki, R., Kawamura, Y., Ugawa, M., Sato, I., Hashimoto, K., et al. (2018). Ghost cytometry. *Science* 360, 1246–1251. doi: 10.1126/science.aan0096
- Peterson, B. Z., Tanada, T. N., and Catterall, W. A. (1996). Molecular determinants of high affinity dihydropyridine binding in L-type calcium channels. *J. Biol. Chem.* 271, 5293–5296. doi: 10.1074/jbc.271.10.5293
- Schneider, C. A., Rasband, W. S., and Eliceiri, K. W. (2012). NIH Image to ImageJ: 25 years of image analysis. *Nat. Methods* 9, 671–675. doi: 10.1038/nmeth.2089
- Sharova, L. V., Sharov, A. A., Nedorezov, T., Piao, Y., Shaik, N., and Ko, M. S. (2009). Database for mRNA half-life of 19 977 genes obtained by DNA microarray analysis of pluripotent and differentiating mouse embryonic stem cells. *DNA Res.* 16, 45–58. doi: 10.1093/dnare/dsn030

- Simms, B. A., and Zamponi, G. W. (2014). Neuronal voltage-gated calcium channels: structure, function and dysfunction. *Neuron* 82, 24–45. doi: 10.1016/j.neuron.2014.03.016
- Thévenaz, P., Ruttimann, U. E., and Unser, M. (1998). A pyramid approach to subpixel registration based on intensity. *IEEE Trans. Image Process.* 7, 27–41. doi: 10.1109/83.650848
- Wahlstrom-Helgren, S., and Klyachko, V. A. (2015). GABA_A receptor-mediated feed-forward circuit dysfunction in the mouse model of fragile X syndrome. *J. Physiol.* 593, 5009–5024. doi: 10.1113/jp271190
- Yue, Q., Jen, J. C., Nelson, S. F., and Baloh, R. W. (1997). Progressive ataxia due to a missense mutation in a calcium-channel gene. *Am. J. Hum. Genet.* 61, 1078–1087. doi: 10.1086/301613
- Zaitsev, A. V., Povysheva, N. V., Lewis, D. A., and Krimer, L. S. (2007). P/Q-type, but not N-type, calcium channels mediate GABA release from fast-spiking interneurons to pyramidal cells in rat prefrontal cortex. *J. Neurophysiol.* 97, 3567–3573. doi: 10.1152/jn.01293.2006
- Zamponi, G. W., Striessnig, J., Koschak, A., and Dolphin, A. C. (2015). The physiology, pathology, and pharmacology of voltage-gated calcium channels and their future therapeutic potential. *Pharmacol. Rev.* 67, 821–870. doi: 10.1124/pr.114.009654
- Zhang, Y., Bonnan, A., Bony, G., Ferezou, I., Pietropaolo, S., Ginger, M., et al. (2014). Dendritic channelopathies contribute to neocortical and sensory hyperexcitability in Fmr1^{-/-} mice. *Nat. Neurosci.* 17, 1701–1709. doi: 10.1038/nn.3864
- Zhuchenko, O., Bailey, J., Bonnen, P., Ashizawa, T., Stockton, D. W., Amos, C., et al. (1997). Autosomal dominant cerebellar ataxia (SCA6) associated with small polyglutamine expansions in the α 1A-voltage-dependent calcium channel. *Nat. Genet.* 15, 62–69. doi: 10.1038/ng0197-62

Conflict of Interest Statement: The authors declare that the research was conducted in the absence of any commercial or financial relationships that could be construed as a potential conflict of interest.

Copyright © 2018 Castagnola, Delhaye, Folci, Paquet, Brau, Duprat, Jarjat, Grossi, Béal, Martin, Mantegazza, Bardoni and Maurin. This is an open-access article distributed under the terms of the Creative Commons Attribution License (CC BY). The use, distribution or reproduction in other forums is permitted, provided the original author(s) and the copyright owner(s) are credited and that the original publication in this journal is cited, in accordance with accepted academic practice. No use, distribution or reproduction is permitted which does not comply with these terms.

Annexe 2

Considérant les résultats précédents, nous avons décidé d'étudier l'interaction dynamique entre les cellules et leur environnement en développant une technique de tri cellulaire, le aiFACS (agonist-induced Functional Analysis and Cell Sorting). Cette technique permet l'enregistrement et le tri simultané des cellules en temps réel en fonction de leur réponse immédiate et individuelle à un stimulus. Comme preuve de concept, nous avons utilisé le aiFACS sur le cerveau de souris dissocié, un tissu très hétérogène, en récupérant les interneurones par stimulation au KCl ou à l'agoniste des récepteurs glutamate AMPA, après les avoir triés par rapport à leur niveau calcique. Après le stimulus par AMPA, un séquençage ARN en single-cell de ces interneurones sélectionnés par aiFACS a abouti à une classification en neuf clusters. De plus, nous avons utilisé le aiFACS sur le cerveau de souris *Fmr1* KO et avons montré que les interneurones *Fmr1* KO ont une réponse défectueuse à l'AMPA comparé aux cellules WT.

Agonist-induced Functional Analysis and Cell Sorting associated with single-cell transcriptome as a novel tool to define molecular phenotypes of cell subtypes in normal and pathological brain

Sara Castagnola¹, Julie Cazareth¹, Kevin Lebrigand¹, Marielle Jarjat¹, Virginie Magnone¹, Sébastien Delhaye¹, Frédéric Brau¹, Barbara Bardoni^{2*} & Thomas Maurin¹

1-Université Côte d'Azur, CNRS, Institute of Molecular Cellular Pharmacology, F-06560 Valbonne – France

2-Université Côte d'Azur, INSERM, CNRS, Institute of Molecular Cellular Pharmacology, F-06560 Valbonne – France

*Corresponding: bardoni@ipmc.cnrs.fr

Key words: aiFACS, single-cell RNA-sequencing, interneurons, Fragile X Syndrome,

ABSTRACT

To get a better insight into the dynamic interaction between cells and their environment, we developed the agonist-induced Functional Analysis and Cell Sorting (aiFACS) technique, which allows the simultaneous recording and sorting of cells in real-time according to their immediate and individual response to a stimulus. By modulating the aiFACS selection parameters, testing different developmental times, using various stimuli and multiplying the analysis of readouts, it is possible to analyze cell populations of any normal or pathological tissue. The association of aiFACS with single-cell transcriptomic allows building a functional tissue cartography based on specific pharmacological response/s of cells. As proof of concept, we used aiFACS on the dissociated mouse brain, a highly heterogenous tissue, enriching it in interneurons upon stimulation with KCl or with an agonist of the glutamate receptors, AMPA, and upon sorting based on calcium levels. After AMPA stimulus, single-cell RNA-sequencing of these aiFACS-selected interneurons resulted in a nine-cluster classification. Furthermore, we used aiFACS on interneurons derived from the brain of the *Fmr1*-KO mouse, a rodent model of Fragile X syndrome. We show here that these interneurons manifest a generalized defective response to AMPA compared to wild type cells, affecting all the analyzed cell clusters at one specific post-natal developmental time.

INTRODUCTION

The selection, cloning and morphological/functional characterization of individual cells in a suspension or from a tissue is a fastidious and lengthy procedure, although several techniques have been set up to reach this goal: limiting dilutions, laser micro-dissection (Datta et al. 2015), cytoplasm aspiration (Cadwell et al. 2016; Fuzik et al. 2016) micro fluidics (Pollen et al. 2014; Tasic et al. 2016; Zeisel et al. 2015) and flow cytometry (Fulwyler 1965). The latter is a robust and powerful technique allowing the fast analysis and sorting of cell subsets from an initial heterogeneous sample. Cells can be sorted according to various parameters and are amenable to further characterization such as single-cell transcriptomics or mass spectrometry. Single-cell transcriptomics is the unique tool providing a precise and simultaneous analysis of the expression levels of thousands of genes in a complex heterogeneous population at the single-cell level (Poulin et al. 2016). Applied to the study of a pharmacological stimulation, this technique can decipher homeostatic gene regulation at the tissue level from the modulation of the abundance of a given cell population, a phenomenon that is widely observed during development (Ofengheim et al. 2017; Poulin et al. 2016).

Coupling flow cytometry analysis and cell sorting with single-cell transcriptomics makes it possible to link a cell phenotype to its genotype, providing a direct access to the molecular cues of a given phenotype. In this context, the key point is to submit the cells under analysis to the same stimulus. The functional FACS analysis of intracellular pH or calcium variations using fluorescent probes (Chow et al. 2001; Vines et al. 2010), commonly consists to add a stimulation (drugs, osmotic variations...) into the sample tube containing the stained cell suspension before to analysis or sorting. While it takes up to 30 seconds for the sample to reach the flow cell (the chamber aligning the cells in order to pass one-by-one through the laser beam for sensing), it can be considered that the fluorescence signal is measured "*at equilibrium*", as its detection and the physiological stimulus are temporally far from each other. This lag time prevents a comparable and accurate analysis of cell to cell calcium variations on commercial flow cytometers, compared to the efficient sampling of calcium imaging (from few milliseconds to seconds) obtained in fluorescence microscopy (due to the combination of quick local delivery of drugs with high recording rates). As the cell suspension in the sample tube is currently injected under pressure into the cytometer fluidics of many commercial flow

cytometers, the removal of the sample tube to study cellular responses to drug stimulations is required. This manual step increases the lag of time and, in turn, contributes to the observation of "stationary" cellular responses. Moreover, this methodology presupposes that the first and last cell analyzed in the tube behave in an equivalent way. With the appearance of sample lines using peristatic pumping in commercial FACS (i.e. sample tube at atmospheric pressure) technical approaches have been proposed to add drugs to the cells without discontinuity (Arnoldini et al. 2013; Vines et al. 2010). While the lag of time corresponding to the tube removal was suppressed, all the cells remained simultaneously exposed to the drug but analyzed at different times. Encouraging approaches to "fast" calcium response measurements by flow cytometry have been proposed in the past, based on a fluidic modification in a FACS analyzer (Tárnok 1996; Zwartz et al. 2011). A way to monitor brief kinetics and the possibility to sort the cells by modifying the tubing configuration of a FACStar Plus cytometer was also described (Dunne 1991). However, no sorting evidence was demonstrated. These approaches remained in the form of prototypes and were only used to carry out analysis (Time zero Instrument).

The agonist-induced Functional Analysis and Cell Sorting (aiFACS) prototype we developed is built on a FACS Aria III as an add-on. It allows to analyze all the aforementioned parameters but also to sort cells according to their immediate and individual response to a stimulus. We used it on mouse brains and we were able to obtain enriched preparations of interneurons. Further application of aiFACS to FXS mouse brains highlights the functional and molecular impairment of interneurons, thus validating in this model the power of this technique as a new tool to study brain disorders. Beside the brain, aiFACS can be employed to analyze cell populations of any normal and pathological tissue including tumors.

RESULTS

Set up of Agonist-Induced Functional Analysis and Cell Sorting (aiFACS)

We designed the aiFACS prototype in order to be able to sort cells according to their response to a pharmacological stimulation that is monitored in real time with a fluorescent calcium indicator (Figure 1A). The sorter fluidics (BD FACARia III) is modified to allow drug injection into the sample line. Thanks to a "Y" connector, a tubing (shown in red, Figure 1A) with a diameter of 0.19 mm that is equivalent to that of the sample line (shown in blue, Figure 1A) is connected to two syringes, upstream of the solenoid valve and the flow cell. Two valves open or closed alternately control the injection syringes containing PBS and agonist and allow the injection pad to be selected. The speed of injection of the solutions is controlled using a peristaltic micro-pump to synchronize it with the FACS flowrate. The incubation time between each cell and the drug is thus controlled (red tubing, Figure 1A). In basal conditions, a sample resuspension buffer (D-PBS) is infused. To induce stimulation, the experimental drug, is injected (1,6X). The cells are sorted according to their response to the drug. The precise dilution of the agonist is determined by the flow rate of the instrument and of the pump. Its definition was possible by using beads (PE and APCCY7, respectively) instead of D-PBS and agonist and counting them before and after aiFACS.

Using the Miltenyi Neuron Isolation kit (Berl et al. 2017; Holt and Olsen 2016), we freshly dissociated 18 Post-Natal Day (PND 18) mouse adult brains to obtain RNA from the neuronal and non-neuronal collected populations that we used to measure the expression of several neuronal markers by RT-qPCR (Supplemental Figure S1). The neuron fraction is enriched in interneuron (*Gad2*, *Cnrl* not shown) and pyramidal cell (*Itpr1*, *Mef2c*, *NeuroD1*, *Nrgn*) markers, and depleted in microglial (*Grn*), immature neuron (*Sox2*), astrocyte (*Gfap*), oligodendrocytes (*Mog2*, *Mbp*) and endothelial cells (*Rapgef4*).

We injected neurons labelled with Fluo-4 AM in order to monitor the calcium response and we set up the machine using the parameters indicated in red in Supplemental Figure S2A. In this first step, based on our previous experience with ratiometric calcium imaging (Castagnola et al. 2018), we

used KCl (63mM final) as agonistic drug to elicit calcium entry into cells. We added fluorescent beads to monitor the agonist perfusion and the increase in K⁺ ion concentration in the sample line. At time t0 the D-PBS perfusion starts and it is stopped at time t1, when the KCl perfusion is opened (Figure 1B). Each cell will be in contact with KCl for 3.2 seconds (Supplemental Figure S2A). The appearance of the beads corresponds to the arrival of cells stimulated with KCl in the flow cell (Figure 1C). The increased level of calcium can be appreciated in the graph in Supplemental Figure S2B. In order to verify the amplitude of neuronal response and have a positive control of stimulation, ionomycin is added to KCl at time t2 (Figure 1B). Pre-sort viability is determined by labeling dissociated neurons with DAPI staining (Figure 1D). The viability of the cells having responded to KCl and after sorting by aiFACS can be monitored with the previous labeling and it is determined through re-analysis of the cells (Figure 1D). Remarkably, post-aiFACS KCl-responsive cells are viable (>90%) and capable of growing neurites when seeded on ornithine-coated glass coverslips (Figure 1E).

aiFACS selection and characterization of AMPA-responding interneuron populations

To obtain a proof of concept that this new method allows to select and study neuronal populations using a pharmacological stimulation, we decided to activate a ionotropic receptor by its agonist and using α- amino-3-hydroxy-5-methyl-4-isoxazolepropionic acid (AMPA). After brain dissociation, cells stained with Fluo-4 were gated based on their fluorescence. We injected the cells in the FACS supplying the flow cell with a neutral D-PBS (baseline condition). After 3 minutes of recording, we stimulated cells with an AMPA solution (126 μM final). Also in this case each cell was in contact with the drug for 3.2 seconds. The gating strategy is detailed in the Methods section and the various steps are shown in Supplemental Figure S3. In our analysis, we focused on the cells that exhibit a homogenous Fluo-4 staining and we called them gating-dependent cell population 1 (GD1 cells; Figure 2A). To be able to quantify precisely the response to the stimulation using the intracellular calcium concentration changes, the ‘resting’/unstimulated/baseline fluorescence of the cell population should be as homogeneous as possible. Indeed, this point is critical to be able to set an activation ‘threshold’ beyond which responding cells are sorted. Resting Ca²⁺ levels in the GD1 population, compared to the remaining cell population (GD2, cells) are less variable allowing to set this threshold

(Figure 2A). This cell population is not contaminated with microglia (Supplemental Figure S4A, B) and is enriched in *Gad2*- and *Calb2*-expressing cells compared to GD2 (Figure 2B). This suggests that our strategy favored the selection of interneurons (Le Magueresse and Monyer 2013). To get more insight in the interneuron sub-population selected, GD1 cells were used to carry out single-cell transcriptomics with the 10x Genomics Chromium and Illumina sequencing platform. After quality control, we analyzed 2,170 cells (1,287 AMPA and 883 baseline), with a median UMI per cell of 6,652. The canonical correspondence analysis (CCA) of the two aggregated samples led to the identification of nine cell clusters (Figure 3A and 3B). The AMPA response of each cluster is illustrated in Figure 3C. The selection of the various markers was carried out on the basis of previous publications (Paul et al. 2017; Rosenberg et al. 2018; Tasic et al. 2016; Mi et al. 2018; Zeisel et al. 2015; Zeisel et al. 2018; La Manno et al. 2016).

GD1 cells are broadly split into inhibitory (*Dcx*, *Gad1*, *Gad2*, *Dlx6*, *Dlx1*, *Dlx5*, and *Dlx2*) and excitatory neurons (*Slc17a7*, *Slc17a6*, *Nrn1*, *Neurod1*, and *Neurod2*) (Figure 3A and 3B). We identified two clusters of cycling progenitors (*Top2a*, *Ube2c*, *Mki67*, *Hmgb2*, and *Cenpf*; Figure 3A and Supplemental Figure S5A) already engaged toward the inhibitory (*Dlx1*, *Dlx5* and *Dlx2*) or excitatory lineages (*Selm*, *Meis1*, *Pax6*, *E2f1*, *Cog7*, and *Cd63*). Inhibitory neurons were split in three main populations that express *Meis2* in combination with other markers: *Tiam2/Nrxn3*, *Pbx1/Sox4* and *Synpr/Calb2/Pbx3*. We also identified two inhibitory neuron clusters further advanced in their maturation process: “*Sema3c*” (*Calb2*, *Sema3c*, *Id2*, and *Cnrl*), composed of VIP neuron precursors, and inhibitory mature neurons composed of “*Rora*” cells (*Cldn3*, *Akap7*, *Ctnbp2*, *Gad1*, and *Gad2*) that may give rise to CCK (Figure 3A, 3B and 3G). Next, we identified a continuum of three excitatory cell clusters, separated by their differentiation status: ventricular zone or dentate gyrus granule cell intermediate progenitors (*Hes6* and *Ccnd2*), and two clusters of further differentiated cells (*Neurod1*, *Neurod2*, *Apc*, *Nrxn1*, *Rbfox3*, and *Map1b*), that could be split according to their intermediate or final maturation, as indicated by the expression of pre- and post-synaptic markers (*Snap25*, *Grin2b* and *Pclo*), cytoskeletal (*Mapt*) and potassium channel expression (*Kcnb2* or *Kcnal* and *Kcnk2*) (Figure 3A and 3B). Distribution of some specific markers (*Meis2*, *NeuroD1*, *NeuroD2*, and *Gad2*) is shown in the context of various clusters (Figure 3D – 3G). The post-aiFACS selection

clearly shows that AMPA stimulation promoted the positive selection of *Meis2* interneurons (12 % to 38 % of the sorted cells; Figure 3H).

In summary, aiFACS is a tool to analyze a tissue response to a pharmacological stimulation, offering new information on ion homeostasis players but also on the cellular specificities that drive the heterogeneity of the cell response.

aiFACS selection through AMPA stimulation unveils impaired *Fmr1*-KO interneurons

In order to validate that aiFACS is helpful to study brain disorders, we applied it to dissociated neurons from mouse *Fmr1*-KO brains, the murine Fragile X Syndrome (FXS) model. This disorder is due to the lack of function of the Fragile X Mental Retardation Protein (FMRP). Indeed, recent studies highlighted interneuron dysfunctions in FXS (Cea-Del Rio and Huntsman 2014; Goel et al. 2018; Le Magueresse and Monyer 2013; Olmos-Serrano et al. 2010; Patel et al. 2013; Yang et al. 2018) as well as their alteration in expression, trafficking and functioning of AMPA receptors (AMPARs) (Cheng et al. 2017). To carry out this part of the study, we implemented the technique by introducing a dynamic selection to simultaneously analyze wild type (WT) and *Fmr1*-KO samples. We dissociated PND 18 WT and *Fmr1*-KO brains and cells from both genotypes were stained with Fluo-4. WT cells were further labeled with Alexa-Fluor 594-coupled Wheat Germ Agglutinin (WGA 594), while *Fmr1*-KO cells were labeled with Alexa-Fluor 647 WGA. This labeling allowed the mixing of cells of both genotypes to perform a combined analysis (Figure 4A). In following experiments the dyes were switched. Following the previous procedure, we selected 5,000 cells for each condition (baseline and upon AMPA stimulation).

Since upon AMPA stimulation GD1 cells are strongly enriched in *Meis2*-expressing cells, we measured the expression levels of *Meis2* by RT-qPCR after AMPA stimulation of both WT and *Fmr1*-KO GD1 cells obtained from new sets of mice by evaluating the fold change respective to the expression of aiFACS selected WT neurons (Figure 4B). Our results show that the response to AMPA of GD1 *Fmr1*-KO neurons compared to WT neurons is impaired for the mRNA levels of *Meis2*, *Neurod1* and *Neurod2* markers, while no changes were observed for mRNA expression of *Gad2* (Figure 4B). This suggests that AMPA-responding *Fmr1*-KO GD1 cells display an abnormal level of

the analyzed genes compared to WT or that a different number of cells express this marker in WT and *Fmr1*-KO. To get more insight, we performed single-cell sequencing on AMPA-stimulated GD1 cells dissociated from *Fmr1*-KO brains. We analyzed 1,047 *Fmr1*-KO GD1 cells with a median UMI per cell of 6,585. Targets mRNAs of FMRP selected by HITS-CLIP (Maurin et al. 2018) were identified in each cluster. We use the top 200 mRNA prominent targets of FMRP from HIT-CLIP we previously carried-out (Maurin et al. 2018). We calculated a signature score (*i.e.* a composite expression score of a set of genes using Seurat's AddModuleScore function using standard parameters. <https://www.rdocumentation.org/packages/Seurat/versions/3.1.4/topics/AddModuleScore>). This score is plotted as a boxplot per cell type (wt/ko samples aggregate) (Supplemental Figure S5B). We identified the same cell clusters present in AMPA stimulated WT GD1 cells, even if their proportions are altered (Figure 4C). This suggests an overall impairment in AMPA response in the absence of FMRP as cells from each cluster are affected. This variability could be explained by the different level of maturity or developmental profile of the cells composing each cluster in WT *vs* *Fmr1*-KO.

To evaluate this hypothesis, we measured the levels of the analyzed markers at baseline (Figure 5A) by using new sets of non-littermates PND 18 and PND 19 WT and *Fmr1*-KO mouse neuronal populations submitted to aiFACS. By RT-qPCR, we observed an elevated expression of the two pro-neuronal genes *Neurod1* and *Neurod2* in *Fmr1*-KO baseline GD1 cells. To assess whether the phenotype we observed is associated to the developmental process, we decided to repeat the analysis in mice older than PND 18. Remarkably, at PND 19 by RT-qPCR we observed that the expression levels of *Meis2* *Neurod1*, *Neurod2* and *Gad2* do not show a significantly different abundance between the two genotypes (Mann-Whitney test, *Meis2*, ns p = 0.285; *Neurod1* ns p = 0.2857; *Neurod2* ns p = 0.5714; *Gad2* ns p = 0.1905. Figure 5B). Consistently, the analysis of PND 19 GD1 *Fmr1*-KO neurons revealed that their response to AMPA is unchanged compared to WT neurons for all the analyzed markers (Supplemental Figure S6). We can therefore suggest that AMPA-responding *Fmr1*-KO GD1 cells might be changed at this time of development, at least for the GD1 cells expressing these markers.

DISCUSSION

A new approach to study pharmacological responses of cells

We developed the agonist-induced Functional Analysis and Cell Sorting (aiFACS) prototype with the need to explore the cell-specific answer to environmental/pharmacological stimuli in particular for fast kinetics studies, since classical FACS analysis does not allow the sorting of living cells all submitted to a same brief stimulus at the same time. Using this technique we demonstrated the calcium monitoring in real time with a fluorescent indicator and sorting of cells according to their calcium answer upon pharmacological treatment. The entry of calcium into the neurons is tightly controlled process and it is due to the opening of Ca^{2+} permeable channels that are known to respond to a large array of stimuli such as membrane depolarization or extracellular chemical messengers that can directly activate the channel or can act indirectly via intracellular molecular signaling (Barrit et al. 1999; Taylor et al. 2002). In particular, fast and brief increases of intracellular calcium levels are known to be involved in various steps of neuronal development. Indeed, calcium transients have a pivotal role in the regulation of neurotransmitter phenotypes, dendritic morphology and axonal growth, and guidance (Rosenberg and Spitzer 2011). The modulation of all these parameters is critical for the specification of the neuronal subtype. Hence, the duration and the quality of the stimulus are the most critical aspects to manage while setting-up the aiFACS method, because they represent the key modulators of the selection. Indeed, the duration of the stimulus is dependent on the length of the red tubing (Figure 1A) and on the speed of the sample flow rate (Supplemental Figure 2A), as mentioned previously by Tarnok et al. (1996) in its fixed time flow cytometry approach. For instance, we decided to use a stimulus of 3.2 sec based on our previous studies by using calcium imaging in cultured neurons. Indeed, after 3.2 sec we observed the appearance of a peak of intracellular calcium in cultured cortical neurons upon various stimuli (Castagnola et al. 2018). This controlled time is a very critical point since a too long time of contact between the neurons and the agonist, due to long process of cell sorting by classical FACS, could result into a modification of neuronal gene expression. For instance activation of Creb by phosphorylation was observed already after one minute (Bito et al. 1996). Moreover, aiFACS allows applying one or more stimuli to the same cells under

analysis in a subsequent manner, as we showed in Figure 1 for KCl and ionomycin. aiFACS-selected cells can be analyzed by various downstream methods, including single-cell sequencing. This technique allows to unravel cell identity, define the molecular determinants of the pharmacological response and directly access gene expression differences including splice variants and edited transcripts. Furthermore, by introducing dynamic selection, WT and one or more mutants can be analyzed simultaneously in the same run or multiple individuals having the same genotype can be multiplexed and analyzed separately, but simultaneously. To show the power of aiFACS, we used the brain as a highly specialized and heterogeneous tissue. By applying this technique to PND 18 mouse brains, we demonstrated the possibility of enriching our samples in interneurons responding rapidly to the pharmacological agonist. To date, the study of interneurons has been confined to restricted brain areas or circuits, due to the limited availability of high throughput analysis tools allowing a thorough and precise analysis of the complex molecular, spatial, anatomical and connection heterogeneities of the brain (Le Magueresse and Monyer 2013). By our approach, we are convinced that it will be possible to provide a novel function-based classification of interneuron cells rather than a classification based on (or in addition to) other parameters such as localization, morphology and gene expression.

The proof of concept in Fragile X syndrome

We compared WT and *Fmr1*-KO aiFACS-selected cell responses to AMPA. Our results show a global altered AMPA response in the *Fmr1*-KO cells, in agreement with other studies (Cheng et al. 2017). The same clusters of cells were selected but their ratio is different between WT and *Fmr1*-KO cells. Indeed, we repeated the aiFACS selection on additional sets of WT and *Fmr1*-KO mouse brains and we validated that *Fmr1*-KO cells display abnormal levels of *Meis2*, *Neurod1* and *Neurod2*, while overall consistent levels of *Gad2* (Figure 4B). These data confirm that the balance of inhibitory/excitatory neuronal activity is abnormal in the FXS brain, as previously suggested (Contractor et al. 2015; Li et al. 2020) Remarkably, we uncover the specific deregulation of *Meis2* interneuron responsiveness to AMPA stimulation. *Meis2* is a crucial transcription factor for interneuron maturation in the rodent brain. Mutations or deletions of this gene have been associated to

neurodevelopmental disorders displaying intellectual disability and autism spectrum disorder (Giliberti et al. 2019; Verheije et al. 2019). *Meis2* is a marker of Lateral Ganglionic Eminence (LGE)-derived interneurons that are Medium Spiny Neurons (MSNs) of the striatum. Moreover, *Meis2* interneurons are in the Rostral Migratory System (RMS), giving rise to dopaminergic periglomerular interneurons of the Olfactory Bulb (OB) (Agoston et al. 2014; Allen et al. 2007; Fujiwara and Cave 2016). *Meis2* interneurons were never involved in the pathophysiology of FXS before and altered levels of *Meis2* (mRNA or protein) were never observed in studies involving large *Fmr1*-KO brain regions. Indeed, the previous analysis of cortex and hippocampus transcriptomics of *Fmr1*-KO mouse did not reveal substantial differences with WT samples (Maurin et al. 2018). Therefore, our data clearly show that aiFACS allows to highlight unexpected impairments in cell subtypes by carrying out a functional sensitive cellular selection.

In summary, our results point out the presence of functional and molecular impairments in *Fmr1*-KO interneurons subtypes that are synchronized with brain development and they open up new research perspectives for FXS. Remarkably, we observed that the expression levels of some markers, such as the two pro-neural genes *Neurod1* and *Neurod2*, which are deregulated at PND 18, appear normalized when analyzed at PND 19. Even if more detailed analysis will be needed for a deep understanding of post-natal neuronal development in *Fmr1*-KO mouse, which has received little attention (Maurin et al. 2019; Tang et al. 2015), we can consider that this different expression could be a consequence of an altered developmental profile of *Fmr1*-KO interneurons dependent on the function of FMRP. This protein is known to modulate a network of pathways, including calcium signaling, which is supposed to be completely disorganized in its absence (Maurin and Bardoni 2018; Maurin et al. 2018; Miyashiro et al. 2003; Richter and Coller 2015; Castagnola et al. 2018; Ferron 2016).

We present aiFACS as a new tool to analyze interneurons from mouse brains. It was developed on a simpler and similar basis of previous technical modifications on commercial flow cytometers designed to optimize Real-Time flow cytometry cellular assays in the past (Dunne et al. 1991; Tárnok et al. 1996; Zwartz et al. 2011; Arnoldini et al. 2013; Vines et al. 2010). Fluidics of flow cytometers use principally two different technologies to inject the sample into the sheath fluid: a

pressure applied on the sample tube or a peristatic pumping. As pressure was the main commercial technology available in the 90's, (Dunne et al. 1991; Tárnok et al. 1996) using an approach similar than one previously described (Kelley 1989) with a derivation of the pressurization from the cytometer to create a stimulus line to mix drugs with the cells. Later, with the Accuri C6 flow cytometer based on a sample injection at atmospheric pressure (Arnoldini et al. 2013; Vines et al. 2010) suggested to simply add the stimulation into the sample tube. While simpler, this latter approach has the main drawback to monitor heterogeneous cellular stimulations as the first and last cell monitored will be exposed for different length of time to the drug. If our aiFACS approach seems closer to the first developments (Dunne et al. 1991; Tárnok et al. 1996), it offers the advantage to be more flexible in connecting a stimulus line to a commercial flow cytometer and manage multiple drug injections and proved to be efficient with sorting strategies, while previous developments only shown cell analysis. This is a key aspect to perform further single-cell Omics studies. The proof of concept on the FXS mouse model confirmed that aiFACS allows the collection of a wealth of new information concerning the molecular pathology of a brain disorder. This was possible by using both a sophisticated approach such as single-cell RNA sequencing and a simple and inexpensive technique like RT-qPCR. We used here well-defined parameters based on our previous experiments and a specific readout, the intracellular calcium level. Our parameters and conditions of works resulted in the study of a specific cell brain population. However, by modulating the aiFACS selection parameters, testing different developmental times, using various stimuli and multiplying the analysis of readouts, we think that it will be possible to extend the use of aiFACS to other brain cell type and also to a large panel of normal pathological tissues, including tumors. Lastly, in perspective, the aiFACS can be applied to study second messenger modulations, kinase activations, ionic fluxes and many other biochemical and pharmacological mechanisms at the level of individual cells.

METHODS

Animal handling and care. Animal care was conducted in accordance with the European Community Directive 2010/63/EU. WT and *Fmr1*-KO mice on a C57BL/6J congenic background were obtained from Prof. R. Willemsen (Mientjes et al. 2006) and reported as *Fmr1*-KO 2. All animals were generated and housed in groups of six in standard laboratory conditions (22°C, 55 ± 10% humidity, 12-h light/12-h dark diurnal cycles) with food and water provided *ad libitum*. Only brains from male animals were analyzed. For timed pregnancies, noon on the day of the vaginal plug was counted as E 0.5. The experiments were performed following the Animals in Research: Reporting In Vivo Experiments (ARRIVE) guidelines (Kilkenny et al. 2010). The experiments were approved by the local ethics committee (Comité d'Ethique en Expérimentation Animale CIEPAL-AZUR N. 00788.01).

Brain dissociation and neuron isolation. Full brains were dissected from PND 18 mice. A brief wash with complete D-PBS (supplemented with 0.5% bovine serum albumin, 1% pyruvate and 15 mM glucose) was performed before cutting the brains in six equally thick sagittal sections (2 mm) using a mouse brain matrix slicer (CellPoint Scientific) and 5 razorblades. Brain slices were dissociated mechanically using a gentleMACS™ Octo Dissociator and enzymatically using the Adult Brain Dissociation kit (Miltenyi Biotec) following the manufacturer's instructions. The Neuron Isolation Kit (Miltenyi Biotec) was used for magnetic selection of neuronal cells.

Neuron labelling. WT and *Fmr1*-KO neuronal suspensions were labelled at 37°C with a combination of the Fluo-4 calcium indicator (5 µg/ml; Invitrogen) and either Alexa-Fluor 594-coupled Wheat Germ Agglutinin (WGA) or Alexa-Fluor 647-coupled WGA (5 µg/ml; Invitrogen) in D-PBS for 20 and 10 min. The dyes were switched at each experiments A centrifugation at 300g for 10 minutes at room temperature was then performed and cells were resuspended in 300 µl of D-PBS. Prior to sorting, neurons were labeled with 0.05 µg/ml DAPI.

aiFACS and cell sorting. Cells were sorted, using a 100 μ m nozzle, on a FACSaria III (BD Biosciences) equipped with four lasers. Fluo-4, Alexa Fluor 594, DAPI, Alexa Fluor 647, and APC-Cy7 (Invitrogen) were excited at 488nm, 561nm, 405nm, and 633nm respectively, and detected through BP530/30, BP610/20, BP450/40, BP660/20, and BP780/60 filters. The sorter was implemented with a homemade injection system (Figure 1A). The sample line was improved, upstream of the solenoid valve, with an injection system composed of two syringes controlled by valves and a peristaltic micro-pump. D-PBS was put in the first syringe. A 1,6X agonist solution (100 mM KCl or 200 μ M AMPA or 10 μ M ionomycin) was prepared and APC-CY7- labeled CompBead compensation particles (BD Biosciences) were added to the solution before putting it in the second injection syringe. Both the MINIPULS 3 peristaltic pump (Gilson) and the cytometer flow rate were set to 39 μ l/min. Baseline acquisition and sorting were done with the valve of the buffer syringe opened. Once the valve of the agonist syringe was opened, the valve of the buffer syringe was closed. The agonist solution running in the flow cell was monitored by the appearance of the beads. In this moment the agonist-responding cells started to be sorted. Cells were collected in D-PBS. Data were analyzed with BD FACSDiva v6 software (BD Biosciences).

Gating strategy. Cells and beads are identified by their size/structure profile. A first region "cells" is drawn around the GD1 population. Next, the living cells are identified as DAPI negative. Doublets are excluded on morphological parameters SSC then FSC. Among the living cells, in singlets, a graph of the fluorescence of WGAs coupled either to Alexa Fluor 594 (605/40 channel) or to Alexa Fluor 647 (APC channel) allows us to identify the cells from each mouse phenotype. For each mouse, the basal level of Fluo-4 is represented as a function of cell size. A region above this baseline is defined and will be used to identify the cells that respond to the agonist so that we can sort them. The appearance of the beads gives the signal for the start of the stimulation and thus the sorting (Supplemental Figure S2).

RNA preparation and RT-qPCR. Total RNA from aiFACS-sorted cells was extracted using Trizol reagent (Sigma) according to the manufacturer's instructions. In each experimental sample 1 μ g of

RNA (Supplemental Figure S1) or 5,000 cells (Fig. 2B, 4B, 5A, 5B and Supplemental Figure S6) per condition were used. RNA was purified using 500 µl of Trizol reagent and precipitated from the aqueous phase with 500 µl of Isopropanol (VWR Medicals) and 1 µl of glycogen (20 µg/µl, Invitrogen). RNA was resuspended in 20 µl (Supplemental Figure S1) or 11 µl (Fig. 2B, 4B, 5A, 5B and Supplemental Figure S6) of Nuclease Free H₂O. Either 1 µg (Supplemental Figure S1) or 11 µl (Fig. 2B, 4B, 5A, 5B and Supplemental Figure S6) of RNA were added to the RT reaction that was performed using the Superscript IV synthesis kit (Invitrogen). An initial amplification was done with a denaturation step at 65°C for 5 min, followed by oligo d(T) annealing at 23°C for 10 min, primer annealing at 53°C for 10 min and primer extension at 80°C for 10 min. Upon completion of the cycling steps, the reactions were stored at -20°C. Quantitative PCR (RT-qPCR) was performed on a Light Cycler 480 (Roche) with MasterMix SYBRGreen (Roche) following the manufacturer's instructions and according to the MIQE guidelines (Bustin et al. 2009). Primer sequences are presented in Supplemental Table S1.

Immunofluorescence and antibodies. aiFACS-sorted neurons were plated on ornithine-coated glass coverslips (35 mm diameter) and cultivated in complete medium: Neurobasal (Invitrogen) supplemented with B-27 (Invitrogen) and GlutaMAX (Invitrogen) as previously described (Abekhoukh et al. 2017; Maurin et al. 2019). Neurons were fixed and immunofluorescence was carried out with Microtubule Associated Protein 2 (MAP2; Bio Legend) antibody detected with a secondary Goat anti-chicken Alexa 594 (Invitrogen) 6 days after the selection as previously described (Drozd et al. 2019). Fluorescent images were taken using a wide-field upright fluorescence microscope (Axioplan2, Carl Zeiss, Marly-le-Roi, France), with an ORCA ER CCD camera (Hamamatsu, Massy, France) through a Rhodamine filter set (BP565/30 ; LP585 ; BP620/60) and a PlanApoChormat 63x/1.4 DIC oil immersion objective (pixel size : 100nm).

Microglia was labeled as previously described (Cazareth et al. 2014) using the following antibodies BV510 anti-mouse CD45: clone 30-F11 (BD Biosciences) and AlexaFluor700 anti-mouse CD11b: clone M1/70 (Sony Biotechnonolgy).

Droplet-based scRNA-seq. Single-cell suspensions were converted to barcoded scRNA-seq libraries using the Chromium Single Cell 3' Library, Gel Bead & Multiplex Kit and Chip Kit (10x Genomics), aiming for an estimated 2,000 cells per library and following manufacturer's instructions. Samples were processed using kits pertaining to V2 barcoding chemistry of 10X Genomics. Libraries were sequenced on an Illumina NextSeq500, and mapped to the mouse genome (build mm10) using Cell Ranger (10X Genomics). Gene positions were annotated as per Ensembl build 84.

Single-cell gene expression quantification and determination of the major cell types. Raw gene expression matrices generated per sample using Cell Ranger (version 2.0.0) were loaded and processed in R (version 3.4.3). Samples were analyzed independently within the Seurat workflow using the Seurat R package (version 3.0.0). First, cells that had over 95% dropouts were removed. Gene expression matrices from remaining cells were normalized using SCTransform from Seurat package. To reduce dimensionality of each dataset, the resulting variably expressed genes were summarized by principal component analysis, and the first 30 principal components further summarized using UMAP dimensionality reduction. The three samples independent analyses were then integrated using Canonical Correlation Analysis (CCA). The analysis workflow was then re-run on an integrated dataset. Cell clusters in the resulting UMAP two-dimensional representation were annotated to known biological cell types using canonical marker genes described in literature (Paul et al. 2017; Rosenberg et al. 2018; Tasic et al. 2016; Mi et al. 2018; Zeisel et al. 2015; Zeisel et al. 2018; La Manno et al. 2016).

Statistics. Statistical tests used in each experiment are indicated in the figure legends. Data are expressed as mean \pm SEM and the p values (or adjusted p values) < 0.05 were considered as statistically significant. Statistical analysis was performed using Prism Software version 7 (GraphPad Software, Inc.).

DATA AVAILABILITY

Single-cell transcriptomic data are deposited in the GEO database, accession number: GSE142274. All single-cell analyses R scripts will be made available through github (<https://github.com/ucagenomix/sc.castagnola.2020>).

ACKNOWLEDGMENTS

The authors are grateful to M. Beal, M. Capovilla, M. Drozd, M. Grossi for discussion, help and encouragement. This study was supported by Inserm, CNRS, Université Côte d’Azur, Fraxa Research Foundation, Fédération Recherche sur le Cerveau, Fondation Jérôme Lejeune and Agence Nationale de la Recherche: ANR-11-LABX-0028-01, ANR-15-CE16-0015 and ANR-15-IDEX-0001. The authors acknowledge the IPMC partner “Microscopie Imagerie Côte d’Azur” (MICA) GIS-IBiSA multi-sites platform supported by the GIS IBiSA. Conseil Départemental 06, Région PACA, ARC and Canceropôle PACA and “UCAGenomiX platform », partner of the National Infrastructure France Génomique, supported by the Commissariat aux Grands Investissements: ANR-10-INBS-09-03, and ANR-10-INBS-09-02.

Conflict of interest statement. None declared.

REFERENCES

- Abekhoukh S, Sahin HB, Grossi M, Zongaro S, Maurin T, Madrigal I, Kazue-Sugioka D, Raas-Rothschild A, Doulazmi M, Carrera P, et al. 2017. New insights into the regulatory function of CYFIP1 in the context of WAVE- and FMRP-containing complexes. *Dis Model Mech* **10**: 463–474.
- Agoston Z, Heine P, Brill MS, Grebbin BM, Hau A-C, Kallenborn-Gerhardt W, Schramm J, Götz M, Schulte D. 2014. Meis2 is a Pax6 co-factor in neurogenesis and dopaminergic periglomerular fate specification in the adult olfactory bulb. *Development* **141**: 28–38.
- Allen ZJ, Waclaw RR, Colbert MC, Campbell K. 2007. Molecular identity of olfactory bulb interneurons: transcriptional codes of periglomerular neuron subtypes. *J Mol Histol* **38**: 517–525.
- Arnoldini M, Heck T, Blanco-Fernández A, Hammes F. 2013. Monitoring of dynamic microbiological processes using real-time flow cytometry. *PloS One* **8**: e80117.
- Barritt GJ. 1999. Receptor-activated Ca²⁺ inflow in animal cells: a variety of pathways tailored to meet different intracellular Ca²⁺ signalling requirements. *Biochem J* **337** (Pt 2): 153–169.
- Berl S, Karram K, Scheller A, Jungblut M, Kirchhoff F, Waisman A. 2017. Enrichment and isolation of neurons from adult mouse brain for ex vivo analysis. *J Neurosci Methods* **283**: 15–22.
- Bito H, Deisseroth K, Tsien RW. 1996. CREB Phosphorylation and Dephosphorylation: A Ca²⁺- and Stimulus Duration-Dependent Switch for Hippocampal Gene Expression. *Cell* **87**: 1203–1214.
- Bustin SA, Benes V, Garson JA, Hellemans J, Huggett J, Kubista M, Mueller R, Nolan T, Pfaffl MW, Shipley GL, et al. 2009. The MIQE guidelines: minimum information for publication of quantitative real-time PCR experiments. *Clin Chem* **55**: 611–622.
- Cadwell CR, Palasantza A, Jiang X, Berens P, Deng Q, Yilmaz M, Reimer J, Shen S, Bethge M, Tolias KF, et al. 2016. Electrophysiological, transcriptomic and morphologic profiling of single neurons using Patch-seq. *Nat Biotechnol* **34**: 199–203.
- Cazareth J, Guyon A, Heurteaux C, Chabry J, Petit-Paitel A. 2014. Molecular and cellular neuroinflammatory status of mouse brain after systemic lipopolysaccharide challenge: Importance of CCR2/CCL2 signaling. *Journal of Neuroinflammation* **11**: undefined-undefined.
- Castagnola S, Delhaye S, Folci A, Paquet A, Brau F, Duprat F, Jarjat M, Grossi M, Béal M, Martin S, et al. 2018. New Insights Into the Role of Cav2 Protein Family in Calcium Flux Deregulation in Fmr1-KO Neurons. *Front Mol Neurosci* **11**: 342.
- Cea-Del Rio CA, Huntsman MM. 2014. The contribution of inhibitory interneurons to circuit dysfunction in Fragile X Syndrome. *Front Cell Neurosci* **8**: 245.
- Cheng G-R, Li X-Y, Xiang Y-D, Liu D, Mcclintock SM, Zeng Y. 2017. The Implication of AMPA Receptor in Synaptic Plasticity Impairment and Intellectual Disability in Fragile X Syndrome. *66*: 13.

- Chow S, Patel H, Hedley DW. 2001. Measurement of MAP kinase activation by flow cytometry using phospho-specific antibodies to MEK and ERK: Potential for pharmacodynamic monitoring of signal transduction inhibitors. *Cytometry* **46**: 72–78.
- Contractor A, Klyachko VA, Portera-Cailliau C. 2015. Altered neuronal and circuit excitability in Fragile X Syndrome. *Neuron* **87**: 699–715.
- Datta S, Malhotra L, Dickerson R, Chaffee S, Sen CK, Roy S. 2015. Laser capture microdissection: Big data from small samples. *Histol Histopathol* **30**: 1255–1269.
- Drozd M, Delhaye S, Maurin T, Castagnola S, Grossi M, Brau F, Jarjat M, Willemse R, Capovilla M, Hukema RK, et al. 2019. Reduction of Fmr1 mRNA Levels Rescues Pathological Features in Cortical Neurons in a Model of FXTAS. *Mol Ther Nucleic Acids* **18**: 546–553.
- Dunne JF. 1991. Time window analysis and sorting. *Cytometry* **12**: 597–601.
- Ferron L. 2016. Fragile X mental retardation protein controls ion channel expression and activity. *J Physiol (Lond)* **594**: 5861–5867.
- Fujiwara N, Cave JW. 2016. Partial Conservation between Mice and Humans in Olfactory Bulb Interneuron Transcription Factor Codes. *Front Neurosci* **10**: 337.
- Fulwyler MJ. 1965. Electronic Separation of Biological Cells by Volume. *Science* **150**: 910–911.
- Fuzik J, Zeisel A, Máté Z, Calvignoni D, Yanagawa Y, Szabó G, Linnarsson S, Harkany T. 2016. Integration of electrophysiological recordings with single-cell RNA-seq data identifies neuronal subtypes. *Nat Biotechnol* **34**: 175–183.
- Giliberti A, Currò A, Papa FT, Frullanti E, Ariani F, Coriolani G, Grosso S, Renieri A, Mari F. 2019. MEIS2 gene is responsible for intellectual disability, cardiac defects and a distinct facial phenotype. *Eur J Med Genet* 103627.
- Goel A, Cantu DA, Guilfoyle J, Chaudhari GR, Newadkar A, Todisco B, de Alba D, Kourdougli N, Schmitt LM, Pedapati E, et al. 2018. Impaired perceptual learning in a mouse model of Fragile X syndrome is mediated by parvalbumin neuron dysfunction and is reversible. *Nat Neurosci* **21**: 1404–1411.
- Holt LM, Olsen ML. 2016. Novel Applications of Magnetic Cell Sorting to Analyze Cell-Type Specific Gene and Protein Expression in the Central Nervous System. *PLOS ONE* **11**: e0150290.
- Kelley KA. 1989. Sample station modification providing on-line reagent addition and reduced sample transit time for flow cytometers. *Cytometry* **10**: 796–800.
- Kilkenny C, Browne WJ, Cuthill IC, Emerson M, Altman DG. 2010. Improving Bioscience Research Reporting: The ARRIVE Guidelines for Reporting Animal Research. *PLOS Biol* **8**: e1000412.
- Le Magueresse C, Monyer H. 2013. GABAergic Interneurons Shape the Functional Maturation of the Cortex. *Neuron* **77**: 388–405.
- La Manno G, Gyllborg D, Codeluppi S, Nishimura K, Salto C, Zeisel A, Borm LE, Stott SRW, Toledo EM, Villaescusa JC, et al. 2016. Molecular Diversity of Midbrain Development in Mouse, Human, and Stem Cells. *Cell* **167**: 566–580.e19.

- Li M, Shin J, Risgaard RD, Parries MJ, Wang J, Chasman D, Liu S, Roy S, Bhattacharyya A, Zhao X. 2020. Identification of FMR1-regulated molecular networks in human neurodevelopment. *Genome Res.* **30**:361–374.
- Maurin T, Bardoni B. 2018. Fragile X Mental Retardation Protein: To Be or Not to Be a Translational Enhancer. *Front Mol Biosci* **5**:113.
- Maurin T, Lebrigand K, Castagnola S, Paquet A, Jarjat M, Popa A, Grossi M, Rage F, Bardoni B. 2018. HITS-CLIP in various brain areas reveals new targets and new modalities of RNA binding by fragile X mental retardation protein. *Nucleic Acids Res* **46**: 6344–6355.
- Maurin T, Melancia F, Jarjat M, Castro L, Costa L, Delhaye S, Khayachi A, Castagnola S, Mota E, Di Giorgio A, et al. 2019. Involvement of Phosphodiesterase 2A Activity in the Pathophysiology of Fragile X Syndrome. *Cereb Cortex* **29**: 3241–3252.
- Mi D, Li Z, Lim L, Li M, Moissidis M, Yang Y, Gao T, Hu TX, Pratt T, Price DJ, et al. 2018. Early emergence of cortical interneuron diversity in the mouse embryo. *Science* **360**: 81–85.
- Mientjes EJ, Nieuwenhuizen I, Kirkpatrick L, Zu T, Hoogeveen-Westerveld M, Severijnen L, Rifé M, Willemsen R, Nelson DL, Oostra BA. 2006. The generation of a conditional Fmr1 knock out mouse model to study Fmrp function in vivo. *Neurobiol Dis* **21**: 549–555.
- Miyashiro KY, Beckel-Mitchener A, Purk TP, Becker KG, Barret T, Liu L, Carbonetto S, Weiler IJ, Greenough WT, Eberwine J. 2003. RNA cargoes associating with FMRP reveal deficits in cellular functioning in Fmr1 null mice. *Neuron* **37**: 417–431.
- Ofengeim D, Mazzitelli S, Ito Y, DeWitt JP, Mifflin L, Zou C, Das S, Adiconis X, Chen H, Zhu H, et al. 2017. RIPK1 mediates a disease-associated microglial response in Alzheimer’s disease. *Proc Natl Acad Sci* **114**: E8788–E8797.
- Olmos-Serrano JL, Palusziewicz SM, Martin BS, Kaufmann WE, Corbin JG, Huntsman MM. 2010. Defective GABAergic Neurotransmission and Pharmacological Rescue of Neuronal Hyperexcitability in the Amygdala in a Mouse Model of Fragile X Syndrome. *J Neurosci* **30**: 9929–9938.
- Patel AB, Hays SA, Bureau I, Huber KM, Gibson JR. 2013. A Target Cell-Specific Role for Presynaptic Fmr1 in Regulating Glutamate Release onto Neocortical Fast-Spiking Inhibitory Neurons. *J Neurosci* **33**: 2593–2604.
- Paul A, Crow M, Raudales R, He M, Gillis J, Huang ZJ. 2017. Transcriptional Architecture of Synaptic Communication Delineates GABAergic Neuron Identity. *Cell* **171**: 522–539.e20.
- Pollen AA, Nowakowski TJ, Shuga J, Wang X, Leyrat AA, Lui JH, Li N, Szpankowski L, Fowler B, Chen P, et al. 2014. Low-coverage single-cell mRNA sequencing reveals cellular heterogeneity and activated signaling pathways in developing cerebral cortex. *Nat Biotechnol* **32**: 1053–1058.
- Poulin J-F, Tasic B, Hjerling-Leffler J, Trimarchi JM, Awatramani R. 2016. Disentangling neural cell diversity using single-cell transcriptomics. *Nat Neurosci* **19**: 1131–1141.
- Richter JD, Coller J. 2015. Pausing on Polyribosomes: Make Way for Elongation in Translational Control. *Cell* **163**: 292–300.
- Rosenberg AB, Roco CM, Muscat RA, Kuchina A, Sample P, Yao Z, Graybuck LT, Peeler DJ, Mukherjee S, Chen W, et al. 2018. Single-cell profiling of the developing mouse brain and spinal cord with split-pool barcoding. *Science* **360**: 176–182.

- Rosenberg SS, Spitzer NC. 2011. Calcium signaling in neuronal development. *Cold Spring Harb Perspect Biol* **3**: a004259.
- Tang B, Wang T, Wan H, Han L, Qin X, Zhang Y, Wang J, Yu C, Berton F, Francesconi W, et al. 2015. Fmr1 deficiency promotes age-dependent alterations in the cortical synaptic proteome. *Proc Natl Acad Sci U S A* **112**: E4697–E4706.
- Tárnok A. 1996. Improved kinetic analysis of cytosolic free calcium in pressure-sensitive neuronal cells by fixed-time flow cytometry. *Cytometry* **23**: 82–89.
- Tasic B, Menon V, Nguyen TN, Kim TK, Jarsky T, Yao Z, Levi B, Gray LT, Sorensen SA, Dolbear T, et al. 2016. Adult Mouse Cortical Cell Taxonomy by Single Cell Transcriptomics. *Nat Neurosci* **19**: 335–346.
- Taylor CW. 2002. Controlling Calcium Entry. *Cell* **111**: 767–769.
- Verheije R, Kupchik GS, Isidor B, Kroes HY, Lynch SA, Hawkes L, Hempel M, Gelb BD, Ghoumid J, D'Amours G, et al. 2019. Heterozygous loss-of-function variants of MEIS2 cause a triad of palatal defects, congenital heart defects, and intellectual disability. *Eur J Hum Genet* **27**: 278–290.
- Vines A, McBean GJ, Blanco-Fernández A. 2010. A flow-cytometric method for continuous measurement of intracellular Ca²⁺ concentration. *Cytometry A* **77A**: 1091–1097.
- Yang Y-M, Arsenault J, Bah A, Krzeminski M, Fekete A, Chao OY, Pacey LK, Wang A, Forman-Kay J, Hampson DR, et al. 2018. Identification of a molecular locus for normalizing dysregulated GABA release from interneurons in the Fragile X brain. *Mol Psychiatry* DOI: [10.1038/s41380-018-0240-0](https://doi.org/10.1038/s41380-018-0240-0)
- Zeisel A, Hochgerner H, Lönnberg P, Johnsson A, Memic F, van der Zwan J, Häring M, Braun E, Borm LE, La Manno G, et al. 2018. Molecular Architecture of the Mouse Nervous System. *Cell* **174**: 999-1014.e22.
- Zeisel A, Muñoz-Manchado AB, Codeluppi S, Lönnberg P, Manno GL, Juréus A, Marques S, Munguba H, He L, Betsholtz C, et al. 2015. Cell types in the mouse cortex and hippocampus revealed by single-cell RNA-seq. *Science* **347**: 1138–1142.
- Zwartz GJ, Chigae A, Foutz TD, Edwards B, Sklar LA. 2011. A miniature Couette to generate shear for flow cytometry: studying real-time modulation of intracellular calcium in monocytic cells. *Cytom Part J Int Soc Anal Cytol* **79**: 233–240.

FIGURE LEGENDS

FIGURE 1. The aiFACS technique. **A)** Schema of the instrumental apparatus: BD FACSaria III implemented with the aiFACS device. The fluidics of the sorter is modified to allow the injection of a pharmacological agonist. Two syringes, one containing D-PBS (in grey) and the other containing the agonist (in green) are connected to their respective tubing: the D-PBS tubing (in grey) and the agonist tubing (in green). These are further connected to a downstream Y-shaped connector that enters the flow cell (the chamber in which the cells are aligned to pass one-by-one through the light beam for sensing). The sample is connected to the sorter through a tubing (in blue) having the same diameter as the agonist tubing (in green). A peristaltic micro-pump (P) allows to control the speed of solution injection and to synchronize it to the speed of sample flow in the sorter. The incubation time between each cell of the sample and the agonist is also controlled (red tubing). **B)** Time *vs* Fluo-4 AM bi-parametric graph showing the response of the cells to different stimuli in real time. At time t0 the opening of the D-PBS valve starts the perfusion and the baseline levels of fluorescence (in the red rectangle) are obtained with continuous perfusion. At time t1 the D-PBS valve is closed and that of the agonist is opened. The magnitude of the cellular calcium response to the KCl agonist (50 mM final) is shown in the light-blue rectangle. At time t2 ionomycin is added to KCl as a positive control of stimulation. The maximal response of the cells is displayed in the green rectangle. **C)** Addition of beads to the agonist solution allows real time detection of the agonist presence. Bead fluorescence is shown in purple. **D)** aiFACS allows viable recovery of stimulated cells. Upper panels: discrimination of cells based on scatter parameters (FSC: forward scatter; SSC: side scatter) before sorting (55.3 % of the total population; left panel). The pre-sort viability is determined by labelling the cells with DAPI (95.5 % of the cells in the red region; right panel). Lower panels: discrimination of cells based on scatter parameters (FSC: forward scatter; SSC: side scatter) after sorting (90.9 % of the total population; left panel). The viability of the cells after KCl stimulation and aiFACS sorting is determined by re-analyzing the DAPI staining (99.7 % of the cells in the red region; right panel). **E)** Sorted neurons are viable and can grow neurites when plated on L-ornitin-coated glass coverslips,

cultivated for up to 6 Days *In Vitro* (DIV 6) in complete neurobasal medium and analyzed by immunocytochemistry (MAP2 staining). 63X Magnification - Scale bars: 10 μm .

FIGURE 2. The gating strategy. **A)** Discrimination of cells based on scatter parameters (FSC: forward scatter; SSC: side scatter). Cells were gated according to their size/structure. GD1: gating-dependent cell population 1; GD2: gating-dependent cell population 2. **B)** RNA was purified from WT GD1 and GD2 cells. Neuronal and non-neuronal marker levels were analyzed in both populations by RT-qPCR. The graph (on the left) shows mRNA expression relative to the total WT neuron suspension (WT input). GD1 and GD2 cells were live-imaged two hours after aiFACS sorting (on the right). 63X Magnification - Scale bars: 15 μm .

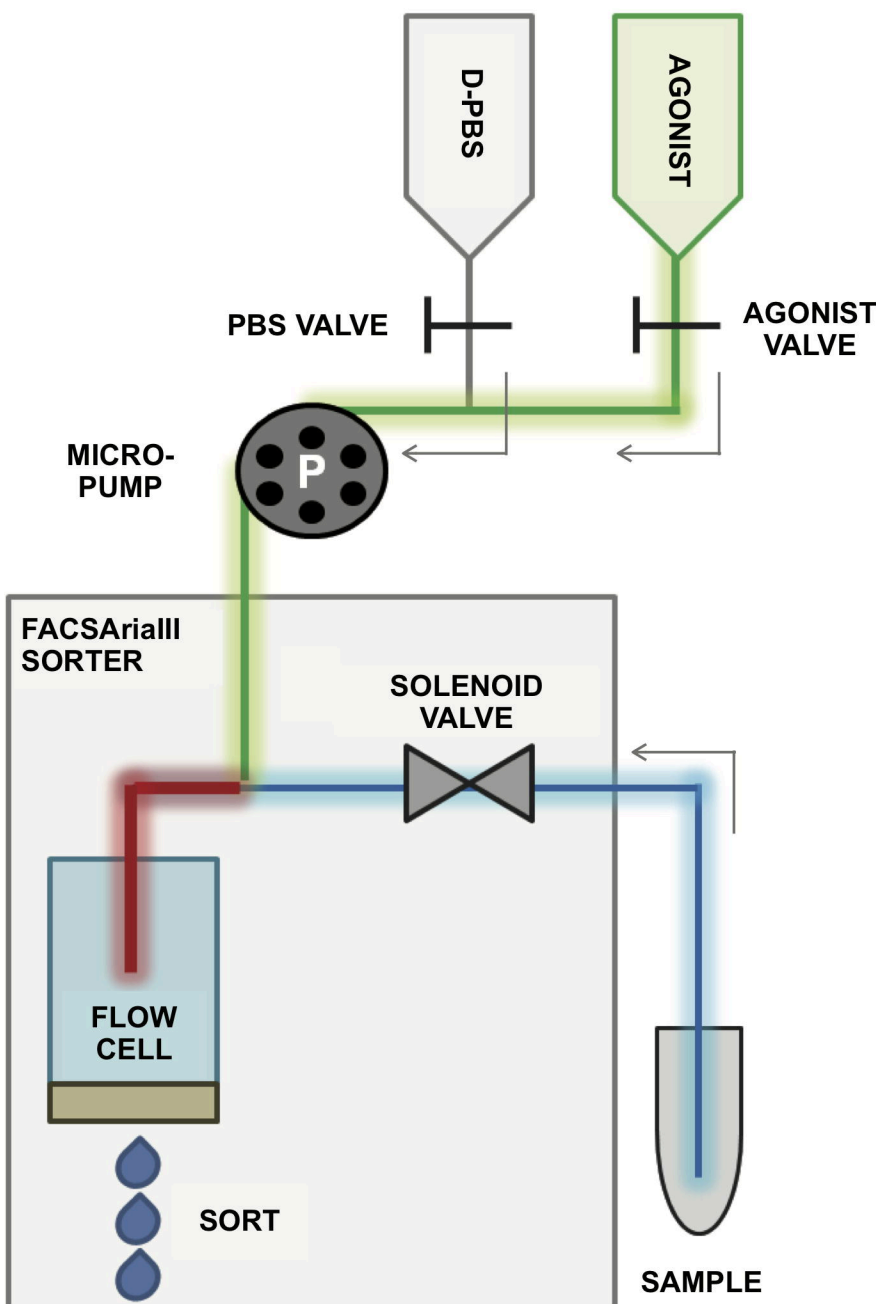
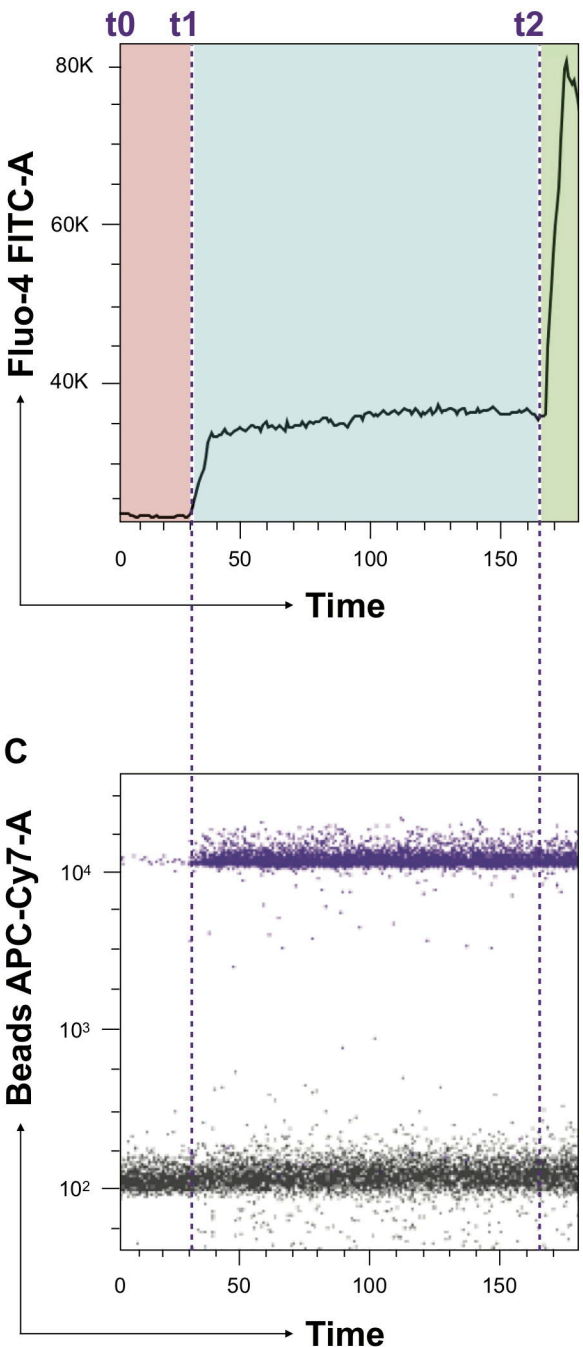
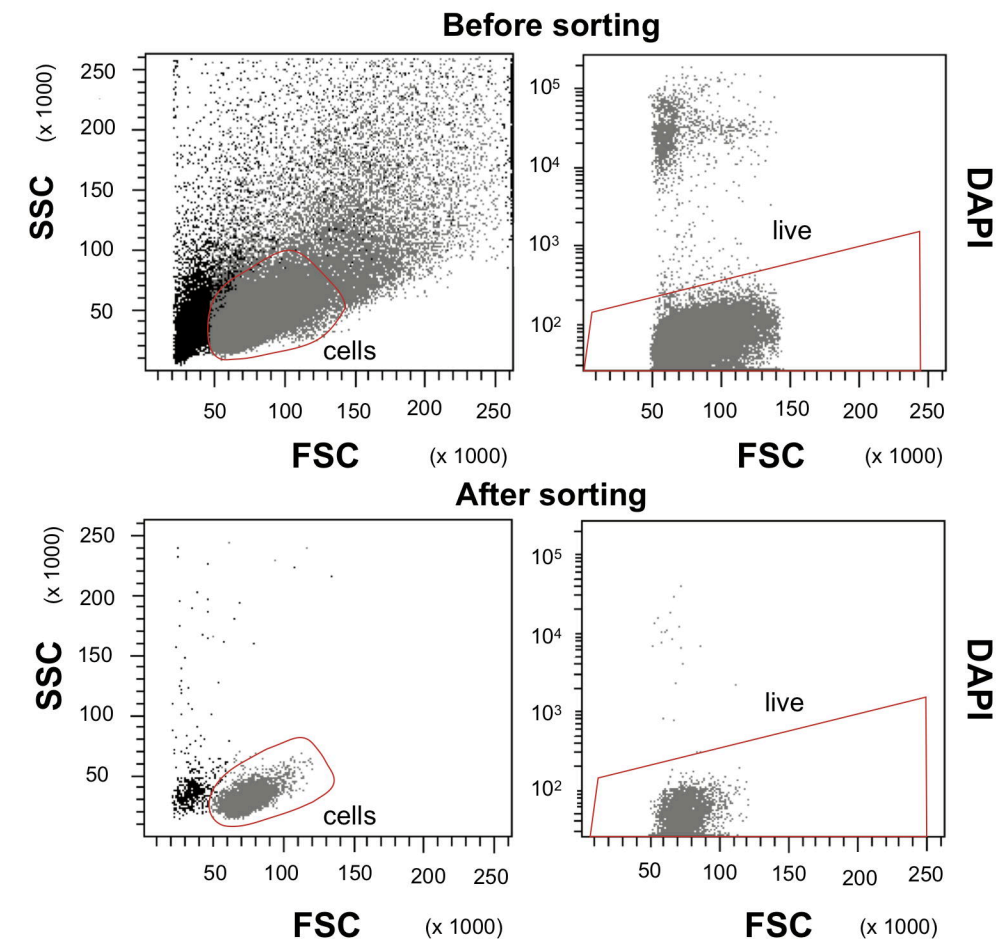
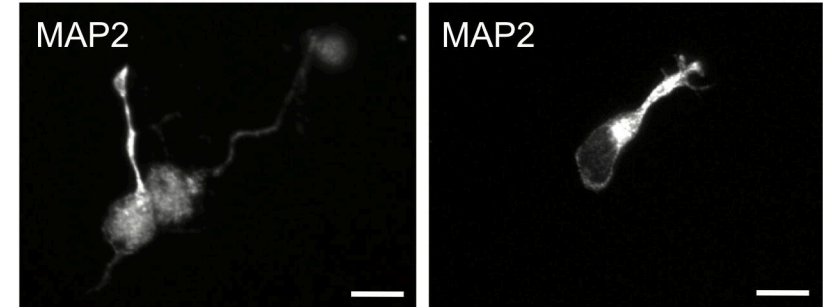
FIGURE 3. Single-cell transcriptomic analysis of GD1 cells. **A)** Heatmap of marker gene expression for the nine identified cell clusters in the aggregated dataset before and after stimulation. Ex-*Neurod2*, Ex-*Sept4*, Ex-*Selm* and Ex-*Top2a*: excitatory clusters; Inh-*Top2a*, Inh-*Sox4*, and Inh-*Synpr*: inhibitory clusters. *Sema3c*: ependymal cells. *Akap7*: oligodendrocytes. **B)** UMAP representation of the distribution of the nine clusters. **C)** UMAP representation of the two aggregated WT samples: baseline and AMPA. **D)** UMAP representation of the *Meis2*-expressing cell cluster. **E)** UMAP representation of the *Neurod1*-expressing cell cluster. **F)** UMAP representation of the *Neurod2*-expressing cell cluster. **G)** UMAP representation of the *Gad2*-expressing cell cluster. **H)** Relative proportion of cells by cluster type for individual samples.

FIGURE 4. aiFACS multiplex analysis. **A)** Left panel: PND 18 WT and *Fmr1*-KO brains were processed by aiFACS. The brain dissociation is carried out mechanically with the gentleMACS™ Octo Dissociator (Miltenyi Biotec) and enzymatically with the Adult Brain Dissociation kit (Miltenyi Biotec). The selection of neuronal cells is performed magnetically with the Neuron Isolation Kit

(Miltenyi Biotec). Central panel: neurons from the two genotypes were multiplexed by fluorescent labeling with Wheat Germ Agglutinin (WGA; WGA647 for WT and WGA594 for *Fmr1*-KO), processed and analyzed simultaneously. Upper right panel: the injection of fluorescently-labeled beads simultaneous to the perfusion with AMPA (100 µM final) allows to monitor the agonist concentration in the flow cell. Central and lower panels: real-time monitoring of neuronal responses to AMPA stimulation through Fluo-4 fluorescence quantification. **B)** mRNA was purified from 5,000 GD1 cells and inhibitory and excitatory marker expression levels were quantified by RT-qPCR and compared in WT and *Fmr1*-KO. Marker expression upon AMPA stimulation at PND 18 in both genotypes is presented as the fold change respective to the expression of aiFACSeD WT neurons (input WT). Results are presented as the mean ± SEM, Mann-Whitney test. p values: *Meis2*, * p = 0.0159; *Neurod1* * p = 0.0317; *Neurod2* * p = 0.0286; *Gad2* ns p = 0.9048. For *Meis2*, *Neurod1* and *Gad2*: WT n = 4; *Fmr1*-KO n = 5. For *Neurod2*: WT n = 4; *Fmr1*-KO n = 4. Each n corresponds to two (non-littermate) mouse brains and it is the mean of two independent replicates. **C)** Percentage of cells belonging to the nine clusters after single-cell analysis of AMPA response in WT and *Fmr1*-KO GD1 cells. Ex-*Neurod2*, Ex-*Sept4*, Ex-Selm and Ex-*Top2a*: excitatory clusters; Inh-*Top2a*, Inh-*Sox4*, and Inh-*Synpr*: inhibitory clusters. *Sema3c*: ependymal cells. *Akap7*: oligodendrocytes.

FIGURE 5. Baseline gene expression at PND 18 and PND 19. A) At PND18, mRNA was purified from 5,000 GD1 cells and inhibitory and excitatory marker expression levels were quantified by RT-qPCR and compared between WT and *Fmr1*-KO brains. Baseline marker expression in both genotypes is presented respective to the expression of aiFACSeD WT neurons (input WT). Results are presented as the mean ± SEM, Mann-Whitney test. p values: *Meis2*, ns p = 0.1905; *Neurod1* * p = 0.00317; *Neurod2* * p = 0.0286; *Gad2* ns p = 0.7302. For *Meis2*, *Neurod1* and *Gad2*: WT n = 4; *Fmr1*-KO n = 5. For *Neurod2*: WT n = 4; *Fmr1*-KO n = 4. Each n corresponds to two non -littermate mouse brains and it is the mean of two independent replicates. **B)** At PN19, mRNA was purified from 5,000 GD1 cells and inhibitory and excitatory marker expression levels were quantified by RT-qPCR and compared between WT and *Fmr1*-KO brains. Baseline marker expression in both genotypes is

presented respective to the expression of aiFACSSed WT neurons (input WT). Results are presented as the mean \pm SEM, Mann-Whitney test. p values: *Meis2*, ns p = 0.285; *Neurod1* ns p = 0.2857; *Neurod2* ns p = 0.5714; *Gad2* ns p = 0.1905. For *Meis2*, *Neurod1* and *Gad2*: WT n = 5; *Fmr1*-KO n = 4. For *Neurod2*: WT n = 5; *Fmr1*-KO n = 3. Each n corresponds to two non-littermate mouse brains and it is the mean of two independent replicates.

A**B****D****E****Figure 1**

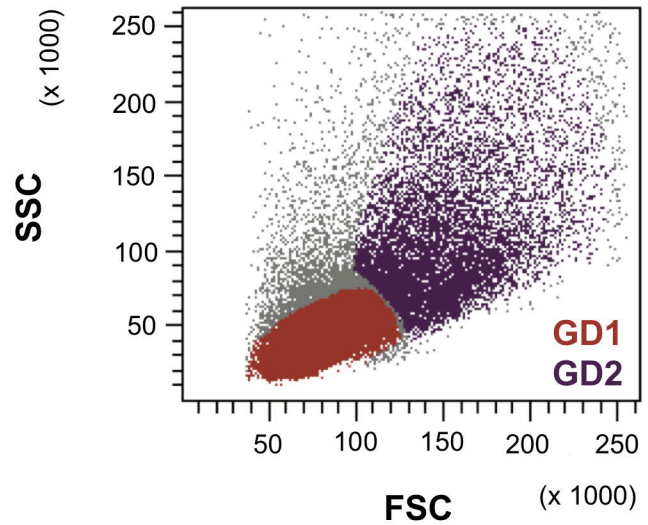
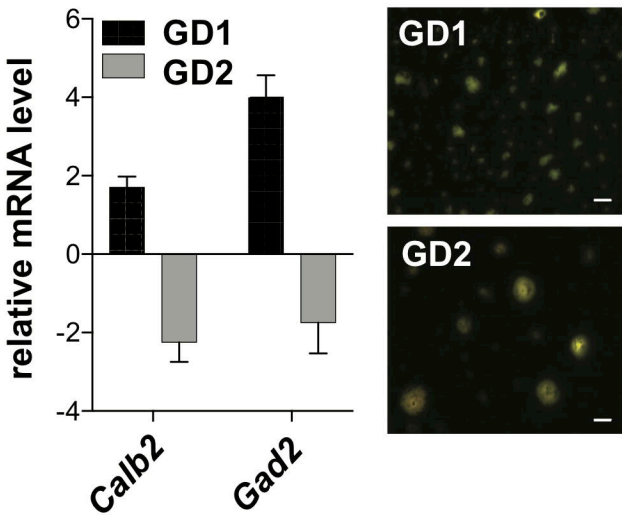
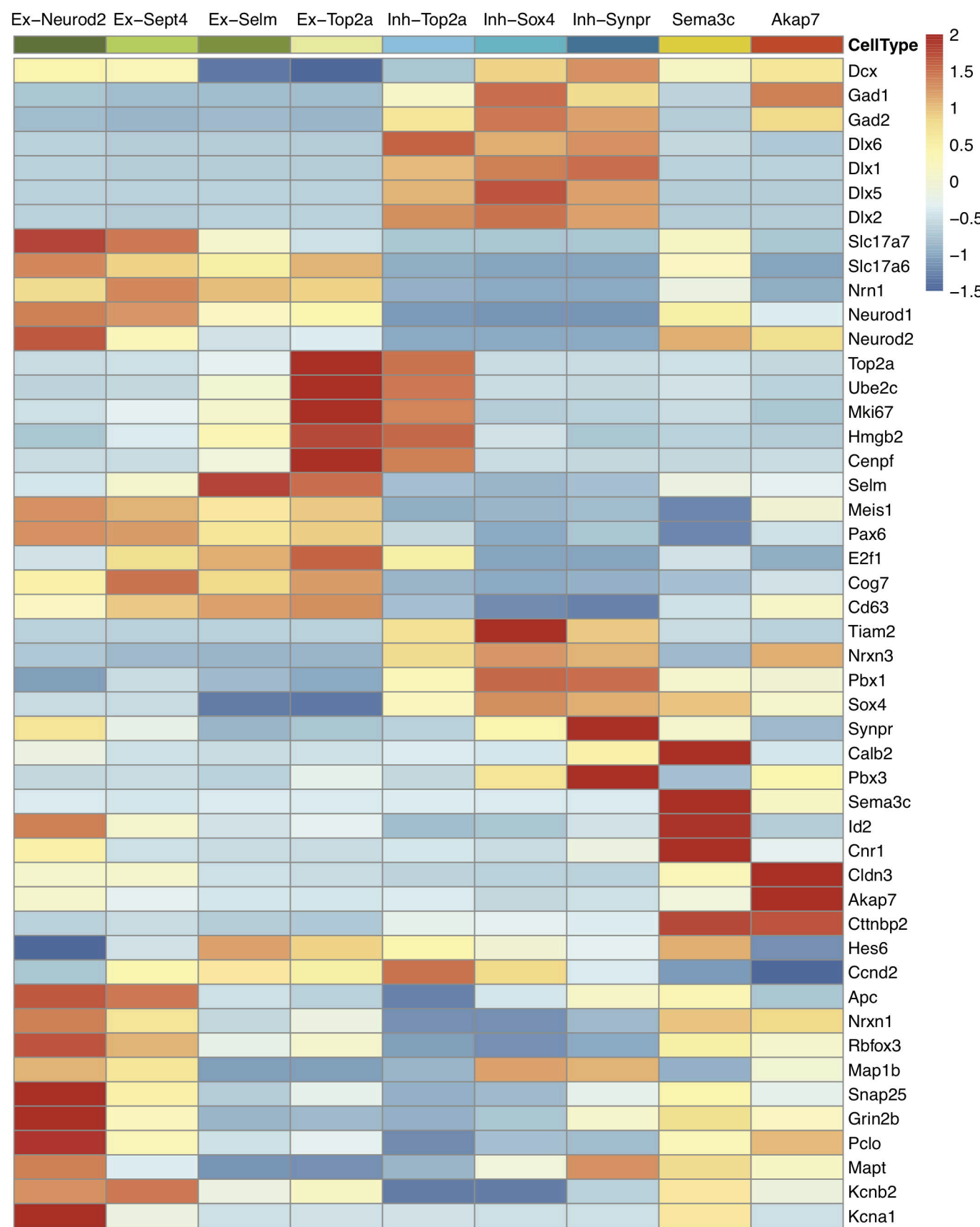
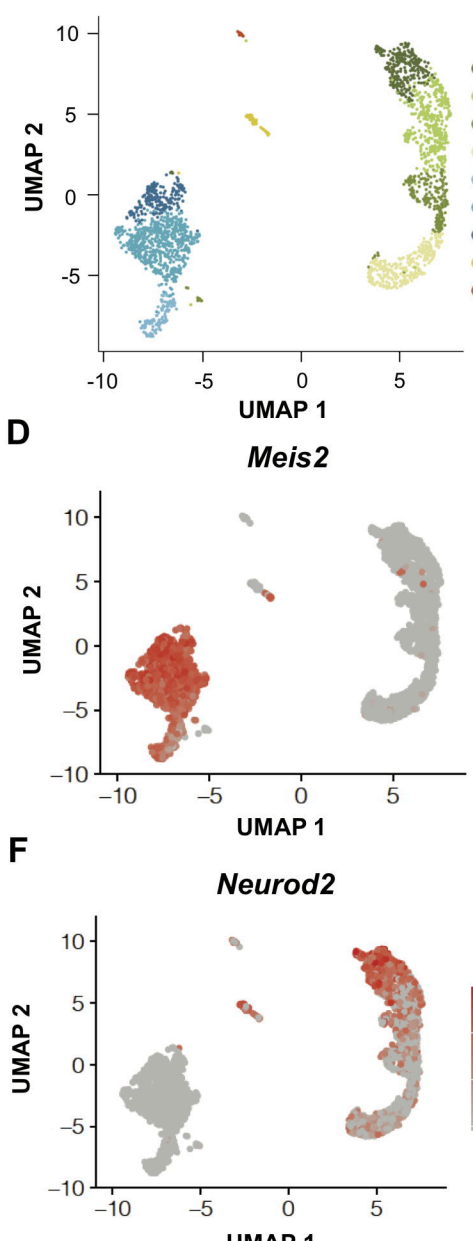
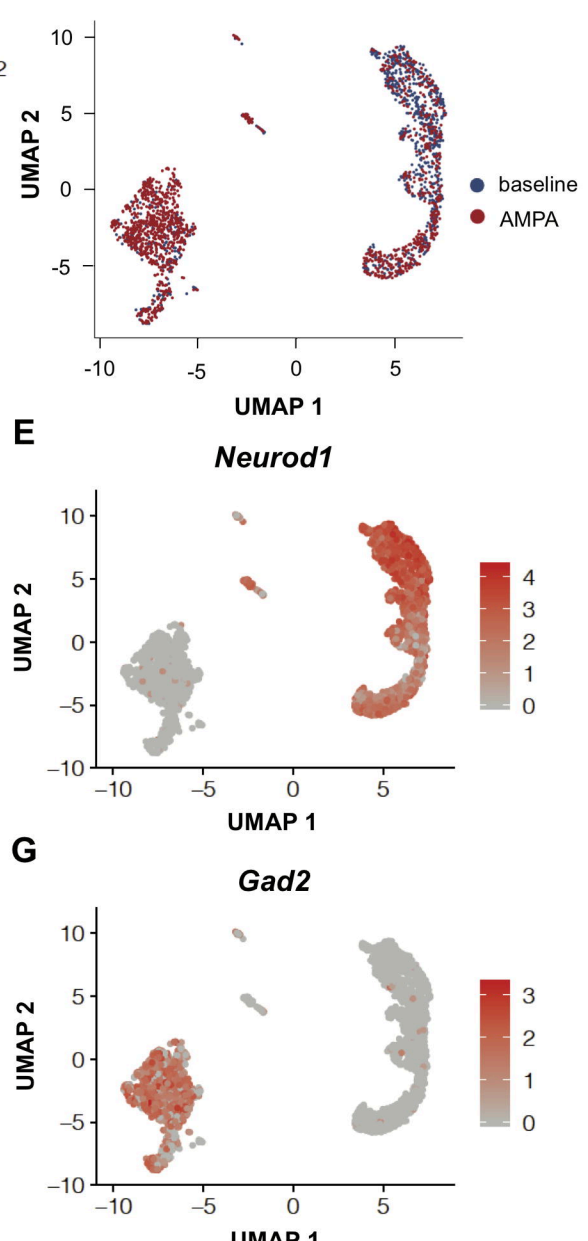
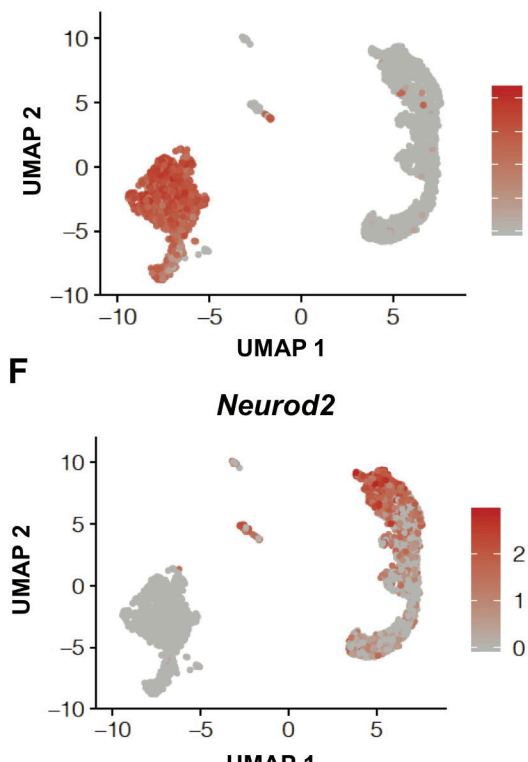
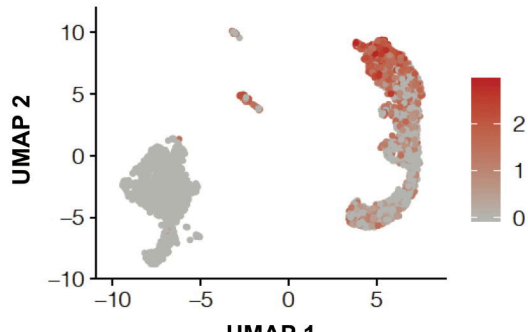
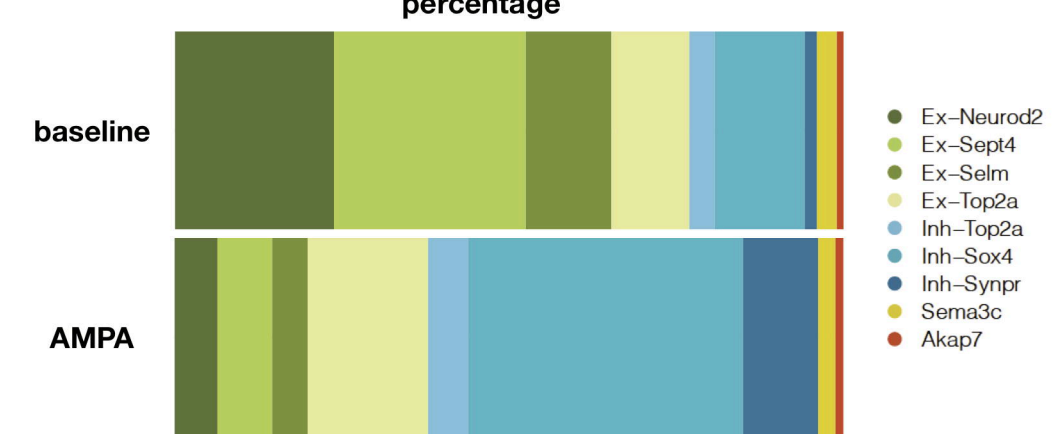
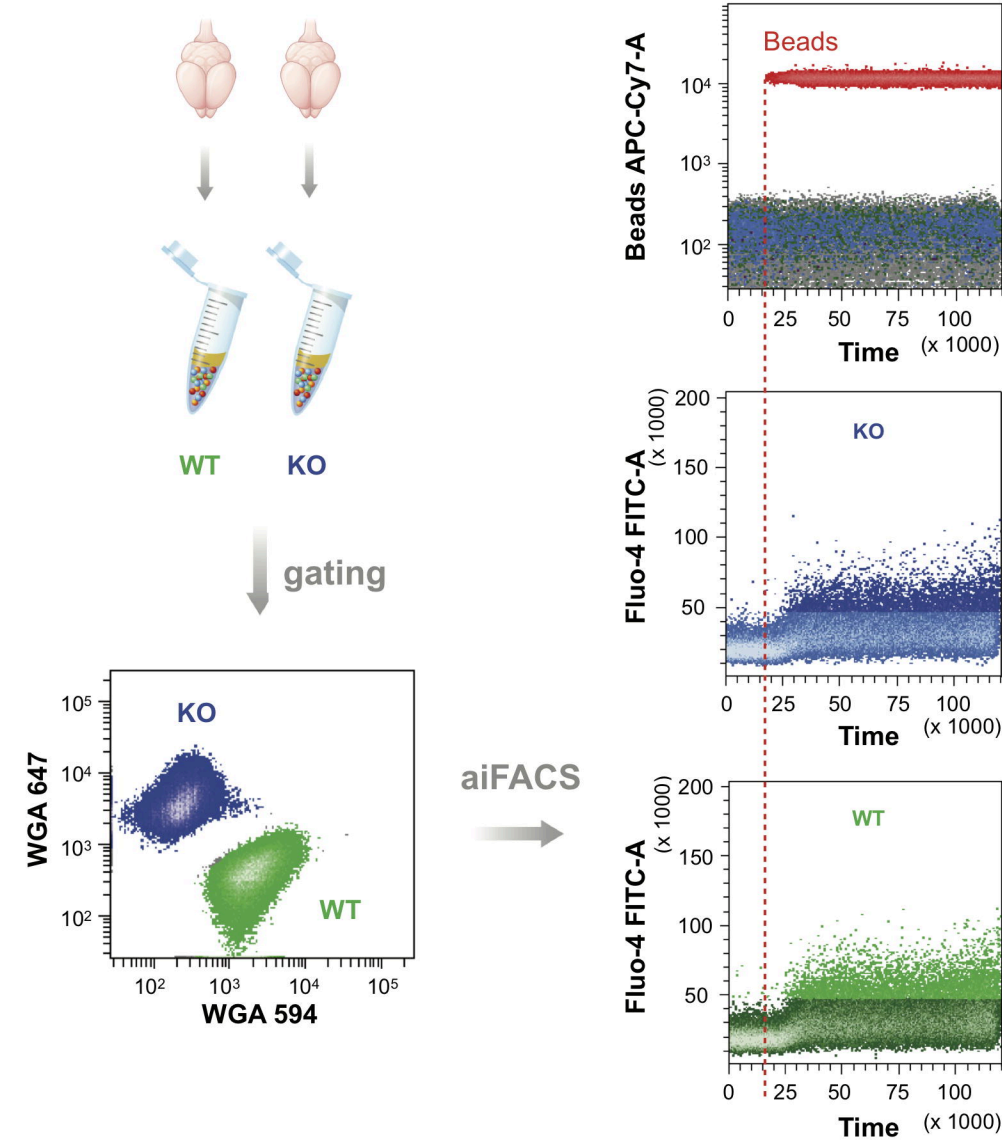
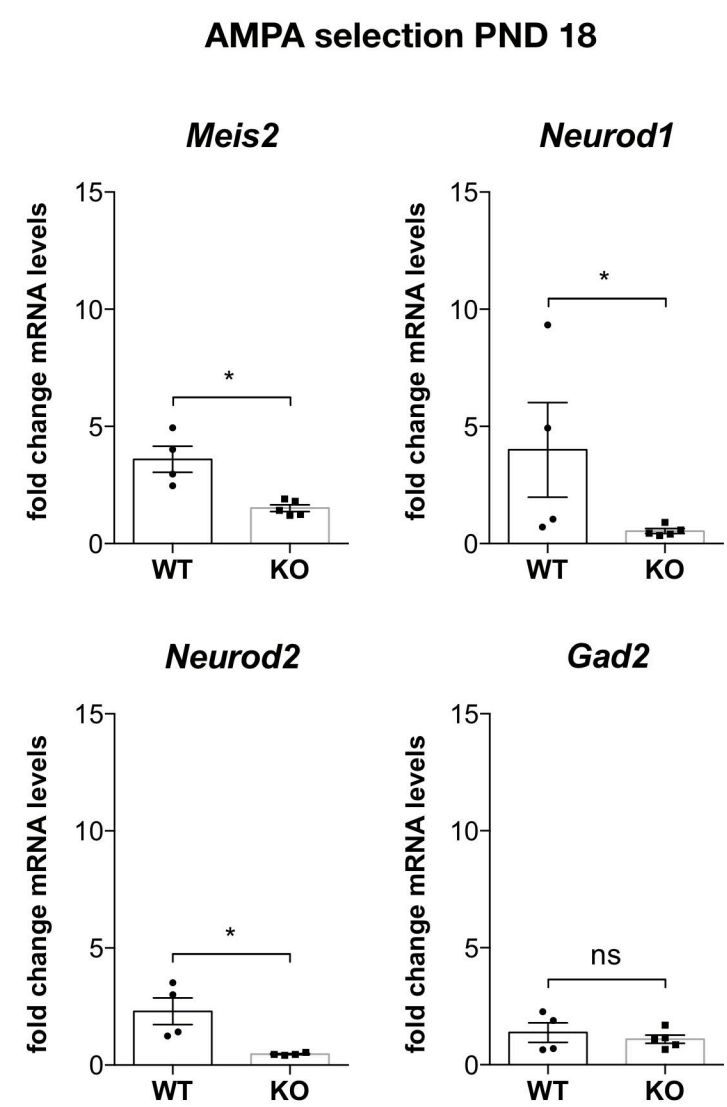
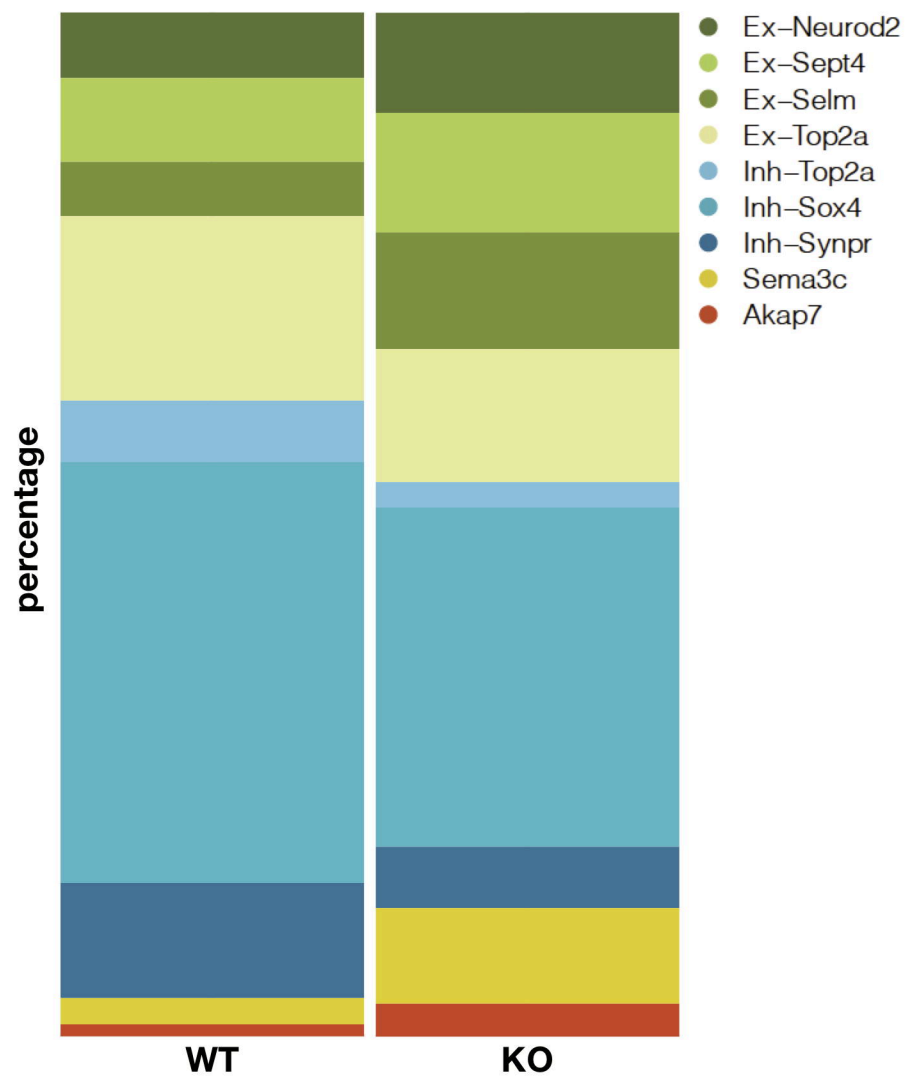
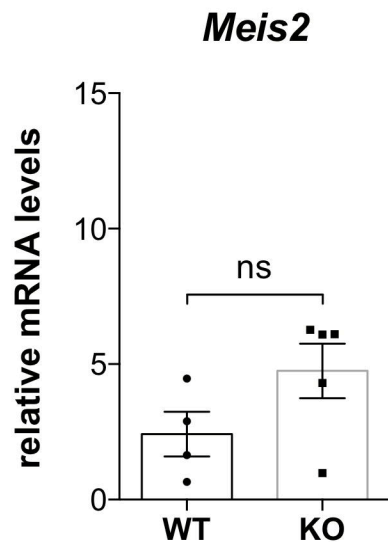
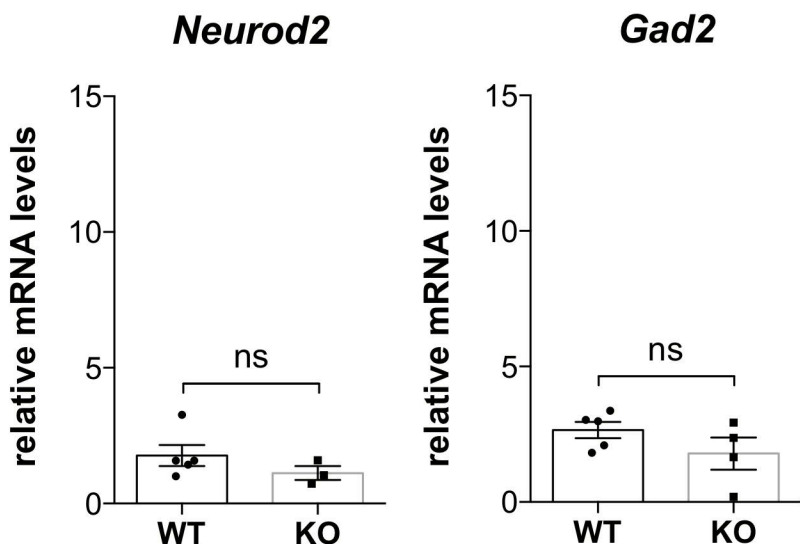
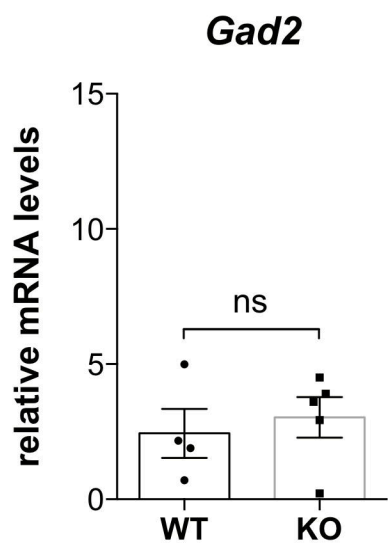
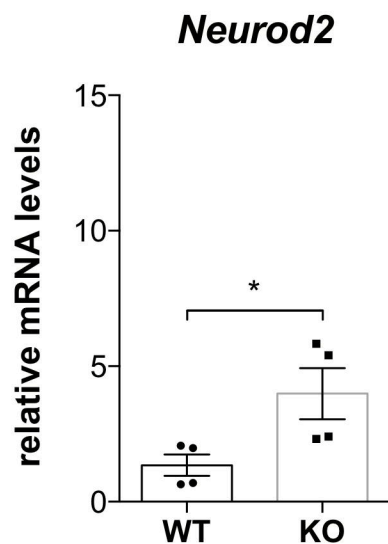
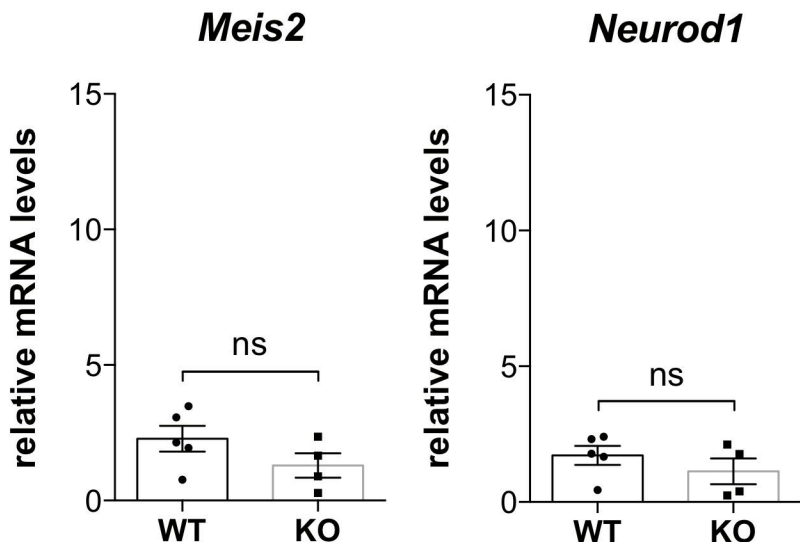
A**B**

Figure 2

Figure 3

A

B

C

D

F

H


A**B****C****Figure 4**

A**Baseline PND 18****B****Baseline PND 19****Figure 5**

Bibliographie

- Abekhoush, S., Bardoni, B., 2014. CYFIP family proteins between autism and intellectual disability: links with Fragile X syndrome. *Front. Cell. Neurosci.* 8.
<https://doi.org/10.3389/fncel.2014.00081>
- Abel, T., Nguyen, P.V., Barad, M., Deuel, T.A., Kandel, E.R., Bourchouladze, R., 1997. Genetic demonstration of a role for PKA in the late phase of LTP and in hippocampus-based longterm memory. *Cell* 88, 615–626. [https://doi.org/10.1016/s0092-8674\(00\)81904-2](https://doi.org/10.1016/s0092-8674(00)81904-2)
- Abitbol, M., Menini, C., Delezoide, A.-L., Rhyner, T., Vekemans, M., Mallet, J., 1993. Nucleus basalis magnocellularis and hippocampus are the major sites of FMR-1 expression in the human fetal brain. *Nat. Genet.* 4, 147–153. <https://doi.org/10.1038/ng0693-147>
- Acin-Perez, R., Russwurm, M., Günnewig, K., Gertz, M., Zoidl, G., Ramos, L., Buck, J., Levin, L.R., Rassow, J., Manfredi, G., Steegborn, C., 2011. A Phosphodiesterase 2A Isoform Localized to Mitochondria Regulates Respiration. *J. Biol. Chem.* 286, 30423–30432.
<https://doi.org/10.1074/jbc.M111.266379>
- Adusei, D.C., Pacey, L.K.K., Chen, D., Hampson, D.R., 2010. Early developmental alterations in GABAergic protein expression in fragile X knockout mice. *Neuropharmacology* 59, 167–171.
<https://doi.org/10.1016/j.neuropharm.2010.05.002>
- Ahi, J., Radulovic, J., Spiess, J., 2004. The role of hippocampal signaling cascades in consolidation of fear memory. *Behav. Brain Res.* 149, 17–31. [https://doi.org/10.1016/S0166-4328\(03\)00207-9](https://doi.org/10.1016/S0166-4328(03)00207-9)
- Alanay, Y., Unal, F., Turanli, G., Alikasifoğlu, M., Alehan, D., Akyol, U., Belgin, E., Sener, C., Aktaş, D., Boduroğlu, K., Utine, E., Volkan-Salancı, B., Ozusta, S., Genç, A., Başar, F., Sevinç, S., Tunçbilek, E., 2007. A multidisciplinary approach to the management of individuals with fragile X syndrome. *J. Intellect. Disabil. Res. JIDR* 51, 151–161.
<https://doi.org/10.1111/j.1365-2788.2006.00942.x>
- Arancio, O., Antonova, I., Gambaryan, S., Lohmann, S.M., Wood, J.S., Lawrence, D.S., Hawkins, R.D., 2001. Presynaptic Role of cGMP-Dependent Protein Kinase during Long-Lasting Potentiation. *J. Neurosci.* 21, 143–149. <https://doi.org/10.1523/JNEUROSCI.21-01-00143.2001>
- Arancio, O., Kiebler, M., Lee, C.J., Lev-Ram, V., Tsien, R.Y., Kandel, E.R., Hawkins, R.D., 1996. Nitric Oxide Acts Directly in the Presynaptic Neuron to Produce Long-Term Potentiationin Cultured Hippocampal Neurons. *Cell* 87, 1025–1035. [https://doi.org/10.1016/S0092-8674\(00\)81797-3](https://doi.org/10.1016/S0092-8674(00)81797-3)
- Armstrong, D., Dunn, J.K., Antalfy, B., Trivedi, R., 1995. Selective dendritic alterations in the cortex of Rett syndrome. *J. Neuropathol. Exp. Neurol.* 54, 195–201.
<https://doi.org/10.1097/00005072-199503000-00006>
- Ascano, M., Mukherjee, N., Bandaru, P., Miller, J.B., Nusbaum, J., Corcoran, D.L., Langlois, C., Munschauer, M., Dewell, S., Hafner, M., Williams, Z., Ohler, U., Tuschl, T., 2012. FMR1 targets distinct mRNA sequence elements to regulate protein expression. *Nature* 492, 382–386.
<https://doi.org/10.1038/nature11737>
- Ashley, Claude T., Sutcliffe, J.S., Kunst, C.B., Leiner, H.A., Eichler, E.E., Nelson, D.L., Warren, S.T., 1993. Human and murine FMR-1 : alternative splicing and translational initiation downstream of the CGG-repeat. *Nat. Genet.* 4, 244–251. <https://doi.org/10.1038/ng0793-244>
- Ashley, C. T., Wilkinson, K.D., Reines, D., Warren, S.T., 1993. FMR1 protein: conserved RNP family domains and selective RNA binding. *Science* 262, 563–566.
<https://doi.org/10.1126/science.7692601>
- Asiminas, A., Jackson, A.D., Louros, S.R., Till, S.M., Spano, T., Dando, O., Bear, M.F., Chattarji, S., Hardingham, G.E., Osterweil, E.K., Wyllie, D.J.A., Wood, E.R., Kind, P.C., 2019. Sustained

- correction of associative learning deficits after brief, early treatment in a rat model of Fragile X Syndrome. *Sci. Transl. Med.* 11. <https://doi.org/10.1126/scitranslmed.aao0498>
- Asperger, H., 1991. 'Autistic psychopathy' in childhood, in: Frith, U. (Ed.), *Autism and Asperger Syndrome*. Cambridge University Press, Cambridge, pp. 37–92.
<https://doi.org/10.1017/CBO9780511526770.002>
- Autism in History: The Case of Hugh Blair of Borgue | Wiley [WWW Document], n.d. . Wiley.com. URL <https://www.wiley.com/enam/Autism+in+History%3A+The+Case+of+Hugh+Blair+of+Borgue-p-9780631220886> (accessed 2.18.21).
- Azevedo, M.F., Faucz, F.R., Bimpaki, E., Horvath, A., Levy, I., de Alexandre, R.B., Ahmad, F., Manganiello, V., Stratakis, C.A., 2014. Clinical and Molecular Genetics of the Phosphodiesterases (PDEs). *Endocr. Rev.* 35, 195–233. <https://doi.org/10.1210/er.2013-1053>
- Bailey, D.B., Raspa, M., Olmsted, M., Holiday, D.B., 2008. Co-occurring conditions associated with FMR1 gene variations: Findings from a national parent survey. *Am. J. Med. Genet. A.* 146A, 2060–2069. <https://doi.org/10.1002/ajmg.a.32439>
- Bakker, C.E., de Diego Otero, Y., Bontekoe, C., Raghoe, P., Luteijn, T., Hoogeveen, A.T., Oostra, B.A., Willemse, R., 2000. Immunocytochemical and Biochemical Characterization of FMRP, FXR1P, and FXR2P in the Mouse. *Exp. Cell Res.* 258, 162–170.
<https://doi.org/10.1006/excr.2000.4932>
- Banke, T.G., Bowie, D., Lee, H.-K., Huganir, R.L., Schousboe, A., Traynelis, S.F., 2000. Control of GluR1 AMPA Receptor Function by cAMP-Dependent Protein Kinase. *J. Neurosci.* 20, 89–102.
<https://doi.org/10.1523/JNEUROSCI.20-01-00089.2000>
- Bardoni, B., Schenck, A., Louis Mandel, J., 1999. A Novel RNA-binding Nuclear Protein That Interacts With the Fragile X Mental Retardation (FMR1) Protein. *Hum. Mol. Genet.* 8, 2557–2566.
<https://doi.org/10.1093/hmg/8.13.2557>
- Bardoni, B., Willemse, R., Weiler, I.J., Schenck, A., Severijnen, L.-A., Hindelang, C., Lalli, E., Mandel, J.-L., 2003. NUFIP1 (nuclear FMRP interacting protein 1) is a nucleocytoplasmic shuttling protein associated with active synaptoneuroosomes. *Exp. Cell Res.* 289, 95–107.
[https://doi.org/10.1016/S0014-4827\(03\)00222-2](https://doi.org/10.1016/S0014-4827(03)00222-2)
- Baron-Cohen, S., Lombardo, M.V., Auyeung, B., Ashwin, E., Chakrabarti, B., Knickmeyer, R., 2011. Why Are Autism Spectrum Conditions More Prevalent in Males? *PLoS Biol.* 9.
<https://doi.org/10.1371/journal.pbio.1001081>
- Barr, M.W., 1904. Mental Defectives: Their History, Treatment, and Training. Blakiston's.
- Bear, M.F., Huber, K.M., Warren, S.T., 2004. The mGluR theory of fragile X mental retardation. *Trends Neurosci.* 27, 370–377. <https://doi.org/10.1016/j.tins.2004.04.009>
- Beavo, J.A., Hardman, J.G., Sutherland, E.W., 1971. Stimulation of Adenosine 3',5'-Monophosphate Hydrolysis by Guanosine 3',5'-Monophosphate. *J. Biol. Chem.* 246, 3841–3846.
[https://doi.org/10.1016/S0021-9258\(18\)62110-6](https://doi.org/10.1016/S0021-9258(18)62110-6)
- Bechara, E.G., Didiot, M.C., Melko, M., Davidovic, L., Bensaid, M., Martin, P., Castets, M., Pognonec, P., Khandjian, E.W., Moine, H., Bardoni, B., 2009. A Novel Function for Fragile X Mental Retardation Protein in Translational Activation. *PLoS Biol.* 7.
<https://doi.org/10.1371/journal.pbio.1000016>
- Belagodu, A.P., Johnson, A.M., Galvez, R., 2016. Characterization of ultrasonic vocalizations of Fragile X mice. *Behav. Brain Res.* 310, 76–83. <https://doi.org/10.1016/j.bbr.2016.04.016>
- Berman, R.F., Buijsen, R.A., Usdin, K., Pintado, E., Kooy, F., Pretto, D., Pessah, I.N., Nelson, D.L., Zalewski, Z., Charlet-Bergereand, N., Willemse, R., Hukema, R.K., 2014. Mouse models of the fragile X premutation and fragile X-associated tremor/ataxia syndrome. *J. Neurodev. Disord.* 6, 25. <https://doi.org/10.1186/1866-1955-6-25>
- Berry-Kravis, E., Huttenlocher, P.R., 1992. Cyclic AMP metabolism in fragile X syndrome. *Ann. Neurol.* 31, 22–26. <https://doi.org/10.1002/ana.410310105>

- Berry-Kravis, E., Raspa, M., Loggin-Hester, L., Bishop, E., Holiday, D., Bailey, D.B., Jr, 2010. Seizures in Fragile X Syndrome: Characteristics and Comorbid Diagnoses. *Am. J. Intellect. Dev. Disabil.* 115, 461–472. <https://doi.org/10.1352/1944-7558-115.6.461>
- Berry-Kravis, E.M., Harnett, M.D., Reines, S.A., Reese, M.A., Ethridge, L.E., Outterson, A.H., Michalak, C., Furman, J., Gurney, M.E., 2021. Inhibition of phosphodiesterase-4D in adults with fragile X syndrome: a randomized, placebo-controlled, phase 2 clinical trial. *Nat. Med.* 1–9. <https://doi.org/10.1038/s41591-021-01321-w>
- Beurel, E., Grieco, S.F., Jope, R.S., 2015. Glycogen synthase kinase-3 (GSK3): regulation, actions, and diseases. *Pharmacol. Ther.* 0, 114–131. <https://doi.org/10.1016/j.pharmthera.2014.11.016>
- Boess, F.G., Hendrix, M., van der Staay, F.-J., Erb, C., Schreiber, R., van Staveren, W., de Vente, J., Prickaerts, J., Blokland, A., Koenig, G., 2004. Inhibition of phosphodiesterase 2 increases neuronal cGMP, synaptic plasticity and memory performance. *Neuropharmacology* 47, 1081–1092. <https://doi.org/10.1016/j.neuropharm.2004.07.040>
- Bolduc, F.V., Valente, D., Nguyen, A.T., Mitra, P.P., Tully, T., 2010. An assay for social interaction in *Drosophila* fragile X mutants. *Fly (Austin)* 4, 216–225. <https://doi.org/10.4161/fly.4.3.12280>
- Bollen, E., Akkerman, S., Puzzo, D., Gulisano, W., Palmeri, A., D'Hooge, R., Balschun, D., Steinbusch, H.W.M., Blokland, A., Prickaerts, J., 2015. Object memory enhancement by combining subefficacious doses of specific phosphodiesterase inhibitors. *Neuropharmacology* 95, 361–366. <https://doi.org/10.1016/j.neuropharm.2015.04.008>
- Bolton, P., Macdonald, H., Pickles, A., Rios, P., Goode, S., Crowson, M., Bailey, A., Rutter, M., 1994. A Case-Control Family History Study of Autism. *J. Child Psychol. Psychiatry* 35, 877–900. <https://doi.org/10.1111/j.1469-7610.1994.tb02300.x>
- Bonaccorso, C.M., Spatuzza, M., Marco, B.D., Gloria, A., Barrancotto, G., Cupo, A., Musumeci, S.A., D'Antoni, S., Bardoni, B., Catania, M.V., 2015. Fragile X mental retardation protein (FMRP) interacting proteins exhibit different expression patterns during development. *Int. J. Dev. Neurosci.* 42, 15–23. <https://doi.org/10.1016/j.ijdevneu.2015.02.004>
- Bontekoe, C.J., de Graaff, E., Nieuwenhuizen, I.M., Willemse, R., Oostra, B.A., 1997. FMR1 premutation allele (CGG)81 is stable in mice. *Eur. J. Hum. Genet.* 5, 293–298.
- Borges, K., Dingledine, R., 2001. Functional Organization of the GluR1 Glutamate Receptor Promoter*. *J. Biol. Chem.* 276, 25929–25938. <https://doi.org/10.1074/jbc.M009105200>
- Boswell-Smith, V., Spina, D., Page, C.P., 2006. Phosphodiesterase inhibitors. *Br. J. Pharmacol.* 147, S252. <https://doi.org/10.1038/sj.bjp.0706495>
- Braat, S., Kooy, R.F., 2015. Insights into GABAergic system deficits in fragile X syndrome lead to clinical trials. *Neuropharmacology, GABAergic Signaling in Health and Disease* 88, 48–54. <https://doi.org/10.1016/j.neuropharm.2014.06.028>
- Brouwer, J., Mientjes, E., Bakker, C., Nieuwenhuizen, I., Severijnen, L., Van der Linde, H., Nelson, D., Oostra, B., Willemse, R., 2007. Elevated Fmr1 mRNA levels and reduced protein expression in a mouse model with an unmethylated Fragile X full mutation. *Exp. Cell Res.* 313, 244–253. <https://doi.org/10.1016/j.yexcr.2006.10.002>
- Brouwer, J.R., Huizer, K., Severijnen, L.-A., Hukema, R.K., Berman, R.F., Oostra, B.A., Willemse, R., 2008. CGG-repeat length and neuropathological and molecular correlates in a mouse model for fragile X-associated tremor/ataxia syndrome. *J. Neurochem.* 107, 1671–1682. <https://doi.org/10.1111/j.1471-4159.2008.05747.x>
- Brown, G.P., Blitzer, R.D., Connor, J.H., Wong, T., Shenolikar, S., Iyengar, R., Landau, E.M., 2000. LongTerm Potentiation Induced by θ Frequency Stimulation Is Regulated by a Protein Phosphatase-1-Operated Gate. *J. Neurosci.* 20, 7880–7887. <https://doi.org/10.1523/JNEUROSCI.20-21-07880.2000>
- Bruno, J.L., Hosseini, S.M.H., Saggar, M., Quintin, E.-M., Raman, M.M., Reiss, A.L., 2017. Altered Brain Network Segregation in Fragile X Syndrome Revealed by Structural Connectomics. *Cereb.*

- Cortex N. Y. NY 27, 2249–2259. <https://doi.org/10.1093/cercor/bhw055>
- Bruno, J.L., Shelly, E.W., Quintin, E.-M., Rostami, M., Patnaik, S., Spielman, D., Mayer, D., Gu, M., Lightbody, A.A., Reiss, A.L., 2013. Aberrant basal ganglia metabolism in fragile X syndrome: a magnetic resonance spectroscopy study. *J. Neurodev. Disord.* 5, 20. <https://doi.org/10.1186/1866-1955-5-20>
- Budimirovic, D.B., Kaufmann, W.E., 2011. What Can We Learn about Autism from Studying Fragile X Syndrome? *Dev. Neurosci.* 33, 379–394. <https://doi.org/10.1159/000330213>
- Butcher, R.W., Sutherland, E.W., 1962. Adenosine 3',5'-Phosphate in Biological Materials I. PURIFICATION AND PROPERTIES OF CYCLIC 3',5'-NUCLEOTIDE PHOSPHODIESTERASE AND USE OF THIS ENZYME TO CHARACTERIZE ADENOSINE 3',5'-PHOSPHATE IN HUMAN URINE. *J. Biol. Chem.* 237, 1244–1250.
- Cai, D., Qiu, J., Cao, Z., McAtee, M., Bregman, B.S., Filbin, M.T., 2001. Neuronal Cyclic AMP Controls the Developmental Loss in Ability of Axons to Regenerate. *J. Neurosci.* 21, 4731–4739. <https://doi.org/10.1523/JNEUROSCI.21-13-04731.2001>
- Castets, M., Schaeffer, C., Bechara, E., Schenck, A., Khandjian, E.W., Luche, S., Moine, H., Rabilloud, T., Mandel, J.-L., Bardoni, B., 2005. FMRP interferes with the Rac1 pathway and controls actin cytoskeleton dynamics in murine fibroblasts. *Hum. Mol. Genet.* 14, 835–844. <https://doi.org/10.1093/hmg/ddi077>
- Ceman, S., Brown, V., Warren, S.T., 1999. Isolation of an FMRP-Associated Messenger Ribonucleoprotein Particle and Identification of Nucleolin and the Fragile X-Related Proteins as Components of the Complex. *Mol. Cell. Biol.* 19, 7925–7932.
- Ceman, S., O'Donnell, W.T., Reed, M., Patton, S., Pohl, J., Warren, S.T., 2003. Phosphorylation influences the translation state of FMRP-associated polyribosomes. *Hum. Mol. Genet.* 12, 3295–3305. <https://doi.org/10.1093/hmg/ddg350>
- Chen, E., Sharma, M.R., Shi, X., Agrawal, R.K., Joseph, S., 2014. Fragile X Mental Retardation Protein Regulates Translation by Binding Directly to the Ribosome. *Mol. Cell* 54, 407–417. <https://doi.org/10.1016/j.molcel.2014.03.023>
- Chen, L., Liu, K., Wang, Y., Liu, N., Yao, M., Hu, J., Wang, G., Sun, Y., Pan, J., 2021. Phosphodiesterase2 inhibitor reverses post-traumatic stress induced fear memory deficits and behavioral changes via cAMP/cGMP pathway. *Eur. J. Pharmacol.* 891, 173768. <https://doi.org/10.1016/j.ejphar.2020.173768>
- Chen, Y., Harry, A., Li, J., Smit, M.J., Bai, X., Magnusson, R., Pieroni, J.P., Weng, G., Iyengar, R., 1997. Adenylyl cyclase 6 is selectively regulated by protein kinase A phosphorylation in a region involved in Galphas stimulation. *Proc. Natl. Acad. Sci. U. S. A.* 94, 14100–14104. <https://doi.org/10.1073/pnas.94.25.14100>
- Chen, Y., Tassone, F., Berman, R.F., Hagerman, P.J., Hagerman, R.J., Willemse, R., Pessah, I.N., 2010. Murine hippocampal neurons expressing Fmr1 gene premutations show early developmental deficits and late degeneration. *Hum. Mol. Genet.* 19, 196–208. <https://doi.org/10.1093/hmg/ddp479>
- Cheng, X., Ji, Z., Tsalkova, T., Mei, F., 2008. Epac and PKA: a tale of two intracellular cAMP receptors. *Acta Biochim. Biophys. Sin.* 40, 651–662.
- Chinwalla, A.T., Cook, L.L., Delehaunty, K.D., Fewell, G.A., Fulton, L.A., Fulton, R.S., Graves, T.A., Hillier, L.W., Mardis, E.R., McPherson, J.D., Miner, T.L., Nash, W.E., Nelson, J.O., Nhan, M.N., Pepin, K.H., Pohl, C.S., Ponce, T.C., Schultz, B., Thompson, J., Trevaskis, E., Waterston, R.H., Wendl, M.C., Wilson, R.K., Yang, S.-P., An, P., Berry, E., Birren, B., Bloom, T., Brown, D.G., Butler, J., Daly, M., David, R., Deri, J., Dodge, S., Foley, K., Gage, D., Gnerre, S., Holzer, T., Jaffe, D.B., Kamal, M., Karlsson, E.K., Kells, C., Kirby, A., Kulbokas, E.J., Lander, E.S., Landers, T., Leger, J.P., Levine, R., Lindblad-Toh, K., Mauceli, E., Mayer, J.H., McCarthy, M., Meldrim, J., Meldrim, J., Mesirov, J.P., Nicol, R., Nusbaum, C., Seaman, S., Sharpe, T., Sheridan, A., Singer,

J. B., Santos, R., Spencer, B., Stange-Thomann, N., Vinson, J.P., Wade, C.M., Wierzbowski, J., Wyman, D., Zody, M.C., Birney, E., Goldman, N., Kasprzyk, A., Mongin, E., Rust, A.G., Slater, G., Stabenau, A., Ureta-Vidal, A., Whelan, S., Ainscough, R., Attwood, J., Bailey, J., Barlow, K., Beck, S., Burton, J., Clamp, M., Clee, C., Coulson, A., Cuff, J., Curwen, V., Cutts, T., Davies, J., Eyras, E., Grafham, D., Gregory, S., Hubbard, T., Hunt, A., Jones, M., Joy, A., Leonard, S., Lloyd, C., Matthews, L., McLaren, S., McLay, K., Meredith, B., Mullikin, J.C., Ning, Z., Oliver, K., Overton-Larty, E., Plumb, R., Potter, S., Quail, M., Rogers, J., Scott, C., Searle, S., Shownkeen, R., Sims, S., Wall, M., West, A.P., Willey, D., Williams, S., Abril, J.F., Guigó, R., Parra, G., Agarwal, P., Agarwala, R., Church, D.M., Hlavina, W., Maglott, D.R., Sapožnikov, V., Alexandersson, M., Pachter, L., Antonarakis, S.E., Dermitzakis, E.T., Reymond, A., UCLA, C., Baertsch, R., Diekhans, M., Furey, T.S., Hinrichs, A., Hsu, F., Karolchik, D., Kent, W.J., Roskin, K.M., Schwartz, M.S., Sugnet, C., Weber, R.J., Bork, P., Letunic, I., Suyama, M., Torrents, D., Zdobnov, E.M., Botcherby, M., Brown, S.D., Campbell, R.D., Jackson, I., Bray, N., Couronne, O., Dubchak, I., Poliakov, A., Rubin, E.M., Brent, M.R., Flieck, P., Keibler, E., Korf, I., Batalov, S., Bult, C., Frankel, W.N., Carninci, P., Hayashizaki, Y., Kawai, J., Okazaki, Y., Cawley, S., Kulp, D., Wheeler, R., Chiaromonte, F., Collins, F.S., Felsenfeld, A., Guyer, M., Peterson, J., Wetterstrand, K., Copley, R.R., Mott, R., Dewey, C., Dickens, N.J., Emes, R.D., Goodstadt, L., Ponting, C.P., Winter, E., Dunn, D.M., von Niederhausern, A.C., Weiss, R.B., Eddy, S.R., Johnson, L.S., Jones, T.A., Elnitski, L., Kolbe, D.L., Eswara, P., Miller, W., O'Connor, M.J., Schwartz, S., Gibbs, R.A., Muzny, D.M., Glusman, G., Smit, A., Green, E.D., Hardison, R.C., Yang, S., Haussler, D., Hua, A., Roe, B.A., Kucherlapati, R.S., Montgomery, K.T., Li, J., Li, M., Lucas, S., Ma, B., McCombie, W.R., Morgan, M., Pevzner, P., Tesler, G., Schultz, J., Smith, D.R., Tromp, J., Worley, K.C., Lander, E.S., Abril, J.F., Agarwal, P., Alexandersson, M., Antonarakis, S.E., Baertsch, R., Berry, E., Birney, E., Bork, P., Bray, N., Brent, M.R., Brown, D.G., Butler, J., Bult, C., Chiaromonte, F., Chinwalla, A.T., Church, D.M., Clamp, M., Collins, F.S., Copley, R.R., Couronne, O., Cawley, S., Cuff, J., Curwen, V., Cutts, T., Daly, M., Dermitzakis, E.T., Dewey, C., Mouse Genome Sequencing Consortium, Genome Sequencing Center:, Whitehead Institute/MIT Center for Genome Research:, European Bioinformatics Institute:, Wellcome Trust Sanger Institute, Research Group in Biomedical Informatics, Bioinformatics, National Center for Biotechnology Information, Department of Mathematics, Division of Medical Genetics, Center for Biomolecular Science and Engineering, EMBL, UK MRC Mouse Sequencing Consortium, Lawrence Berkeley National Laboratory, Department of Computer Science, School of Computer Science, The Jackson Laboratory, Laboratory for Genome Exploration, Affymetrix Inc., Departments of Statistics and Health Evaluation Sciences, National Human Genome Research Institute, Wellcome Trust Centre for Human Genetics, Department of Electrical Engineering, Department of Human Anatomy and Genetics, Department of Human Genetics, Howard Hughes Medical Institute and Department of Genetics, Departments of Biochemistry and Molecular Biology and Computer Science and Engineering, Department of Computer Science and Engineering, Baylor College of Medicine, The Institute for Systems Biology, Department of Biochemistry and Molecular Biology, Howard Hughes Medical Institute, Department of Chemistry and Biochemistry, Departments of Genetics and Medicine and Harvard-Partners Center for Genetics and Genomics, Department of Statistics, US DOE Joint Genome Institute, Cold Spring Harbor Laboratory, Wellcome Trust, Max Planck Institute for Molecular Genetics, Genome Therapeutics Corporation, Bioinformatics Solutions Inc., Department of Molecular and Human Genetics, Department of Biology, Members of the Mouse Genome Analysis Group, 2002. Initial sequencing and comparative analysis of the mouse genome. *Nature* 420, 520–562.
<https://doi.org/10.1038/nature01262>

- Christensen, D.L., Baio, J., Van Naarden Braun, K., Bilder, D., Charles, J., Constantino, J.N., Daniels, J., Durkin, M.S., Fitzgerald, R.T., Kurzius-Spencer, M., Lee, L.-C., Pettygrove, S., Robinson, C., Schulz, E., Wells, C., Wingate, M.S., Zahorodny, W., Yeargin-Alsopp, M., Centers for Disease Control and Prevention (CDC), 2016. Prevalence and Characteristics of Autism Spectrum Disorder Among Children Aged 8 Years--Autism and Developmental Disabilities Monitoring Network, 11 Sites, United States, 2012. *Morb. Mortal. Wkly. Rep. Surveill. Summ. Wash. DC* 2002 65, 1–23. <https://doi.org/10.15585/mmwr.ss6503a1>
- Clifford, S., Dissanayake, C., Bui, Q.M., Huggins, R., Taylor, A.K., Loesch, D.Z., 2007. Autism Spectrum Phenotype in Males and Females with Fragile X Full Mutation and Premutation. *J. Autism. Dev. Disord.* 37, 738–747. <https://doi.org/10.1007/s10803-006-0205-z>
- Comery, T.A., Harris, J.B., Willems, P.J., Oostra, B.A., Irwin, S.A., Weiler, I.J., Greenough, W.T., 1997. Abnormal dendritic spines in fragile X knockout mice: Maturation and pruning deficits. *Proc. Natl. Acad. Sci. U. S. A.* 94, 5401–5404.
- Costa, L., Sardone, L.M., Bonaccorso, C.M., D'Antoni, S., Spatuzza, M., Gulisano, W., Tropea, M.R., Puzzo, D., Leopoldo, M., Lacivita, E., Catania, M.V., Ciranna, L., 2018. Activation of Serotonin 5-HT7 Receptors Modulates Hippocampal Synaptic Plasticity by Stimulation of Adenylate Cyclases and Rescues Learning and Behavior in a Mouse Model of Fragile X Syndrome. *Front. Mol. Neurosci.* 11. <https://doi.org/10.3389/fnmol.2018.00353>
- Cribbs, J.T., Strack, S., 2007. Reversible phosphorylation of Drp1 by cyclic AMP-dependent protein kinase and calcineurin regulates mitochondrial fission and cell death. *EMBO Rep.* 8, 939–944. <https://doi.org/10.1038/sj.embo.7401062>
- Cronister, A., Schreiner, R., Wittenberger, M., Amiri, K., Harris, K., Hagerman, R.J., 1991. Heterozygous fragile X female: historical, physical, cognitive, and cytogenetic features. *Am. J. Med. Genet.* 38, 269–274. <https://doi.org/10.1002/ajmg.1320380221>
- Dahlhaus, R., 2018. Of Men and Mice: Modeling the Fragile X Syndrome. *Front. Mol. Neurosci.* 11. <https://doi.org/10.3389/fnmol.2018.00041>
- Dahlhaus, R., El-Husseini, A., 2010. Altered neuroligin expression is involved in social deficits in a mouse model of the fragile X syndrome. *Behav. Brain Res.* 208, 96–105. <https://doi.org/10.1016/j.bbr.2009.11.019>
- Darnell, J.C., Fraser, C.E., Mostovetsky, O., Stefani, G., Jones, T.A., Eddy, S.R., Darnell, R.B., 2005. Kissing complex RNAs mediate interaction between the Fragile-X mental retardation protein KH2 domain and brain polyribosomes. *Genes Dev.* 19, 903–918. <https://doi.org/10.1101/gad.1276805>
- Darnell, J.C., Jensen, K.B., Jin, P., Brown, V., Warren, S.T., Darnell, R.B., 2001. Fragile X Mental Retardation Protein Targets G Quartet mRNAs Important for Neuronal Function. *Cell* 107, 489–499. [https://doi.org/10.1016/S0092-8674\(01\)00566-9](https://doi.org/10.1016/S0092-8674(01)00566-9)
- Darnell, J.C., Van Driesche, S.J., Zhang, C., Hung, K.Y.S., Mele, A., Fraser, C.E., Stone, E.F., Chen, C., Fak, J.J., Chi, S.W., Licatalosi, D.D., Richter, J.D., Darnell, R.B., 2011. FMRP stalls ribosomal translocation on mRNAs linked to synaptic function and autism. *Cell* 146, 247–261. <https://doi.org/10.1016/j.cell.2011.06.013>
- Davis, N.O., Kollins, S.H., 2012. Treatment for Co-Occurring Attention Deficit/Hyperactivity Disorder and Autism Spectrum Disorder. *Neurotherapeutics* 9, 518–530. <https://doi.org/10.1007/s13311-012-0126-9>
- de la Cruz, F.F., 1985. Fragile X syndrome. *Am. J. Ment. Defic.* 90, 119–123.
- de Rooij, J., Zwartkruis, F.J.T., Verheijen, M.H.G., Cool, R.H., Nijman, S.M.B., Wittinghofer, A., Bos, J.L., 1998. Epac is a Rap1 guanine-nucleotide-exchange factor directly activated by cyclic AMP. *Nature* 396, 474–477. <https://doi.org/10.1038/24884>
- Delhaye, S., Bardoni, B., 2021. Role of phosphodiesterases in the pathophysiology of neurodevelopmental disorders. *Mol. Psychiatry* 1–13. <https://doi.org/10.1038/s41380-020-0488-1>

- 00997-9 den Broeder, M.J., van der Linde, H., Brouwer, J.R., Oostra, B.A., Willemse, R., Ketting, R.F., 2009. Generation and Characterization of Fmr1 Knockout Zebrafish. PLoS ONE 4. <https://doi.org/10.1371/journal.pone.0007910>
- Devys, D., Lutz, Y., Rouyer, N., Bellocq, J.P., Mandel, J.L., 1993. The FMR-1 protein is cytoplasmic, most abundant in neurons and appears normal in carriers of a fragile X premutation. Nat. Genet. 4, 335–340. <https://doi.org/10.1038/ng0893-335>
- Dewachter, I., Ris, L., Jaworski, T., Seymour, C.M., Kremer, A., Borghgraef, P., De Vijver, H., Godaux, E., Van Leuven, F., 2009. GSK3 β , a centre-staged kinase in neuropsychiatric disorders, modulates long term memory by inhibitory phosphorylation at Serine-9. Neurobiol. Dis., Biomarkers of Neuropsychiatric Disease 35, 193–200. <https://doi.org/10.1016/j.nbd.2009.04.003>
- Ding, Q., Liu, G., Zeng, Y., Zhu, J., Liu, Z., Jiang, J., Huang, J., 2017. Glycogen synthase kinase-3 β inhibitor reduces LPS-induced acute lung injury in mice. Mol. Med. Rep. 16, 6715–6721. <https://doi.org/10.3892/mmr.2017.7469>
- Domek-Łopacińska, K., Strosznajder, J.B., 2008. The effect of selective inhibition of cyclic GMP hydrolyzing phosphodiesterases 2 and 5 on learning and memory processes and nitric oxide synthase activity in brain during aging. Brain Res. 1216, 68–77. <https://doi.org/10.1016/j.brainres.2008.02.108>
- Douummar, D., Dentel, C., Lyautey, R., Metreau, J., Keren, B., Drouot, N., Malherbe, L., Bouilleret, V., Courraud, J., Valenti-Hirsch, M.P., Minotti, L., Dozieres-Puyravel, B., Bär, S., Scholly, J., Schaefer, E., Nava, C., Wirth, T., Nasser, H., de Salins, M., de Saint Martin, A., Warde, M.T.A., Kahane, P., Hirsch, E., Anheim, M., Friant, S., Chelly, J., Mignot, C., Rudolf, G., 2020. Biallelic PDE2A variants: a new cause of syndromic paroxysmal dyskinesia. Eur. J. Hum. Genet. 28, 1403–1413. <https://doi.org/10.1038/s41431-020-0641-9>
- Du, F., 2019. Golgi-Cox Staining of Neuronal Dendrites and Dendritic Spines With FD Rapid GolgiStain™ Kit. Curr. Protoc. Neurosci. 88, e69. <https://doi.org/10.1002/cpns.69>
- Eichler, E.E., Richards, S., Gibbs, R.A., Nelson, D.L., 1993. Fine structure of the human FMR1 gene. Hum. Mol. Genet. 2, 1147–1153. <https://doi.org/10.1093/hmg/2.8.1147>
- Einfeld, S.L., Ellis, L.A., Emerson, E., 2011. Comorbidity of intellectual disability and mental disorder in children and adolescents: A systematic review. J. Intellect. Dev. Disabil. 36, 137–143. <https://doi.org/10.1080/13668250.2011.572548>
- Esteban, J.A., Shi, S.-H., Wilson, C., Nuriya, M., Huganir, R.L., Malinow, R., 2003. PKA phosphorylation of AMPA receptor subunits controls synaptic trafficking underlying plasticity. Nat. Neurosci. 6, 136–143. <https://doi.org/10.1038/nn997>
- Esvold, E.-E., Tuvikene, J., Sirp, A., Patil, S., Bramham, C.R., Timmusk, T., 2020. CREB Family Transcription Factors Are Major Mediators of BDNF Transcriptional Autoregulation in Cortical Neurons. J. Neurosci. 40, 1405–1426. <https://doi.org/10.1523/JNEUROSCI.0367-19.2019>
- Evidence for social anxiety and impaired social cognition in a mouse model of fragile X syndrome. - PsycNET [WWW Document], n.d. URL <https://content.apa.org/record/2008-03769-005> (accessed 2.27.21).
- Farmer, R., Burbano, S.D., Patel, N.S., Sarmiento, A., Smith, A.J., Kelly, M.P., 2020. Phosphodiesterases PDE2A and PDE10A both change mRNA expression in the human brain with age, but only PDE2A changes in a region-specific manner with psychiatric disease. Cell. Signal. 70, 109592. <https://doi.org/10.1016/j.cellsig.2020.109592>
- Felgerolle, C., Hébert, B., Ardourel, M., Meyer-Dilhet, G., Menuet, A., Pinto-Morais, K., Bizot, J.-C., Pichon, J., Briault, S., Perche, O., 2019. Visual Behavior Impairments as an Aberrant Sensory Processing in the Mouse Model of Fragile X Syndrome. Front. Behav. Neurosci. 13. <https://doi.org/10.3389/fnbeh.2019.00228>

- Feng, Y., Gutekunst, C.-A., Eberhart, D.E., Yi, H., Warren, S.T., Hersch, S.M., 1997. Fragile X Mental Retardation Protein: Nucleocytoplasmic Shuttling and Association with Somatodendritic Ribosomes. *J. Neurosci.* 17, 1539–1547. <https://doi.org/10.1523/JNEUROSCI.17-0501539.1997>
- Ferrer, I., Gullotta, F., 1990. Down's syndrome and Alzheimer's disease: dendritic spine counts in the hippocampus. *Acta Neuropathol. (Berl.)* 79, 680–685. <https://doi.org/10.1007/BF00294247>
- Fischer, J., Hammerschmidt, K., 2011. Ultrasonic vocalizations in mouse models for speech and sociocognitive disorders: insights into the evolution of vocal communication. *Genes Brain Behav.* 10, 17–27. <https://doi.org/10.1111/j.1601-183X.2010.00610.x>
- Fmr1 knockout mice: A model to study fragile X mental retardation, 1994. *.. Cell* 78, 23–33. [https://doi.org/10.1016/0092-8674\(94\)90569-X](https://doi.org/10.1016/0092-8674(94)90569-X)
- Frame, S., Cohen, P., Biondi, R.M., 2001. A Common Phosphate Binding Site Explains the Unique Substrate Specificity of GSK3 and Its Inactivation by Phosphorylation. *Mol. Cell* 7, 1321–1327. [https://doi.org/10.1016/S1097-2765\(01\)00253-2](https://doi.org/10.1016/S1097-2765(01)00253-2)
- Frey, U., Huang, Y.Y., Kandel, E.R., 1993. Effects of cAMP simulate a late stage of LTP in hippocampal CA1 neurons. *Science* 260, 1661–1664. <https://doi.org/10.1126/science.8389057>
- Galvez, R., Greenough, W.T., 2005. Sequence of abnormal dendritic spine development in primary somatosensory cortex of a mouse model of the fragile X mental retardation syndrome. *Am. J. Med. Genet. A* 135A, 155–160. <https://doi.org/10.1002/ajmg.a.30709>
- Gelinas, J.N., Banko, J.L., Peters, M.M., Klann, E., Weeber, E.J., Nguyen, P.V., 2008. Activation of exchange protein activated by cyclic-AMP enhances long-lasting synaptic potentiation in the hippocampus. *Learn. Mem.* 15, 403–411. <https://doi.org/10.1101/lm.830008>
- Geurts, A.M., Cost, G.J., Freyvert, Y., Zeitler, B., Miller, J.C., Choi, V.M., Jenkins, S.S., Wood, A., Cui, X., Meng, X., Vincent, A., Lam, S., Michalkiewicz, M., Schilling, R., Foeckler, J., Kalloway, S., Weiler, H., Ménoret, S., Anegon, I., Davis, G.D., Zhang, L., Rebar, E.J., Gregory, P.D., Urnov, F.D., Jacob, H.J., Buelow, R., 2009. Knockout Rats Produced Using Designed Zinc Finger Nucleases. *Science* 325, 433. <https://doi.org/10.1126/science.1172447>
- Gholizadeh, S., Arsenault, J., Xuan, I.C.Y., Pacey, L.K., Hampson, D.R., 2014. Reduced Phenotypic Severity Following Adeno-Associated Virus-Mediated Fmr1 Gene Delivery in Fragile X Mice. *Neuropharmacology* 39, 3100–3111. <https://doi.org/10.1038/npp.2014.167>
- Gomez, T.M., Spitzer, N.C., 1999. In vivo regulation of axon extension and pathfinding by growthcone calcium transients. *Nature* 397, 350–355. <https://doi.org/10.1038/16927>
- Gomis-González, M., Busquets-Garcia, A., Matute, C., Maldonado, R., Mato, S., Ozaita, A., 2016. Possible Therapeutic Doses of Cannabinoid Type 1 Receptor Antagonist Reverses Key Alterations in Fragile X Syndrome Mouse Model. *Genes* 7. <https://doi.org/10.3390/genes7090056>
- Gonzalez-Billault, C., Muñoz-Llancao, P., Henriquez, D.R., Wojnacki, J., Conde, C., Caceres, A., 2012. The role of small GTPases in neuronal morphogenesis and polarity. *Cytoskeleton* 69, 464–485. <https://doi.org/10.1002/cm.21034>
- Gorbunova, Y.V., Spitzer, N.C., 2002. Dynamic interactions of cyclic AMP transients and spontaneous Ca²⁺ spikes. *Nature* 418, 93–96. <https://doi.org/10.1038/nature00835>
- Gotheil, D., Furfarro, J.A., Hoeft, F., Eckert, M.A., Hall, S.S., O'Hara, R., Erba, H.W., Ringel, J., Hayashi, K.M., Patnaik, S., Golianu, B., Kraemer, H.C., Thompson, P.M., Piven, J., Reiss, A.L., 2008. Neuroanatomy of Fragile X Syndrome Is Associated with Aberrant Behavior and the Fragile X Mental Retardation Protein (FMRP). *Ann. Neurol.* 63, 40–51. <https://doi.org/10.1002/ana.21243>

- Greco, C.M., Hagerman, R.J., Tassone, F., Chudley, A.E., Del Bigio, M.R., Jacquemont, S., Leehey, M., Hagerman, P.J., 2002. Neuronal intranuclear inclusions in a new cerebellar tremor/ataxia syndrome among fragile X carriers. *Brain* 125, 1760–1771.
<https://doi.org/10.1093/brain/awf184>
- Grewal, S.S., Horgan, A.M., York, R.D., Withers, G.S., Banker, G.A., Stork, P.J., 2000. Neuronal calcium activates a Rap1 and B-Raf signaling pathway via the cyclic adenosine monophosphate-dependent protein kinase. *J. Biol. Chem.* 275, 3722–3728.
<https://doi.org/10.1074/jbc.275.5.3722>
- Grimes, C.A., Jope, R.S., 2001. CREB DNA binding activity is inhibited by glycogen synthase kinase-3 β and facilitated by lithium. *J. Neurochem.* 78, 1219–1232.
- Gross, C., Chang, C.-W., Kelly, S.M., Bhattacharya, A., McBride, S.M.J., Danielson, S.W., Jiang, M.Q., Chan, C.B., Ye, K., Gibson, J.R., Klann, E., Jongens, T.A., Moberg, K.H., Huber, K.M., Bassell, G.J., 2015. Increased expression of the PI3K enhancer PIKE mediates deficits in synaptic plasticity and behavior in Fragile X syndrome. *Cell Rep.* 11, 727–736.
<https://doi.org/10.1016/j.celrep.2015.03.060>
- Grossman, A.W., Elisseou, N.M., McKinney, B.C., Greenough, W.T., 2006. Hippocampal pyramidal cells in adult Fmr1 knockout mice exhibit an immature-appearing profile of dendritic spines. *Brain Res.* 1084, 158–164. <https://doi.org/10.1016/j.brainres.2006.02.044>
- Guo, W., Murthy, A.C., Zhang, L., Johnson, E.B., Schaller, E.G., Allan, A.M., Zhao, X., 2012. Inhibition of GSK3 β improves hippocampus-dependent learning and rescues neurogenesis in a mouse model of fragile X syndrome. *Hum. Mol. Genet.* 21, 681–691.
<https://doi.org/10.1093/hmg/ddr501>
- Gurney, M.E., 2019. Genetic Association of Phosphodiesterases With Human Cognitive Performance. *Front. Mol. Neurosci.* 12, 22. <https://doi.org/10.3389/fnmol.2019.00022>
- Guthrie, W., Swineford, L.B., Nottke, C., Wetherby, A.M., 2013. Early diagnosis of autism spectrum disorder: Stability and change in clinical diagnosis and symptom presentation. *J. Child Psychol. Psychiatry* 54, 582–590. <https://doi.org/10.1111/jcpp.12008>
- Hagerman, P., 2013. Fragile X-associated tremor/ataxia syndrome (FXTAS): Pathology and mechanisms. *Acta Neuropathol. (Berl.)* 126, 1–19. <https://doi.org/10.1007/s00401-013-11381>
- Hagerman, R., Hagerman, P., 2013. Advances in clinical and molecular understanding of the FMR1 premutation and fragile X-associated tremor/ataxia syndrome. *Lancet Neurol.* 12, 786–798.
[https://doi.org/10.1016/S1474-4422\(13\)70125-X](https://doi.org/10.1016/S1474-4422(13)70125-X)
- Hagerman, R.J., Hagerman, P.J., 2002. The fragile X premutation: into the phenotypic fold. *Curr. Opin. Genet. Dev.* 12, 278–283. [https://doi.org/10.1016/S0959-437X\(02\)00299-X](https://doi.org/10.1016/S0959-437X(02)00299-X)
- Hagerman, R.J., Leehey, M., Heinrichs, W., Tassone, F., Wilson, R., Hills, J., Grigsby, J., Gage, B., Hagerman, P.J., 2001. Intention tremor, parkinsonism, and generalized brain atrophy in male carriers of fragile X. *Neurology* 57, 127–130. <https://doi.org/10.1212/WNL.57.1.127>
- Haidar, Z., Jalkh, N., Corbani, S., Abou-Ghoch, J., Fawaz, A., Mehawej, C., Chouery, E., 2020. A Homozygous Splicing Mutation in PDE2A in a Family with Atypical Rett Syndrome. *Mov. Disord.* n/a. <https://doi.org/10.1002/mds.28023>
- Haify, S.N., Mankoe, R.S.D., Boumeester, V., van der Toorn, E.C., Verhagen, R.F.M., Willemse, R., Hukema, R.K., Bosman, L.W.J., 2020. Lack of a Clear Behavioral Phenotype in an Inducible FXTAS Mouse Model Despite the Presence of Neuronal FMRpolyG-Positive Aggregates. *Front. Mol. Biosci.* 7. <https://doi.org/10.3389/fmolsb.2020.599101>
- Hallahan, B.P., Craig, M.C., Toal, F., Daly, E.M., Moore, C.J., Ambikapathy, A., Robertson, D., Murphy, K.C., Murphy, D.G.M., 2011. In vivo brain anatomy of adult males with Fragile X syndrome: An MRI study. *NeuroImage* 54, 16–24. <https://doi.org/10.1016/j.neuroimage.2010.08.015>
- Hallmayer, J., Cleveland, S., Torres, A., Phillips, J., Cohen, B., Torigoe, T., Miller, J., Fedele, A., Collins, J., Smith, K., Lotspeich, L., Croen, L.A., Ozonoff, S., Lajonchere, C., Grether, J.K., Risch, N.,

2011. Genetic Heritability and Shared Environmental Factors Among Twin Pairs With Autism. *Arch. Gen. Psychiatry* 68, 1095–1102. <https://doi.org/10.1001/archgenpsychiatry.2011.76>
- Hamilton, S.M., Green, J.R., Veeraragavan, S., Yuva, L., McCoy, A., Wu, Y., Warren, J., Little, L., Ji, D., Cui, X., Weinstein, E., Paylor, R., 2014. Fmr1 and Nlgn3 knockout rats: novel tools for investigating autism spectrum disorders. *Behav. Neurosci.* 128, 103–109. <https://doi.org/10.1037/a0035988>
- Han, J., Liu, S., Rose, D.M., Schlaepfer, D.D., McDonald, H., Ginsberg, M.H., 2001. Phosphorylation of the Integrin α 4 Cytoplasmic Domain Regulates Paxillin Binding*. *J. Biol. Chem.* 276, 40903–40909. <https://doi.org/10.1074/jbc.M102665200>
- Hartley, S.L., Sikora, D.M., 2009. Sex Differences in Autism Spectrum Disorder: An Examination of Developmental Functioning, Autistic Symptoms, and Coexisting Behavior Problems in Toddlers. *J. Autism. Dev. Disord.* 39, 1715–1722. <https://doi.org/10.1007/s10803-009-0810-8>
- Hecht, F., Kaiser-McCaw, B., 1979. The importance of being a fragile site. *Am. J. Hum. Genet.* 31, 223–225.
- Heine, C., Scherf, N., Sygnecka, K., Egerland, U., Hage, T., Franke, H., 2011. Inhibitors of the phosphodiesterase 2 increased axonal fibre growth in a dopaminergic organotypic ex vivo slice co-culture model. *BMC Pharmacol.* 11, P34. <https://doi.org/10.1186/1471-2210-11-S1P34>
- Heine, C., Sygnecka, K., Scherf, N., Berndt, A., Egerland, U., Hage, T., Franke, H., 2013. Phosphodiesterase 2 Inhibitors Promote Axonal Outgrowth in Organotypic Slice Co-Cultures. *Neurosignals* 21, 197–212. <https://doi.org/10.1159/000338020>
- Hersh, J.H., Saul, R.A., Genetics, C. on, 2011. Health Supervision for Children With Fragile X Syndrome. *Pediatrics* 127, 994–1006. <https://doi.org/10.1542/peds.2010-3500>
- Hessl, D., Berry-Kravis, E., Cordeiro, L., Yuhas, J., Ornitz, E.M., Campbell, A., Chruscinski, E., Hervey, C., Long, J.M., Hagerman, R.J., 2009a. Prepulse Inhibition in Fragile X Syndrome: Feasibility, Reliability, and Implications for Treatment. *Am. J. Med. Genet. Part B Neuropsychiatr. Genet. Off. Publ. Int. Soc. Psychiatr. Genet.* 150B, 545–553. <https://doi.org/10.1002/ajmg.b.30858>
- Hessl, D., Nguyen, D.V., Green, C., Chavez, A., Tassone, F., Hagerman, R.J., Senturk, D., Schneider, A., Lightbody, A., Reiss, A.L., Hall, S., 2009b. A solution to limitations of cognitive testing in children with intellectual disabilities: the case of fragile X syndrome. *J. Neurodev. Disord.* 1, 33–45. <https://doi.org/10.1007/s11689-008-9001-8>
- Hinds, H.L., Ashley, C.T., Sutcliffe, J.S., Nelson, D.L., Warren, S.T., Housman, D.E., Schalling, M., 1993. Tissue specific expression of FMR-1 provides evidence for a functional role in fragile X syndrome. *Nat. Genet.* 3, 36–43. <https://doi.org/10.1038/ng0193-36>
- Hinton, V.J., Brown, W.T., Wisniewski, K., Rudelli, R.D., 1991. Analysis of neocortex in three males with the fragile X syndrome. *Am. J. Med. Genet.* 41, 289–294. <https://doi.org/10.1002/ajmg.1320410306>
- Hodges, S.L., Nolan, S.O., Reynolds, C.D., Lugo, J.N., 2017. Spectral and temporal properties of calls reveal deficits in ultrasonic vocalizations of adult Fmr1 knockout mice. *Behav. Brain Res.* 332, 50–58. <https://doi.org/10.1016/j.bbr.2017.05.052>
- Hoeft, F., Carter, J.C., Lightbody, A.A., Cody Hazlett, H., Piven, J., Reiss, A.L., 2010. Region-specific alterations in brain development in one- to three-year-old boys with fragile X syndrome. *Proc. Natl. Acad. Sci. U. S. A.* 107, 9335–9339. <https://doi.org/10.1073/pnas.1002762107>
- Hoeft, F., Lightbody, A.A., Hazlett, H., Patnaik, S., Piven, J., Reiss, A.L., 2008. Morphometric Spatial Patterns Differentiate Fragile X Syndrome, Typical Developing and Developmentally Delayed Boys of Ages One to Three. *Arch. Gen. Psychiatry* 65, 1087–1097. <https://doi.org/10.1001/archpsyc.65.9.1087>
- Hooper, C., Markevich, V., Plattner, F., Killick, R., Schofield, E., Engel, T., Hernandez, F., Anderton, B.,

- Rosenblum, K., Bliss, T., Cooke, S.F., Avila, J., Lucas, J.J., Giese, K.P., Stephenson, J., Lovestone, S., 2007. Glycogen synthase kinase-3 inhibition is integral to long-term potentiation. *Eur. J. Neurosci.* 25, 81–86. <https://doi.org/10.1111/j.1460-9568.2006.05245.x>
- Howe, A.K., 2004. Regulation of actin-based cell migration by cAMP/PKA. *Biochim. Biophys. Acta BBA - Mol. Cell Res., Cell Adhesion and Signalling* 1692, 159–174.
<https://doi.org/10.1016/j.bbamcr.2004.03.005>
- Huang, Y.Y., Kandel, E.R., 1994. Recruitment of long-lasting and protein kinase A-dependent longterm potentiation in the CA1 region of hippocampus requires repeated tetanization. *Learn. Mem. Cold Spring Harb. N* 1, 74–82.
- Huber, K.M., Gallagher, S.M., Warren, S.T., Bear, M.F., 2002. Altered synaptic plasticity in a mouse model of fragile X mental retardation. *Proc. Natl. Acad. Sci. U. S. A.* 99, 7746–7750.
<https://doi.org/10.1073/pnas.122205699>
- Hufgard, J.R., Williams, M.T., Skelton, M.R., Grubisha, O., Ferreira, F.M., Sanger, H., Wright, M.E., Reed-Kessler, T.M., Rasmussen, K., Duman, R.S., Vorhees, C.V., 2017. Phosphodiesterase-1b (Pde1b) knockout mice are resistant to forced swim and tail suspension induced immobility and show upregulation of Pde10a. *Psychopharmacology (Berl.)* 234, 1803–1813.
<https://doi.org/10.1007/s00213-017-4587-8>
- Hunsaker, M.R., Wenzel, H.J., Willemse, R., Berman, R.F., 2009. Progressive Spatial Processing Deficits in a Mouse Model of the Fragile X Premutation. *Behav. Neurosci.* 123, 1315–1324.
<https://doi.org/10.1037/a0017616>
- Hunter, J., Rivero-Arias, O., Angelov, A., Kim, E., Fotheringham, I., Leal, J., 2014. Epidemiology of fragile X syndrome: A systematic review and meta-analysis. *Am. J. Med. Genet. A.* 164, 1648–1658. <https://doi.org/10.1002/ajmg.a.36511>
- Hur, E.-M., Zhou, F.-Q., 2010. GSK3 signaling in neural development. *Nat. Rev. Neurosci.* 11, 539–551.
<https://doi.org/10.1038/nrn2870>
- Impey, S., Mark, M., Villacres, E.C., Poser, S., Chavkin, C., Storm, D.R., 1996. Induction of CREmediated gene expression by stimuli that generate long-lasting LTP in area CA1 of the hippocampus. *Neuron* 16, 973–982. [https://doi.org/10.1016/s0896-6273\(00\)80120-8](https://doi.org/10.1016/s0896-6273(00)80120-8)
- Impey, S., Obrietan, K., Wong, S.T., Poser, S., Yano, S., Wayman, G., Deloulme, J.C., Chan, G., Storm, D.R., 1998. Cross Talk between ERK and PKA Is Required for Ca²⁺ Stimulation of CREBDependent Transcription and ERK Nuclear Translocation. *Neuron* 21, 869–883.
[https://doi.org/10.1016/S0896-6273\(00\)80602-9](https://doi.org/10.1016/S0896-6273(00)80602-9)
- Inagaki, N., Chihara, K., Arimura, N., Ménager, C., Kawano, Y., Matsuo, N., Nishimura, T., Amano, M., Kaibuchi, K., 2001. CRMP-2 induces axons in cultured hippocampal neurons. *Nat. Neurosci.* 4, 781–782. <https://doi.org/10.1038/90476>
- Irwin, S.A., Patel, B., Idupulapati, M., Harris, J.B., Crisostomo, R.A., Larsen, B.P., Kooy, F., Willems, P.J., Cras, P., Kozlowski, P.B., Swain, R.A., Weiler, I.J., Greenough, W.T., 2001a. Abnormal dendritic spine characteristics in the temporal and visual cortices of patients with fragile-X syndrome: a quantitative examination. *Am. J. Med. Genet.* 98, 161–167. [https://doi.org/10.1002/1096-8628\(20010115\)98:2<161::aid-ajmg1025>3.0.co;2-b](https://doi.org/10.1002/1096-8628(20010115)98:2<161::aid-ajmg1025>3.0.co;2-b)
- Irwin, S.A., Patel, B., Idupulapati, M., Harris, J.B., Crisostomo, R.A., Larsen, B.P., Kooy, F., Willems, P.J., Cras, P., Kozlowski, P.B., Swain, R.A., Weiler, I.J., Greenough, W.T., 2001b. Abnormal dendritic spine characteristics in the temporal and visual cortices of patients with fragile-X syndrome: a quantitative examination. *Am. J. Med. Genet.* 98, 161–167.
[https://doi.org/10.1002/1096-8628\(20010115\)98:2<161::aid-ajmg1025>3.0.co;2-b](https://doi.org/10.1002/1096-8628(20010115)98:2<161::aid-ajmg1025>3.0.co;2-b)
- Iwahashi, C.K., Yasui, D.H., An, H.-J., Greco, C.M., Tassone, F., Nannen, K., Babineau, B., Lebrilla, C.B., Hagerman, R.J., Hagerman, P.J., 2006. Protein composition of the intranuclear inclusions of FXTAS. *Brain J. Neurol.* 129, 256–271. <https://doi.org/10.1093/brain/awh650>

- Iwami, G., Kawabe, J., Ebina, T., Cannon, P.J., Homcy, C.J., Ishikawa, Y., 1995. Regulation of adenylyl cyclase by protein kinase A. *J. Biol. Chem.* 270, 12481–12484.
<https://doi.org/10.1074/jbc.270.21.12481>
- Izquierdo, L.A., Vianna, M., Barros, D.M., Mello e Souza, T., Ardenghi, P., Sant' Anna, M.K., Rodrigues, C., Medinam, J.H., Izquierdo, I., 2000. Short- and Long-Term Memory Are Differentially Affected by Metabolic Inhibitors Given into Hippocampus and Entorhinal Cortex. *Neurobiol. Learn. Mem.* 73, 141–149. <https://doi.org/10.1006/nlme.1999.3925>
- Jacquemont, S., Hagerman, R.J., Leehey, M., Grigsby, J., Zhang, L., Brunberg, J.A., Greco, C., Des Portes, V., Jardini, T., Levine, R., Berry-Kravis, E., Brown, W.T., Schaeffer, S., Kissel, J., Tassone, F., Hagerman, P.J., 2003. Fragile X Premutation Tremor/Ataxia Syndrome: Molecular, Clinical, and Neuroimaging Correlates. *Am. J. Hum. Genet.* 72, 869–878.
- Jacquemont, S., Hagerman, R.J., Leehey, M.A., Hall, D.A., Levine, R.A., Brunberg, J.A., Zhang, L., Jardini, T., Gane, L.W., Harris, S.W., Herman, K., Grigsby, J., Greco, C.M., Berry-Kravis, E., Tassone, F., Hagerman, P.J., 2004. Penetrance of the fragile X-associated tremor/ataxia syndrome in a premutation carrier population. *JAMA* 291, 460–469.
<https://doi.org/10.1001/jama.291.4.460>
- Jacquemont, S., Pacini, L., Jønch, A.E., Cencelli, G., Rozenberg, I., He, Y., D'Andrea, L., Pedini, G., Eldeeb, M., Willemsen, R., Gasparini, F., Tassone, F., Hagerman, R., Gomez-Mancilla, B., Bagni, C., 2018. Protein synthesis levels are increased in a subset of individuals with fragile X syndrome. *Hum. Mol. Genet.* 27, 2039–2051. <https://doi.org/10.1093/hmg/ddy099>
- Johannesson, R., Rehder, H., Wendt, V., Schwinger, E., 1987. Spermatogenesis in two patients with the fragile X syndrome. I. Histology: light and electron microscopy. *Hum. Genet.* 76, 141–147.
<https://doi.org/10.1007/BF00284911>
- John, J., Bhattacharyya, U., Yadav, N., Kukshal, P., Bhatia, T., Nimgaonkar, V.L., Deshpande, S.N., Thelma, B.K., 2019. Multiple rare inherited variants in a four generation schizophrenia family offer leads for complex mode of disease inheritance. *Schizophr. Res.*
<https://doi.org/10.1016/j.schres.2019.11.041>
- Jokiranta, E., Brown, A.S., Heinimaa, M., Cheslack-Postava, K., Partanen, A., Sourander, A., 2013. Parental psychiatric disorders and autism spectrum disorders. *Psychiatry Res.* 207, 203–211.
<https://doi.org/10.1016/j.psychres.2013.01.005>
- Jope, R.S., Johnson, G.V.W., 2004. The glamour and gloom of glycogen synthase kinase-3. *Trends Biochem. Sci.* 29, 95–102. <https://doi.org/10.1016/j.tibs.2003.12.004>
- Kamenetsky, M., Middelhaufe, S., Bank, E.M., Levin, L.R., Buck, J., Steegborn, C., 2006. Molecular Details of cAMP Generation in Mammalian Cells: A Tale of Two Systems. *J. Mol. Biol.* 362, 623–639. <https://doi.org/10.1016/j.jmb.2006.07.045>
- Kanner, L., 1968. Autistic disturbances of affective contact. *Acta Paedopsychiatr.* 35, 100–136.
- Kaufmann, W.E., Moser, H.W., 2000. Dendritic anomalies in disorders associated with mental retardation. *Cereb. Cortex N. Y. N* 1991 10, 981–991.
<https://doi.org/10.1093/cercor/10.10.981>
- Kelly, M.P., 2017. A Role for Phosphodiesterase 11A (PDE11A) in the Formation of Social Memories and the Stabilization of Mood. *Adv. Neurobiol.* 17, 201–230. https://doi.org/10.1007/978-3319-58811-7_8
- Kelly, M.P., Logue, S.F., Brennan, J., Day, J.P., Lakkaraju, S., Jiang, L., Zhong, X., Tam, M., Rizzo, S.J.S., Platt, B.J., Dwyer, J.M., Neal, S., Pulito, V.L., Agostino, M.J., Grauer, S.M., Navarra, R.L., Kelley, C., Comery, T.A., Murrills, R.J., Houslay, M.D., Brandon, N.J., 2010. Phosphodiesterase 11A in brain is enriched in ventral hippocampus and deletion causes psychiatric disease-related phenotypes. *Proc. Natl. Acad. Sci.* 107, 8457–8462.
<https://doi.org/10.1073/pnas.1000730107>

- Khandjian, E.W., Corbin, F., Woerly, S., Rousseau, F., 1996. The fragile X mental retardation protein is associated with ribosomes. *Nat. Genet.* 12, 91–93. <https://doi.org/10.1038/ng0196-91>
- Kidd, S.A., Lachiewicz, A., Barbouth, D., Blitz, R.K., Delahunty, C., McBrien, D., Visootsak, J., BerryKravis, E., 2014. Fragile X Syndrome: A Review of Associated Medical Problems. *Pediatrics* 134, 995–1005. <https://doi.org/10.1542/peds.2013-4301>
- Kong, A., Frigge, M.L., Masson, G., Besenbacher, S., Sulem, P., Magnusson, G., Gudjonsson, S.A., Sigurdsson, A., Jonasdottir, Aslaug, Jonasdottir, Adalbjorg, Wong, W.S.W., Sigurdsson, G., Walters, G.B., Steinberg, S., Helgason, H., Thorleifsson, G., Gudbjartsson, D.F., Helgason, A., Magnusson, O.T., Thorsteinsdottir, U., Stefansson, K., 2012. Rate of de novo mutations and the importance of father's age to disease risk. *Nature* 488, 471–475. <https://doi.org/10.1038/nature11396>
- Kooy, R.F., Reyniers, E., Verhoye, M., Sijbers, J., Bakker, C.E., Oostra, B.A., Willems, P.J., Van Der Linden, A., 1999. Neuroanatomy of the fragile X knockout mouse brain studied using in vivo high resolution magnetic resonance imaging. *Eur. J. Hum. Genet.* 7, 526–532. <https://doi.org/10.1038/sj.ejhg.5200348>
- Korsak, L.I.T., Shepard, K.A., Akins, M.R., 2017. Cell type-dependent axonal localization of translational regulators and mRNA in mouse peripheral olfactory neurons. *J. Comp. Neurol.* 525, 2202–2215. <https://doi.org/10.1002/cne.24199>
- Krawczun, M.S., Jenkins, E.C., Brown, W.T., 1985. Analysis of the fragile-X chromosome: localization and detection of the fragile site in high resolution preparations. *Hum. Genet.* 69, 209–211. <https://doi.org/10.1007/BF00293026>
- Kumari, D., Usdin, K., 2001. Interaction of the Transcription Factors USF1, USF2, and α-Pal/Nrf-1 with the FMR1 Promoter: IMPLICATIONS FOR FRAGILE X MENTAL RETARDATION SYNDROME*. *J. Biol. Chem.* 276, 4357–4364. <https://doi.org/10.1074/jbc.M009629200>
- Kwon, H., Menon, V., Eliez, S., Warsofsky, I.S., White, C.D., Dyer-Friedman, J., Taylor, A.K., Glover, G.H., Reiss, A.L., 2001. Functional Neuroanatomy of Visuospatial Working Memory in Fragile X Syndrome: Relation to Behavioral and Molecular Measures. *Am. J. Psychiatry* 158, 1040–1051. <https://doi.org/10.1176/appi.ajp.158.7.1040>
- La Fata, G., Gärtner, A., Domínguez-Iturza, N., Dresselaers, T., Dawitz, J., Poorthuis, R.B., Averna, M., Himmelreich, U., Meredith, R.M., Achsel, T., Dotti, C.G., Bagni, C., 2014. FMRP regulates multipolar to bipolar transition affecting neuronal migration and cortical circuitry. *Nat. Neurosci.* 17, 1693–1700. <https://doi.org/10.1038/nn.3870>
- Lachiewicz, A.M., Dawson, D.V., Spiridigliozzi, G.A., 2000. Physical characteristics of young boys with fragile X syndrome: reasons for difficulties in making a diagnosis in young males. *Am. J. Med. Genet.* 92, 229–236. [https://doi.org/10.1002/\(sici\)1096-8628\(20000605\)92:4<229::aidajmg1>3.0.co;2-k](https://doi.org/10.1002/(sici)1096-8628(20000605)92:4<229::aidajmg1>3.0.co;2-k)
- Lai, J.K.Y., Lerch, J.P., Doering, L.C., Foster, J.A., Ellegood, J., 2016. Regional brain volumes changes in adult male FMR1-KO mouse on the FVB strain. *Neuroscience* 318, 12–21. <https://doi.org/10.1016/j.neuroscience.2016.01.021>
- Lai, M.-C., Kassee, C., Besney, R., Bonato, S., Hull, L., Mandy, W., Szatmari, P., Ameis, S.H., 2019. Prevalence of co-occurring mental health diagnoses in the autism population: a systematic review and meta-analysis. *Lancet Psychiatry* 6, 819–829. [https://doi.org/10.1016/S22150366\(19\)30289-5](https://doi.org/10.1016/S22150366(19)30289-5)
- Lee, F.H.F., Lai, T.K.Y., Su, P., Liu, F., 2019. Altered cortical Cytoarchitecture in the Fmr1 knockout mouse. *Mol. Brain* 12. <https://doi.org/10.1186/s13041-019-0478-8>
- Lee, H.-K., Barbarosie, M., Kameyama, K., Bear, M.F., Huganir, R.L., 2000. Regulation of distinct AMPA receptor phosphorylation sites during bidirectional synaptic plasticity. *Nature* 405, 955–959. <https://doi.org/10.1038/35016089>

- Lee, H.-K., Takamiya, K., Han, J.-S., Man, H., Kim, C.-H., Rumbaugh, G., Yu, S., Ding, L., He, C., Petralia, R.S., Wenthold, R.J., Gallagher, M., Huganir, R.L., 2003. Phosphorylation of the AMPA receptor GluR1 subunit is required for synaptic plasticity and retention of spatial memory. *Cell* 112, 631–643. [https://doi.org/10.1016/s0092-8674\(03\)00122-3](https://doi.org/10.1016/s0092-8674(03)00122-3)
- Lee, H.-K., Takamiya, K., He, K., Song, L., Huganir, R.L., 2010. Specific roles of AMPA receptor subunit GluR1 (GluA1) phosphorylation sites in regulating synaptic plasticity in the CA1 region of hippocampus. *J. Neurophysiol.* 103, 479–489. <https://doi.org/10.1152/jn.00835.2009>
- Lee, J.J., Wedow, R., Okbay, A., Kong, E., Maghzian, O., Zacher, M., Nguyen-Viet, T.A., Bowers, P., Sidorenko, J., Linnér, R.K., Fontana, M.A., Kundu, T., Lee, C., Li, H., Li, R., Royer, R., Timshel, P.N., Walters, R.K., Willoughby, E.A., Yengo, L., Alver, M., Bao, Y., Clark, D.W., Day, F.R., Furlotte, N.A., Joshi, P.K., Kemper, K.E., Kleinman, A., Langenberg, C., Mägi, R., Trampush, J.W., Verma, S.S., Wu, Y., Lam, M., Zhao, J.H., Zheng, Z., Boardman, J.D., Campbell, H., Freese, J., Harris, K.M., Hayward, C., Herd, P., Kumari, M., Lencz, T., Luan, J., Malhotra, A.K., Metspalu, A., Milani, L., Ong, K.K., Perry, J.R.B., Porteous, D.J., Ritchie, M.D., Smart, M.C., Smith, B.H., Tung, J.Y., Wareham, N.J., Wilson, J.F., Beauchamp, J.P., Conley, D.C., Esko, T., Lehrer, S.F., Magnusson, P.K.E., Oskarsson, S., Pers, T.H., Robinson, M.R., Thom, K., Watson, C., Chabris, C.F., Meyer, M.N., Laibson, D.I., Yang, J., Johannesson, M., Koellinger, P.D., Turley, P., Visscher, P.M., Benjamin, D.J., Cesaroni, D., 2018. Gene discovery and polygenic prediction from a genome-wide association study of educational attainment in 1.1 million individuals. *Nat. Genet.* 50, 1112–1121. <https://doi.org/10.1038/s41588-018-0147-3>
- Leehey, M.A., Berry-Kravis, E., Min, S.-J., Hall, D.A., Rice, C.D., Zhang, L., Grigsby, J., Greco, C.M., Reynolds, A., Lara, R., Cogswell, J., Jacquemont, S., Hessl, D.R., Tassone, F., Hagerman, R., Hagerman, P.J., 2007. Progression of tremor and ataxia in male carriers of the FMR1 premutation. *Mov. Disord. Off. J. Mov. Disord. Soc.* 22, 203–206. <https://doi.org/10.1002/mds.21252>
- Leitner, Y., 2014. The Co-Occurrence of Autism and Attention Deficit Hyperactivity Disorder in Children – What Do We Know? *Front. Hum. Neurosci.* 8. <https://doi.org/10.3389/fnhum.2014.00268>
- Lejeune, J., Turpin, R., Gautier, M., 1959. [Mongolism; a chromosomal disease (trisomy)]. *Bull. Acad. Natl. Med.* 143, 256–265.
- Leonard, H., Wen, X., 2002. The epidemiology of mental retardation: Challenges and opportunities in the new millennium. *Ment. Retard. Dev. Disabil. Res. Rev.* 8, 117–134. <https://doi.org/10.1002/mrdd.10031>
- Li, J., Pelletier, M.R., Perez Velazquez, J.-L., Carlen, P.L., 2002. Reduced Cortical Synaptic Plasticity and GluR1 Expression Associated with Fragile X Mental Retardation Protein Deficiency. *Mol. Cell. Neurosci.* 19, 138–151. <https://doi.org/10.1006/mcne.2001.1085>
- Lin, C.-F., Chen, C.-L., Chiang, C.-W., Jan, M.-S., Huang, W.-C., Lin, Y.-S., 2007. GSK-3beta acts downstream of PP2A and the PI 3-kinase-Akt pathway, and upstream of caspase-2 in ceramide-induced mitochondrial apoptosis. *J. Cell Sci.* 120, 2935–2943. <https://doi.org/10.1242/jcs.03473>
- Linglart, A., Fryssira, H., Hiort, O., Holterhus, P.-M., Perez de Nanclares, G., Argente, J., Heinrichs, C., Kuechler, A., Mantovani, G., Leheup, B., Wicart, P., Chassot, V., Schmidt, D., Rubio-Cabezas, Ó., Richter-Unruh, A., Berrade, S., Pereda, A., Boros, E., Muñoz-Calvo, M.T., Castori, M., Gunes, Y., Bertrand, G., Bougnères, P., Clauser, E., Silve, C., 2012. PRKAR1A and PDE4D Mutations Cause Acrodysostosis but Two Distinct Syndromes with or without GPCR-Signaling Hormone Resistance. *J. Clin. Endocrinol. Metab.* 97, E2328–E2338. <https://doi.org/10.1210/jc.2012-2326>

- Liu, L., Zheng, J., Huang, X.-F., Zhu, X., Ding, S.-M., Ke, H.-M., O'Donnell, J.M., Zhang, H.-T., Song, G.Q., Xu, Y., 2018. The neuroprotective and antidepressant-like effects of Hcyb1, a novel selective PDE2 inhibitor. *CNS Neurosci. Ther.* 24, 652–660.
<https://doi.org/10.1111/cns.12863>
- Liu, Z.-H., Smith, C.B., 2009. Dissociation of social and nonsocial anxiety in a mouse model of fragile X syndrome. *Neurosci. Lett.* 454, 62–66. <https://doi.org/10.1016/j.neulet.2009.02.066>
- Loomes, R., Hull, L., Mandy, W.P.L., 2017. What Is the Male-to-Female Ratio in Autism Spectrum Disorder? A Systematic Review and Meta-Analysis. *J. Am. Acad. Child Adolesc. Psychiatry* 56, 466–474. <https://doi.org/10.1016/j.jaac.2017.03.013>
- Lu, Y.-F., Hawkins, R.D., 2002. Ryanodine Receptors Contribute to cGMP-Induced Late-Phase LTP and CREB Phosphorylation in the Hippocampus. *J. Neurophysiol.* 88, 1270–1278.
<https://doi.org/10.1152/jn.2002.88.3.1270>
- Lubs, H.A., 1969. A marker X chromosome. *Am. J. Hum. Genet.* 21, 231–244.
- Lyall, K., Croen, L., Daniels, J., Fallin, M.D., Ladd-Acosta, C., Lee, B.K., Park, B.Y., Snyder, N.W., Schendel, D., Volk, H., Windham, G.C., Newschaffer, C., 2017. The Changing Epidemiology of Autism Spectrum Disorders. *Annu. Rev. Public Health* 38, 81–102.
<https://doi.org/10.1146/annurev-publhealth-031816-044318>
- Ma, L., Herren, A.W., Espinal, G., Randol, J., McLaughlin, B., Martinez-Cerdeño, V., Pessah, I.N., Hagerman, R.J., Hagerman, P.J., 2019. Composition of the Intranuclear Inclusions of Fragile X-associated Tremor/Ataxia Syndrome. *Acta Neuropathol. Commun.* 7, 143.
<https://doi.org/10.1186/s40478-019-0796-1>
- Maenner, M.J., Shaw, K.A., Baio, J., Washington, A., Patrick, M., DiRienzo, M., Christensen, D.L., Wiggins, L.D., Pettygrove, S., Andrews, J.G., Lopez, M., Hudson, A., Baroud, T., Schwenk, Y., White, T., Rosenberg, C.R., Lee, L.-C., Harrington, R.A., Huston, M., Hewitt, A., Esler, A., HallLandé, J., Poynter, J.N., Hallas-Muchow, L., Constantino, J.N., Fitzgerald, R.T., Zahorodny, W., Shenouda, J., Daniels, J.L., Warren, Z., Vehorn, A., Salinas, A., Durkin, M.S., Dietz, P.M., 2020. Prevalence of Autism Spectrum Disorder Among Children Aged 8 Years — Autism and Developmental Disabilities Monitoring Network, 11 Sites, United States, 2016. *MMWR Surveill. Summ.* 69, 1–12. <https://doi.org/10.15585/mmwr.ss6904a1>
- Malakhova, A.V., Rudko, O.I., Sobolev, V.V., Tretiakov, A.V., Naumova, E.A., Kokaeva, Z.G., Azimova, J.E., Klimov, E.A., 2019. PDE4B gene polymorphism in Russian patients with panic disorder. *AIMS Genet.* 6, 55–63. <https://doi.org/10.3934/genet.2019.3.55>
- Marrus, N., Hall, L., 2017. Intellectual Disability and Language Disorder. *Child Adolesc. Psychiatr. Clin. N. Am.* 26, 539–554. <https://doi.org/10.1016/j.chc.2017.03.001>
- Martin, J.P., Bell, J., 1943. A PEDIGREE OF MENTAL DEFECT SHOWING SEX-LINKAGE. *J. Neurol. Psychiatry* 6, 154–157.
- Masood, A., Huang, Y., Hajjhussein, H., Xiao, L., Li, H., Wang, W., Hamza, A., Zhan, C.-G., O'Donnell, J.M., 2009. Anxiolytic Effects of Phosphodiesterase-2 Inhibitors Associated with Increased cGMP Signaling. *J. Pharmacol. Exp. Ther.* 331, 690–699.
<https://doi.org/10.1124/jpet.109.156729>
- Maurin, T., Lebrigand, K., Castagnola, S., Paquet, A., Jarjat, M., Popa, A., Grossi, M., Rage, F., Bardoni, B., 2018. HITS-CLIP in various brain areas reveals new targets and new modalities of RNA binding by fragile X mental retardation protein. *Nucleic Acids Res.* 46, 6344–6355.
<https://doi.org/10.1093/nar/gky267>
- Maurin, T., Melancia, F., Jarjat, M., Castro, L., Costa, L., Delhaye, S., Khayachi, A., Castagnola, S., Mota, E., Di Giorgio, A., Servadio, M., Drozd, M., Poupon, G., Schiavi, S., Sardone, L., Azoulay, S., Ciranna, L., Martin, S., Vincent, P., Trezza, V., Bardoni, B., 2019a. Involvement of Phosphodiesterase 2A Activity in the Pathophysiology of Fragile X Syndrome. *Cereb. Cortex*

- 29, 3241–3252. <https://doi.org/10.1093/cercor/bhy192>
- Maurin, T., Melancia, F., Jarjat, M., Castro, L., Costa, L., Delhaye, S., Khayachi, A., Castagnola, S., Mota, E., Di Giorgio, A., Servadio, M., Drozd, M., Poupon, G., Schiavi, S., Sardone, L., Azoulay, S., Ciranna, L., Martin, S., Vincent, P., Trezza, V., Bardoni, B., 2019b. Involvement of Phosphodiesterase 2A Activity in the Pathophysiology of Fragile X Syndrome. *Cereb. Cortex* 29, 3241–3252. <https://doi.org/10.1093/cercor/bhy192>
- Mazefsky, C.A., Oswald, D.P., Day, T.N., Eack, S.M., Minshew, N.J., Lainhart, J.E., 2012. ASD, a psychiatric disorder, or both? Psychiatric diagnoses in adolescents with high-functioning ASD. *J. Clin. Child Adolesc. Psychol. Off. J. Soc. Clin. Child Adolesc. Psychol. Am. Psychol. Assoc. Div. 53* 41, 516–523. <https://doi.org/10.1080/15374416.2012.686102>
- McKinney, B.C., Grossman, A.W., Elisseou, N.M., Greenough, W.T., 2005. Dendritic spine abnormalities in the occipital cortex of C57BL/6 Fmr1 knockout mice. *Am. J. Med. Genet. B Neuropsychiatr. Genet.* 136B, 98–102. <https://doi.org/10.1002/ajmg.b.30183>
- McNaughton, C.H., Moon, J., Strawderman, M.S., Maclean, K.N., Evans, J., Strupp, B.J., 2008. Evidence for social anxiety and impaired social cognition in a mouse model of fragile X syndrome. *Behav. Neurosci.* 122, 293–300. <https://doi.org/10.1037/0735-7044.122.2.293>
- McQuown, S., Xia, S., Baumgärtel, K., Barido, R., Anderson, G., Dyck, B., Scott, R., Peters, M., 2019. Phosphodiesterase 1b (PDE1B) Regulates Spatial and Contextual Memory in Hippocampus. *Front. Mol. Neurosci.* 12, 21. <https://doi.org/10.3389/fnmol.2019.00021>
- Melko, M., Bardoni, B., 2010. The role of G-quadruplex in RNA metabolism: Involvement of FMRP and FMR2P. *Biochimie* 92, 919–926. <https://doi.org/10.1016/j.biochi.2010.05.018>
- Mendelsohn, N.J., Schaefer, G.B., 2008. Genetic Evaluation of Autism. *Semin. Pediatr. Neurol.*, Advances in Clinical Genetics (Part III) 15, 27–31. <https://doi.org/10.1016/j.spen.2008.01.005>
- Michot, C., Le Goff, C., Goldenberg, A., Abhyankar, A., Klein, C., Kinning, E., Guerrot, A.-M., Flahaut, P., Duncombe, A., Baujat, G., Lyonnet, S., Thalassinos, C., Nitschke, P., Casanova, J.-L., Le Merrer, M., Munnich, A., Cormier-Daire, V., 2012. Exome Sequencing Identifies PDE4D Mutations as Another Cause of Acrodysostosis. *Am. J. Hum. Genet.* 90, 740–745. <https://doi.org/10.1016/j.ajhg.2012.03.003>
- Mientjes, E.J., Nieuwenhuizen, I., Kirkpatrick, L., Zu, T., Hoogeveen-Westerveld, M., Severijnen, L., Rifé, M., Willemse, R., Nelson, D.L., Oostra, B.A., 2006. The generation of a conditional Fmr1 knock out mouse model to study Fmrp function in vivo. *Neurobiol. Dis.* 21, 549–555. <https://doi.org/10.1016/j.nbd.2005.08.019>
- Mildly impaired water maze performance in maleFmr1 knockout mice, 1997. *Neuroscience* 76, 367–376. [https://doi.org/10.1016/S0306-4522\(96\)00224-2](https://doi.org/10.1016/S0306-4522(96)00224-2)
- Millar, J.K., 2005. DISC1 and PDE4B Are Interacting Genetic Factors in Schizophrenia That Regulate cAMP Signaling. *Science* 310, 1187–1191. <https://doi.org/10.1126/science.1112915>
- Min, W.W., Yuskaitis, C.J., Yan, Q., Sikorski, C., Chen, S., Jope, R.S., Bauchwitz, R.P., 2009. Elevated glycogen synthase kinase-3 activity in Fragile X mice: Key metabolic regulator with evidence for treatment potential. *Neuropharmacology* 56, 463–472. <https://doi.org/10.1016/j.neuropharm.2008.09.017>
- Mizunami, M., Nemoto, Y., Terao, K., Hamanaka, Y., Matsumoto, Y., 2014. Roles of calcium/calmodulin-dependent kinase II in long-term memory formation in crickets. *PloS One* 9, e107442. <https://doi.org/10.1371/journal.pone.0107442>
- Monterisi, S., Lobo, M.J., Livie, C., Castle, J.C., Weinberger, M., Baillie, G., Surdo, N.C., Musheshe, N., Stangherlin, A., Gottlieb, E., Maizels, R., Bortolozzi, M., Micaroni, M., Zaccolo, M., 2020. PDE2A2 regulates mitochondria morphology and apoptotic cell death via local modulation of cAMP/PKA signalling. *eLife* 6. <https://doi.org/10.7554/eLife.21374>
- Monyak, R.E., Emerson, D., Schoenfeld, B.P., Zheng, X., Chambers, D.B., Rosenfelt, C., Langer, S.,

- Hinchey, P., Choi, C.H., McDonald, T.V., Bolduc, F.V., Sehgal, A., McBride, S.M.J., Jongens, T.A., 2017. Insulin Signaling Misregulation underlies Circadian and Cognitive Deficits in a Drosophila Fragile X Model. *Mol. Psychiatry* 22, 1140–1148.
<https://doi.org/10.1038/mp.2016.51>
- Morales, J., Hiesinger, P.R., Schroeder, A.J., Kume, K., Verstreken, P., Jackson, F.R., Nelson, D.L., Hassan, B.A., 2002. Drosophila Fragile X Protein, DFXR, Regulates Neuronal Morphology and Function in the Brain. *Neuron* 34, 961–972. [https://doi.org/10.1016/S0896-6273\(02\)00731-6](https://doi.org/10.1016/S0896-6273(02)00731-6)
- Morgan-Smith, M., Wu, Y., Zhu, X., Pringle, J., Snider, W.D., 2014. GSK-3 signaling in developing cortical neurons is essential for radial migration and dendritic orientation. *eLife* 3.
<https://doi.org/10.7554/eLife.02663>
- Morris, R., 1984. Developments of a water-maze procedure for studying spatial learning in the rat. *J. Neurosci. Methods* 11, 47–60. [https://doi.org/10.1016/0165-0270\(84\)90007-4](https://doi.org/10.1016/0165-0270(84)90007-4)
- Mostofsky, S.H., Mazzocco, M.M., Aakalu, G., Warsofsky, I.S., Denckla, M.B., Reiss, A.L., 1998. Decreased cerebellar posterior vermis size in fragile X syndrome: correlation with neurocognitive performance. *Neurology* 50, 121–130. <https://doi.org/10.1212/wnl.50.1.121> Muhle, R., Trentacoste, S.V., Rapin, I., 2004. The Genetics of Autism. *Pediatrics* 113, e472–e486.
<https://doi.org/10.1542/peds.113.5.e472>
- Musumeci, S.A., Hagerman, R.J., Ferri, R., Bosco, P., Bernardino, B.D., Tassinari, C.A., Sarro, G.B.D., Elia, M., 1999. Epilepsy and EEG Findings in Males with Fragile X Syndrome. *Epilepsia* 40, 1092–1099. <https://doi.org/10.1111/j.1528-1157.1999.tb00824.x>
- Myrick, L.K., Hashimoto, H., Cheng, X., Warren, S.T., 2015. Human FMRP contains an integral tandem Agenet (Tudor) and KH motif in the amino terminal domain. *Hum. Mol. Genet.* 24, 1733–1740. <https://doi.org/10.1093/hmg/ddu586>
- Myrick, L.K., Nakamoto-Kinoshita, M., Lindor, N.M., Kirmani, S., Cheng, X., Warren, S.T., 2014. Fragile X syndrome due to a missense mutation. *Eur. J. Hum. Genet.* 22, 1185–1189.
<https://doi.org/10.1038/ejhg.2013.311>
- Najmabadi, H., Hu, H., Garshasbi, M., Zemojtel, T., Abedini, S.S., Chen, W., Hosseini, M., Behjati, F., Haas, S., Jamali, P., Zecha, A., Mohseni, M., Püttmann, L., Vahid, L.N., Jensen, C., Moheb, L.A., Bienek, M., Larti, F., Mueller, I., Weissmann, R., Darvish, H., Wrogemann, K., Hadavi, V., Lipkowitz, B., Esmaeeli-Nieh, S., Wieczorek, D., Kariminejad, R., Firouzabadi, S.G., Cohen, M., Fattah, Z., Rost, I., Mojahedi, F., Hertzberg, C., Dehghan, A., Rajab, A., Banavandi, M.J.S., Hoffer, J., Falah, M., Musante, L., Kalscheuer, V., Ullmann, R., Kuss, A.W., Tzschach, A., Kahrizi, K., Ropers, H.H., 2011. Deep sequencing reveals 50 novel genes for recessive cognitive disorders. *Nature* 478, 57–63. <https://doi.org/10.1038/nature10423>
- Nakamoto, M., Nalavadi, V., Epstein, M.P., Narayanan, U., Bassell, G.J., Warren, S.T., 2007. Fragile X mental retardation protein deficiency leads to excessive mGluR5-dependent internalization of AMPA receptors. *Proc. Natl. Acad. Sci.* 104, 15537–15542.
<https://doi.org/10.1073/pnas.0707484104>
- Nakashima, M., Imada, H., Shiraishi, E., Ito, Y., Suzuki, N., Miyamoto, M., Taniguchi, T., Iwashita, H., 2018. Phosphodiesterase 2A Inhibitor TAK-915 Ameliorates Cognitive Impairments and Social Withdrawal in N-Methyl-d-Aspartate Receptor Antagonist-Induced Rat Models of Schizophrenia. *J. Pharmacol. Exp. Ther.* 365, 179–188.
<https://doi.org/10.1124/jpet.117.245506>
- Nakashima, M., Suzuki, N., Shiraishi, E., Iwashita, H., 2019. TAK-915, a phosphodiesterase 2A inhibitor, ameliorates the cognitive impairment associated with aging in rodent models. *Behav. Brain Res.* 376, 112192. <https://doi.org/10.1016/j.bbr.2019.112192>
- Nalavadi, V.C., Muddashetty, R.S., Gross, C., Bassell, G.J., 2012. Dephosphorylation-Induced Ubiquitination and Degradation of FMRP in Dendrites: A Role in Immediate Early mGluRStimulated Translation. *J. Neurosci.* 32, 2582–2587.

<https://doi.org/10.1523/JNEUROSCI.5057-11.2012>

Narayanan, U., Nalavadi, V., Nakamoto, M., Pallas, D.C., Ceman, S., Bassell, G.J., Warren, S.T., 2007a. FMRP Phosphorylation Reveals an Immediate-Early Signaling Pathway Triggered by Group I mGluR and Mediated by PP2A. *J. Neurosci.* 27, 14349–14357.

<https://doi.org/10.1523/JNEUROSCI.2969-07.2007>

Narayanan, U., Nalavadi, V., Nakamoto, M., Pallas, D.C., Ceman, S., Bassell, G.J., Warren, S.T., 2007b. FMRP Phosphorylation Reveals an Immediate-Early Signaling Pathway Triggered by Group I mGluR and Mediated by PP2A. *J. Neurosci.* 27, 14349–14357.

<https://doi.org/10.1523/JNEUROSCI.2969-07.2007>

Newschaffer, C.J., Croen, L.A., Daniels, J., Giarelli, E., Grether, J.K., Levy, S.E., Mandell, D.S., Miller, L.A., Pinto-Martin, J., Reaven, J., Reynolds, A.M., Rice, C.E., Schendel, D., Windham, G.C., 2007. The Epidemiology of Autism Spectrum Disorders. *Annu. Rev. Public Health* 28, 235–258. <https://doi.org/10.1146/annurev.publhealth.28.021406.144007>

Ng, M.-C., Yang, Y.-L., Lu, K.-T., 2013. Behavioral and Synaptic Circuit Features in a Zebrafish Model of Fragile X Syndrome. *PLoS ONE* 8. <https://doi.org/10.1371/journal.pone.0051456>

Nimchinsky, E.A., Oberlander, A.M., Svoboda, K., 2001. Abnormal Development of Dendritic Spines in FMR1 Knock-Out Mice. *J. Neurosci.* 21, 5139–5146.
<https://doi.org/10.1523/JNEUROSCI.2114-05139.2001>

Nolan, S.O., Lugo, J.N., 2018. Reversal learning paradigm reveals deficits in cognitive flexibility in the Fmr1 knockout male mouse. *F1000Research* 7.
<https://doi.org/10.12688/f1000research.14969.1>

Noyama, K., Maekawa, S., 2003. Localization of cyclic nucleotide phosphodiesterase 2 in the brain-derived Triton-insoluble low-density fraction (raft). *Neurosci. Res.* 45, 141–148.
[https://doi.org/10.1016/s0168-0102\(02\)00208-0](https://doi.org/10.1016/s0168-0102(02)00208-0)

Oberlé, I., Rousseau, F., Heitz, D., Kretz, C., Devys, D., Hanauer, A., Boué, J., Bertheas, M.F., Mandel, J.L., 1991. Instability of a 550-base pair DNA segment and abnormal methylation in fragile X syndrome. *Science* 252, 1097–1102. <https://doi.org/10.1126/science.252.5009.1097>

Ohta, Y., Akiyama, T., Nishida, E., Sakai, H., 1987. Protein kinase C and cAMP-dependent protein kinase induce opposite effects on actin polymerizability. *FEBS Lett.* 222, 305–310.
[https://doi.org/10.1016/0014-5793\(87\)80391-5](https://doi.org/10.1016/0014-5793(87)80391-5)

Opitz, J.M., Westphal, J.M., Daniel, A., 1984. Discovery of a connective tissue dysplasia in the Martin-Bell syndrome. *Am. J. Med. Genet.* 17, 101–109.
<https://doi.org/10.1002/ajmg.1320170105>

Osterweil, E.K., Krueger, D.D., Reinhold, K., Bear, M.F., 2010. Hypersensitivity to mGluR5 and ERK1/2 Leads to Excessive Protein Synthesis in the Hippocampus of a Mouse Model of Fragile X Syndrome. *J. Neurosci.* 30, 15616–15627. <https://doi.org/10.1523/JNEUROSCI.3888-10.2010>

Pickard, B.S., Thomson, P.A., Christoforou, A., Evans, K.L., Morris, S.W., Porteous, D.J., Blackwood, D.H.R., Muir, W.J., 2007. The PDE4B gene confers sex-specific protection against schizophrenia. *Psychiatr. Genet.* 17, 129–133.
<https://doi.org/10.1097/YGP.0b013e328014492b>

Pieretti, S., Dominici, L., Di Giannuario, A., Cesari, N., Dal Piaz, V., 2006. Local anti-inflammatory effect and behavioral studies on new PDE4 inhibitors. *Life Sci.* 79, 791–800.
<https://doi.org/10.1016/j.lfs.2006.02.026>

Pietropaolo, S., Guilleminot, A., Martin, B., D'Amato, F.R., Crusio, W.E., 2011. Genetic-Background Modulation of Core and Variable Autistic-Like Symptoms in Fmr1 Knock-Out Mice. *PLoS ONE* 6. <https://doi.org/10.1371/journal.pone.0017073>

Potter, L.R., 2011. Guanylyl cyclase structure, function and regulation. *Cell. Signal.* 23, 1921–1926.
<https://doi.org/10.1016/j.cellsig.2011.09.001>

- Prabu, S.K., Anandatheerthavarada, H.K., Raza, H., Srinivasan, S., Spear, J.F., Avadhani, N.G., 2006. Protein kinase A-mediated phosphorylation modulates cytochrome c oxidase function and augments hypoxia and myocardial ischemia-related injury. *J. Biol. Chem.* 281, 2061–2070. <https://doi.org/10.1074/jbc.M507741200>
- Prickaerts, J., de Vente, J., Honig, W., Steinbusch, H.W.M., Blokland, A., 2002. cGMP, but not cAMP, in rat hippocampus is involved in early stages of object memory consolidation. *Eur. J. Pharmacol.* 436, 83–87. [https://doi.org/10.1016/s0014-2999\(01\)01614-4](https://doi.org/10.1016/s0014-2999(01)01614-4)
- Quartier, A., Poquet, H., Gilbert-Dussardier, B., Rossi, M., Casteleyn, A.-S., Portes, V. des, Feger, C., Nourisson, E., Kuentz, P., Redin, C., Thevenon, J., Mosca-Boidron, A.-L., Callier, P., Muller, J., Lesca, G., Huet, F., Geoffroy, V., El Chehadeh, S., Jung, M., Trojak, B., Le Gras, S., Lehalle, D., Jost, B., Maury, S., Masurel, A., Edery, P., Thauvin-Robinet, C., Gérard, B., Mandel, J.-L., Faivre, L., Piton, A., 2017. Infragenic FMR1 disease-causing variants: a significant mutational mechanism leading to Fragile-X syndrome. *Eur. J. Hum. Genet.* 25, 423–431. <https://doi.org/10.1038/ejhg.2016.204>
- Rall, T.W., Sutherland, E.W., 1958. Formation of a cyclic adenine ribonucleotide by tissue particles. *J. Biol. Chem.* 232, 1065–1076.
- Ramírez-Cheyne, J.A., Duque, G.A., Ayala-Zapata, S., Saldarriaga-Gil, W., Hagerman, P., Hagerman, R., Payán-Gómez, C., 2019. Fragile X syndrome and connective tissue dysregulation. *Clin. Genet.* 95, 262–267. <https://doi.org/10.1111/cge.13469>
- Ramos, A., Hollingworth, D., Adinolfi, S., Castets, M., Kelly, G., Frenkiel, T.A., Bardoni, B., Pastore, A., 2006. The Structure of the N-Terminal Domain of the Fragile X Mental Retardation Protein: A Platform for Protein-Protein Interaction. *Structure* 14, 21–31. <https://doi.org/10.1016/j.str.2005.09.018>
- Rapoport, J., Chavez, A., Greenstein, D., Addington, A., Gogtay, N., 2009. Autism-Spectrum Disorders and Childhood Onset Schizophrenia: Clinical and Biological Contributions to a Relationship Revisited. *J. Am. Acad. Child Adolesc. Psychiatry* 48, 10–18. <https://doi.org/10.1097/CHI.0b013e31818b1c63>
- Reed, T.M., Repaske, D.R., Snyder, G.L., Greengard, P., Vorhees, C.V., 2002. Phosphodiesterase 1B Knock-Out Mice Exhibit Exaggerated Locomotor Hyperactivity and DARPP-32 Phosphorylation in Response to Dopamine Agonists and Display Impaired Spatial Learning. *J. Neurosci.* 22, 5188–5197. <https://doi.org/10.1523/JNEUROSCI.22-12-05188.2002>
- Reiss, A.L., Abrams, M.T., Greenlaw, R., Freund, L., Denckla, M.B., 1995. Neurodevelopmental effects of the FMR-1 full mutation in humans. *Nat. Med.* 1, 159–167. <https://doi.org/10.1038/nm0295-159>
- Reschly, D.J., 2009. Documenting the Developmental Origins of Mild Mental Retardation. *Appl. Neuropsychol.* 16, 124–134. <https://doi.org/10.1080/09084280902864469>
- Reyes-Harde, M., Empson, R., Potter, B.V.L., Gajone, A., Stanton, P.K., 1999. Evidence of a role for cyclic ADP-ribose in long-term synaptic depression in hippocampus. *Proc. Natl. Acad. Sci. U. S. A.* 96, 4061–4066.
- Reynolds, C.D., Nolan, S.O., Jefferson, T., Lugo, J.N., 2016. Sex- & Genotype-Specific Differences in Vocalization Development in FMR1 Knockout Mice. *Neuroreport* 27, 1331–1335. <https://doi.org/10.1097/WNR.0000000000000701>
- Richards, S.B., Brady, M.P., Taylor, R.L., 2014. Cognitive and Intellectual Disabilities: Historical Perspectives, Current Practices, and Future Directions. Routledge.
- Rodríguez-Moreno, A., Sihra, T.S., 2013. Presynaptic kainate receptor-mediated facilitation of glutamate release involves Ca²⁺-calmodulin and PKA in cerebrocortical synaptosomes. *FEBS Lett.* 587, 788–792. <https://doi.org/10.1016/j.febslet.2013.01.071>
- Roisen, F.J., Murphy, R.A., Braden, W.G., 1972. Neurite development in vitro. I. The effects of adenosine 3'5'-cyclic monophosphate (cyclic AMP). *J. Neurobiol.* 3, 347–368.

<https://doi.org/10.1002/neu.480030408>

Ronemus, M., Iossifov, I., Levy, D., Wigler, M., 2014. The role of de novo mutations in the genetics of autism spectrum disorders. *Nat. Rev. Genet.* 15, 133–141. <https://doi.org/10.1038/nrg3585>

Rosenberg, R.E., Law, J.K., Yenokyan, G., McGready, J., Kaufmann, W.E., Law, P.A., 2009.

Characteristics and concordance of autism spectrum disorders among 277 twin pairs. *Arch. Pediatr. Adolesc. Med.* 163, 907–914. <https://doi.org/10.1001/archpediatrics.2009.98>

Rosman, G.J., Martins, T.J., Sonnenburg, W.K., Beavo, J.A., Ferguson, K., Loughney, K., 1997. Isolation and characterization of human cDNAs encoding a cGMP-stimulated 3',5'-cyclic nucleotide phosphodiesterase1The nucleotide sequence reported in this paper has been submitted to the GenBankTM/EMBL Data Bank with accession No. U67733.1. *Gene* 191, 89–95.

[https://doi.org/10.1016/S0378-1119\(97\)00046-2](https://doi.org/10.1016/S0378-1119(97)00046-2)

Ruan, L., Du, K., Tao, M., Shan, C., Ye, R., Tang, Y., Pan, H., Lv, J., Zhang, M., Pan, J., 2019.

Phosphodiesterase-2 Inhibitor Bay 60-7550 Ameliorates Aβ-Induced Cognitive and Memory Impairment via Regulation of the HPA Axis. *Front. Cell. Neurosci.* 13.

<https://doi.org/10.3389/fncel.2019.00432>

Rubeis, S.D., He, X., Goldberg, A.P., Poultney, C.S., Samocha, K., Cicek, A.E., Kou, Y., Liu, L., Fromer, M., Walker, S., Singh, T., Klei, L., Kosmicki, J., Fu, S.-C., Aleksic, B., Biscaldi, M., Bolton, P.F., Brownfeld, J.M., Cai, J., Campbell, N.G., Carracedo, A., Chahrour, M.H., Chiocchetti, A.G., Coon, H., Crawford, E.L., Crooks, L., Curran, S.R., Dawson, G., Duketis, E., Fernandez, B.A., Gallagher, L., Geller, E., Guter, S.J., Hill, R.S., Ionita-Laza, I., Gonzalez, P.J., Kilpinen, H., Klauck, S.M., Kolevzon, A., Lee, I., Lei, J., Lehtimäki, T., Lin, C.-F., Ma'ayan, A., Marshall, C.R., McInnes, A.L., Neale, B., Owen, M.J., Ozaki, N., Parellada, M., Parr, J.R., Purcell, S., Puura, K., Rajagopalan, D., Rehnström, K., Reichenberg, A., Sabo, A., Sachse, M., Sanders, S.J., Schafer, C., Schulte-Rüther, M., Skuse, D., Stevens, C., Szatmari, P., Tammimies, K., Valladares, O., Voran, A., Wang, L.-S., Weiss, L.A., Willsey, A.J., Yu, T.W., Yuen, R.K.C., Cook, E.H., Freitag, C.M., Gill, M., Hultman, C.M., Lehner, T., Palotie, A., Schellenberg, G.D., Sklar, P., State, M.W., Sutcliffe, J.S., Walsh, C.A., Scherer, S.W., Zwick, M.E., Barrett, J.C., Cutler, D.J., Roeder, K., Devlin, B., Daly, M.J., Buxbaum, J.D., 2014. Synaptic, transcriptional and chromatin genes disrupted in autism. *Nature* 515, 209–215. <https://doi.org/10.1038/nature13772>

Rudelli, R.D., Brown, W.T., Wisniewski, K., Jenkins, E.C., Laure-Kamionowska, M., Connell, F., Wisniewski, H.M., 1985. Adult fragile X syndrome. Clinico-neuropathologic findings. *Acta Neuropathol. (Berl.)* 67, 289–295. <https://doi.org/10.1007/BF00687814>

Russwurm, C., Zoidl, G., Koesling, D., Russwurm, M., 2009. The neuronal PDE2A3 splice variant is targeted to membranes via dual acylation. *BMC Pharmacol.* 9, P61.

<https://doi.org/10.1186/1471-2210-9-S1-P61>

Rutten, K., Wallace, T.L., Works, M., Prickaerts, J., Blokland, A., Novak, T.J., Santarelli, L., Misner, D.L., 2011. Enhanced long-term depression and impaired reversal learning in phosphodiesterase 4B-knockout (PDE4B-/-) mice. *Neuropharmacology* 61, 138–147.

<https://doi.org/10.1016/j.neuropharm.2011.03.020>

Sabaratnam, M., Vroegop, P.G., Gangadharan, S.K., 2001. Epilepsy and EEG findings in 18 males with fragile X syndrome. *Seizure* 10, 60–63. <https://doi.org/10.1053/seiz.2000.0492>

Salcedo-Arellano, M.J., Lozano, R., Tassone, F., Hagerman, R.J., Saldarriaga, W., 2016. Alcohol use dependence in fragile X syndrome. *Intractable Rare Dis. Res.* 5, 207–213.

<https://doi.org/10.5582/irdr.2016.01046>

Saldarriaga, W., Forero-Forero, J.V., González-Teshima, L.Y., Fandiño-Losada, A., Isaza, C., Tovar-Cuevas, J.R., Silva, M., Choudhary, N.S., Tang, H.-T., Aguilar-Gaxiola, S., Hagerman, R.J., Tassone, F., 2018. Genetic cluster of fragile X syndrome in a Colombian district. *J. Hum. Genet.* 63, 509–516. <https://doi.org/10.1038/s10038-017-0407-6>

- Salpietro, V., Perez-Dueñas, B., Nakashima, K., San Antonio-Arce, V., Manole, A., Efthymiou, S., Vandrovčová, J., Bettencourt, C., Mencacci, N.E., Klein, C., Kelly, M.P., Davies, C.H., Kimura, H., Macaya, A., Houlden, H., 2018. A homozygous loss-of-function mutation in PDE2A associated to early-onset hereditary chorea. *Mov. Disord.* 33, 482–488.
<https://doi.org/10.1002/mds.27286>
- Sanders, S.J., Murtha, M.T., Gupta, A.R., Murdoch, J.D., Raubeson, M.J., Willsey, A.J., Ercan-Sencicek, A.G., DiLullo, N.M., Parikhshak, N.N., Stein, J.L., Walker, M.F., Ober, G.T., Teran, N.A., Song, Y., El-Fishawy, P., Murtha, R.C., Choi, M., Overton, J.D., Bjornson, R.D., Carriero, N.J., Meyer, K.A., Bilguvar, K., Mane, S.M., Sestan, N., Lifton, R.P., Günel, M., Roeder, K., Geschwind, D.H., Devlin, B., State, M.W., 2012. De novo mutations revealed by whole-exome sequencing are strongly associated with autism. *Nature* 485, 237–241. <https://doi.org/10.1038/nature10945>
- Sanderson, J.L., Gorski, J.A., Dell'Acqua, M.L., 2016. NMDA Receptor-Dependent LTD Requires Transient Synaptic Incorporation of Ca²⁺-Permeable AMPARs Mediated by AKAP150Anchored PKA and Calcineurin. *Neuron* 89, 1000–1015.
<https://doi.org/10.1016/j.neuron.2016.01.043>
- Sandin, S., Lichtenstein, P., Kuja-Halkola, R., Hultman, C., Larsson, H., Reichenberg, A., 2017. The Heritability of Autism Spectrum Disorder. *JAMA* 318, 1182–1184.
<https://doi.org/10.1001/jama.2017.12141>
- Sandoval, G.M., Shim, S., Hong, D.S., Garrett, A.S., Quintin, E.-M., Marzelli, M.J., Patnaik, S., Lightbody, A.A., Reiss, A.L., 2018. Neuroanatomical abnormalities in fragile X syndrome during the adolescent and young adult years. *J. Psychiatr. Res.* 107, 138–144.
<https://doi.org/10.1016/j.jpsychires.2018.10.014>
- Sass, P., Field, J., Nikawa, J., Toda, T., Wigler, M., 1986. Cloning and characterization of the highaffinity cAMP phosphodiesterase of *Saccharomyces cerevisiae*. *Proc. Natl. Acad. Sci. U. S. A.* 83, 9303–9307.
- Schaeffer, C., Bardoni, B., Mandel, J.-L., Ehresmann, B., Ehresmann, C., Moine, H., 2001. The fragile X mental retardation protein binds specifically to its mRNA via a purine quartet motif. *EMBO J.* 20, 4803–4813. <https://doi.org/10.1093/emboj/20.17.4803>
- Scharkowski, F., Frotscher, M., Lutz, D., Korte, M., Michaelsen-Preusse, K., 2018. Altered Connectivity and Synapse Maturation of the Hippocampal Mossy Fiber Pathway in a Mouse Model of the Fragile X Syndrome. *Cereb. Cortex* 28, 852–867. <https://doi.org/10.1093/cercor/bhw408>
- Scheerenberger, R.C., 1983. A History of Mental Retardation. P.H. Brookes Publishing Company.
- Schenck, A., Bardoni, B., Langmann, C., Harden, N., Mandel, J.-L., Giangrande, A., 2003. CYFIP/Sra-1 Controls Neuronal Connectivity in *Drosophila* and Links the Rac1 GTPase Pathway to the Fragile X Protein. *Neuron* 38, 887–898. [https://doi.org/10.1016/S0896-6273\(03\)00354-4](https://doi.org/10.1016/S0896-6273(03)00354-4)
- Schneider, A., Hagerman, R.J., Hessl, D., 2009. Fragile X syndrome—From genes to cognition. *Dev. Disabil. Res. Rev.* 15, 333–342. <https://doi.org/10.1002/ddrr.80>
- Schneider, A., Seritan, A., Tassone, F., Rivera, S.M., Hagerman, R., Hessl, D., 2013. Psychiatric Features in High-Functioning Adult Brothers With Fragile X Spectrum Disorders. *Prim. Care Companion CNS Disord.* 15. <https://doi.org/10.4088/PCC.12l01492>
- Schneider, A., Winarni, T.I., Cabal-Herrera, A.M., Bacalman, S., Gane, L., Hagerman, P., Tassone, F., Hagerman, R., 2020. Elevated FMR1-mRNA and lowered FMRP – A double-hit mechanism for psychiatric features in men with FMR1 premutations. *Transl. Psychiatry* 10.
<https://doi.org/10.1038/s41398-020-00863-w>
- Schoffelmeer, A.N., Wardeh, G., Mulder, A.H., 1985. Cyclic AMP facilitates the electrically evoked release of radiolabelled noradrenaline, dopamine and 5-hydroxytryptamine from rat brain slices. *Naunyn. Schmiedebergs Arch. Pharmacol.* 330, 74–76.
<https://doi.org/10.1007/BF00586712>

- Seese, R.R., Le, A.A., Wang, K., Cox, C.D., Lynch, G., Gall, C.M., 2020. A TrkB agonist and ampakine rescue synaptic plasticity and multiple forms of memory in a mouse model of intellectual disability. *Neurobiol. Dis.* 134, 104604. <https://doi.org/10.1016/j.nbd.2019.104604>
- Sellier, C., Buijsen, R.A.M., He, F., Natla, S., Jung, L., Tropel, P., Gaucherot, A., Jacobs, H., Meziane, H., Vincent, A., Champy, M.-F., Sorg, T., Pavlovic, G., Wattenhofer-Donze, M., Birling, M.-C., Oulad-Abdelghani, M., Eberling, P., Ruffenach, F., Joint, M., Anheim, M., Martinez-Cerdeno, V., Tassone, F., Willemse, R., Hukema, R.K., Viville, S., Martinat, C., Todd, P.K., Charlet-Berguerand, N., 2017. Translation of Expanded CGG Repeats into FMRpolyG Is Pathogenic and May Contribute to Fragile X Tremor Ataxia Syndrome. *Neuron* 93, 331–347. <https://doi.org/10.1016/j.neuron.2016.12.016>
- Semple, B.D., Blomgren, K., Gimlin, K., Ferriero, D.M., Noble-Haeusslein, L.J., 2013. Brain development in rodents and humans: Identifying benchmarks of maturation and vulnerability to injury across species. *Prog. Neurobiol.* 0, 1–16. <https://doi.org/10.1016/j.pneurobio.2013.04.001>
- Shah, S., Molinaro, G., Liu, B., Wang, R., Huber, K.M., Richter, J.D., 2020. FMRP Control of Ribosome Translocation Promotes Chromatin Modifications and Alternative Splicing of Neuronal Genes Linked to Autism. *Cell Rep.* 30, 4459–4472.e6. <https://doi.org/10.1016/j.celrep.2020.02.076>
- Sharifzadeh, M., Sharifzadeh, K., Naghdi, N., Ghahremani, M.H., Roghani, A., 2005. Posttraining intrahippocampal infusion of a protein kinase AII inhibitor impairs spatial memory retention in rats. *J. Neurosci. Res.* 79, 392–400. <https://doi.org/10.1002/jnr.20358>
- Shelly, M., Cancedda, L., Heilshorn, S., Sumbre, G., Poo, M.-M., 2007. LKB1/STRAD promotes axon initiation during neuronal polarization. *Cell* 129, 565–577. <https://doi.org/10.1016/j.cell.2007.04.012>
- Shelly, M., Lim, B.K., Cancedda, L., Heilshorn, S.C., Gao, H., Poo, M., 2010a. Local and Long-Range Reciprocal Regulation of cAMP and cGMP in Axon/Dendrite Formation. *Science* 327, 547–552. <https://doi.org/10.1126/science.1179735>
- Shelly, M., Lim, B.K., Cancedda, L., Heilshorn, S.C., Gao, H., Poo, M., 2010b. Local and Long-Range Reciprocal Regulation of cAMP and cGMP in Axon/Dendrite Formation. *Science* 327, 547–552. <https://doi.org/10.1126/science.1179735>
- Sheng, M., Mcfadden, G., Greenberg, M., 1990. Membrane depolarization and calcium induce c-fos transcription via phosphorylation of transcription factor CREB. *Neuron*. [https://doi.org/10.1016/0896-6273\(90\)90115-V](https://doi.org/10.1016/0896-6273(90)90115-V)
- Shi, J., Liu, H., Pan, J., Chen, J., Zhang, N., Liu, K., Fei, N., O'Donnell, J.M., Zhang, H.-T., Xu, Y., 2018. Inhibition of phosphodiesterase 2 by Bay 60-7550 decreases ethanol intake and preference in mice. *Psychopharmacology (Berl.)* 235, 2377–2385. <https://doi.org/10.1007/s00213-0184934-4>
- Simonoff, E., Pickles, A., Charman, T., Chandler, S., Loucas, T., Baird, G., 2008. Psychiatric Disorders in Children With Autism Spectrum Disorders: Prevalence, Comorbidity, and Associated Factors in a Population-Derived Sample. *J. Am. Acad. Child Adolesc. Psychiatry* 47, 921–929. <https://doi.org/10.1097/CHI.0b013e318179964f>
- Siuciak, J.A., Chapin, D.S., McCarthy, S.A., Martin, A.N., 2007. Antipsychotic profile of rolipram: efficacy in rats and reduced sensitivity in mice deficient in the phosphodiesterase-4B (PDE4B) enzyme. *Psychopharmacology (Berl.)* 192, 415–424. <https://doi.org/10.1007/s00213-0070727-x>
- Siuciak, J.A., McCarthy, S.A., Chapin, D.S., Martin, A.N., Harms, J.F., Schmidt, C.J., 2008. Behavioral characterization of mice deficient in the phosphodiesterase-10A (PDE10A) enzyme on a C57/Bl6N congenic background. *Neuropharmacology* 54, 417–427. <https://doi.org/10.1016/j.neuropharm.2007.10.009>

- Soares, L.M., Meyer, E., Milani, H., Steinbusch, H.W.M., Prickaerts, J., Oliveira, R.M.W. de, 2017. The phosphodiesterase type 2 inhibitor BAY 60-7550 reverses functional impairments induced by brain ischemia by decreasing hippocampal neurodegeneration and enhancing hippocampal neuronal plasticity. *Eur. J. Neurosci.* 45, 510–520. <https://doi.org/10.1111/ejn.13461>
- Sominsky, L., De Luca, S., Spencer, S.J., 2018. Microglia: Key players in neurodevelopment and neuronal plasticity. *Int. J. Biochem. Cell Biol.* 94, 56–60. <https://doi.org/10.1016/j.biocel.2017.11.012>
- Son, H., Lu, Y.-F., Zhuo, M., Arancio, O., Kandel, E.R., Hawkins, R.D., 1998. The Specific Role of cGMP in Hippocampal LTP. *Learn. Mem.* 5, 231–245.
- Spencer, C.M., Alekseyenko, O., Hamilton, S.M., Thomas, A.M., Serysheva, E., Yuva-Paylor, L.A., Paylor, R., 2011. Modifying Behavioral Phenotypes in Fmr1 KO Mice: Genetic Background Differences Reveal Autistic-Like Responses. *Autism Res. Off. J. Int. Soc. Autism Res.* 4, 40–56. <https://doi.org/10.1002/aur.168>
- Spencer, C.M., Alekseyenko, O., Serysheva, E., Yuva-Paylor, L.A., Paylor, R., 2005. Altered anxietyrelated and social behaviors in the Fmr1 knockout mouse model of fragile X syndrome. *Genes Brain Behav.* 4, 420–430. <https://doi.org/10.1111/j.1601-183X.2005.00123.x>
- Spitzer, N.C., Root, C.M., Borodinsky, L.N., 2004. Orchestrating neuronal differentiation: patterns of Ca²⁺ spikes specify transmitter choice. *Trends Neurosci.* 27, 415–421. <https://doi.org/10.1016/j.tins.2004.05.003>
- Stefani, G., Fraser, C.E., Darnell, J.C., Darnell, R.B., 2004. Fragile X Mental Retardation Protein Is Associated with Translating Polyribosomes in Neuronal Cells. *J. Neurosci.* 24, 7272–7276. <https://doi.org/10.1523/JNEUROSCI.2306-04.2004>
- Stephenson, D.T., Coskran, T.M., Kelly, M.P., Kleiman, R.J., Morton, D., O’neill, S.M., Schmidt, C.J., Weinberg, R.J., Menniti, F.S., 2012. The Distribution of Phosphodiesterase 2a in the Rat Brain. *Neuroscience* 226, 145–155. <https://doi.org/10.1016/j.neuroscience.2012.09.011>
- Stephenson, D.T., Coskran, T.M., Wilhelms, M.B., Adamowicz, W.O., O’Donnell, M.M., Muravnick, K.B., Menniti, F.S., Kleiman, R.J., Morton, D., 2009. Immunohistochemical Localization of Phosphodiesterase 2A in Multiple Mammalian Species. *J. Histochem. Cytochem.* 57, 933–949. <https://doi.org/10.1369/jhc.2009.953471>
- Ster, J., de Bock, F., Bertaso, F., Abitbol, K., Daniel, H., Bockaert, J., Fagni, L., 2009. Epac mediates PACAP-dependent long-term depression in the hippocampus. *J. Physiol.* 587, 101–113. <https://doi.org/10.1113/jphysiol.2008.157461>
- Streisinger, G., Walker, C., Dower, N., Knauber, D., Singer, F., 1981. Production of clones of homozygous diploid zebra fish (Brachydanio rerio). *Nature* 291, 293–296. <https://doi.org/10.1038/291293a0>
- Sutherland, C., 2011. What Are the bona fide GSK3 Substrates? *Int. J. Alzheimers Dis.* 2011. <https://doi.org/10.4061/2011/505607>
- Sutherland, G.R., 1977. Fragile sites on human chromosomes: demonstration of their dependence on the type of tissue culture medium. *Science* 197, 265–266. <https://doi.org/10.1126/science.877551>
- Suzuki, K., Sugihara, G., Ouchi, Y., Nakamura, K., Futatsubashi, M., Takebayashi, K., Yoshihara, Y., Omata, K., Matsumoto, K., Tsuchiya, K.J., Iwata, Y., Tsujii, M., Sugiyama, T., Mori, N., 2013. Microglial activation in young adults with autism spectrum disorder. *JAMA Psychiatry* 70, 49–58. <https://doi.org/10.1001/jamapsychiatry.2013.272>
- Swerdlow, N.R., Light, G.A., Thomas, M.L., Srock, J., Calkins, M.E., Green, M.F., Greenwood, T.A., Gur, R.E., Gur, R.C., Lazzeroni, L.C., Nuechterlein, K.H., Radant, A.D., Seidman, L.J., Siever, L.J.,

- Silverman, J.M., Stone, W.S., Sugar, C.A., Tsuang, D.W., Tsuang, M.T., Turetsky, B.I., Braff, D.L., 2018. Deficient prepulse inhibition in schizophrenia in a multi-site cohort: Internal replication and extension. *Schizophr. Res.*, Impaired sensorimotor Gating in Schizophrenia 198, 6–15. <https://doi.org/10.1016/j.schres.2017.05.013>
- Tabet, R., Moutin, E., Becker, J.A.J., Heintz, D., Fouillen, L., Flatter, E., Kręzel, W., Alunni, V., Koebel, P., Dembélé, D., Tassone, F., Bardoni, B., Mandel, J.-L., Vitale, N., Muller, D., Merrer, J.L., Moine, H., 2016. Fragile X Mental Retardation Protein (FMRP) controls diacylglycerol kinase activity in neurons. *Proc. Natl. Acad. Sci.* 113, E3619–E3628. <https://doi.org/10.1073/pnas.1522631113>
- Tamanini, F., Willemsen, R., van Unen, L., Bontekoe, C., Galjaard, H., Oostra, B.A., Hoogeveen, A.T., 1997. Differential Expression of FMR1, FXR1 and FXR2 Proteins in Human Brain and Testis. *Hum. Mol. Genet.* 6, 1315–1322. <https://doi.org/10.1093/hmg/6.8.1315>
- Tan, M., Ma, S., Huang, Q., Hu, K., Song, B., Li, M., 2013. GSK-3 α / β -mediated phosphorylation of CRMP-2 regulates activity-dependent dendritic growth. *J. Neurochem.* 125, 685–697. <https://doi.org/10.1111/jnc.12230>
- Tan, W., Schauder, C., Naryshkina, T., Minakhina, S., Steward, R., 2016. Zfrp8 forms a complex with Fragile-X Mental Retardation Protein and regulates its localization and function. *Dev. Biol.* 410, 202–212. <https://doi.org/10.1016/j.ydbio.2015.12.008>
- Tang, F., Dent, E.W., Kalil, K., 2003. Spontaneous Calcium Transients in Developing Cortical Neurons Regulate Axon Outgrowth. *J. Neurosci.* 23, 927–936. <https://doi.org/10.1523/JNEUROSCI.2303-00927.2003>
- Tassone, F., Hagerman, R.J., Taylor, A.K., Gane, L.W., Godfrey, T.E., Hagerman, P.J., 2000. Elevated Levels of FMR1 mRNA in Carrier Males: A New Mechanism of Involvement in the Fragile-X Syndrome. *Am. J. Hum. Genet.* 66, 6–15.
- Taylor, S.S., Buechler, J.A., Yonemoto, W., 1990. cAMP-dependent protein kinase: framework for a diverse family of regulatory enzymes. *Annu. Rev. Biochem.* 59, 971–1005. <https://doi.org/10.1146/annurev.bi.59.070190.004543>
- Teixeira, M.M., Gristwood, R.W., Cooper, N., Hellewell, P.G., 1997. Phosphodiesterase (PDE)4 inhibitors: anti-inflammatory drugs of the future? *Trends Pharmacol. Sci.* 18, 164–171. [https://doi.org/10.1016/s0165-6147\(97\)01049-3](https://doi.org/10.1016/s0165-6147(97)01049-3)
- The Autism Spectrum Disorders Working Group of The Psychiatric Genomics Consortium, 2017. Meta-analysis of GWAS of over 16,000 individuals with autism spectrum disorder highlights a novel locus at 10q24.32 and a significant overlap with schizophrenia. *Mol. Autism* 8, 21. <https://doi.org/10.1186/s13229-017-0137-9>
- Thomas, A.M., Bui, N., Graham, D., Perkins, J.R., Yuva-Paylor, L.A., Paylor, R., 2011. Genetic reduction of group 1 metabotropic glutamate receptors alters select behaviors in a mouse model for fragile X syndrome. *Behav. Brain Res.* 223, 310–321. <https://doi.org/10.1016/j.bbr.2011.04.049>
- Thomas, A.M., Bui, N., Perkins, J.R., Yuva-Paylor, L.A., Paylor, R., 2012. Group I metabotropic glutamate receptor antagonists alter select behaviors in a mouse model for fragile X syndrome. *Psychopharmacology (Berl.)* 219, 47–58. <https://doi.org/10.1007/s00213-012-2375-4>
- Tian, Y., Yang, C., Shang, S., Cai, Y., Deng, X., Zhang, J., Shao, F., Zhu, D., Liu, Y., Chen, G., Liang, J., Sun, Q., Qiu, Z., Zhang, C., 2017. Loss of FMRP Impaired Hippocampal Long-Term Plasticity and Spatial Learning in Rats. *Front. Mol. Neurosci.* 10. <https://doi.org/10.3389/fnmol.2017.00269>
- Till, S.M., Asiminas, A., Jackson, A.D., Katsanevakis, D., Barnes, S.A., Osterweil, E.K., Bear, M.F., Chattarji, S., Wood, E.R., Wyllie, D.J.A., Kind, P.C., 2015. Conserved hippocampal cellular pathophysiology but distinct behavioural deficits in a new rat model of FXS. *Hum. Mol. Genet.* 24, 5977–5984. <https://doi.org/10.1093/hmg/ddv299>

- Turner, G., Daniel, A., Frost, M., 1980. X-linked mental retardation, macro-orchidism, and the Xq27 fragile site. *J. Pediatr.* 96, 837–841. [https://doi.org/10.1016/s0022-3476\(80\)80552-x](https://doi.org/10.1016/s0022-3476(80)80552-x)
- Undi, R.B., Gutti, U., Gutti, R.K., 2017. LiCl regulates mitochondrial biogenesis during megakaryocyte development. *J. Trace Elem. Med. Biol. Organ Soc. Miner. Trace Elel. GMS* 39, 193–201. <https://doi.org/10.1016/j.jtemb.2016.10.003>
- Valverde, R., Edwards, L., Regan, L., 2008. Structure and function of KH domains. *FEBS J.* 275, 2712–2726. <https://doi.org/10.1111/j.1742-4658.2008.06411.x>
- Valverde, R., Pozdnyakova, I., Kajander, T., Venkatraman, J., Regan, L., 2007. Fragile X mental retardation syndrome: structure of the KH1-KH2 domains of fragile X mental retardation protein. *Struct. Lond. Engl.* 1993 15, 1090–1098. <https://doi.org/10.1016/j.str.2007.06.022>
- Van Dam, D., Errijgers, V., Kooy, R.F., Willemse, R., Mientjes, E., Oostra, B.A., De Deyn, P.P., 2005. Cognitive decline, neuromotor and behavioural disturbances in a mouse model for fragile-X-associated tremor/ataxia syndrome (FXTAS). *Behav. Brain Res.* 162, 233–239. <https://doi.org/10.1016/j.bbr.2005.03.007>
- Veloz, M.F.V., Buijsen, R.A.M., Willemse, R., Cupido, A., Bosman, L.W.J., Koekkoek, S.K.E., Potters, J.W., Oostra, B.A., De Zeeuw, C.I., 2012. The effect of an mGluR5 inhibitor on procedural memory and avoidance discrimination impairments in Fmr1 KO mice. *Genes Brain Behav.* 11, 325–331. <https://doi.org/10.1111/j.1601-183X.2011.00763.x>
- Ventura, R., Pascucci, T., Catania, M.V., Musumeci, S.A., Puglisi-Allegra, S., 2004. Object recognition impairment in Fmr1 knockout mice is reversed by amphetamine: involvement of dopamine in the medial prefrontal cortex. *Behav. Pharmacol.* 15, 433–442.
- Verkerk, A.J., Pieretti, M., Sutcliffe, J.S., Fu, Y.H., Kuhl, D.P., Pizzuti, A., Reiner, O., Richards, S., Victoria, M.F., Zhang, F.P., 1991. Identification of a gene (FMR-1) containing a CGG repeat coincident with a breakpoint cluster region exhibiting length variation in fragile X syndrome. *Cell* 65, 905–914. [https://doi.org/10.1016/0092-8674\(91\)90397-h](https://doi.org/10.1016/0092-8674(91)90397-h)
- Verkerk, A.J.M.H., de Graaff, E., De Boulle, K., Eichler, E.E., Konecki, D.S., Reyniers, E., Manca, A., Poustka, A., Willems, P.J., Nelson, D.L., Oostra, B.A., 1993. Alternative splicing in the fragile X gene FMR1. *Hum. Mol. Genet.* 2, 399–404. <https://doi.org/10.1093/hmg/2.4.399>
- Vincent, A., Hertz, D., Petit, C., Kretz, C., Oberlé, I., Mandel, J.-L., 1991. Abnormal pattern detected in fragile-X patients by pulsed-field gel electrophoresis. *Nature* 349, 624–626. <https://doi.org/10.1038/349624a0>
- Volkmar, F.R., McPartland, J.C., 2014. From Kanner to DSM-5: Autism as an Evolving Diagnostic Concept. *Annu. Rev. Clin. Psychol.* 10, 193–212. <https://doi.org/10.1146/annurev-clinpsy032813-153710>
- Volkmar, F.R., Reichow, B., McPartland, J., 2012. Classification of autism and related conditions: progress, challenges, and opportunities. *Dialogues Clin. Neurosci.* 14, 229–237.
- Wang, J.-N., Zhao, Xue-jun, Liu, Z., Zhao, Xu-li, Sun, T., Fu, Z., 2017. Selective phosphodiesterase-2A inhibitor alleviates radicular inflammation and mechanical allodynia in non-compressive lumbar disc herniation rats. *Eur. Spine J.* 26, 1961–1968. <https://doi.org/10.1007/s00586017-5023-9>
- Wang, L., Xiaokaiti, Y., Wang, G., Xu, X., Chen, L., Huang, X., Liu, L., Pan, J., Hu, S., Chen, Z., Xu, Y., 2017. Inhibition of PDE2 reverses beta amyloid induced memory impairment through regulation of PKA/PKG-dependent neuro-inflammatory and apoptotic pathways. *Sci. Rep.* 7, 12044. <https://doi.org/10.1038/s41598-017-08070-2>
- Westmark, C.J., Malter, J.S., 2007. FMRP Mediates mGluR5-Dependent Translation of Amyloid Precursor Protein. *PLoS Biol.* 5. <https://doi.org/10.1371/journal.pbio.0050052>
- Willemse, R., Bontekoe, C.J., Severijnen, L.-A., Oostra, B.A., 2002. Timing of the absence of FMR1 expression in full mutation chorionic villi. *Hum. Genet.* 110, 601–605. <https://doi.org/10.1007/s00439-002-0723-5>

- Wincott, C.M., Kim, S., Titcombe, R.F., Tukey, D.S., Girma, H.K., Pick, J.E., Devito, L.M., Hofmann, F., Hoeffer, C., Ziff, E.B., 2013. Spatial memory deficits and motor coordination facilitation in cGMP-dependent protein kinase type II-deficient mice. *Neurobiol. Learn. Mem.* 99, 32–37. <https://doi.org/10.1016/j.nlm.2012.10.003>
- Wing, L., 1981. Asperger's syndrome: a clinical account. *Psychol. Med.* 11, 115–129. <https://doi.org/10.1017/S0033291700053332>
- Wu, J., Wang, Y., Rowan, M.J., Anwyl, R., 1998. Evidence for Involvement of the cGMP–Protein Kinase G Signaling System in the Induction of Long-Term Depression, But Not Long-Term Potentiation, in the Dentate Gyrus In Vitro. *J. Neurosci.* 18, 3589–3596. <https://doi.org/10.1523/JNEUROSCI.18-10-03589.1998>
- Wu, Y.-J., Hsu, M.-T., Ng, M.-C., Amstislavskaya, T.G., Tikhonova, M.A., Yang, Y.-L., Lu, K.-T., 2017. Fragile X Mental Retardation-1 Knockout Zebrafish Shows Precocious Development in Social Behavior. *Zebrafish* 14, 438–443. <https://doi.org/10.1089/zeb.2017.1446>
- Xu, B., Roos, J.L., Dexheimer, P., Boone, B., Plummer, B., Levy, S., Gogos, J.A., Karayiorgou, M., 2011. Exome sequencing supports a de novo mutational paradigm for schizophrenia. *Nat. Genet.* 43, 864–868. <https://doi.org/10.1038/ng.902>
- Yan, Q.J., Asafo-Adjei, P.K., Arnold, H.M., Brown, R.E., Bauchwitz, R.P., 2004. A phenotypic and molecular characterization of the fmr1-tm1Cgr Fragile X mouse. *Genes Brain Behav.* 3, 337–359. <https://doi.org/10.1111/j.1601-183X.2004.00087.x>
- Yang, K., Chen, Z., Gao, J., Shi, W., Li, L., Jiang, S., Hu, H., Liu, Z., Xu, D., Wu, L., 2017. The Key Roles of GSK-3 β in Regulating Mitochondrial Activity. *Cell. Physiol. Biochem.* 44, 1445–1459. <https://doi.org/10.1159/000485580>
- Yoshimura, T., Arimura, N., Kawano, Y., Kawabata, S., Wang, S., Kaibuchi, K., 2006. Ras regulates neuronal polarity via the PI3-kinase/Akt/GSK-3 β /CRMP-2 pathway. *Biochem. Biophys. Res. Commun.* 340, 62–68. <https://doi.org/10.1016/j.bbrc.2005.11.147>
- Yuskaitis, C.J., Mines, M.A., King, M.K., Sweatt, J.D., Miller, C.A., Jope, R.S., 2010a. Lithium ameliorates altered glycogen synthase kinase-3 and behavior in a mouse model of Fragile X syndrome. *Biochem. Pharmacol.* 79, 632–646. <https://doi.org/10.1016/j.bcp.2009.09.023>
- Yuskaitis, C.J., Mines, M.A., King, M.K., Sweatt, J.D., Miller, C.A., Jope, R.S., 2010b. Lithium ameliorates altered glycogen synthase kinase-3 and behavior in a mouse model of Fragile X syndrome. *Biochem. Pharmacol.* 79, 632–646. <https://doi.org/10.1016/j.bcp.2009.09.023> Zhang, H.-T., Huang, Y., Jin, S.-L.C., Frith, S.A., Suvarna, N., Conti, M., O'Donnell, J.M., 2002. Antidepressant-like Profile and Reduced Sensitivity to Rolipram in Mice Deficient in the PDE4D Phosphodiesterase Enzyme. *Neuropsychopharmacology* 27, 587–595. [https://doi.org/10.1016/S0893-133X\(02\)00344-5](https://doi.org/10.1016/S0893-133X(02)00344-5)
- Zhang, H.-T., Huang, Y., Masood, A., Stolinski, L.R., Li, Y., Zhang, L., Dlaboga, D., Jin, S.-L.C., Conti, M., O'Donnell, J.M., 2008. Anxiogenic-Like Behavioral Phenotype of Mice Deficient in Phosphodiesterase 4B (PDE4B). *Neuropsychopharmacol. Off. Publ. Am. Coll. Neuropsychopharmacol.* 33, 1611–1623. <https://doi.org/10.1038/sj.npp.1301537>
- Zhang, K.Y.J., Card, G.L., Suzuki, Y., Artis, D.R., Fong, D., Gillette, S., Hsieh, D., Neiman, J., West, B.L., Zhang, C., Milburn, M.V., Kim, S.-H., Schlessinger, J., Bollag, G., 2004. A Glutamine Switch Mechanism for Nucleotide Selectivity by Phosphodiesterases. *Mol. Cell* 15, 279–286. <https://doi.org/10.1016/j.molcel.2004.07.005>
- Zhang, Y.Q., Bailey, A.M., Matthies, H.J.G., Renden, R.B., Smith, M.A., Speese, S.D., Rubin, G.M., Broadie, K., 2001. Drosophila Fragile X-Related Gene Regulates the MAP1B Homolog Futsch to Control Synaptic Structure and Function. *Cell* 107, 591–603. [https://doi.org/10.1016/S0092-8674\(01\)00589-X](https://doi.org/10.1016/S0092-8674(01)00589-X)

Zumbrunn, J., Kinoshita, K., Hyman, A.A., Näthke, I.S., 2001. Binding of the adenomatous polyposis coli protein to microtubules increases microtubule stability and is regulated by GSK3 β phosphorylation. *Curr. Biol.* 11, 44–49. [https://doi.org/10.1016/S0960-9822\(01\)00002-1](https://doi.org/10.1016/S0960-9822(01)00002-1)